

**Synthesis of novel organic solvent-free
waterborne poly(urethane-urea)s.
Nanocomposites, hydrogels and
adhesives**



emari ta zabal zazu
Universidad del País Vasco Euskal Herriko Unibertsitatea

Iñigo Díez García

2020



GIPUZKOAKO
INGENIARITZA
ESKOLA
ESCUELA
DE INGENIERÍA
DE GIPUZKOA

**Synthesis of novel organic solvent-free
waterborne poly(urethane-urea)s.
Nanocomposites, hydrogels and adhesives.**

Iñigo Díez García
PhD Program of Renewable Materials Engineering

Thesis supervisors:
Dr Arantxa Eceiza
Dr Agnieszka Tercjak

Donostia-San Sebastian, 2020

Acknowledgments

“And in the end it's not the years in your life that count; it's the life in your years.”

(Abraham Lincoln)

El camino emprendido hace cuatro años toca a su fin. Un camino lleno de buenas persona y experiencias que me han permitido desarrollarme profesionalmente, pero sobre todo en lo personal. Es por ello que me gustaría agradecer a todas ellas lo que han supuesto en mi vida estos últimos años.

Las primeras palabras son para agradecer a mis directoras de tesis, la Dra. Arantxa Eceiza y la Dra. Agnieszka Tercjak, por haberme dado la oportunidad y la confianza para desarrollar este trabajo. Agradecerles también su inestimable ayuda con sus conocimientos y consejos durante estos años, los cuales me han permitido aprender, ampliar mi visión sobre la investigación y la ciencia, así como mejorar los artículos publicados y el presente trabajo. Asimismo, agradecerles también el apoyo brindado en los momentos en los que se presentaba algún tipo de obstáculo.

Por otra parte, agradecer al Gobierno Vasco por la ayuda económica concedida para la realización de la presente tesis doctoral (PRE_2018_2_0217), así como por la concesión de la beca que me permitió realizar la estancia de movilidad (EGONLABUR2018). Así como al Gobierno Polaco por permitirme, dentro del programa NAWA, realizar una corta estancia de movilidad.

Asimismo, me gustaría agradecer al Departamento de Ingeniería Química y del Medio Ambiente por facilitarme el uso de las instalaciones necesarias para desarrollar la presente tesis doctoral. También agradecer a los Servicios Generales (SGIker) de la UPV/EHU el apoyo técnico proporcionado, especialmente a la Dra. Loli Martín, técnico del servicio de Macroconducta-Mesoestructura-Nanotecnología, por su inestimable ayuda.

I would like to thank Professor Joseph L. Keddie for the opportunity of staying for three months in his research group at University of Surrey researching and learning about adhesive properties. I want to appreciate also the kindness of all the members of the group, who made me feel like I was home. I will not forget all the coffee breaks,

lunches, conversations, and all the time I spent there. You all have a special place in my heart. I would also like to thank Professor Adriana Zaleska-Medynska and her group at University of Gdansk, especially to Marek, for the time I spent there researching and learning.

También quisiera agradecer a todos mis compañeros de laboratorio por su apoyo, conversaciones, confianzas, ayuda y los buenos momentos que me habéis hecho pasar estos años. No me olvido de quienes habéis estado desde el primer día, ni de los que os fuisteis, ni de los que llegasteis más recientemente. Gracias. Habéis sido uno de los pilares más importantes de mi vida durante estos últimos años.

Por último, quiero agradecer a toda a mí familia. En especial a mis padres. Aita, ama, gracias por haber estado hay todos estos años, por vuestro apoyo, ayuda, por vuestra confianza y creer en mí. Por todos vuestros esfuerzos para que yo pueda haber llegado aquí, sin los cuales no hubiera sido posible. Muchísimas gracias por todo. A mi hermana, a ti Maider, por estar siempre ahí, por ayudarme siempre que la he necesitado, desde txiki hasta ahora. Gracias. A ti, Amatxi, por las tardes de café al salir del laboratorio, por tu cariño todos estos años, por creer en mí. Y no puedo olvidarme de vosotras, Amoña y tía, desgraciadamente no habéis podido ser partícipes del final de estos años de tesis doctoral, pero, por suerte, sí llegastéis a saber que la empezaba. Sé que desde algún lugar habréis observado mis progresos y sabréis que he llegado a terminarla.

*Para vosotros,
aita, ama, Mainer*

Summary

The present research work is focused on the synthesis and the characterization of novel organic solvent-free waterborne poly(urethane-urea)s, and based on them nanocomposites and hydrogels. Moreover, the adhesive performance of synthesized waterborne poly(urethane-urea)s was evaluated and an adhesive system for base of Pressure Sensitive Adhesive (PSA) was achieved.

The first objective was to synthesize environmentally friendly waterborne poly(urethane-urea)s. In order to achieve such a goal, 100% renewable carbon bio-based macrodiol and poly(ethylene oxide) were employed for the synthesis of waterborne poly(urethane-urea)s through a novel and non-common organic solvent-free synthesis procedure. Then, the versatility of the synthesis procedure was proved by synthesizing waterborne poly(urethane-urea)s based on triblock copolymers as macrodiols. Furthermore, nanocomposites based on synthesized waterborne poly(urethane-urea)s were prepared by incorporation of inorganic nanoparticles (TiO_2). Moreover, the self-healing ability displayed by the waterborne poly(urethane-urea) and nanocomposite films was analyzed. In addition, sodium alginate was used together with poly(ethylene oxide) based and triblock copolymers based waterborne poly(urethane-urea)s, as well as with those containing TiO_2 nanoparticles, for the preparation of hydrogels.

Finally, the adhesive performance of both poly(ethylene oxide) based and triblock copolymers based waterborne poly(urethane-urea)s was studied. Bilayer systems creating a gradient in viscoelasticity were designed in order to improve the adhesive performance. Considering the results obtained for the designed bilayer systems, the application as PSA adhesive tape was evaluated.

This work highlights the potential of the developed novel organic solvent-free waterborne poly(urethane-urea) synthesis, besides proving the versatility of prepared waterborne poly(urethane-urea)s for the development of new materials, which can find application in different fields, such as coatings, adhesives, wound dressing or tissue engineering.

General index

Chapter 1: Introduction	1
Chapter 2: Materials and characterization techniques	35
Chapter 3: Waterborne poly(urethane-urea)s based on a bio-based macrodiol	51
Chapter 4: Triblock copolymers as macrodiols for the synthesis of waterborne poly(urethane-urea)s	75
Chapter 5: Nanocomposites prepared by incorporation of TiO₂ nanoparticles	101
Chapter 6: Self-healing ability of waterborne poly(urethane-urea) and nanocomposite films	129
Chapter 7: Development of hydrogels by incorporation of sodium alginate	147
Chapter 8: Adhesive performance of waterborne poly(urethane-urea)s	173
Chapter 9: General conclusions, future works and publications	197
Annexes	211

Chapter



"A journey of a thousand miles begins with a single step."

(Laozi)

Introduction

1. Introduction

1.1. Motivation	5
1.2. Polyurethanes and poly(urethane-urea)s	6
1.2.1. Brief history	6
1.2.2. Chemistry and synthesis	6
1.2.3. Waterborne polyurethanes and poly(urethane-urea)s	10
1.3. Block copolymers	10
1.3.1. Characteristics of block copolymers	10
1.3.2. Triblock copolymers formed by PEO and PPO blocks	11
1.4. Nanocomposites	12
1.4.1. Overview of nanocomposites	12
1.4.2. Nanocomposites based on polyurethanes and poly(urethane-urea)s	13
1.5. Self-healing	14
1.5.1. Healable polymers and healing mechanisms	14
1.5.2. Healable polyurethanes and poly(urethane-urea)s	16
1.6. Hydrogels	16
1.6.1. Overview of hydrogels	16
1.6.2. Hydrogels based on polyurethanes and poly(urethane-urea)s	17
1.6.3. Applications of hydrogels	18
1.7. Adhesion	19
1.7.1. Development of adhesives	19
1.7.2. Adhesion mechanism	20
1.7.3. Types of polymer adhesives	20
1.7.4. Applications of polyurethane and poly(urethane-urea) adhesives	21
1.8. General objectives	22
1.9. References	25

1.1. Motivation

In recent years, the society has started to demand the development of more environmentally friendly materials. The problems caused by the production, use, and waste of plastics, have generated considerable social awareness, largely motivated by the fact that the media focuses on highlighting their drawbacks downplaying their benefits. Despite all, the life quality enjoyed today is largely thanks to polymer materials. Nevertheless, it is true that there is a huge problem when it comes down to these materials. It must be understood that a rational use of polymer materials, such as criticized plastic bags, ought to be carried out. In addition, human population must accept its responsibility in the disposal of plastic residue. Every single person should make its own contribution to the recycling process by properly getting rid of polymer residues. Notwithstanding, scientists from different research fields play an important role in finding solutions to the problems generated by the production of plastics. On the one hand, designing biodegradable and bio-based polymers and, on the other hand, developing new greener synthesis protocols and recycling procedures.

Therefore, in this work, the development of an organic solvent-free synthesis procedure for waterborne poly(urethane-urea)s is presented. In quest of developing more sustainable waterborne poly(urethane-urea)s, a corn-based 100% renewable carbon content precursor is employed. Moreover, different systems are prepared using block copolymers with blocks of different chemical structure, molecular weights and blocks architectures, demonstrating the versatility of the developed synthesis process. Additionally, with the aim of improving the performance of synthesized waterborne poly(urethane-urea)s, nanocomposites were developed through the incorporation of TiO₂ nanoparticles as nanofillers, leading to improved mechanical properties, thermal stability and self-healing efficiency. Furthermore, due to the increasing interest in hydrogels, especially for biomedical applications, synthesized waterborne poly(urethane-urea)s are used for their preparation. Finally, the potential application of synthesized waterborne poly(urethane-urea)s as adhesives is also studied.

1.2. Polyurethanes and poly(urethane-urea)s

1.2.1. Brief history

In 1849, Wurtz synthesized the first ever urethane¹. Almost a century later, in 1937, in Germany, Bayer et al.¹⁻³, at IG Farbenindustrie^{4,5}, published the first patent on polyurethanes and polyureas, which was related to the synthesis of these polymers based on 1,6-hexane diisocyanate and 1,6-hexadamine. Authors were searching for new fibers which could compete with polyamide (PA, trade name Nylon) fibers that had been synthesized by Carothers et al.^{4,6} at Du-Pont. Later, in 1938, Rinke et al.^{4,5} were successful in the synthesis of polyurethanes taking advantage of the reaction between an aliphatic diisocyanate and a macrodiol.

Research on polyurethanes had barely started when World War II began. Europe was at war and terror had spread over the continent. It was in this very dark moment of history when employment of polyurethanes began. They were first utilized as coatings and foams for aircrafts^{1,3,7}. Once the war was over, in the 1950s, industrial production of polyurethanes started to grow³. They became important polymeric materials with application as foams, coatings and adhesives³. In this decade, DuPont developed Spandex fibers, commercially known as Lycra^{4,5,8,9}. From that moment, research on polyurethanes and their precursors increased^{3,5}, and with the years they have become one of the most versatile and most employed polymers^{3,4}.

1.2.2. Chemistry and synthesis

The global production of polyurethane products reached 22,300 kt in 2016, and is expected to increase to 28,600 kt by 2020¹⁰. In fact, the polyurethane industry was directly responsible for 55,600 jobs in the United States of America in 2017, and for a total of 270,000 jobs when adding the indirect ones¹¹. This high demand is the result of the vast number of applications of polyurethanes, which include adhesives, coatings, paints, foams and sealants, among others^{4,12}. This means that they can be found in different fields such as automotive, textile, construction, medicine, among others^{4,11,12}.

The synthesis of polyurethanes is based on a polycondensation reaction between a diisocyanate and a polyol^{3,5}. Nevertheless, isocyanate group can react with compounds containing active hydrogens^{4,13} (hydroxyl, amine, water, carboxylic acid)¹³ (Figure 1.1). Polyureas are synthesized by reaction of a diisocyanate and an amine with at least two active hydrogens^{4,5,7,13}. Isocyanate group can also react with urethane and urea groups leading to allophanate and biuret groups, respectively¹³ (Figure 1.1).

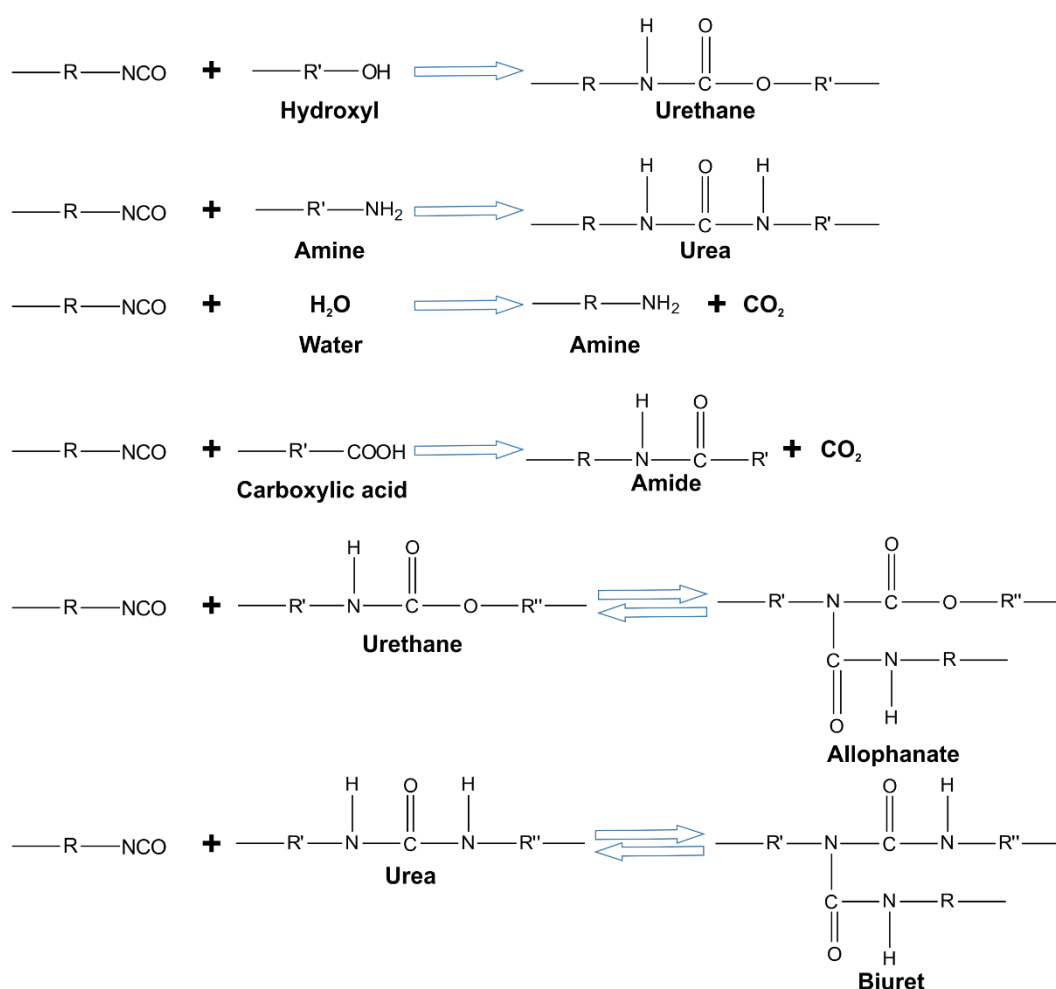


Figure 1.1. Most common reactions of isocyanate group.

1.2.2.1. Diisocyanates

As mentioned, diisocyanates are the basic building block for synthesis of classic polyurethanes. They are industrially produced by the phosgene-amine synthesis route^{14,15}. Among them, both aliphatic and aromatic diisocyanates can be found. Toluene diisocyanate (TDI) and 4,4'-diphenylmethane diisocyanate (MDI) are the

most common ones^{3,16}. Nonetheless, there are also other commonly used diisocyanates, which chemical structures are shown in Figure 1.2.

The choice of the type of diisocyanate has a crucial effect on the final properties of synthesized material. On the one hand, the reactivity of each isocyanate group in a diisocyanate molecule towards an active hydrogen can be different, especially in the case of non-symmetric diisocyanates^{5,13}. Usually, aromatic diisocyanates are more reactive than aliphatic ones¹⁶. On the other hand, the structure of the diisocyanate affects crystallinity, hydrophilicity, mechanical properties, biodegradability as well as biocompatibility of synthesized materials¹⁷⁻¹⁹. Aliphatic diisocyanates, such as hexamethylene diisocyanate (HDI) and 4,4'-dicyclohexylmethane diisocyanate (H₁₂MDI) are preferred for UV light and oxidative resistance^{5,16,17}, since materials based on aromatic diisocyanate tend to yellowing¹⁷. For the synthesis of rigid polyurethanes, aromatic diisocyanates are usually selected⁵.

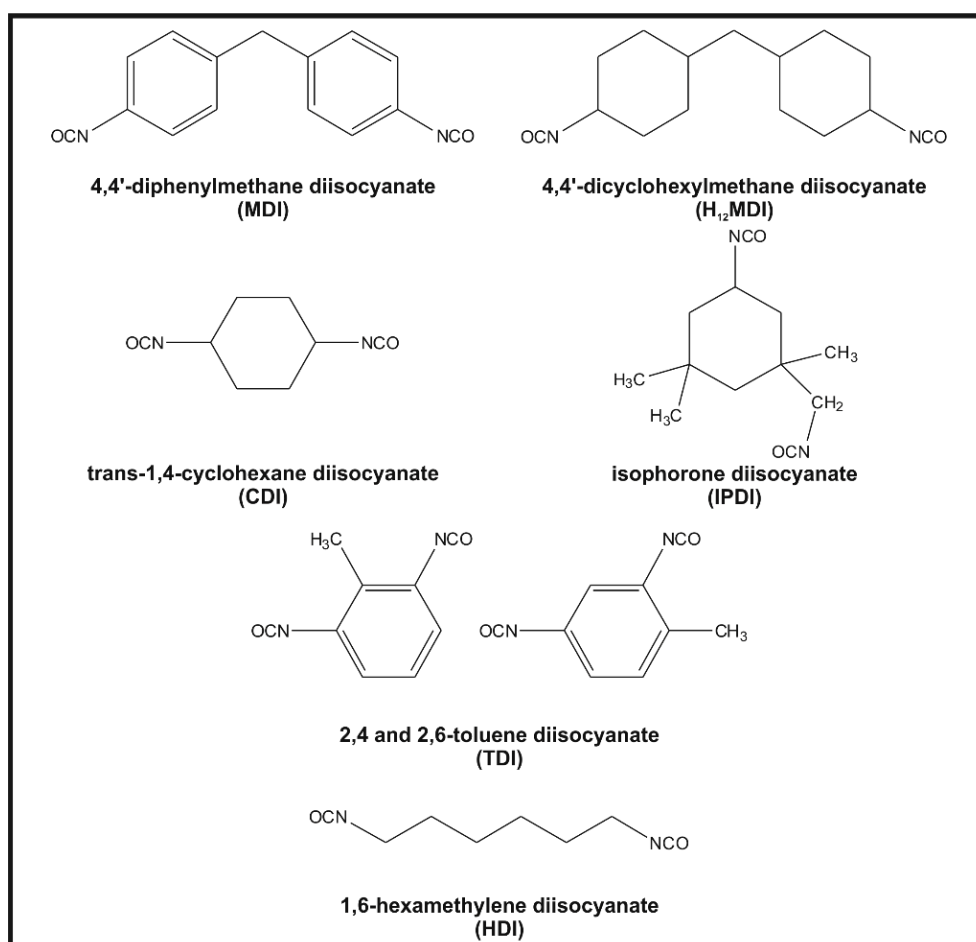


Figure 1.2. Most common diisocyanates.

1.2.2.2. Polyols

Polyols are molecules with at least two hydroxyl functional groups^{3,20,21}. Difunctional polyols are referred as macrodiols²². They are responsible for the flexible long segments of the polyurethane chains³, denominated soft segment²⁰ (Figure 1.3). The molecular weight of polyols employed in the synthesis of polyurethanes generally varies between 300 and 10,000 g mol⁻¹, with hydroxyl groups ranging from 2 to 8 as commonly reported²⁰. Elastic polyurethanes are obtained when the functionality of the polyol is low, 2 or 3 hydroxyl groups, and the molecular weight is high. Meanwhile, low molecular weight and functionality higher than 3 lead to rigid cross-linked polyurethanes^{3,20}. The chemical structure and characteristic of the employed polyol have a strong effect on the final properties of synthesized polyurethanes^{21,23}. Therefore, different types of polyols are used, as they are polyethers, polyesters, polycaprolactones, polycarbonates as well as copolymers^{3,21,23-25}.

1.2.2.3. Chain extender

The chain extender, together with the diisocyanate, forms the hard segment of both polyurethanes and poly(urethane-urea)s^{3,26} (Figure 1.3). This is a segment that plays a crucial role in the final properties of the material, particularly in mechanical properties and thermal stability²⁶. They are usually low molecular weight amines and hydroxyl terminated molecules³, which are difunctional in the case of thermoplastic polyurethanes and poly(urethane-urea)s. Hydroxyl terminated chain extenders produce urethane groups, whereas amine terminated ones lead to urea groups^{23,26}. Therefore, diamine chain extenders lead to formation of poly(urethane-urea)s. Ethylene glycol, 1,4-butanediol, 1,6-hexanediol and ethylene diamine are the most utilized ones^{23,26}.

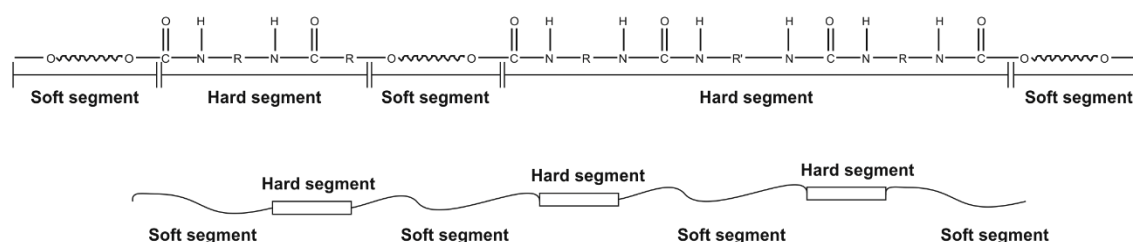


Figure 1.3. Structure of segmented poly(urethane-urea)s.

1.2.3. Waterborne polyurethanes and poly(urethane-urea)s

Waterborne polyurethanes and poly(urethane-urea)s consist of water dispersed polyurethanes or poly(urethane-urea)s synthesized from the classic precursors (diisocyanate, polyol and chain extender)²⁷. These waterborne polyurethanes and poly(urethane-urea)s have been developed as substitutes of solvent-borne ones due to increasing regulations on Volatile Organic Compounds (VOCs)²⁷⁻³⁰. These dispersions are especially appealing for painting, coating and adhesive applications^{28,29,31}. Polyurethane and poly(urethane-urea)s are hydrophobic, therefore, different strategies are followed in order to disperse polyurethanes and poly(urethane-urea)s in aqueous phase. The most employed ones are (i) acetone process, (ii) prepolymer mixing process, (iii) melt-dispersion process and (iv) ketamine-ketazine process^{27,30}. Among these, industrially the acetone process is the most employed one³⁰.

Regardless of the method, a solubilizing group, which acts as internal emulsifier, is required^{29,31,32}. This group is responsible for the dispersion of the polyurethane or poly(urethane-urea) chains in water. The internal emulsifier can be either anionic, cationic or nonionic^{25,28-30}. Anionic includes carboxylated or sulphonated groups, cationic consists of ammonium groups, while nonionic internal emulsifier must be hydrophilic segments, as it is the poly(ethylene oxide) (PEO)^{28,29,33}.

1.3. Block copolymers

1.3.1. Characteristics of block copolymers

Block copolymers consist of monomer units grouped in discrete blocks³⁴. Depending on the number of different blocks, copolymers can be classified as diblock, triblock or any higher multiblock configuration^{35,36}. The interest on block copolymers is based on their ability to self-organize at the nanometric scale^{35,37}. They tend to separate into microdomains creating a phase separation and self-organizing into various morphologies^{16,35} depending on block configuration, degree of polymerization, and other parameters³⁶. These different morphologies include spheres, cylinders, gyroids and lamellae structure^{34-36,38}. The spacing between domains depends on molecular

weight, segment size and strength of interactions between blocks³⁸. The result of all these mentioned features is that block copolymers can act as templates for different applications, for example for integrated circuits³⁹ or for preparation of inorganic/organic hybrid materials^{38,40,41}. Moreover, they present distinct architectures depending on the configuration of their blocks. Therefore, they can arrange into linear, branched and cyclic architectures, among others^{34,36}.

The self-organization of block copolymers is even more complex when they are introduced in a solution, as it is water³⁶. If the solvent is capable of dissolving at least one of the blocks, block copolymer molecules self-organizes in order to avoid contact between the solvent and the non-soluble block or blocks³⁷. Amphiphilic copolymers are one of the most interesting class of block copolymers when it comes to self-organization in solvents, including water. They are formed by both hydrophilic and hydrophobic blocks³⁷. In water, these block copolymers tend to organize into spherical micelles and other structures, as vesicles, cylinders, tubules, bi-continuous, onions, and others.^{34,36,38,42}. The structure of the spherical micelles is often denominated core-corona, where the hydrophobic block forms the core and the hydrophilic block constitutes the corona, which is in contact with water^{36,43,44}.

1.3.2. Triblock copolymers formed by PEO and PPO blocks

Triblock copolymers based on PEO and poly(propylene oxide) (PPO) belong to the class of amphiphilic block copolymers. In this case, PEO is the hydrophilic block whereas PPO constitutes the hydrophobic block^{37,43,44}. PEO-b-PPO-b-PEO and PPO-b-PEO-b-PPO triblock copolymers belong to this class of block copolymers (Figure 1.4). These two triblock copolymers are known with the trade name Pluronic⁴³⁻⁴⁵. The field of application of these triblock copolymers is large, with application as detergents⁴⁶, foaming agents⁴⁷, emulsifiers⁴⁸, dispersion stabilizers⁴⁹, drug delivery⁵⁰ as well as in other areas of medicine⁵¹, and even in petroleum industries⁴³. The ratio between PEO/PPO and the molecular weight of each block and the triblock copolymer influence the final properties of these triblock copolymers⁴³⁻⁴⁵. Furthermore, micelle formation in water is also affected by the formulation of the triblock copolymers as well as by their concentration in water and the temperature⁴⁵. This is the consequence of the fact that the hydrophobic PPO block is soluble in water at temperatures lower

than 15 °C⁴² and at low copolymer concentration⁴⁴. In the case of PEO-b-PPO-b-PEO triblock copolymers, as previously mentioned, formed micelles are reported to have core-corona structure, with PEO blocks forming the corona and PPO block the core^{43,44,51}. Nonetheless, for PPO-b-PEO-b-PPO triblock copolymers it has been reported that they do not form spherical micelles in dilute solution⁵². Increasing the concentration of the copolymer results in the formation of micelles in which the external PPO blocks may join creating looping shaped micelles⁴³⁻⁴⁵. In addition, micelles can be interconnected when the external PPO blocks join with other micelles⁴³.

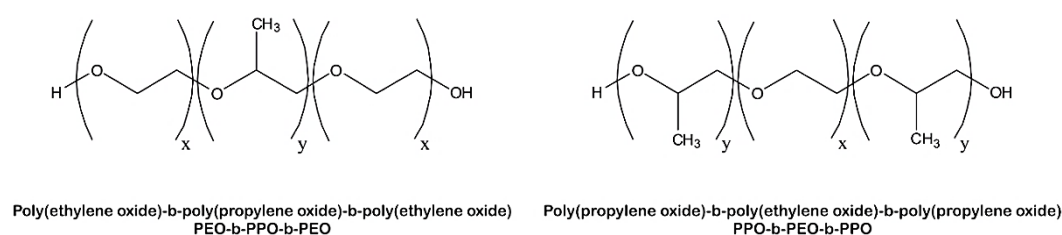


Figure 1.4. Structure of the triblock copolymers based on PEO and PPO blocks.

1.4. Nanocomposites

1.4.1. Overview of nanocomposites

The inception of nanotechnology concept dates back to December of 1959, when Richard Feynman presented the lecture titled: *There is plenty of room at the bottom*⁵³⁻⁵⁵. In the field of nanotechnology, nanocomposites are defined as materials in which at least one of the phases presents a dimension at nanoscale^{56,57} (Figure 1.5). There are different types of nanocomposites depending on the matrix: ceramic matrix nanocomposites, metal matrix nanocomposites and polymer matrix nanocomposites⁵⁶. Even if the concept of nanotechnology is new, Roman glassmakers already fabricated nanocomposite materials consisting of glasses incorporating nanosized metals. The color of the cups made with that glass changed from green to red when a light source is placed inside⁵³. Moreover, the colorful windows of medieval cathedrals are also consequence of metal nanoparticles well-dispersed in the glass at the nanoscale level⁵³.

In the last years, the interest on nanocomposites has dramatically increased⁵⁶. This is mainly due to the effect that the incorporation of a nanofiller into a matrix has on the properties of the material^{56,58}. Often, incorporation of small nanofiller contents leads to an improvement in the properties of the matrix^{56,58}. Furthermore, addition of nanofillers might provide new properties to the matrix, such as conductivity⁵⁹, self-cleaning ability⁶⁰, antibacterial activity^{61,62}, etc. Among nanofillers used to provide these properties, carbon nanotubes, inorganic nanoparticles, nanofibers, nanocrystals, nanowhiskers, graphene, as well as other can be listed^{56,59–66}.

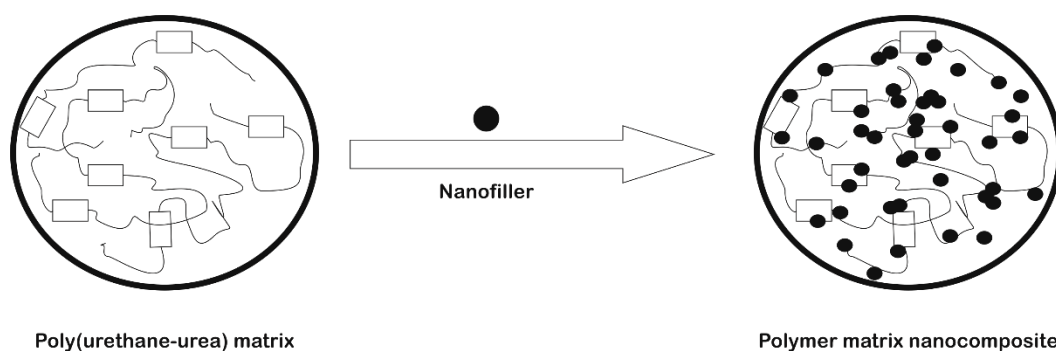


Figure 1.5. Scheme of the poly(urethane-urea) matrix and the polymer matrix nanocomposite after dispersion of the nanofiller.

1.4.2. Nanocomposites based on polyurethanes and poly(urethane-urea)s

Nanocomposites based on polyurethanes and poly(urethane-urea)s are part of polymer matrix nanocomposites. Different nanofillers have been incorporated to polyurethane and poly(urethane-urea) matrices. The main objective when dispersing a nanofiller, as mentioned above, is to improve some properties or provide new ones. In this field, CaCO_3 nanoparticles were successfully used to improve the tensile strength and thermal stability of a waterborne polyurethane⁶⁷. ZnO nanowhiskers also improved the tensile strength, by a 34%, besides providing with antibacterial activity to waterborne polyurethane based nanocomposites⁶⁸. Antibacterial activity was also reported by Zhong et al.⁶⁹ for nanocomposites consisting of *in-situ* formation of Ag nanoparticles in a waterborne polyurethane matrix, by Han et al.⁶² for nanocomposites prepared by incorporation of Au nanoparticles into a waterborne polyurethane, and by Charpentier et al.⁶¹, who controlled the dispersion of TiO_2

nanoparticles into a polyurethane. Cakic et al.⁷⁰ and Yang et al.⁷¹ incorporated SiO₂ nanoparticles to waterborne polyurethanes, which led to an increase in the thermal stability, as well as in the mechanical properties. Furthermore, electrical conductive nanocomposites has also been obtained in the cases of incorporation of Cu nanowires⁷², TiO₂ nanoparticles⁵⁹, carbon nanotubes⁷³ and graphene oxide⁶⁴.

1.5. Self-healing

1.5.1. Healable polymers and healing mechanisms

Plastic waste is a great problem. In 2010, in coastal regions of the world, 99.5 millions of metric tons of plastic waste were generated⁷⁴. Recycling is a solution, nevertheless recycling rates are still low. In Europe, 30% of plastic wastes are recycled, 25% in China and just a 9% in the United States of America⁷⁵. Incineration for energy recovery is also carried out, but still more than 50% of global plastic wastes end up discarded (Figure 1.6). Therefore, extending the life of use of plastics is essential, as well as it is a sustainable consumption, in order to put an end to the throwaway culture⁷⁶. It is here where self-healing polymers become interesting, since this ability increases the lifetime of a product⁷⁷⁻⁷⁹.

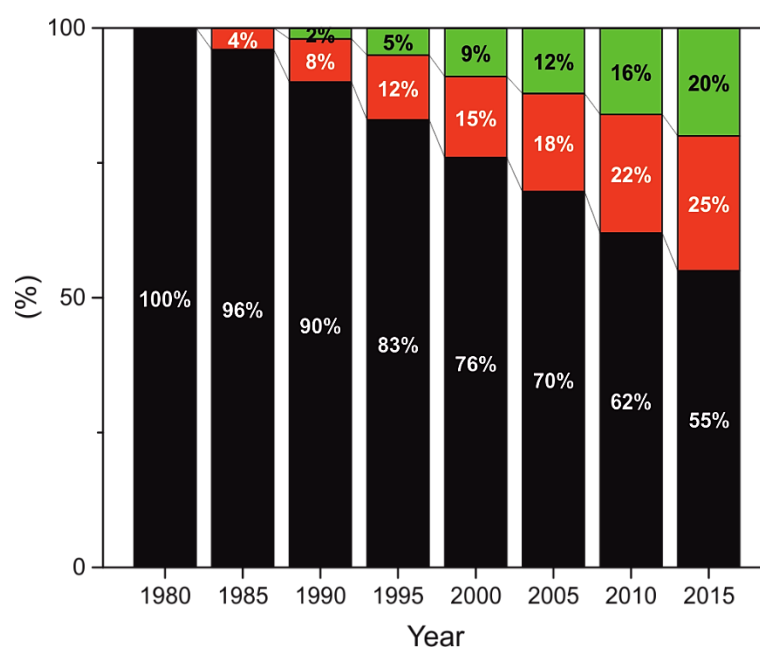


Figure 1.6. Estimated disposal method of global plastic wastes⁷⁵. In black, discarded, in red, incinerated, and in green, recycled plastic wastes.

Self-healing is defined as the ability of a material to fully or partially recover a functionality from a physical or a chemical damage⁸⁰⁻⁸². This is a similar process to the one that takes place in the skin for wound-healing^{83,84}, which takes place thanks to highly coordinated actions⁸⁵. Some of these complex events are coagulation, vasoconstriction and vasodilation, remodeling, scar formation and, finally, scar resolution⁸⁵. Due to the complexity of wound-healing process, it is a challenge to imitate this mechanism. Nonetheless, research on self-healing materials has increased over time, and polymers are not an exception⁸⁶.

The mechanism for self-healing of polymers after crack formation takes place in five stages, as proposed by Wool et al.⁸⁷ (Figure 1.7): (1) surface rearrangement, (2) surface approach that leads to (3) wetting and then to a (4) diffusion of polymer chains. Finally, (5) randomization resulting in the loss of memory of the crack interface.

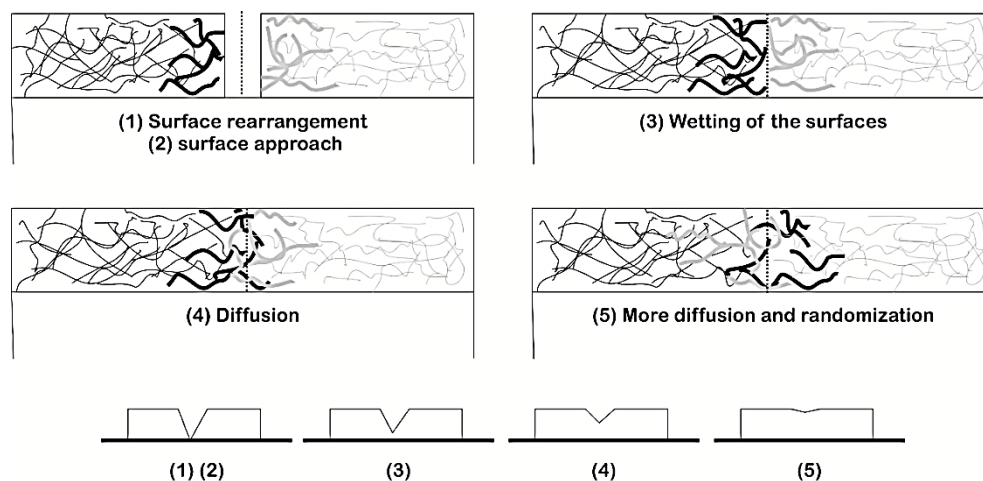


Figure 1.7. Crack healing mechanism.

Self-healable polymers can be classified into two categories: extrinsic and intrinsic. The first one relies on embedding microcapsules containing a healing agent into the polymer matrix^{81,88,89}. On the contrary, intrinsic self-healing polymers do not require the help of an external healing agent thanks to their polymer matrix structure. These polymers present reversible covalent and/or non-covalent bonds^{88,89}. It is important to remark that in some cases an external stimuli such as light or heat is needed. These last ones are called non-autonomous healable polymers^{81,90}.

1.5.2. Healable polyurethanes and poly(urethane-urea)s

Polyurethanes and poly(urethane-urea)s are great candidates for the development of self-healable materials. In fact, research on self-healable polyurethanes is a subject undergoing intense study⁹¹. The versatility of their synthesis makes it possible to prepare materials with a wide range of properties and structures. Functionalizing the polymer structure allows designing intrinsic self-healable polyurethanes and poly(urethane-urea)s by introduction of reversible bonds into the backbone. These interactions can be either dynamic covalent reactions, such as Diels-Alder^{90,92}, or supramolecular interactions, as it is hydrogen bonding^{89,93}.

Different self-healable polyurethanes and poly(urethane-urea)s have been developed. Irusta et al.⁹⁰ synthesized a self-healable polyurethane based on thermal reversible Diels-Alder reaction, whereas Fang et al.⁹² prepared a waterborne polyurethane with a thermally activated Diels-Alder reaction. A photochemical self-healable polyurethane was designed by Ling et al.⁹⁴ using coumarin as cross-linker. Yuan et al.⁸⁸ made use of alkoxyamines as cross-linkers. Disulfide bonds were the reversible bonds in the self-healable polyurethanes synthesized by Xu et al.⁹⁵ and on the thermally activated self-healable poly(urethane-urea) synthesized by Nevejans et al.⁹⁶. Hydrogen bonding was the reversible bond responsible for the self-healing of poly(urethane-urea)s prepared by Kim et al.⁹¹.

1.6. Hydrogels

1.6.1. Overview of hydrogels

Research on hydrogels started in 1960 when Wichterle and Lim⁹⁷ published their pioneering work on preparation of hydrogels from cross-linked methacrylate. They were searching for biocompatible materials. This was an starting point for intensive research on hydrogels⁹⁸⁻¹⁰¹, especially as biomaterials^{100,102-107}.

An hydrogel is defined as a three dimensional expandable polymer network that may absorb high amounts of water^{101,102,108-111}. Hydrogels can be divided into two categories attending to the way the cross-linking of the polymer network is achieved.

These two groups are chemically cross-linked gels and physically cross-linked gels^{106,108,111–114} (Figure 1.8). Besides this classification, hydrogels can also be categorized according to their physical state into solid, semi-solid and liquid hydrogels¹¹¹.

The strategies for the preparation of hydrogels are numerous^{110,111} (Figure 1.8). On the one hand, synthesis of chemically cross-linked hydrogels can be achieved by free radical polymerization, Diels-Alder click reaction, Schiff base formation, enzymatic induced cross-linking, photopolymerization or grafting^{106,110,111,115,116}. On the other hand, physically cross-linked hydrogels are prepared by taking advantage of ionic interactions, hydrogen bonding, hydrophobic interactions, crystallization or metal coordination^{106,111}. Methods such as freeze-thawing¹¹⁷ or incorporation of cations^{118,119} are also commonly used.

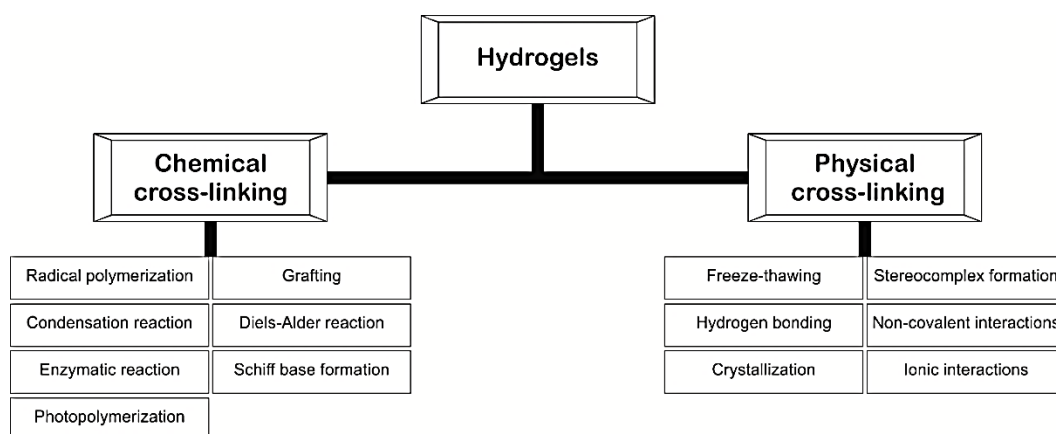


Figure 1.8. General methods for preparation of hydrogels.

1.6.2. Polyurethane and pol(urethane-urea) based hydrogels

Regarding polyurethane based hydrogels, some research has been carried out in this field. Hydrogels based on the incorporation of alginate to polyurethanes have already been prepared by Travinskaya et al.¹²⁰, Bhattacharyya et al.¹²¹ and Wang et al.¹¹⁸. This has not been the only strategy followed. For example, Wang et al.¹²² made use of the freeze-thawing strategy, whereas Sirkecioglu et al.¹²³ and Petrini et al.¹²⁴ designed hydrogels based on PEO by using trifunctional cross-linking agents.

Concerning poly(urethane-urea)s based hydrogels, they have also been reported. Some research detailed the use of an excess of diisocyanate and water as *in-situ* chain extender to synthesize poly(urethane-urea) hydrogels^{125,126}. Hydrogen bonding between multiple urethane and urea linkages of a poly(urethane-urea) has been proved successful for the synthesis of physical hydrogels¹²⁷. Incorporation of PEO chains to the poly(urethane-urea) backbone has also been reported to lead to hydrogels formation^{128,129}.

1.6.3. Applications of hydrogels

Regardless of the formulation of polymer hydrogels, their field of applications is vast. As previously mentioned, biomedical application is the main field in which hydrogels find applications^{106,108}. They have been employed in tissue engineering^{108,124,130}, neural electrodes^{131,132}, contact lenses¹³³, wound dressing^{109,134}, drug delivery^{107,135,136}, etc.

In addition to applications as biomaterials, hydrogels can be used for other purposes. Wang et al.¹³⁷ synthesized hydrogels based on poly(ethylene oxide) methyl ether methacrylate and 2-methacryloyloxyethyl phosphorylcholine for marine antifouling. Removal of heavy metal ions from water was achieved by hydrogels prepared by Hong et al.¹³⁸ and by Yu et al.¹³⁹. Moreover, Ramos et al.¹⁴⁰ designed chitosan hydrogels reinforced with TiO₂ nanoparticles as arsenic sorbent, whereas chitosan based hydrogels obtained by Ebrahimi et al.¹⁴¹ served as detectors for *Escherichia coli* bacteria. Essawy et al.¹⁴² used the hydrogels designed by them for controlled release of soil nutrients. Meanwhile, Jia et al.¹⁴³ utilized hydrogels for a more technological application, which was as a component of a soft robotic microgripper. These are just some examples of the broad range of applications of hydrogels.

When it comes to polyurethane or poly(urethane-urea) based hydrogels, biological nitrogen removal process for wastewater was accomplished by Sato et al.¹²⁶, whereas Bhattacharyya et al.¹²¹ developed hydrogels for safe and efficient oral insulin delivery. Wang et al.¹²² and Petrini et al.¹²⁴ designed hydrogels for wound dressing and tissue engineering, respectively. Furthermore, ultrastrong and tough hydrogels for precise fabrication of 3D biomaterials were prepared by Yang et al.¹²⁷.

1.7. Adhesion

1.7.1. Development of adhesives

Adhesion property, defined as the interaction, either interatomic or intermolecular, that takes place at the interface of two surfaces¹⁴⁴, has been useful to join different materials. Diverse adhesives have been used throughout history, and they have become indispensable for modern life. Egyptians and Chinese used casein glue^{145,146}, while both Greeks and Romans mixed slaked lime with volcanic ash and sand to produce *pozzolanic cement*¹⁴⁵. This archaic cement was employed in the construction of the Roman Colosseum and Pantheon¹⁴⁵.

It was in 1690 when the first glue factory was built in Europe, in the Netherlands^{145,146}. Nonetheless, the first US patent on a glue dates back to 1840, which was a glue based on animal bones¹⁴⁵. In the 20th Century, research on polymer materials and the development of new synthetic polymers led to a revolution in the field of adhesives. Dating back again to World War II, Bayer¹⁴⁵ developed a polyisocyanate adhesive. Synthetic rubber and modified phenolic resin were used during that war¹⁴⁵. Epoxy-phenolic adhesives were also developed at that time¹⁴⁵. A great lay forward in synthetic adhesive took place during World War II. From that moment, research related to adhesive materials has been especially carried out by the automotive and aerospace industries, encouraging knowledge in this field, and consequently the knowledge on the adhesion mechanism¹⁴⁴.

Despite all the research on new synthetic adhesives, due to economic reason and regardless of the country, natural adhesives dominate the adhesive market¹⁴⁵. A market that is advancing in the direction of becoming more environmentally friendly. In fact, in 2017, two major industry sectors led the use of bio-based adhesives, as they were the building and construction industry and the paper and packaging industry¹⁴⁷. Nevertheless, most of adhesives utilized today are petroleum derived and VOCs are released in their production and manipulation¹⁴⁷. The good news is that, from available data before the global crisis, 37% of the European adhesives and sealants market consisted on waterborne products¹⁴⁸.

1.7.2. Adhesion mechanism

When referring to adhesion two different mechanisms have to be taken into account: bonding and debonding. The first one takes place when the adhesive is applied onto a surface. In this stage, the topography of the surface plays a key role, since its roughness affects the extent of real contact with the adhesive¹⁴⁹. For a good contact, a liquid-like behavior of the adhesive is desired¹⁵⁰, maximizing the interfacial contact¹⁵¹. At this point, the wetting ability of the adhesive on the surface is of a great importance for a good adhesion¹⁵². Nevertheless, for the debonding stage a more solid-like behavior of the adhesive is needed.

Debonding can take place in different ways¹⁵³. This is influenced by the relationship between adhesion and cohesion¹⁵¹. Molecular forces determine the cohesive strength: chemical bonds, intermolecular interactions and mechanical bonds¹⁵². Different debonding failures can be listed attending to the relationship between adhesion and cohesion: cohesion failure, substrate failure, mixed failure and adhesive failure (Figure 1.9).

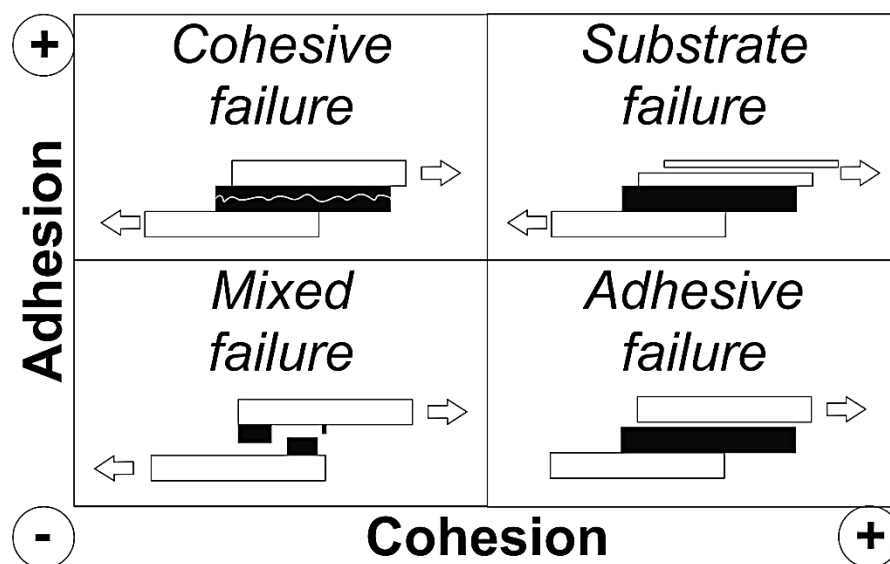


Figure 1.9. Adhesion failure mechanisms depending on the adhesion-cohesion balance.

1.7.3. Types of polymer adhesives

Adhesives can be presented in three different physical forms: liquid, solid or as a paste^{145,154}. The physical state of the adhesive depends on the application. Adhesives

can be classified according to their chemical nature. The most important adhesives are acrylic and acrylates, epoxies, polyimides, silicones, cyanate esters and polyurethanes¹⁵⁴. These polymers can be divided, at the same time, in thermoplastic and thermosetting. The first ones present a linear or a branched structure, whereas the structure of the latter ones is cross-linked^{154,155}.

From all possible classifications, one of the main division for polymer adhesives is according to their functionality. Structural adhesives are commonly thermosetting polymers that are used to transfer loads between adherends⁶⁵. Meanwhile, thermoplastic polymers might be used as hot-melt adhesives, which can be utilized in diverse applications⁶⁵. Waterborne adhesives are employed in packaging and are a more environmentally friendly alternative⁶⁵. Ultraviolet/visible light curing adhesives find application in electronic, automotive, medical, optical and packaging industries thanks to their fast curing process¹⁵⁴. High temperature adhesives cure with heat and are used in aircraft, satellites, missiles, electronics, and automotive industries^{65,154}. Nanocomposite adhesives is a new class of adhesives that is growing fast in the last years as a consequence of the intensive research on nanomaterials⁶⁵. Nonetheless, pressure sensitive adhesives (PSAs), consisting on viscoelastic polymers that adhere fast to any surface applying low pressures^{65,156-158}, are the type of adhesives that are most commonly found as consumer products¹⁵⁹. Even if noncross-linked, thus thermoplastic, polymers are not ideal candidates as PSAs¹⁵⁰, some research, especially by Piau et al.¹⁶⁰, has been carried out on noncross-linked PSAs^{161,162}.

1.7.4. Applications of polyurethane and poly(urethane-urea) adhesives

Polyurethane and poly(urethane-urea) adhesives are used for many applications^{3,163}, with the textile industry as the main consumer¹⁵¹ (Figure 1.10). Polyurethane adhesives represented the 12% of the adhesive market value¹². These kind of adhesives present advantages such as an excellent adhesion due to their polar nature, a high-strength as a consequence of their segmented structure and the possibility of

cross-linking¹⁵¹. Their cost is also an advantage¹⁵¹. Nevertheless, their limited thermal and hydrolytic stability are the drawbacks of polyurethane adhesives¹⁵¹.

Polyurethane adhesives have been in the adhesive market for many years. Nowadays, research is focused on moving forward more environmentally friendly polyurethane adhesives. For this reason, the adhesive industry is replacing classical solvent-borne polyurethanes for waterborne polyurethanes^{12,70,164}. Many research works can be found in waterborne polyurethane adhesives^{70,164-168}, some of them for the preparation of PSAs^{165,167}.

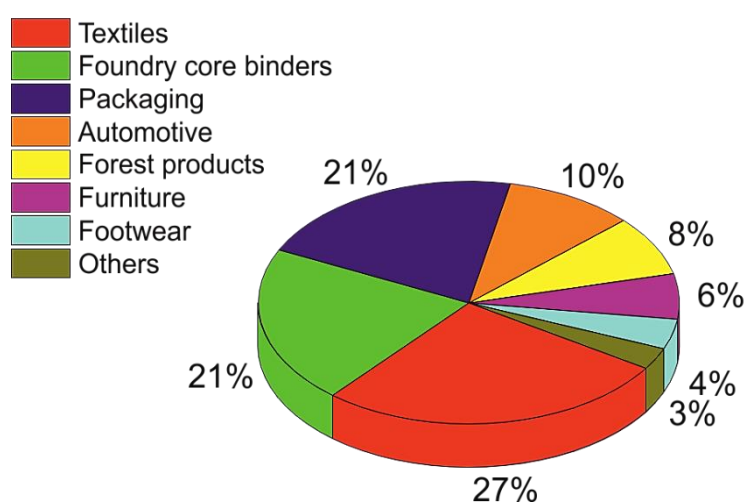


Figure 1.10. Percentage of the market value (in millions of \$) of adhesive applications of polyurethanes¹⁵¹.

1.8. General objectives

The main objectives of this investigation work was to synthesize bio-based waterborne poly(urethane-urea)s following a novel organic-solvent free synthesis procedure and to prove that the developed synthesis procedure is also useful for synthesis of waterborne poly(urethane-urea)s based on triblock copolymers. Furthermore, this investigation work was also focused on the development of nanocomposites with the intention of improving their final properties if compared to synthesized waterborne poly(urethane-urea)s. The self-healing ability displayed by synthesized waterborne poly(urethane-urea) and their nanocomposite films was also studied. In addition, the feasibility of preparation of hydrogels based on synthesized waterborne poly(urethane-urea)s was also proved. Finally, possible application of

synthesized waterborne poly(urethane-urea)s as adhesives was analyzed. Therefore, the main objectives of each Chapter, as shown in Figure 1.11, are the following:

The main goal of the Chapter 3 is establishing a new procedure for the synthesis of waterborne poly(urethane-urea)s based on a 100% renewable carbon content corn-based macrodiol, poly(trimethylene ether glycol) (P3MG), together with PEO as precursors for the synthesis of environmentally friendly waterborne poly(urethane-urea)s. The effect of the variation of the ratio between PEO and P3MG macrodiols on the final properties of synthesized waterborne poly(urethane-urea)s is studied.

In Chapter 4 the possibility of using block copolymers with PEO and PPO blocks as macrodiols for the synthesis of waterborne poly(urethane-urea)s following the synthesis procedure developed in Chapter 3 is verified. The influence of the soft segment composition, formed by the triblock copolymers, on the final properties of synthesized waterborne poly(urethane-urea)s is studied.

Chapter 5 focuses on the development of nanocomposites based on selected synthesized waterborne poly(urethane-urea)s improving their final properties by incorporation of TiO₂ nanoparticles. The effect of TiO₂ nanoparticles on thermal and mechanical properties, thermal stability, morphology and electrical conductivity is investigated.

In Chapter 6 the self-healing ability of synthesized waterborne poly(urethane-urea) and prepared nanocomposite films is studied. For this purpose, depending on synthesized waterborne poly(urethane-urea) and nanocomposite films, either mechanical properties of original and healed films are determined or the healing process is observed by optical microscopy.

In Chapter 7 the preparation of hydrogels based on selected synthesized waterborne poly(urethane-urea)s is described. Sodium alginate (SA) is incorporated into selected synthesized waterborne poly(urethane-urea)s and then hydrogels are obtained by addition of CaCl₂. The thermal properties and stability, swelling ability, mechanical properties, rheology, and morphology of obtained hydrogels are analyzed. In addition, the biocompatibility of the prepared hydrogels is also studied.

In Chapter 8 the application of synthesized waterborne poly(urethane-urea)s as adhesives is proven. The adhesive performance of selected waterborne poly(urethane-urea) films is determined. Additionally, different strategies for improvement of the adhesive performance are considered and tested, as they were blending and designing of bilayer systems. Finally, application as pressure sensitive adhesive (PSA) tape is examined.

In Chapter 9 the general conclusions of this work are summarized. The proposed future works, publications and list of communications are also presented.

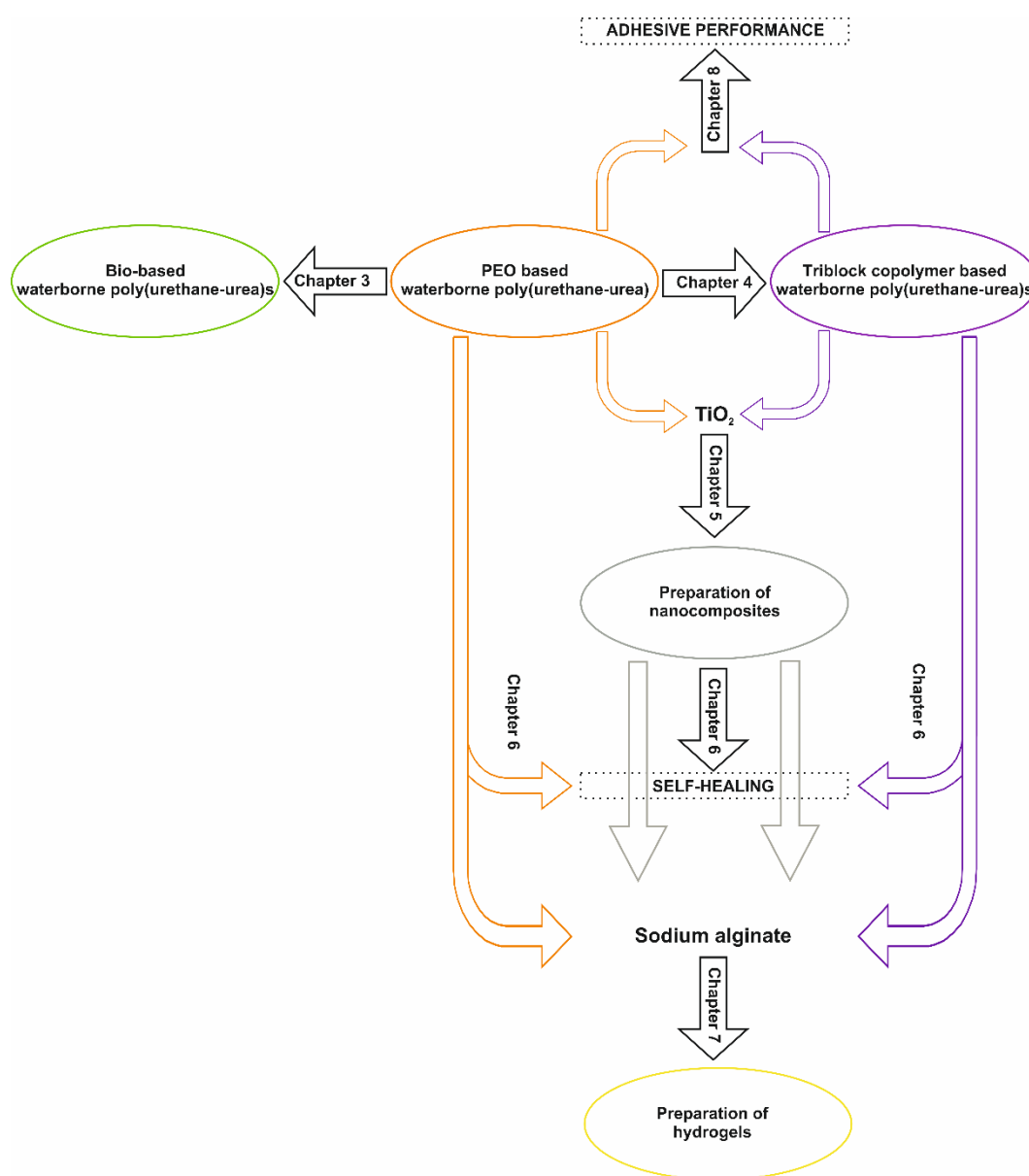


Figure 1.11. Schematic description of the work presented in this thesis.

1.9. References

- [1] B. Samali, S. Nemati, P. Sharafi, F. Tahmoorian, F. Sanati, Structural performance of polyurethane foam-filled building composite panels: a state-of-the-art, *Journal of Composite Science* 3 (2019) 1-30.
- [2] I. G. Farbenindustrie AG, verfahren zur herstellung von polyurethanen bzw. Polyharnstoffen, Reichspatentamp Patentschrift N° 728981, December 7, 1942.
- [3] J. O. Akindoyo, M. D. H. Beg, S. Ghazali, M. R. Islam, N. Jeyaratnam, A. R. Yuvaraj, Polyurethane types, synthesis and applications - a review, *RSC Advances* 6 (2016) 114453-114482.
- [4] M. Szycher, *Szycher's handbook of polyurethanes*, 2nd Ed., CRC press Taylor and Francis Group, 2013, p. 1-12.
- [5] E. Sharmin, F. Zafar, *Polyurethane: An Introduction*, IntechOpen (2012) 3-16.
- [6] W. H. Carothers, Linear polyamides and their production, United States Patent Office 2130523, September 20, 1938.
- [7] R. B. Seymour, G. B. Kauffman, Polyurethanes: a class of modern versatile materials, *Products of Chemistry* 69 (1992) 909-910.
- [8] J. C. Shivers, Segmented copolyetheresther elastomers, United States Patent Office 3023192, February 27, 1962.
- [9] D. K. Chattopadhyay, K. V. S. N. Raju, Structural engineering of polyurethane coatings for high performance applications, *Progress in Polymer Science* 32 (2007) 352-418.
- [10] A. Austin, D. A. Hicks, A review of the global PU industry 2016 and outlook for 2017, *PU Magazine* 14 (2017).
- [11] Economics & Statistics Department American Chemistry Council, The economic benefits of the U.S. polyurethanes industry 2017, October (2018).
- [12] H. Engels, H. Pirkl, R. Albers, R. W. Albach, J. Krause, A. Hoffmann, H. Casselmann, J. Dormish, Polyurethanes: Versatile materials and sustainable problem solvers for today's challenges, *Angewandte Chemie* 52 (2013) 9422-9441.
- [13] M. Ionescu, *Chemistry and Technology of Polyols for Polyurethanes*, 1st Ed., Rapra Technology, 2005, p. 13-30.
- [14] M. Szycher, *Szycher's Handbook of Polyurethanes*, 2nd Ed., CRC press Taylor and Francis Group, 2013, p. 87-134.
- [15] P. Wang, S. Liu, Y. Deng, Important green chemistry and catalysis: non-phosgene syntheses of isocyanates - thermal cracking way, *Chinese Journal of Chemistry* 35 (2017) 821-835.
- [16] M. Szycher, *Szycher's Handbook of Polyurethanes*, 2nd Ed., CRC press Taylor and Francis Group, 2013, p. 37-86.
- [17] D. Lee, H. Tsai, Properties of segmented polyurethanes derived from different diisocyanates, *Journal of Applied Polymer Science* 75 (1999) 167-174.
- [18] Y. W. Tang, R. S. Labow, J. P. Santerre, Enzyme-induced biodegradation of polycarbonate-polyurethanes: Dependence on hard-segment chemistry, *Journal of Biomedical Materials Research* 57 (2001) 597-611.

- [19] A. B. Mathur, T. O. Collier, W. J. Kao, M. Wiggins, M. A. Schubert, A. Hiltner, J. M. Anderson, In vivo biocompatibility and biostability of modified polyurethanes, *Journal of Biomedical Materials Research* 36 (1997) 246-257.
- [20] M. Ionescu, *Chemistry and Technology of Polyols for Polyurethanes*, 1st Ed., Rapra Technology, 2005, p. 1-12.
- [21] M. Szycher, *Szycher's Handbook of Polyurethanes*, 2nd Ed., CRC press Taylor and Francis Group, 2013, p. 135-154.
- [22] M. Szycher, *Szycher's Handbook of Polyurethanes*, 2nd Ed., CRC press Taylor and Francis Group, 2013, p. 633-670.
- [23] S. Mondal, J. L. Hu, Structural characterization and mass transfer properties of nonporous segmented polyurethane membrane: Influence of hydrophilic and carboxylic group, *Journal of Membrane Science* 274 (2006) 219-226.
- [24] M. Ionescu, *Chemistry and Technology of Polyols for Polyurethanes*, 1st Ed., Rapra Technology, 2005, p. 55-166.
- [25] H. Wang, Y. Zhou, M. He, Z. Dai, Effects of soft segments on the waterproof of anionic waterborne polyurethane, *Colloid and Polymer Science* 293 (2015) 875-881.
- [26] M. Szycher, *Szycher's Handbook of Polyurethanes*, 2nd Ed., CRC press Taylor and Francis Group, 2013, p. 155-180.
- [27] K. Noble, *Waterborne polyurethanes*, *Progress in Organic Coatings* 32 (1997) 131-136.
- [28] A. Noreen, K. M. Zia, M. Zuber, S. Tabasum, M. J. Saif, Recent trends in environmentally friendly water-borne polyurethane coatings: A review, *Korean Journal of Chemical Engineering* 33 (2016) 388-400.
- [29] M. Szycher, *Szycher's Handbook of Polyurethanes*, 2nd Ed., CRC press Taylor and Francis Group, 2013, p. 417-448.
- [30] V. D. Athawale, R. V. Nimbalkar, Waterborne coatings based on renewable oil resources: An overview, *Journal of American Oil Chemists' Society* 88 (2011) 159-185.
- [31] B. K. Kim, Aqueous polyurethane dispersions, *Colloid and Polymer Science* 274 (1996) 599-611.
- [32] V. García-Pacios, V. Costa, M. Colera, J. M. Martín-Martnez, Affect of polydispersity on the properties of waterborne polyurethane dispersions based on polycarbonate polyol, *International Journal of Adhesion & Adhesives* 30 (2010) 456-465.
- [33] J. Xia, Y. Xu, C. Gong, D. Gao, Design strategy for waterborne polyurethane with sodium sulfonate groups on the soft segments, *Journal of Applied Polymer Science* 131 (2014) 39657.
- [34] H. Feng, X. Lu, W. Wang, N.-G. Kang, J. Mays, Block copolymers: synthesis, self-assembly, and applications, *Polymers* 9 (2017) 494/1-494/31.
- [35] H. Kim, S. Park, W. D. Hinsberg, Block copolymer based nanostructures: materials, processes, and applications to electronics, *Chemical Reviews* 110 (2010) 146-177.
- [36] Y. Mai, A. Eisenberg, Self-assembly of block copolymers, *Chemical Society Reviews* 41 (2012) 5969-5985.

- [37] R. Jiang, Q. Jin, B. Li, D. Ding, A. C. Shi, Phase diagram of poly(ethylene oxide) and poly(propylene oxide) triblock copolymers in aqueous solutions, *Macromolecules* 39 (2006) 5891-5896.
- [38] A. Tercjak, J. Gutierrez, G. Mondragon, I. Mondragon, Cellulose nanocrystals and Au nanoparticles well-dispersed in a poly(styrene-*b*-ethylene oxide) block copolymer matrix, *The Journal of Physical Chemistry C* 115 (2011) 22180-22185.
- [39] J. Gutierrez, A. Tercjak, L. Peponi, I. Mondragon, Conductive properties of inorganic and organic TiO₂/polystyrene-block-poly(ethylene oxide) nanocomposites, *Journal of Physical Chemistry C* 113 (2009) 8601-8605.
- [40] J. Kirschner, J. Will, T. J. Rejek, L. Portilla, M. Berlinghof, P. Schweizer, E. Spiecker, H. Steinrück, T. Unruh, M. Halik, Memory effect of self-assembled PS-*b*-PEO block copolymer films with selectively embedded functionalized TiO₂ nanoparticles, *Advanced Materials Interfaces* 4 (2017) 1700230/1-1700230/8.
- [41] J. H. Pan, X. S. Zhao, W. I. Lee, Block copolymer-templated synthesis of highly organized mesoporous TiO₂-based films and their photoelectrochemical applications, *Chemical Engineering Journal* 170 (2011) 363-380.
- [42] D. H. Builes, H. Hernandez, I. Mondragon, A. Tercjak, Relationship between the morphology of nanostructured unsaturated polyesters modified with PEO-*b*-PPO-*b*-PEO triblock copolymer and their optical and mechanical properties, *Journal of Physical Chemistry C* 117 (2013) 3563-3571.
- [43] Q. Wang, L. Li, S. Jiang, Effects of a PPO-PEO-PPO triblock copolymer on micellization and gelation of a PEO-PPO-PEO triblock copolymer in aqueous solution, *Langmuir* 21 (2005) 9068-9075.
- [44] S. Liu, H. Bao, L. Li, Role of PPO-PEO-PPO triblock copolymers in phase transitions of a PEO-PPO-PEO triblock copolymer in aqueous solution, *European Polymer Journal* 71 (2015) 423-439.
- [45] S. Liu, L. Li, Molecular interactions between PEO-PPO-PEO and PPO-PEO-PPO triblock copolymers in aqueous solution, *Colloids Surfaces A Physicochemical and Engineering Aspects* 484 (2015) 485-497.
- [46] R. J. Green, S. Tasker, J. Davies, M. C. Davies, C. J. Roberts, S. J. B. Tandler, Adsorption of PEO-PPO-PEO triblock copolymers at the solid/liquid interface: A surface plasmon resonance study, *Langmuir* 13 (1997) 6510-6515.
- [47] H. Maekawa, J. Esquena, S. Bishop, C. Solans, B. F. Chmelka, Meso/macroporous inorganic oxide monoliths from polymer foams, *Advanced Materials* 15 (2003) 591-596.
- [48] A. A. Atta, H. I. Al-Shafy, Z. M. Mohamed, Application of hydrophobically modified water-soluble polyacrylamide conjugated with poly(oxyethylene)-co-poly(oxypropylene) surfactant as emulsifier, *Polymers Advanced Technologies* 22 (2011) 1879-1887.
- [49] G. Fritz, G. Scherf, O. Glatter, Applications of densimetry, ultrasonic speed measurements, and ultralow shear viscosimetry to aqueous fluids, *Journal of Physical Chemistry B* 104 (2000) 3463-3470.
- [50] K. H. Bae, Y. Lee, T. G. Park, Oil-encapsulating PEO-PPO-PEO/PEG shell cross-linked nanocapsules for target-specific delivery of paclitaxel, *Biomacromolecules* 8 (2007) 650-656.
- [51] M. Johnsson, M. Silvander, G. Karlsson, K. Edwards, Effect of PEO-PPO-PEO Triblock copolymers on structure and stability of phosphatidylcholine liposomes, *Langmuir* 15 (1999) 6314-6325.

- [52] G. D. Errico, L. Paduano, A. Khan, Temperature and concentration effects on supramolecular aggregation and phase behavior for poly(propylene oxide)-b-poly(ethylene oxide)-b-poly(propylene oxide) copolymers of different composition in aqueous mixtures, *Journal of Colloid and Interface Science* 279 (2004) 379-390.
- [53] C. P. Poole, F. J. Owens, *Introduction to Nanotechnology*, 1st Ed., John Wiley & Sons, 2003, p. 1-7.
- [54] M. F. Hochella, There's plenty of room at the bottom: Nanoscience in geochemistry, *Geochimica et Cosmochimica Acta* 66 (2002) 735-743.
- [55] R. P. Feynman, There's Plenty of room at the bottom, *Engineering and Science* 23 (1960) 22-36.
- [56] P. H. C. Camargo, K. G. Satyanarayana, F. Wypych, Nanocomposites: synthesis, structure, properties and new application opportunities, *Materials Research* 12 (2009) 1-39.
- [57] L. Cano, A. Evelyn, D. Mauro, M. Striccoli, M. L. Curri, A. Tercjak, Optical and conductive properties of as-synthesized organic-capped TiO₂ nanorods highly dispersible in polystyrene-block-poly(methyl methacrylate) diblock copolymer, *Applied Materials and Interfaces* 6 (2014) 11805-11814.
- [58] L. S. Schadler, L. C. Brinson, W. G. Sawyer, Polymer Nanocomposites: A small part of the story, *The Journal of the Minerals, Metals & Materials Society* 59 (2007) 53-60.
- [59] J. Gutierrez, A. Tercjak, I. Mondragon, Conductive behavior of high TiO₂ nanoparticle content of inorganic/organic nanostructured composites, *Journal of the American Chemical Society* 132 (2010) 873-878.
- [60] C. Zheng, Z. Qi, W. Shen, G. Chen, Self-cleaning bombyx mori silk: Room-temperature preparation of anatase nano-TiO₂ by the sol-gel method and its application, *Coloration Technology* 130 (2014) 280-287.
- [61] P. A. Charpentier, K. Burgess, L. Wang, R. R. Chowdhury, A. F. Lotus, G. Moula, Nano-TiO₂/polyurethane composites for antibacterial and self-cleaning coatings, *Nanotechnology* 23 (2012) 425606/1-425606/9.
- [62] J. G. Han, Y. Q. Xiang, Y. Zhu, New antibacterial composites: waterborne polyurethane/gold nanocomposites synthesized via self-emulsifying method, *Journal of Inorganic and Organometallic Polymers and Materials* 24 (2014) 283-290.
- [63] A. Santamaria-Echart, I. Fernandes, L. Ugarte, F. Barreiro, A. Arbelaiz, M. A. Corcuera, A. Eceiza, Waterborne polyurethane-urea dispersion with chain extension step in homogeneous medium reinforced with cellulose nanocrystals, *Composites Part B: Engineering* 137 (2018) 31-38.
- [64] J. N. Ding, Y. Fan, C. X. Zhao, Y. B. Liu, C. T. Yu, N. Y. Yuan, Electrical conductivity of waterborne polyurethane/graphene composites prepared by solution mixing, *Journal of Composite Materials* 46 (2011) 747-752.
- [65] L. F. M. da Silva, A. Ochsner, R. D. Adams, *Handbook of Adhesion Technology*, 1st Ed., Springer, 2003, p. 261-290.
- [66] L. Ugarte, S. Gómez-Fernández, A. Tercjak, A. Martínez-Amesti, M. A. Corcuera, A. Eceiza, Strain sensitive conductive polyurethane foam/graphene nanocomposites prepared by impregnation method, *European Polymer Journal* 90 (2017) 323-333.

- [67] X. Gao, Y. Zhu, S. Zhou, W. Gao, Z. Wang, B. Zhou, Preparation and characterization of well-dispersed waterborne polyurethane/CaCO₃ nanocomposites, *Colloids and Surfaces A: Physicochemical and Engineering Aspects* 377 (2011) 312-317.
- [68] X. Y. Ma, W. D. Zhang, Effects of flower-like ZnO nanowhiskers on the mechanical, thermal and antibacterial properties of waterborne polyurethane, *Polymer Degradation and Stability* 94 (2009) 1103-1109.
- [69] Z. Zhong, S. Luo, K. Yang, X. Wu, T. Ren, High-performance anionic waterborne polyurethane/Ag nanocomposites with excellent antibacterial property via in situ synthesis of Ag nanoparticles, *RSC Advances* 7 (2017) 42296-42304.
- [70] S. M. Cakić, I. S. Ristić, M. M. Cincović, D. T. Stojiljković, J. B. Simendi Preparation and characterization of waterborne polyurethane/silica hybrid dispersions from castor oil polyols obtained by glycolysis poly(ethylene terephthalate) waste, *International Journal of Adhesion & Adhesives* 70 (2016) 329-341.
- [71] C. H. Yang, F. J. Liu, Y. P. Liu, W. T. Liao, Hybrids of colloidal silica and waterborne polyurethane, *Journal of Colloid and Interface Science* 302 (2006) 123-132.
- [72] X. Zhang, Z. Tang, D. Tian, K. Liu, W. Wu, A self-healing flexible transparent conductor made of copper nanowires and polyurethane, *Materials Research Bulletin* 90 (2017) 175-181.
- [73] H. Li, D. Yuan, P. Li, C. He, High conductive and mechanical robust carbon nanotubes/waterborne polyurethane composite films for efficient electromagnetic interference shielding, *Composites Part A: Applied Science and Manufacturing* 121 (2019) 411-417.
- [74] J. R. Jambeck, R. Geyer, C. Wilcox, T. R. Siegler, M. Perryman, A. Andrady, R. Narayan, K. L. Law, Plastic waste inputs from land into the ocean, *Science* 347 (2015) 768-771.
- [75] R. Geyer, J. R. Jambeck, K. L. Law, Production, use, and fate of all plastics ever made, *Science Advances* 3 (2017) e1700782.
- [76] E. Ritch, C. Brennan, C. Macleod, Plastic bag politics: Modifying consumer behaviour for sustainable development, *International Journal of Consumer Studies* 33 (2009) 168-174.
- [77] S. Thakur, S. Barua, N. Karak, Self-healable castor oil based tough smart hyperbranched polyurethane nanocomposite with antimicrobial attributes, *RSC Advances* 5 (2015) 2167-2176.
- [78] Q. Zheng, Z. Ma, S. Gong, Multi-stimuli-responsive self-healing metallo-supramolecular polymer nanocomposites, *Journal of Materials Chemistry* 4 (2016) 3324-3334.
- [79] J. T. Kim, B. K. Kim, E. Y. Kim, S. H. Kwon, H. M. Jeong, Synthesis and properties of near IR induced self-healable polyurethane/graphene nanocomposites, *European Polymer Journal* 49 (2013) 3889-3896.
- [80] D. G. Bekas, K. Tsirka, D. Baltzis, A. S. Paipetis, Self-healing materials: A review of advances in materials, evaluation, characterization and monitoring techniques, *Composites Part B: Engineering* 87 (2016) 92-119.
- [81] A. Nellesen, A. M. Schmidt, I. P. Bond, R. Martin, A. Rekondo, Review of research and developments in self healing composite materials, *IOP Conf. Series: Materials Science and Engineering* 346 (2018) 12011/1-12011/16.
- [82] M. W. Urban, D. Davydovich, Y. Yang, T. Demir, Y. Zhang, L. Casabianca, Key-and-lock commodity self-healing copolymers, *Science* 362 (2018) 220-225.
- [83] C. Willyard, The secrets of healing without scars, *Nature* 563 (2018) S86-S88.

- [84] F. Table, Formation of the scab and the rate of epithelization of superficial wounds in the skin of the young domestic pig, *Nature* 193 (1962) 293-294.
- [85] S. E. Mutsaers, G. J. Laurent, E. Bishop, G. Mcgrouter, G. J. Laurent, Mechanisms of tissue repair: from wound healing to fibrosis, *The International Journal of Biochemistry & Cell Biology* 29 (1997) 5-17.
- [86] B. Aisa, D. Therriault, E. Haddad, W. Jamroz, Self-healing materials systems: Overview of major approaches and recent developed technologies, *Advances in Materials Science and Engineering* (2012) 1-17.
- [87] R. P. Wool, K. M. O'Connor, A theory of crack healing in polymers, *Journal of Applied Physics* 52 (1981) 5953-5963.
- [88] C. Yuan, M. Z. Rong, M. Q. Zhang, Self-healing polyurethane elastomer with thermally reversible alkoxyamines as crosslinkages, *Polymer* 55 (2014) 1782-1791.
- [89] S. J. Garcia, Effect of polymer architecture on the intrinsic self-healing character of polymers, *European Polymer Journal* 53 (2014) 118-125.
- [90] L. Irusta, M. J. Fernández-Berridi, J. Aizpurua, Polyurethanes based on isophorone diisocyanate trimer and polypropylene glycol crosslinked by thermal reversible diels alder reactions, *Journal of Applied Polymer Science* 134 (2017) 1-9.
- [91] Y. J. Kim, P. H. Huh, B. K. Kim, Synthesis of self-healing polyurethane urea-based supramolecular materials, *Journal of Polymer Science Part B Polymer Physics* 53 (2015) 468-474.
- [92] Y. Fang, X. Du, Y. Jiang, Z. Du, P. Pan, X. Cheng, H. Wang, Thermal-driven self-healing and recyclable waterborne polyurethane films based on reversible covalent interaction, *ACS Sustainable Chemistry and Engineering* 6 (2018) 14490-14500.
- [93] Y. Xiao, H. Huang, X. Peng, Synthesis of self-healing waterborne polyurethanes containing sulphonate groups, *RSC Advances* 7 (2017) 20093-20100.
- [94] J. Ling, M. Z. Rong, M. Q. Zhang, Coumarin imparts repeated photochemical remendability to polyurethane, *Journal of Materials Chemistry* 21 (2011) 18373-18380.
- [95] Y. Xu, D. Chen, A novel self-healing polyurethane based on disulfide bonds, *Macromolecular Chemistry and Physics* 217 (2016) 1191-1196.
- [96] S. Nevejans, N. Ballard, I. Rivilla, M. Fernández, A. Santamaria, Synthesis of mechanically strong waterborne poly(urethane-urea)s capable of self-healing at elevated temperatures, *European Polymer Journal* 112 (2019) 411-422.
- [97] O. Wichterle, D; Lim, Hydrophilic gels for biological use, *Nature* 185 (1960) 117-118.
- [98] M. F. Refojo, H. Yasuda, Hydrogels from 2-hydroxyethyl methacrylate and propylene glycol monoacrylate, *Journal of Applied Polymer Science* 9 (1965) 2425-2435.
- [99] A. S. Hoffman, G. Schmer, C. Harris, W. G. Kraft, Covalent binding of biomolecules to radiation-grafted hydrogels on inert polymer surfaces, *Transactions of the American Society for Artificial Internal Organs* 18 (1972) 10-18.
- [100] J. H. Gouda, K. Povodator, T. C. Warren, W. Prins, Evidence for a micro-mesomorphic structure in poly(2-hydroxyethyl methacrylate) hydrogels, *Journal of Polymer Science Part B: Polymer Letters* 8 (1970) 1970.

- [101] O. Erol, A. Pantula, W. Liu, D. H. Gracias, Transformer hydrogels: A review, *Advanced Materials Technologies* 4 (2019) 1900043/1-1900043/27.
- [102] B. D. Ratner, A. S. Hoffman, Synthetic hydrogels for biomedical applications in hydrogels for medical and related applications, *ACS Symposium Series; American Chemical Society* 31 (1976) 1-36.
- [103] M. Barvic, K. Kliment, M. Zavadil, Biologic properties and possible uses of polymer-like sponges, *Journal of Biomedical Materials Research* 1 (1967) 313-323.
- [104] K. Kliment, M. Stol, K. Fahoun, B. Stockar, Use of spongy hydron in plastic surgery, *Journal of Biomedical Materials Research* 2 (1968) 237-243
- [105] J. Drobnik, P. Spacek, O. Wichterle, Diffusion of anti-tumor drugs through membranes from hydrophilic methacrylate gels, *Journal of Biomedical Materials Research* 8 (1974) 45-51.
- [106] W. Hu, Z. Wang, Y. Xiao, S. Zhang, J. Wang, Advances in crosslinking strategies of biomedical hydrogels, *Biomaterials Science* 7 (2019) 843-855.
- [107] K. Ulbrich, V. Subr, P. Podprrova, M. Buresova, Synthesis of novel hydrolytically degradable hydrogels for controlled drug release, *Journal of Controlled Release* 34 (1995) 155-165.
- [108] A. S. Hoffman, Hydrogels for biomedical applications, *Advanced Drug Delivery Reviews* 54 (2002) 3-12.
- [109] S. Oh, S. Kim, H. Jeong, J. Lee, J. W. Cho, J. Park, The mechanical properties of polyurethane foam wound dressing hybridized with alginate hydrogel and jute fiber, *Fibers and Polymers* 14 (2013) 173-181.
- [110] W. E. Hennink, C. F. Van Nostrum, Novel crosslinking methods to design hydrogels, *Advanced Drug Delivery Reviews* 54 (2002) 13-36.
- [111] K. Varaprasad, G. Malegowd, T. Jayaramudu, M. Mohan, R. Sadiku, A mini review on hydrogels classification and recent developments in miscellaneous applications, *Materials Science and Engineering C* 79 (2017) 958-971.
- [112] R. Dash, M. Foston, A. J. Ragauskas, Improving the mechanical and thermal properties of gelatin hydrogels cross-linked by cellulose nanowhiskers, *Carbohydrate Polymers* 91 (2013) 638- 645.
- [113] W. A. Petka, J. L. Harden, K. P. Mcgrath, D. Wirtz, D. A. Tirrell, Reversible hydrogels from self-assembling artificial proteins, *Science* 281 (1998) 389-393.
- [114] O. Guaresti, C. García-Astrain, R. H. Aguirresarobe, A. Eceiza, N. Gabilondo, Synthesis of stimuli-responsive chitosan-based hydrogels by Diels-Alder cross-linking 'click' reaction as potential carriers for drug administration, *Carbohydrate Polymers* 183 (2018) 278-286.
- [115] K. González, T. Gurrea, O. Guaresti, I. Algar, A. Eceiza, N. Gabilondo, Maleimide-grafted cellulose nanocrystals as cross-linkers for bionanocomposite hydrogels, *Carbohydrate Polymers* 149 (2016) 94-101.
- [116] C. García-Astrain, R. Hernández, O. Guaresti, L. Fruk, C. Mijangos, A. Eceiza, N. Gabilondo, Click crosslinked chitosan/gold nanocomposite hydrogels, *Macromolecular Materials and Engineering* 301 (2016) 1295-1300.
- [117] H. Zhang, F. Zhang, J. Wu, Physically crosslinked hydrogels from polysaccharides prepared by freeze-thaw technique, *Reactive & Functional Polymers* 73 (2013) 923-92.
- [118] J. Wang, X. Ying, X. Li, W. Zhang, Preparation, characterization and swelling behaviors of polyurethane-grafted calcium alginate hydrogels, *Materials Letters* 126 (2014) 263-266.

- [119] Y. Huang, H. Yu, C. Xiao, Effects of Ca²⁺ crosslinking on structure and properties of waterborne polyurethane-carboxymethylated guar gum films, *Carbohydrate Polymers* 66 (2006) 500-513.
- [120] T. V. Travinskaya, Y. V. Savelyev, Aqueous polyurethane-alginate compositions: Peculiarities of behavior and performance, *European Polymer Journal* 42 (2006) 388-394.
- [121] A. Bhattacharyya, D. Mukherjee, R. Mishra, P. P. Kundu, Development of pH sensitive polyurethane-alginate nanoparticles for safe and efficient oral insulin delivery in animal models, *RSC Advances* 6 (2016) 41835-41846.
- [122] C. Wang, Y. Zheng, K. Qiao, Y. Xie, X. Zhou, An environmentally friendly preparation and characterization of waterborne polyurethane hydrogels by polyvinyl alcohol physical cross-linking to improve water absorption, *RSC Advances* 5 (2015) 73882-73891.
- [123] A. Sirkecioglu, H. B. Mutlu, C. Citak, A. Koc, Physical and surface properties of polyurethane hydrogels in relation with their chemical structure, *Polymer Engineering and Science* 54 (2014) 1182-1191.
- [124] P. Petrini, S. Farè, A. Piva, M. C. Tanzi, Design, synthesis and properties of polyurethane hydrogels for tissue engineering, *Journal of Materials Science: Materials in Medicine* 14 (2003) 683-686.
- [125] C. Deng, Y. Cui, T. Zhao, M. Tan, H. Huang, M. Guo, Mechanically strong and stretchable polyurethane-urea supramolecular hydrogel using water as an additional in situ chain extender, *RSC Advances* 4 (2014) 24095-24102.
- [126] T. Sato, T. Uehara, H. Yoshida, New application of polyurethane as porous hydrogel carrier for microorganisms of waste water treatment, *Cellular Polymer* 23 (2004) 145-160.
- [127] N. Yang, H. Yang, Z. Shao, M. Guo, Ultrastrong and tough supramolecular hydrogels from multiurea linkage segmented copolymers with tractable processability and recyclability, *Macromolecular Rapid Communications* 38 (2017) 1-6.
- [128] Y. Cui, M. Tan, A. Zhu, M. Guo, Non-covalent interaction cooperatively induced stretchy, tough and stimuli-responsive polyurethane-urea supramolecular (PUUS) hydrogels, *Journal of Materials Chemistry B* 3 (2015) 2834-2841.
- [129] Q. Xia, L. Chen, Y. Zhu, Z. Shao, M. Guo, Stretchy and strong polyurethane-urea supramolecular (PUUS) hydrogels with various stimulus-responsive behaviours: the effect of chain-extenders, *Journal of Materials Chemistry B* 7 (2019) 1734-1740.
- [130] C. Zhu, R. Yang, X. Hua, H. Chen, J. Xu, R. Wu, L. Cen, Highly stretchable HA/SA hydrogels for tissue engineering, *Journal of Biomaterials Science, Polymer Edition* 29 (2018) 543-561.
- [131] L. Rao, H. Zhou, T. Li, C. Li, Y. Y. Duan, Polyethylene glycol-containing polyurethane hydrogel coatings for improving the biocompatibility of neural electrodes, *Acta Biomaterialia* 8 (2012) 2233-2242.
- [132] K. González, C. García-Astrain, A. Santamaria-Echart, L. Ugarte, L. Avérous, A. Eceiza, N. Gabilondo, Starch/graphene hydrogels via click chemistry with relevant electrical and antibacterial properties, *Carbohydrate Polymers* 202 (2018) 372-381.
- [133] P. C. Nicolson, Soft contact lens polymers: An evolution, *Biomaterials* 22 (2001) 3273-3283.
- [134] S. T. Oh, W. Kim, S. Kim, Y. Chung, J. Park, The preparation of polyurethane foam combined with pH-sensitive alginate/bentonite hydrogel for wound dressings, *Fibers and Polymers* 12 (2011) 159-165.

- [135] O. Guaresti, C. García-Astrain, T. Palomares, A. A. Varona, A. Eceiza, N. Gabilondo, Synthesis and characterization of a biocompatible chitosan-based hydrogel cross-linked via “click” chemistry for controlled drug release, *International Journal of Biological Macromolecules* 102 (2017) 1-9.
- [136] R. Barbucci, G. Giani, S. Fedi, S. Bottari, M. Casolaro, Biohydrogels with magnetic nanoparticles as crosslinker: Characteristics and potential use for controlled antitumor drug-delivery, *Acta Biomaterialia* 8 (2012) 4244-4252.
- [137] J. Wang, J. Wei, Hydrogel brushes grafted from stainless steel via surface-initiated atom transfer radical polymerization for marine antifouling, *Applied Surface Science* 382 (2016) 202-216.
- [138] T. T. Hong, H. Okabe, Y. Hidaka, K. Hara, Removal of metal ions from aqueous solutions using carboxymethyl cellulose/sodium styrene sulfonate gels prepared by radiation grafting, *Carbohydrate Polymers* 157 (2017) 335-343.
- [139] K. Yu, D. Wang, Q. Wang, Tough and self-healable nanocomposite hydrogels for repeatable water treatment, *Polymers* 10 (2018) 880/1-880/12.
- [140] M. L. P. Ramos, J. A. González, S. G. Albornoz, C. J. Pérez, M. E. Villanueva, S. A. Giorgieri, G. J. Copello, Chitin hydrogel reinforced with TiO₂ nanoparticles as an arsenic sorbent, *Chemical Engineering Journal* 285 (2016) 581-587.
- [141] M. S. Ebrahimi, Y. Voss, H. Schonherr, Rapid detection of escherichia coli via enzymatically triggered reactions in self-reporting chitosan hydrogels, *ACS Applied Materials & Interfaces* 7 (2015) 20190-20199.
- [142] H. A. Essawy, M. B. M. Ghazy, F. A. El-Hai, M. F. Mohamed, Superabsorbent hydrogels via graft polymerization of acrylic acid from chitosan-cellulose hybrid and their potential in controlled release of soil nutrients, *International Journal of Biological Macromolecules* 89 (2016) 144-151.
- [143] H. Jia, E. Mailand, J. Zhou, Z. Huang, G. Dietler, J. M. Kolinski, X. Wang, M. S. Sakar, Universal soft robotic microgripper, *Nano-Micro Small* 15 (2019) 1803870/1-1803870/8.
- [144] F. Awaja, M. Gilbert, G. Kelly, B. Fox, P. J. Pigram, Adhesion of polymers, *Progress in Polymer Science* 34 (2009) 948-968.
- [145] F. A. Kema, *Handbook of Adhesive Technology*, 1st Ed., MARCEL DEKK, 1994, p. 10-21.
- [146] B. Berge, *The Ecology of Building Materials*, 2nd Ed., Elsevier-Architectural press, 2009, p. 369-380.
- [147] A. S. Matharu, K. Lokesh, *Green Chemistry for Surface Coatings, Inks and Adhesives: Sustainable Applications*, 1st Ed., RSC, 2019, pp. 1-17.
- [148] Adhesives and sealants: The european market, *European Coatings Journal* 6 (2009) 12-15.
- [149] C. Creton, M. Ciccotti, Fracture and adhesion of soft materials: A review, *Reports on Progress in Physics* 79 (2016) 046601/1-046601/57.
- [150] C. Carelli, F. Déplace, L. Boissonnet, C. Creton, Effect of a gradient in viscoelastic properties on the debonding mechanisms of soft adhesives, *The Journal of Adhesion* 83 (2010) 409-505.
- [151] M. Szycher, *Szycher's handbook of polyurethanes*, 2nd Ed., CRC press Taylor and Francis Group, 2013, p. 393-416.
- [152] J. A. von Fraunhofer, Adhesion and cohesion, *International Journal of Dentistry* (2012) 1-8.
- [153] A. J. Crosby, K. R. Shull, H. Lakrout, C. Creton, Deformation and failure modes of adhesively bonded elastic layers, *Journal of Applied Physics* 88 (2000) 2956/1-2956/11.

- [154] J. J. Licari, D. W. Swason, *Adhesives Technology for Electronic Applications*. Materials, Processing, Reliability, 2nd Ed., Elsevier, 2011, p. 1-34.
- [155] W. F. Harrington, *Handbook of Adhesive Technology*, 2nd Ed., MARCEL DEKK, 2003, p. 502-517.
- [156] Y. Peykova, O. V Lebedeva, A. Diethert, M. Peter, N. Willenbacher, Adhesive properties of acrylate copolymers: Effect of the nature of the substrate and copolymer functionality, *International Journal of Adhesion & Adhesives* 34 (2012) 107-116.
- [157] M. M. Feldstein, E. E. Dormidontova, A. R. Khokhlov, Pressure sensitive adhesives based on interpolymer complexes, *Progress in Polymer Science* 42 (2015) 79-153.
- [158] F. Deplace, C. Carelli, S. Mariot, H. Retsos, A. Chateauminois, K. Ouzineb, C. Creton, Fine tuning the adhesive properties of a soft nanostructured adhesive with rheological measurements, *The Journal of Adhesion* 85 (2009) 18-54.
- [159] A. Kowalski, Z. Czech, How does the surface free energy influence the tack of acrylic pressure-sensitive adhesives (PSAs)?, *Journal of Coatings Technology and Research* 10 (2013) 879-885.
- [160] J. Piau, C. Verdier, L. Benyahia, Influence of rheology and surface properties in the adhesion of uncross-linked pressure sensitive adhesives, *Rheologica Acta* 36 (1997) 449-461.
- [161] L. Benyahia, C. Verdier, J. Piau, The mechanisms of peeling of uncross-linked pressure sensitive adhesives, *The Journal of Adhesion* 62 (1997) 45-73.
- [162] M. Micutz, L. Aricov, C. Ilie, T. Staicu, Tailoring rheological properties of uncrosslinked waterborne pressure-sensitive adhesives by means of polymer maximum volume fraction, *International Journal of Adhesion & Adhesives* 70 (2016) 10-16.
- [163] J. L. Zhang, D. M. Wu, D. Y. Yang, F. X. Qiu, Environmentally friendly polyurethane composites: Preparation, characterization and mechanical properties, *Journal of Polymers and the Environment* 18 (2010) 128-134.
- [164] Y. K. Jhon, I. W. Cheong, J. H. Kim, Chain extension study of aqueous polyurethane dispersions, *Colloids and Surfaces A: Physicochemical and Engineering Aspects* 179 (2001) 71-78.
- [165] A. Lopez, E. Degrandi-Contraires, E. Canetta, C. Creton, J. L. Keddie, M. Asua, Waterborne polyurethane-acrylic hybrid nanoparticles by miniemulsion polymerization: Applications in pressure-sensitive adhesives, *Lagmuir* 27 (2011) 3878-3888.
- [166] M. A. Pérez-Limiñana, F. Arán-Aís, A. M. Torró-Palau, A. C. Orgilés-Barceló, J. M. Martín-Martínez, Characterization of waterborne polyurethane adhesives containing different amounts of ionic groups, *International Journal of Adhesion and Adhesives* 25 (2005) 507-517.
- [167] N. Akram, R. S. Gurney, M. Zuber, M. Ishaq, J. L. Keddie, Influence of polyol molecular weight and type on the tack and peel properties of waterborne polyurethane pressure-sensitive adhesives, *Macromolecular Reaction Engineering* 7 (2013) 493-503.
- [168] S. M. Cakic, I. S. Ristic, M. Marinovic-Cincovic, M. Spirkova, The effects of the structure and molecular weight of the macrodiol on the properties polyurethane anionic adhesives, *International Journal of Adhesion and Adhesives* 41 (2013) 132-139.

Chapter

2

"Failure is simply the opportunity to begin again, this time more intelligently."

(Henry Ford)

Materials and characterization techniques

2. Materials and characterization techniques

2.1. Chapter overview	39
2.2. Materials	39
2.3. Characterization techniques	41
2.3.1. Physicochemical characterization	41
2.3.2. Thermal characterization	43
2.3.3. Mechanical characterization	44
2.3.4. Morphological characterization	45
2.3.5. Electrical conductivity properties	46
2.3.6. Hydrophilicity	46
2.3.7. Swelling degree	46
2.3.8. Cell proliferation	47
2.3.9. Adhesive properties	47
2.4. References	50

2.1. Chapter overview

This Chapter introduces materials as well as characterization techniques employed through the work presented in this investigation work. Materials and characterization techniques are listed, as approximately as possible, in their order of appearance in the following Chapters.

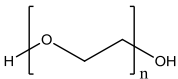
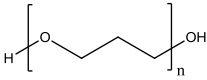
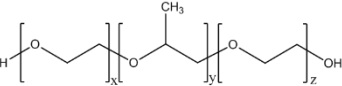
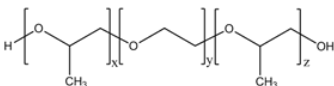
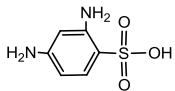
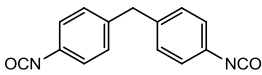
2.2. Materials

Poly(ethylene-oxide) (PEO), purchased from Sigma-Aldrich ($^1\text{H-NMR}$ spectra shown in Figure A.1 in Annexes), and with a molecular weight of 1000 g mol^{-1} , was used as macrodiol for the organic solvent-free synthesis of waterborne poly(urethane-urea)s. Corn sugar derived poly(trimethylene ether glycol) (P3MG) ($^1\text{H-NMR}$ spectra shown in Figure A.2 in Annexes), with 100% renewable carbon content according to ASTM D6866-04 and a molecular weight of 1000 g mol^{-1} , was also utilized as macrodiol. In the case of P3MG, it was mixed with PEO, in different ratios, for the synthesis of organic solvent-free waterborne poly(urethane-urea)s since it was not possible to synthesize waterborne poly(urethane-urea)s just with P3MG following the developed synthesis procedure.

Triblock copolymers based waterborne poly(urethane-urea)s were also synthesized. In this case, poly(ethylene oxide-b-propylene oxide-b-ethylene oxide) (PEO-b-PPO-b-PEO), with molecular weights of 1900 and 2900 g mol^{-1} , and poly(propylene oxide-b-ethylene oxide-b-propylene oxide) (PPO-b-PEO-b-PPO), with molecular weights of 2000 and 2700 g mol^{-1} , triblock copolymers were employed as macrodiols. Hydroxyl index of each macrodiol were determined by titration according to ASTM D4274-99 and are displayed in Annexes (Table A.1).

For the hard segment of synthesized waterborne poly(urethane-urea)s, 4,4'-diphenylmethane diisocyanate (MDI), provided by Covestro, and neutralized 2,4-diamino-benzenesulfonic acid (DBSA), supplied by Sigma Aldrich, were used. Neutralization of ionic groups of DBSA was carried out with sodium hydroxide (NaOH), purchased from POCH S.A, obtaining sodium 2,4-diamino-benzene sulfonate (SDBS).

Table 2.1. Raw materials employed for the synthesis of waterborne poly(urethane-urea). Their chemical structure, molecular weight and PEO content.

Raw materials	Chemical structure	Molecular weight (g mol ⁻¹)	PEO content (wt%)
Poly(ethylene oxide) (PEO)		1023 ^a	100
Poly(trimethylene ether glycol) (P3MG)		985 ^a	—
Poly(ethylene oxide-b-propylene oxide-b-ethylene oxide) (BCPEPE)		1910 ^a	50 ^b
Poly(propylene oxide-b-ethylene oxide-b-propylene oxide) (BCPPEP)		2918 ^a	40 ^b
2,4-Diaminobenzenesulfonic acid (DBSA)		2019 ^a	50 ^b
4,4'-Diphenylmethane diisocyanate (MDI)		2705 ^a	40 ^b
		188	—
		250	—

a) Molecular weight calculated from the hydroxyl index value determined by ASTM D4274-99.

b) PEO content as indicated by the provider.

For the preparation of nanocomposites based on synthesized waterborne poly(urethane-urea)s, aqueous dispersion of TiO₂ nanoparticles (33-37 wt%), mixture of rutile and anatase with particle size <150 nm, supplied by Sigma-Aldrich, was used.

Sodium alginate (SA) (Figure 2.1) of medium viscosity obtained from brown algae, supplied by Sigma-Aldrich, was utilized together with calcium chloride dehydrate (CaCl₂), also provided by Sigma-Aldrich, as reactives to achieve a cross-linked network after mixture with synthesized waterborne poly(urethane-urea)s leading to hydrogels.

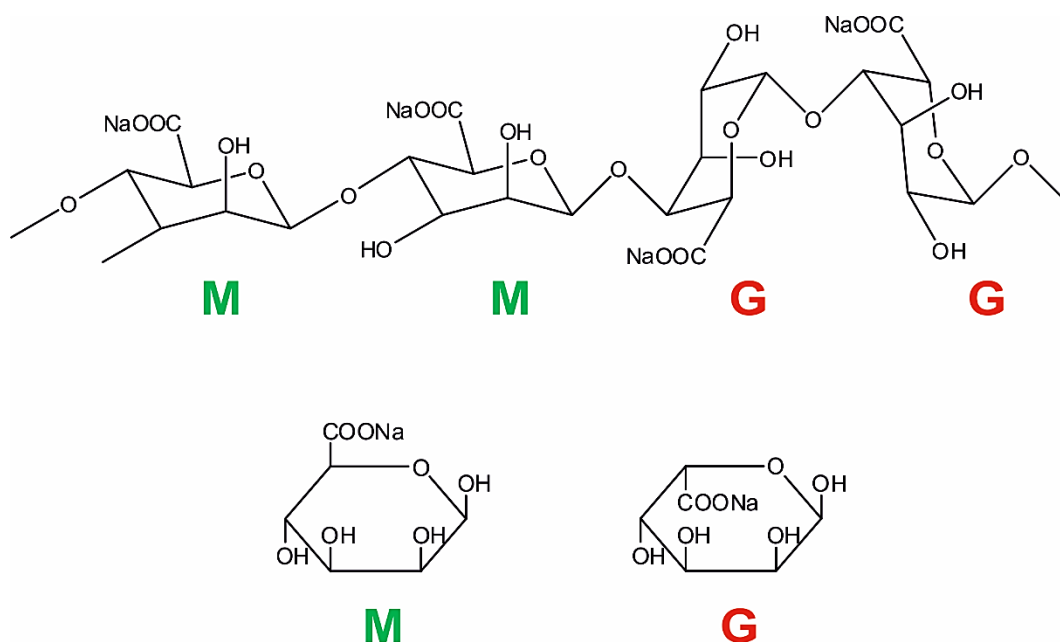


Figure 2.1. Structures of sodium alginate and sodium β-D-mannuronate (M) and sodium α-L-gulonate (G) units.

2.3. Characterization techniques

2.3.1. Physicochemical characterization

2.3.1.1. Experimental solid content

Experimental solid content of synthesized waterborne poly(urethane-urea) dispersions was determined by drying a small volume of each dispersion in an oven at 105 °C for 3 h. Measurements were carried out by triplicate and experimental solid content was calculated using Equation 2.1 as the ratio between dried sample and wet sample.

$$\% \text{ solid content} = \frac{\text{dried sample weight}}{\text{wet sample weight}} \quad (2.1)$$

2.3.1.2. Fourier transformed infrared spectroscopy

Characteristic functional groups were identified by Fourier transformed infrared (FTIR) spectroscopy using a Nicolet Nexus 670 spectrometer which was equipped with a MKII Golden Gate accessory (Specac) with diamond crystal at a nominal

incidence angle of 45°. FTIR spectra were obtained averaging 32 scans with a resolution of 8 cm⁻¹ in the range from 650 to 4000 cm⁻¹ at room temperature.

2.3.1.3. Light scattering

Dynamic light scattering (DLS) is a technique based on scattering of photons that takes place when a light beam passes through a liquid sample with dispersed particles. These colloidal particles are experiencing a random motion as consequence of multiple collisions with the thermally driven molecules of the liquid, which is known as Brownian motion. DLS was employed in order to determine particle size of synthesized waterborne poly(urethane-urea) dispersions as well as their distribution using a BI-200SM goniometer from Brookhaven. Intensity of dispersed light was measured at 90° employing a luminous source of He-Ne laser (Mini L-30, wavelength $\lambda=637$ nm, 400 mW) and a detector (BI-APD) placed on a rotary arm. Measurements were carried out at 25 °C by triplicate. Samples preparation consisted of mixing a small amount of waterborne poly(urethane-urea) dispersion with filtered distilled water fulfilling adequate concentration for a proper DLS measurement.

2.3.1.4. Size exclusion chromatography

Weight average molecular weight (\bar{M}_w) and polydispersity index (IP), as the ratio between \bar{M}_w and number average molecular weight (\bar{M}_n), of synthesized waterborne poly(urethane-urea) films were calculated by size exclusion chromatography (SEC) using a Jasco LC Net II/ADC chromatograph equipped with a RI-2031 Plus refractive index detector. Dimethylformamide (DMF) at a flow rate of 0.7 mL min⁻¹ was selected as mobile phase, whereas separation took place at 40 °C within two PolarGel-M columns (300 mm x 7.5 mm). Waterborne poly(urethane-urea) films were dissolved in DMF at 0.5 wt% for sample preparation. Calculated weight average molecular weight and polydispersity index were referred to monodispersed polystyrene (PS) standards.

2.3.1.5. Ultraviolet-visible spectroscopy

Ultraviolet-visible (UV-vis) spectroscopy transmission spectra were carried out scanning from 200 to 800 nm utilizing a Shimadzu 3600 UV-vis spectrophotometer. Thickness of synthesized waterborne poly(urethane-urea) films was around 0.1 mm. This technique was utilized in order to analyze the transparency of prepared waterborne poly(urethane-urea) films.

2.3.1.6. Rheology

Viscoelastic behavior was studied using a Haake Viscotester IQ (Thermo Fisher Scientific) equipped with parallel plate geometry employing discs with 35 mm of diameter. Preliminary strain sweep tests were carried out to determine the strain dependence of storage (G') and loss (G'') moduli selecting the deformation imposed ($\gamma=1$ for waterborne poly(urethane-urea) dispersions and $\gamma=0.05$ for hydrogels) in the Linear Viscoelastic Range (LVR). Once deformation was selected isothermal frequency sweeps from 10^{-1} to 10 Hz were carried out measuring G' , G'' and complex viscosity (η^*). $\tan \delta$ was calculated from relation between G' and G'' (Equation 2.2).

$$\tan \delta = \frac{G''}{G'} \quad (2.2)$$

2.3.2. Thermal characterization

2.3.2.1. Differential scanning calorimetry

Differential scanning calorimetry (DSC) was used to analyze thermal properties of investigated materials. A DSC 3+ Mettler Toledo equipment provided with an autosampler and an electric intracooler as refrigerator unit was employed. An aluminum pan containing the sample (5-8 mg) was heated from -85 to 200 °C at scanning rate of 5 °C min⁻¹ in nitrogen atmosphere. DSC thermograms reflect variations in the heat required by the sample when it undergoes a thermal transition with respect to a reference. Therefore, glass transition temperature (T_g) was determined as the mid-point of slope change inflection point of the heat capacity

change, while melting temperature (T_m) and enthalpy (ΔH_m) were taken as the maximum and area under the endotherm peak, respectively.

2.3.2.2. Thermogravimetric analysis

Thermal stability of investigated material films was studied employing a TGA/SDTA 851 Mettler Toledo for thermogravimetric analysis (TGA). Dynamic runs from 25 to 800 °C at a heating rate of 10 °C min⁻¹ were carried out for samples with weights between 5 to 10 mg, and in nitrogen atmosphere. Degradation temperature was estimated as the temperature of the minimum in the dTGA curve.

2.3.3. Mechanical characterization

2.3.3.1. Tensile testing

Mechanical properties of investigated material films were determined using an Instron 5967 testing machine operated with a 500 N load cell and pneumatic grips to hold samples at room temperature and at a crosshead speed of 10 mm min⁻¹. At least, 6 specimens (10 mm x 3 mm x 0.7 mm, for synthesized waterborne poly(urethane-urea) films, and 10 mm x 4.5 mm x 0.3 mm for the nanocomposite films) of each composition were tested. Films were kept at 60 °C in vacuum just before cutting the specimens in order to avoid moisture absorption. Young's modulus (E), tensile strength (σ_{max}), stress at break (σ_b) and deformation at break (ϵ_b) were determined from obtained stress-strain curves.

2.3.3.2. Compression testing

Compression test was performed for prepared hydrogels based on synthesized waterborne poly(urethane-urea)s with an Instron 5967 testing machine operated with a 500 N load cell at a crosshead speed of 2 mm min⁻¹ at room temperature. Hydrogel cylindrical blocks (height: 10-13 mm, diameter: 12-14 mm) were tested until a deformation of 90%. Compressive modulus and compressive stress, at strains of 60% and 70%, were determined.

2.3.4. Morphological characterization

2.3.3.1. Atomic force microscopy

Atomic force microscopy (AFM) was used to characterize the morphology of investigated materials by attractive-repulsion interactions between the tip and the investigated sample. AFM images were captured at room temperature, in tapping mode, by a NanoScope V scanning probe microscope (Multimode 8, Bruker) with an integrated force generated by cantilever/silicon probes, applying a resonance frequency of about 320 kHz. Tip radius was of 5-10 nm and the length of cantilever was 125 μm . Morphology of different areas of each investigated sample were scanned in order to ensure that the morphology was representative. AFM height and phase images were collected simultaneously, obtaining similar AFM images and, consequently, only phase images will be presented in this investigation work.

2.3.4.2. Optical microscopy

Optical microscopy (OM) was employed in order to ensure that morphology of prepared nanocomposites was homogeneous at microscopic level. Images of films with thickness of ~ 0.3 mm were obtained with the x10 objective of a Nikon Eclipse E600. Moreover, OM was also used to study the self-healing process of nanocomposites prepared from triblock copolymers based waterborne poly(urethane-urea)s, as it is explained with more detail in the Chapter 6.

2.3.4.3. Scanning electron microscopy

Morphology of prepared hydrogels was observed by a Hitachi S-4800 scanning electron microscope (SEM). Analyzed samples were previously freeze-fractured with liquid nitrogen, in order to expose the cross section, and metallically covered. Samples were scanned at an accelerated voltage of 10 kV at a working distance of 8 mm.

2.3.5. Electrostatic force microscopy

Electrostatic force microscopy (EFM) was used to evaluate whether TiO₂ nanoparticles conserved their electrical properties at the nanometric level when embedded in synthesized waterborne poly(urethane-urea) matrices. This is a qualitative measurement, which was performed with an Icon scanning probe operating in lift mode (lift height ~400 nm) equipped with a Pt/Ir coated tip. The resonance frequency was about 75 kHz. A voltage was applied to the cantilever tip in order to detect the secondary imaging mode derived from tapping mode, which measures the electric field gradient.

2.3.6. Hydrophilicity

Static water contact angle (WCA) was the technique utilized to investigate the hydrophilic character of surfaces of synthesized waterborne poly(urethane-urea) and designed nanocomposite films. Tests were carried out by a SEO Phoenix300 equipment, at room temperature, performing at least 10 measurements for each investigated sample. Sessile drop method was followed, which consists on depositing a deionized water drop on the surface of the film by a syringe tip.

2.3.7. Swelling degree

In order to study the swelling ability of prepared hydrogels, freeze-dried hydrogels (W_0) were immersed in a 0.1 M citric acid solution (pH=2) for 72 h. Samples were removed from water and wiped with filter paper for free water removal and then weighed. Therefore, wet weight (W_w) of different hydrogels at different times ($\frac{1}{4}$, $\frac{1}{2}$, 1, 2, 6, 24, 48 and 72 h) was measured. Measurements were done by triplicate at room temperature. Wet hydrogels were freeze-dried after 72 h of immersion in order to determine the mass loss and correct the swelling degree (%SD), which was determined from Equation 2.3.

$$\%SD = \frac{W_w - W_0}{W_0} \times 100 \quad (2.3)$$

2.3.8. Cell proliferation

The cell proliferation on prepared hydrogels was studied following ISO 10993 standard. Human Fibroblasts Cell (GM07982) were cultured at 37 °C, under humidified 5% CO₂ atmosphere, in DMEM medium (Dulbecco's modified essential medium) supplemented with 10% FBM and (fetal bovine serum), 2 mM L-glutamine, 100 µg mL⁻¹ penicillin and 100 µg mL⁻¹ streptomycin. Cell were used for cytotoxicity experiment at density of 1x10⁴cells mL⁻¹ in 96-well cell culture plates. The wells were previously filled, in triplicate, with investigated hydrogels that were extensively washed with PBS (phosphate-buffered saline) buffer. The control group were cell cultured without the presence of investigated hydrogels. All the cell experimental groups were cultivated for 48 h after cell seeding.

Cell proliferation was determined by 3-(4,5-dimethylthiazol-2-yl)-2,5-diphenyltetrazolium bromide (MTT) colorimetric method. After incubation period, the culture medium was removed from each well followed by the washing with PBS buffer. Then the MTT solution (0.005 mg mL⁻¹) was added in each well and the plate was incubated at 37 °C for 4 h. The MTT solution was removed and the formazan crystals were solubilized in dimethyl sulfoxide (DMSO) for 10 min. A volume of 100 µl from each well was transferred to a 96-well plate and the absorbance was read on a plate reader at wavelength 570 nm.

Statistical analysis was performed with GraphPad Prism software. The ANOVA and Student's t-test were used. Values were considered significantly different if p<0.05.

2.3.9. Adhesive properties

2.3.9.1. Probe-tack adhesion analysis

Probe-tack adhesion analysis were carried out employing a TA-XT Plus Texture Analyser (Stable Micro Systems) with a load cell of 1 kg, using 2.54 cm diameter spherical probes of high surface energy¹ (steel, ~500 mJ m⁻²) and of low surface energy² (polypropylene (PP), ~27 mJ m⁻²) materials at room temperature.

Analyzed dispersions were applied on glass surface utilizing a 200 μm cube applicator and left drying for 24 h at room temperature in order to form a homogeneous film. For probe-tack test, probes were brought into contact with the film for 1 s under a load of 4.9 N. To evaluate the detachment process, probe withdrawal speed was set at 0.1 mm s^{-1} . At least five measurements were done for each investigated film, with thicknesses, determined as the average of 10 measurements, varying from 70 to 100 μm . The probe was cleaned with deionized water and acetone after each test.

During each test, probe displacement and nominal force were measured. Contact area was determined after each test by OM and with the help of a caliper. Stress (σ), calculated as division of force (F) and contact area (A),

$$\sigma = \frac{F}{A} \quad (2.4)$$

and strain (ε), calculated by dividing the travel distance (d) of the probe by the initial thickness of the film (h_{film}), were determined for each test.

$$\varepsilon = \frac{d}{h_{\text{film}}} \quad (2.5)$$

Debonding energy (W_{deb}) was calculated from the area under the stress-strain curve as

$$W_{\text{deb}} = h_{\text{film}} \int_0^{\varepsilon_{\text{film}}} \sigma(\varepsilon) d\varepsilon \quad (2.6)$$

2.3.9.2. 180° peel-off test

180° peel-off test was carried out using a TA-XT Plus Texture Analyser (Stable Micro Systems) in tensile mode with a load cell of 5 kg at a constant speed of 2 mm s^{-1} and at room temperature. For the test, long strips of 25 mm wide were cut from prepared sheets of polyethylene terephthalate (PET) and PP with corona treatment² onto which dispersions were applied, which is explained with more detail in the Chapter 8. Glass and aluminum surfaces, onto which the tapes were adhered, were hold by an static

grip, whereas the strips were hold with a pneumatic grip. Peel-off force was considered as the plateau-like zone of the obtained curves.

2.4. References

- [1] C. Carelli, F. Déplace, L. Boissonnet, C. Creton, Effect of a gradient in viscoelastic properties on the debonding mechanisms of soft adhesives, *The Journal of Adhesion* 83 (2010). 409-505.
- [2] R. Dorai, M. J. Kushner, A model for plasma modification of polypropylene using atmospheric pressure discharges, *Journal of Physics D: Applied Physics* 36 (2003) 666-685.

Chapter

3

"Don't judge each day by the harvest you reap but by the seeds that you plant."

(Robert Louis Stevenson)

Waterborne poly(urethane-urea)s based on a bio-based macrodiol

3. Waterborne poly(urethane-urea)s based on a bio-based macrodiol

3.1. Chapter overview	55
3.2. Introduction	55
3.3. Synthesis of waterborne poly(urethane-urea)s based on poly(ethylene oxide) and poly(trimethylene ether glycol) macrodiols	56
3.3.1. Preparation of poly(urethane-urea) films	58
3.4. Characterization of waterborne poly(urethane-urea)s	59
3.4.1. Characterization of dispersions	59
3.4.2. Characterization of films	62
3.5. Conclusions	69
3.6. References	71

3.1. Chapter overview

This Chapter focuses on the synthesis of different waterborne poly(urethane-urea)s based on mixtures of PEO and corn-based fully renewable carbon content P3MG. Additionally, and as a reference, a waterborne poly(urethane-urea) based on neat PEO homopolymer as macrodiol is also presented. Synthesis of waterborne poly(urethane-urea)s were carried out by a novel procedure, which avoids emissions of VOCs to the atmosphere since organic solvent are not employed. The ratio of PEO/P3MG in the macrodiol mixture was varied for each synthesized waterborne poly(urethane-urea) in order to study its influence on the final properties.

3.2. Introduction

In recent years, mainly in response to the increasing regulations on emissions of VOCs to the atmosphere^{1,2}, research on waterborne polyurethanes and poly(urethane-urea)s has grown considerably¹⁻⁷. As explained in the Chapter 1, acetone process is the most common procedure followed to synthesize waterborne polyurethanes and poly(urethane-urea)s. Nevertheless, it requires using small amounts of organic solvent. It is for this reason that new processes have been developed in order to avoid utilizing organic solvents^{8,9}. These processes take advantage of the faster reactivity between amine and isocyanate groups in comparison to isocyanate group with water or hydroxyl group. The reactivity of aromatic amines with isocyanate groups is 2-3 times faster, whereas aliphatic amines react 200-1000 times faster¹⁰ (Figure 3.1).

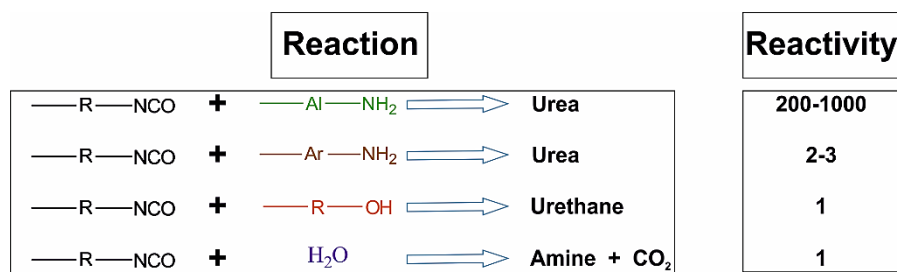


Figure 3.1. Reactions and reactivity of aliphatic amines (-Al-NH₂) and aromatic amines (-Ar-NH₂) compared to hydroxyl groups and water with diisocyanate group.

This faster reactivity allows addition of amine chain extender together with water in the chain extension step, controlling the viscosity and assuring an effective chain extension.

Furthermore, in the search of more environmentally friendly polymers, bio-based precursors play a key role^{2,3,11,12}. In the case of polyurethanes and poly(urethane-urea)s, these are the macrodiol, the diisocyanate and the chain extender^{2,11}. Tannic acid¹, castor oil^{11,13,14}, soybean oil¹², fully renewable sourced polyether^{4,11}, rosin³, natural rubber based macrodiol², fatty acid based diisocyanate¹¹, L-lysine derived diisocyanate¹⁵ and amino acid based chain extender¹⁵, among others, have been used as a bio-based precursors.

3.3. Synthesis of waterborne poly(urethane-urea)s based on mixtures of poly(ethylene oxide) and poly(trimethylene ether glycol) macrodiols

The waterborne poly(urethane-urea)s were synthesized using different molar ratios of macrodiols (PEO/P3MG). The synthesis of a waterborne poly(urethane-urea) based just on P3MG homopolymer was discarded since P3MG was not soluble in water and for an optimal chain extension PEO, as solubilizing agent¹⁶, was required. For the synthesis, the relation of NCO to OH groups (diisocyanate to macrodiols) was equal to 2 and 1. The first step of the synthesis procedure was the synthesis of the prepolymer by reaction of the diisocyanate and the macrodiol, or the mixture of macrodiols. This reaction was carried out in a 250 mL five-necked flask placed in an oil bath and equipped with a mechanical stirrer, a thermometer and a nitrogen inlet by mixing the precursors at 80 °C for 2 h stirring at 300 rpm (Figure 3.2). The conditions were selected after evaluation of the reaction kinetic by determining the NCO content by the dibutylamine back titration method (DBBTM) according to ASTM D2572-97 (see Figure A.3 in Annexes).

Once the prepolymer was synthesized, it was left slowly cooling down to 30 °C keeping the stirring. The next step was the addition of SDBS dissolved in water to the prepolymer for chain extension. This reaction was carried out for 30 min stirring at

400 rpm. The viscosity was controlled by addition of distilled water. Finally, 100 mL of distilled water were added dropwise for 40 min with a vigorous stirring at 700 rpm. Theoretical solid contents of prepared dispersions were around 25%. Samples designation, molar composition and MDI-SDBS segment, acid group and renewable carbon contents are shown in Table 3.1.

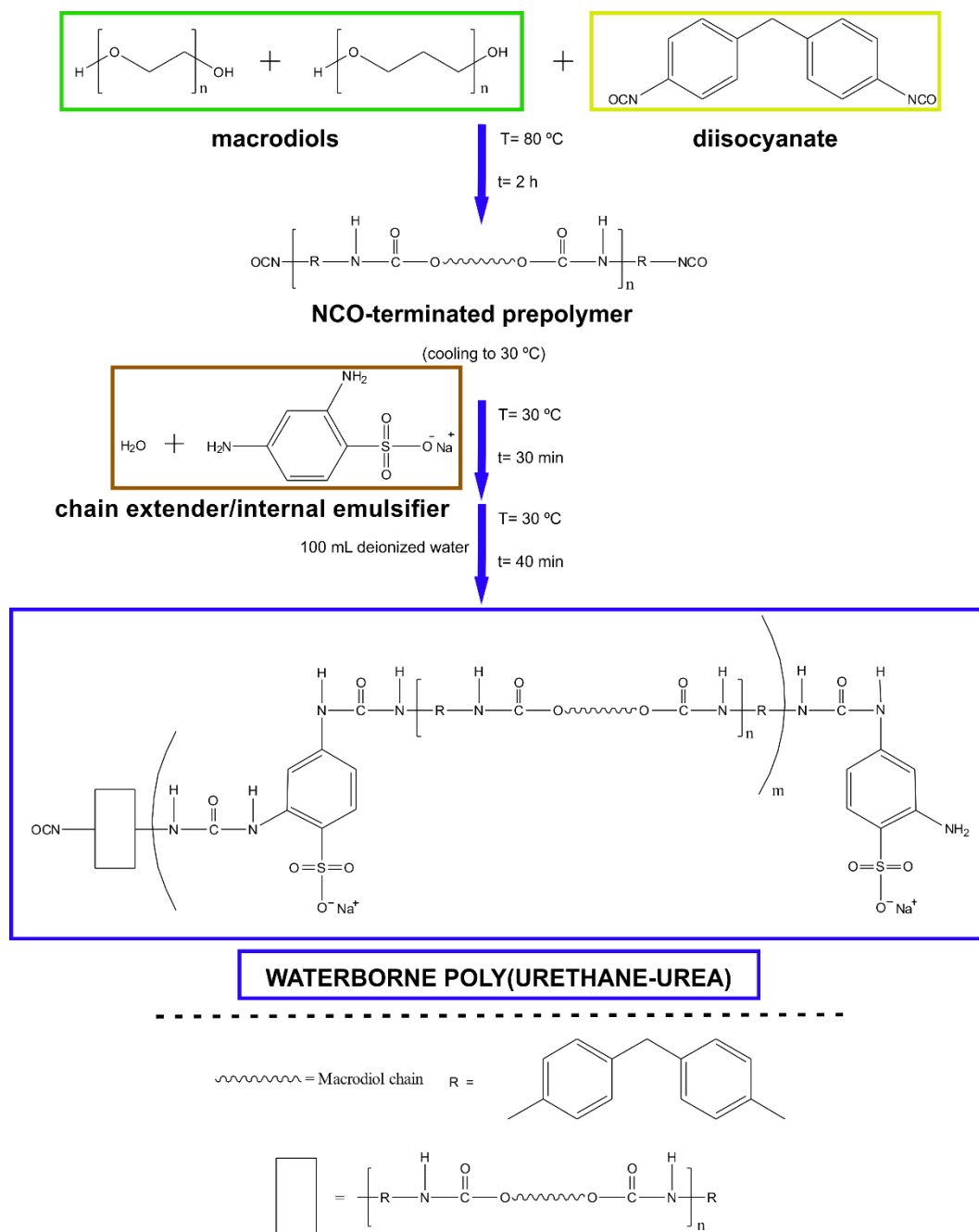


Figure 3.2. Schematic illustration of synthesized PEO and P3MG based waterborne poly(urethane-urea)s.

Table 3.1. Designation of samples, molar composition, MDI-SBBS segment content, acid group content and renewable macrodiol content of synthesized waterborne poly(urethane-urea)s.

Sample	Molar composition (mol)				MDI-SBBS ^a (wt%)	SO ₃ H _{tot} ^a (wt%)	Renewable ^b (wt%)
	MDI	P3MG	PEO	SDBS			
PU0	2	0.00	1.00	1	42.3	4.6	0.0
PU60	2	0.60	0.40	1	42.3	4.6	35.5
PU70	2	0.70	0.30	1	42.3	4.6	41.4
PU80	2	0.80	0.20	1	42.3	4.6	47.3
PU85	2	0.85	0.15	1	42.3	4.6	50.3
PU90	2	0.90	0.10	1	42.3	4.6	53.2

a) Theoretical stoichiometry values.

b) P3MG wt% content.

Prepared dispersions based on PEO/P3MG macrodiol mixture were filtered using a Whatman 1001-125 filter paper with a pore size of 11 μm in order to remove non-dispersed solid precipitate. Homogeneous dispersions with solid contents lower than the theoretical were obtained. The visual appearance of synthesized waterborne poly(urethane-urea) dispersion is shown in Figure 3.3.

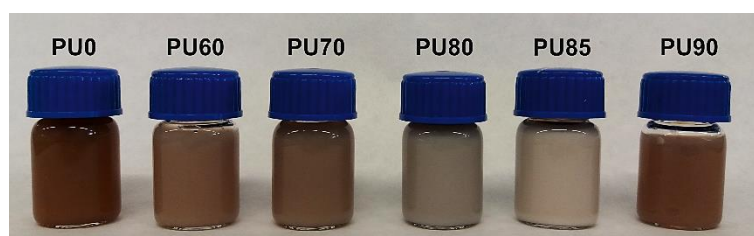


Figure 3.3. Visual appearance of synthesized PEO and P3MG based waterborne poly(urethane-urea) dispersions.

3.3.1. Preparation of waterborne poly(urethane-urea) films

Films were prepared by drying a calculated volume of each dispersion, regarding their solid content, in Teflon covered glass keeping them in vacuum for 5 days and then for overnight at open air at room conditions. Films were kept at 60 °C in vacuum in order to protect them from moisture absorbance before characterization. Film of PU90 dispersion was not optimal due to its low solid content, thus it was not characterized with all the employed characterization techniques. Visual appearances of waterborne poly(urethane-urea) films are shown in Figure 3.4.



Figure 3.4. Visual aspect of synthesized PE0 and P3MG based waterborne poly(urethane-urea) films.

3.4. Characterization of PE0 and P3MG based waterborne poly(urethane-urea)s

3.4.1. Characterization of PE0 and P3MG based waterborne poly(urethane-urea) dispersions

The solid content of synthesized waterborne poly(urethane-urea) dispersions (Table 3.2) reflected the performance of each synthesis since the reaction of diisocyanate and amine groups was not equally optimal for all carried out synthesis due to the competitive reaction of diisocyanate groups with water¹⁰.

Table 3.2. Average particle size, experimental solid content and solid content yield of synthesized PE0 and P3MG based waterborne poly(urethane-urea) dispersions.

Sample	Average particle size (nm)	Solid content (%)	Solid content yield (%)
PU0	2267 ± 60	22.8 ± 0.7	93.3 ± 2.7
PU60	402 ± 5	14.3 ± 0.3	58.3 ± 1.3
PU70	266 ± 5	17.1 ± 0.2	69.3 ± 0.9
PU80	102 ± 1	24.5 ± 0.1	98.7 ± 0.2
PU85	208 ± 1	19.1 ± 0.1	77.9 ± 0.3
PU90	187 ± 2	8.8 ± 0.1	36.0 ± 0.4

The solid contents of prepared dispersions ranged from 9 to 25%. PU0 and PU80 were the ones with solid contents closer to the theoretical one, concluding that PE0 homopolymer and 20/80 ratio of PE0/P3MG macrodiol mixture were the most effective for an optimal chain extension. The lower solid content of the rest of dispersions was the consequence of the formation of non-dispersible particles as result of the mentioned competitive reaction between diisocyanate groups of the prepolymer with water. In contraposition to PE0, which is hydrophilic and water soluble, P3MG is not a hydrophilic macrodiol. Therefore, as it was previously

mentioned, it was not possible to synthesize a waterborne poly(urethane-urea) based on neat P3MG homopolymer. In the cases of PU60 and PU70, two different kinds of prepolymer chains can be formed. On the one hand, PEO rich prepolymer chains, and on the other hand, P3MG rich prepolymer chains. Consequently, PEO rich prepolymer chains can react faster with the diamine chain extender, since they showed higher water solubility. Therefore, P3MG rich prepolymer chains, with lower water solubility, can react in a small extent with the chain extender, hence reacting predominantly with water molecules and leading to the formation of non-dispersible particles (Figure 3.5). As the P3MG content increased to 20/80, the prepolymer chains can be formed by an optimally balanced content of macrodiols leading to higher reaction yield. A further increased resulted in imbalance again diminishing the reaction yield, especially for PU90.

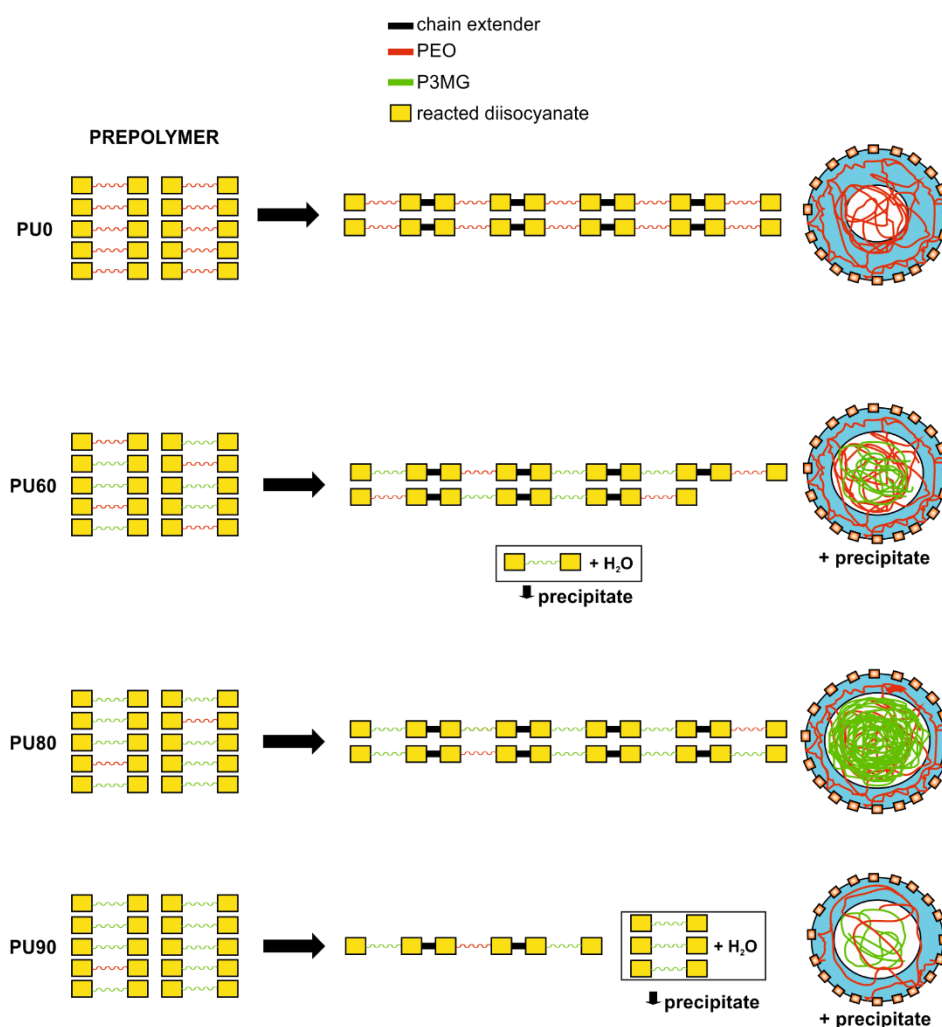


Figure 3.5. Proposed scheme for the particle arrangement in synthesized waterborne poly(urethane-urea)s regarding their chain extension yield.

Waterborne poly(urethane-urea)s in water are arranged into nano-sized particles adopting a core-shell structure in which hydrophilic segments locate on the surface forming the shell, while hydrophobic segments form the core^{16,17}. In the case of synthesized waterborne poly(urethane-urea) dispersions, the shell was formed by sulfonate groups of neutralized DBSA, PEO chains as well as urethane and urea groups, whereas the core consisted of P3MG chains and a few PEO chain segments linked and close to P3MG segments (Figure 3.6).

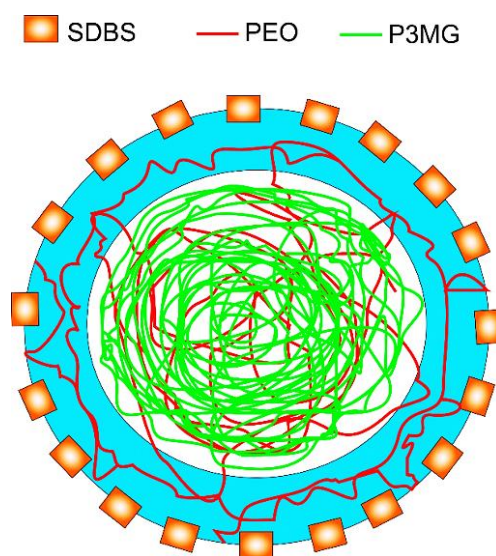


Figure 3.6. Proposed arrangement for core-shell particles of synthesized PEO and P3MG based waterborne poly(urethane-urea) dispersions.

The particle size is a crucial parameter for dispersion stability, as the stability decreases when the particle size increases resulting in the precipitation of the particles with the highest particle size^{9,18,19}. Synthesized waterborne poly(urethane-urea) dispersions exhibited lower particle sizes for PEO/P3MG macrodiol mixture based dispersions than for PU0 (Table 3.2). The largest particle size of PU0 can be a consequence of the interactions of hydrophilic PEO with water molecules forming hydrogen bonds^{8,20}. Due to its hydrophobic character, P3MG does not interact with water molecules, therefore increase of its content resulted in lower particle size. The increase that occurred from PU80 to PU85 can be result of the previously mentioned imbalance between PEO and P3MG contents in prepolymer chains as PEO played the role of the solubilizing agent¹⁶.

3.4.2. Characterization of PEO and P3MG based waterborne poly(urethane-urea) films

Structural characterization measured by FTIR (Figure 3.7) allowed discarding the presence of N=C=O groups in synthesized waterborne poly(urethane-urea) films due to the absence of a band at 2270 cm^{-1} , associated to the stretching vibration band of N=C=O group¹⁹. Broad bands between 3500 and 3200 cm^{-1} corresponded to the stretching vibrations of N–H of urea and urethane groups. Bands at lower wavenumber were associated to hydrogen bonded N–H groups, while bands at higher wavenumber corresponded to non-hydrogen bonded N–H groups²¹. As observed in more detail in Figure 3.7a, FTIR spectra of PU60 and PU85 clearly showed non-hydrogen bonded N–H bands, whereas FTIR spectra of PU0, PU70 and PU80 exhibited mainly bands at lower wavenumber associated to hydrogen bonded N–H groups. The information obtained from analysis of N–H group bands was confirmed when looking at Figure 3.7b where amide I region, 1750 - 1650 cm^{-1} , is displayed. In this region the hydrogen bonded stretching vibrations of C=O groups appeared around and below 1700 cm^{-1} and non-hydrogen bonded free C=O groups appeared at higher wavenumber^{21,22}. In the case of PU70 and PU80, the band associated to hydrogen bonded C=O groups was more intense than the one associated to non-hydrogen bonded C=O, what agreed with what can be observed in the region of stretching vibration of N–H groups. This suggested that hydrogen bonds were formed between MDI-SDBS segment (hard segment)²³. Nonetheless, in the case of PU0, the band associated to free C=O groups was more intense than the one associated to hydrogen bonded C=O groups. This seemed to contradict what can be observed in the region of 3500 - 3200 cm^{-1} . Nevertheless, what this would imply is that, in PU0, N–H preferentially formed hydrogen bonds with the ether oxygen of PEO rather than with C=O of urethane and urea groups^{21,24}. This would result in mixture of MDI-SDBS segment and macrodiol formed segment (soft segment)²⁵. The band at 1070 cm^{-1} corresponded to the hydrogen bonded C–O–C stretching vibration of PEO²⁴, while the bands at higher wavenumber were associated to free ether groups of both macrodiols²⁴. The band at 1018 cm^{-1} was linked to the vibration of the SO_3^- groups within the chain extender/internal emulsifier structure²⁶.

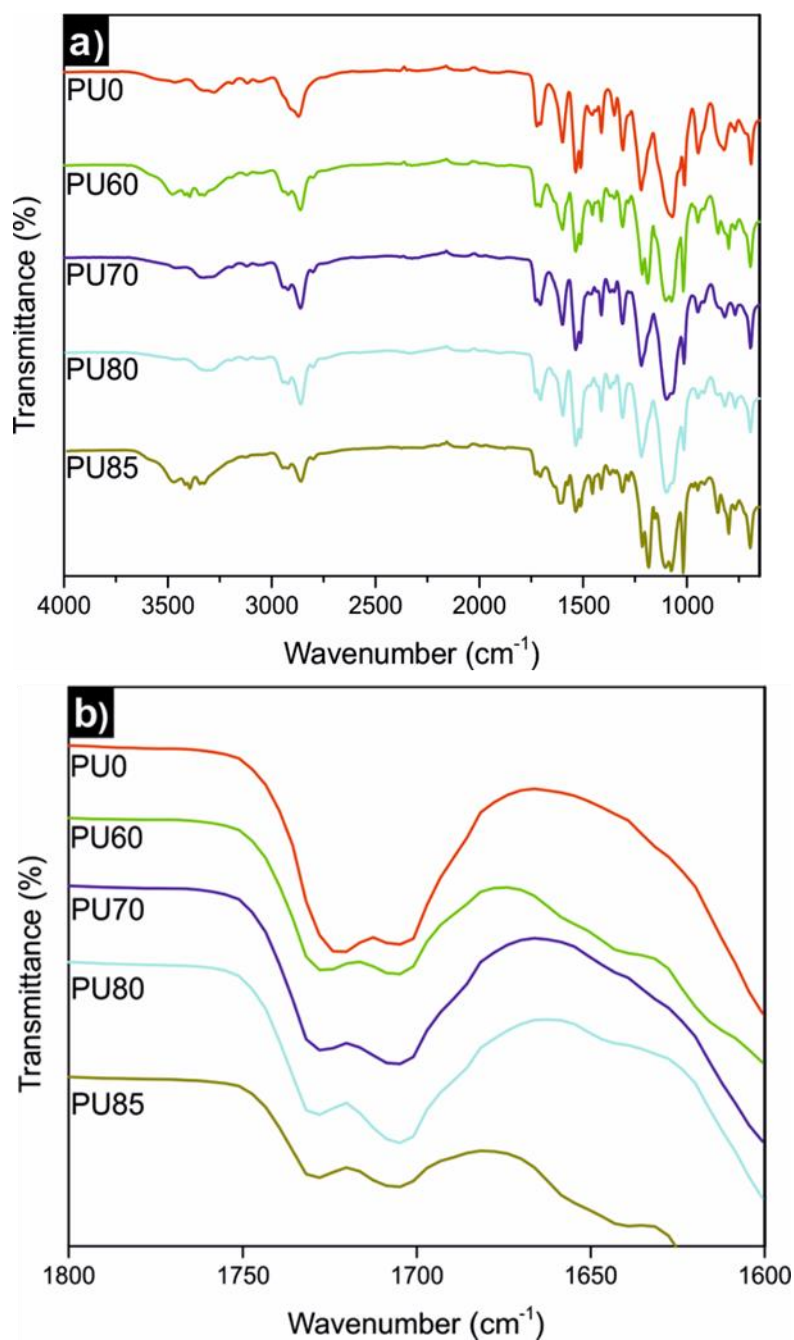


Figure 3.7. FTIR spectra of synthesized (a) PEO and P3MG based waterborne poly(urethane-urea) films and (b) amplification of their carbonyl stretching region.

The \bar{M}_w of investigated waterborne poly(urethane-urea) films were calculated from SEC curves (see Figure A.4 in Annexes) obtaining the values that are displayed in Table 3.3. Synthesized waterborne poly(urethane-urea)s based on macrodiol mixtures of PEO/P3MG presented higher \bar{M}_w than PU0. The \bar{M}_w increased with the increase of the P3MG content until PU80, which was the sample with the highest \bar{M}_w of all synthesized waterborne poly(urethane-urea) films. IP followed the same trend. These results were in concordance with the ones obtained for the solid content yield,

what implied that, for waterborne poly(urethane-urea)s based on PEO/P3MG macrodiol mixtures, the chain extension step led to longer chains. This resulted in the increase of the solid content and, as a consequence, led to dispersions with solid contents close to the theoretical value.

Table 3.3. Average weight molecular weight (\bar{M}_w) and polydispersity index (IP) of synthesized PEO and P3MG based waterborne poly(urethane-urea) films.

Sample	\bar{M}_w	IP (\bar{M}_w/\bar{M}_n)
PU0	31,750	1.9
PU60	41,500	2.2
PU70	42,150	2.2
PU80	87,360	4.1
PU85	67,410	3.3

Thermal behavior was studied by DSC and thermograms are represented in Figure 3.8 (thermal properties are presented in Table 3.4), where absence of crystallization processes for all synthesized waterborne poly(urethane-urea) films was evident. On the contrary, all waterborne poly(urethane-urea) films presented T_g , as displayed in Table 3.4. In addition, synthesized waterborne poly(urethane-urea) films with P3MG in their structure exhibited an endotherm (T_E). This is probably overlapped by the T_g in the case of PU0. This endotherm could be related to a relaxation phenomena consequence of the disordering of short-range ordered MDI-SDBS segments, a similar endotherm was observed by Seymour et al.²⁷. The absence of symmetry in the SDBS chain extender can hinder the long-range ordering of the MDI-SDBS segment²⁸ resulting in a non-ideally packed hard segment, which located within the soft segment formed by the macrodiols^{27,29}. As the P3MG content increased, until PU80, T_E shifted to higher temperature, what can be the result of an increase in the MDI-SDBS segment content in the poly(urethane-urea) chains^{29,30}. The shift of T_E to lower values for PU85 and PU90 can be explained by their lower solid content, what would support the idea of a lower chain extension yield, thus, shorter chains.

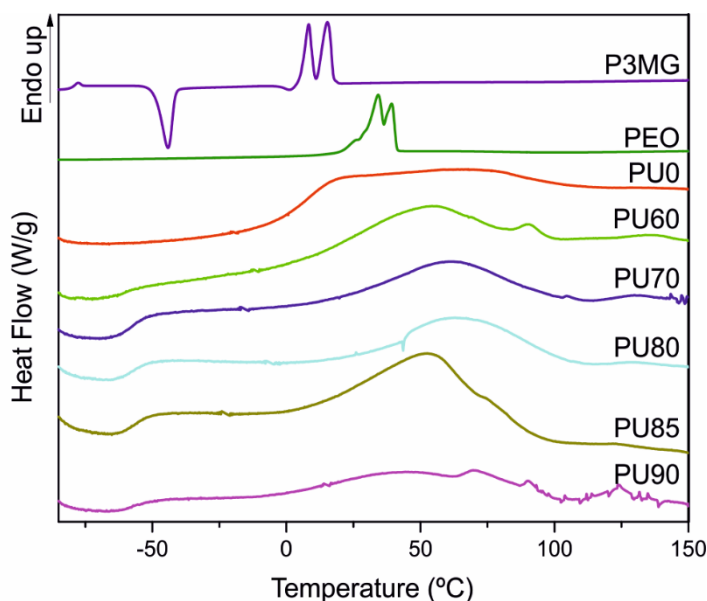


Figure 3.8. DSC heating scan curves of PEO and P3MG macrodiols as well as of synthesized PEO and P3MG based waterborne poly(urethane-urea) films.

Regarding the T_g values, PU0 was the only composition with a T_g over $0\text{ }^\circ\text{C}$, herein the highest of all synthesized waterborne poly(urethane-urea) films. This can be explained taking into consideration that polyurethanes based on PEO can exhibit higher T_g than polyurethanes based on other polyether macrodiols, as a consequence of the compact morphology generated by its more efficient packing than other polyether macrodiols^{31,32}. In the case of formulations based on the renewable macrodiol, the T_g increased with the increase of the P3MG content. This can be related to the previously mentioned MDI-SDBS packing, which, even though it was not ideal, can reduce the mobility of the soft segment leading to increase of the T_g ³³⁻³⁵.

Table 3.4. Glass transition temperature of the soft segment (T_g) and endotherm temperature (T_E) of synthesized waterborne poly(urethane-urea) films.

Sample	T_g ($^\circ\text{C}$)	T_E ($^\circ\text{C}$)
PU0	7	—
PU60	-62	51
PU70	-60	61
PU80	-58	63
PU85	-55	53
PU90	-53	45

Figure 3.9 shows the AFM images obtained for synthesized waterborne poly(urethane-urea) films. PU0 did not present a phase separation in contrast to samples based on PEO/P3MG macrodiol mixtures.

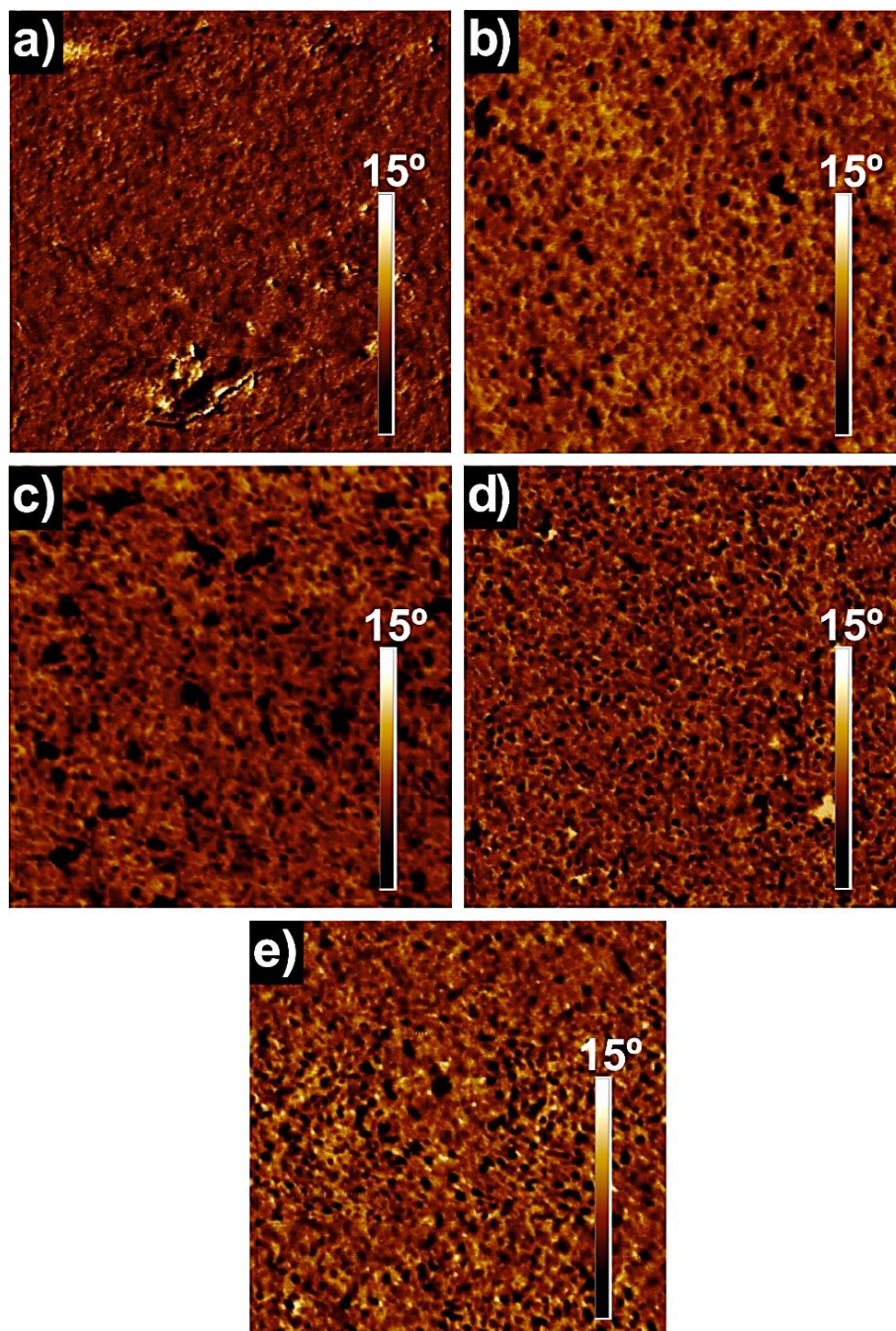


Figure 3.9. AFM phase images (750 nm x 750 nm) of synthesized (a) PU0, (b) PU60, (c) PU70, (d) PU80, (e) PU85 waterborne poly(urethane-urea) films.

The lack of phase separation in PU0 (Figure 3.9a) supported the idea deduced from FTIR spectra analysis that urethane and urea groups formed hydrogen bonding with the ether oxygen of PEO leading to mixture of MDI-SDBS and soft segments. The dark

and bright areas that can be clearly distinguished in Figure 3.9 correspond to soft and MDI-SDBS segments, respectively^{25,36}. The amount of darker domains homogeneously dispersed throughout the brighter continuous area increased when increasing the P3MG content in the macrodiol mixture (Figure 3.9b-e). As it was previously concluded from FTIR analysis, N-H groups presented an inferior tendency to interact with the ether oxygen of P3MG than with the one of PEO³⁷. The phase separation at the nanoscale observed in AFM images supported this conclusion. Therefore, a decrease in interactions between soft and hard segments was promoted when PEO content decreased. The increase of the P3MG content resulted, as previously concluded, in longer polymer chains. Thus, increasing the P3MG content led to an increase in the phase separation at the nanoscale as a consequence of a decrease in interactions between soft and hard segment.

Mechanical properties determined from stress-strain curves, listed in Table 3.5, strongly depended on the macrodiol mixture. In the case of synthesized waterborne poly(urethane-urea) films based on PEO/P3MG macrodiol mixture, increasing P3MG content led to higher mechanical properties in terms of modulus, yield stress, stress at break and elongation at break increased until PU80. Mechanical properties declined from PU80 to PU85, concluding that the increase in the \bar{M}_w was responsible for the improvement in mechanical properties.

Table 3.5. Yield stress (σ_y), stress at break (σ_b), Young's modulus (E) and deformation at break (ϵ_b) of synthesized PEO and P3MG based waterborne poly(urethane-urea) films determined from strain-stress curves.

Sample	E (MPa)	σ_b (MPa)	ϵ_b (%)	σ_y (MPa)
PU0	5.8 ± 0.4	0.3 ± 0.1	573 ± 45	0.7 ± 0.1
PU60	116 ± 38	4.4 ± 0.3	71 ± 10	5.0 ± 0.3
PU70	139 ± 15	5.4 ± 0.7	181 ± 64	7.0 ± 1.0
PU80	216 ± 18	9.1 ± 0.4	418 ± 85	10.7 ± 0.4
PU85	131 ± 13	6.2 ± 0.8	78 ± 13	6.9 ± 0.1

Nevertheless, not many systems present an increase at the same time in modulus and elongation at break since usually one increases and the other one decreases^{2,17,19,38}. Xia et al.³⁹ reported the synthesis of a waterborne polyurethane based on sodium

sulfonate as the internal emulsifier in which both the modulus and elongation at break increased at the same time. This effect can be the result of the absence of crystallization inside the soft segment and of the dispersion within this segment of discrete MDI-SDBS domains¹⁴, what would provoke an increase in the modulus without lessening the elongation at break. PU0, which presented the lowest \bar{M}_w of all synthesized waterborne poly(urethane-urea) films, exhibited the lowest modulus, yield stress and stress at break, however was the film with the highest elongation at break. As it has been previously reported by Xiao et al.⁸ and Jiang et al.³⁸, a decrease in PEO content in waterborne polyurethanes resulted in a lower elongation at break. It is worth mentioning that mechanical properties of synthesized waterborne poly(urethane-urea) films were in the range of similar systems that can be found in literature⁴⁰.

Regarding the transparency in the visible region of the prepared waterborne poly(urethane-urea) film, it was studied by means of UV-vis transmittance, as shown in Figure 3.10.

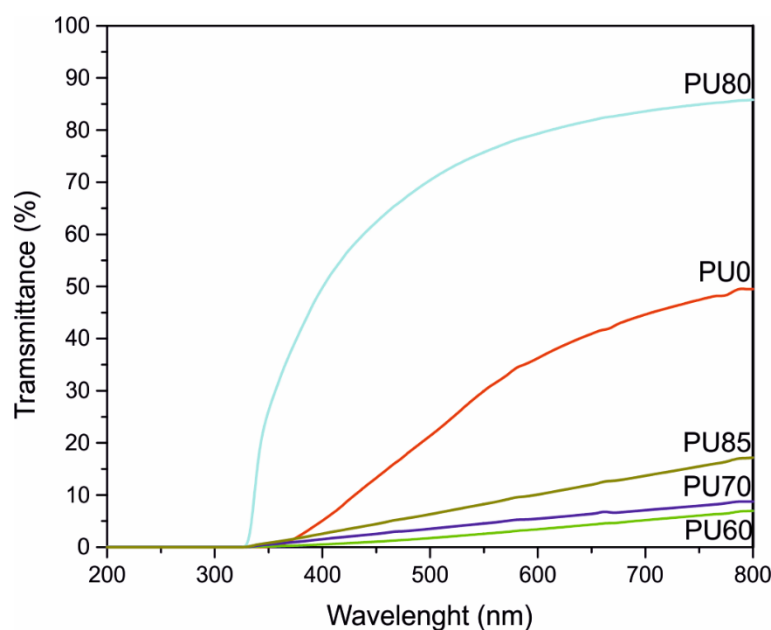


Figure 3.10. UV-vis spectra of synthesized PEO and P3MG based waterborne poly(urethane-urea) films.

At $\lambda=600$ nm, PU60 presented a transmittance of 3%, whereas PU80 showed a transmittance of 79%. Cao et al.⁴¹ reported that, for waterborne polyurethane systems, an increase of the sulfate sodium salt content and a decrease of the particle

size of the dispersion are associated with a higher transparency. This agreed with results obtained by us, as PU80, the synthesized waterborne poly(urethane-urea) with the lowest particle size and the highest \bar{M}_w , meaning it has the highest sodium sulfonate content, was the most transparent one. The lower transparency of PU0 if compare to PU80 can be related to its higher particle size⁴¹, as reported in Table 3.2.

3.5. Conclusions

This Chapter focused on the synthesis and characterization of organic solvent-free waterborne poly(urethane-urea)s synthesized following a novel synthesis procedure. Waterborne poly(urethane-urea)s based on mixtures of a fully renewable carbon content corn-based macrodiol and a biocompatible and biodegradable macrodiol, as it is PEO, were successfully synthesized. From this part of the investigation work the following conclusions can be drawn:

- Waterborne poly(urethane-urea)s with a high renewable carbon content were synthesized through a novel organic solvent-free synthesis procedure,
- PU0 and PU80 were the dispersions with the highest solid content yield,
- A competitive reaction took place between diisocyanate groups of the prepolymer towards water and amine groups of chain extender, modulated by the solubility of the prepolymer in water, thus by the PEO/P3MG ratio. Consequently, non-dispersible particles were formed for PU60, PU70, PU85 and PU90,
- Hydrophilic nature of PEO led to higher particle size waterborne poly(urethane-urea) dispersions with the increase of the PEO content in P3MG/PEO macrodiol mixture,
- PU0 presented the lowest \bar{M}_w from all synthesized waterborne poly(urethane-urea)s,
- For synthesized waterborne poly(urethane-urea)s based on P3MG/PEO macrodiol mixtures, the \bar{M}_w increased in concordance with the increase of the solid content yield,
- PU0 exhibited the lowest T_g , while, for synthesized waterborne poly(urethane-urea)s based on P3MG/PEO macrodiol mixtures, the increase of the P3MG content resulted in higher T_g and T_E ,

- PU0 displayed the highest elongation at break but also the lowest modulus, yield stress and stress at break from all investigated waterborne poly(urethane-urea) films,
- Increase of the P3MG content resulted in waterborne poly(urethane-urea) films with higher mechanical properties by means of modulus, yield stress, stress at break and elongation at break,
- Transparency of films increased in agreement with the solid content yield since less sulfonate groups and higher particle size led to lower transparency.

3.6. References

- [1] S. Gogoi, N. Karak, Biobased biodegradable waterborne hyperbranched polyurethane as an ecofriendly sustainable material, *ACS Sustainable Chemistry and Engineering* 2 (2014) 2730-2738.
- [2] A. Saetung, P. T. Ake, T. Tulyapituk, N. Saetung, P. Phinyocheep, J.-F. Pilard, The chain extender content and NCO/OH ratio flexibly tune the properties of natural rubber-based waterborne polyurethanes, *Journal of Applied Polymer Science* 132 (2015) 42505/1-42505/12.
- [3] X. Xu, Z. Song, S. Shang, X. Rao, Synthesis and properties of novel rosin-based water-borne polyurethane, *Polymer International* 60 (2011) 1521-1526.
- [4] S. Y. Bae, S. H. Jeong, B. K. Kim, Waterborne polyurethane elastomer using renewable polyols, *Journal of Elastomers and Plastics* 48 (2016) 47-57.
- [5] C. Fang, S. Pan, Z. Wang, X. Zhou, W. Lei, Synthesis of waterborne polyurethane using snow as dispersant: Structures and properties controlled by polyols utilization, *Journal of Materials Science & Technology* 35 (2019) 1491-1498.
- [6] J. Wen, Z. Sun, H. Fan, Y. Chen, J. Yan, Synthesis and characterization of a novel fluorinated waterborne polyurethane, *Progress in Organic Coatings* 131 (2019) 291-300.
- [7] S. Zhang, X. Jiang, Synthesis and characterization of non-ionic and anionic two-component aromatic waterborne polyurethane, *Pigment & Resin Technology* 47 (2018) 290-299.
- [8] Y. Xiao, X. Fu, Y. Zhang, Z. Liu, L. Jiang, J. Lei, Preparation of waterborne polyurethanes based on the organic solvent-free process, *Green Chemistry* 18 (2016) 412-416.
- [9] D. H. Park, J. K. Oh, S. B. Kim, W. N. Kim, Synthesis and characterization of sulfonated polyol-based waterborne polyurethane-polyacrylate hybrid emulsions, *Macromolecular Research* 21 (2013). 1247-1253.
- [10] H. T. Lee, S. Y. Wu, R. J. Jeng, Effects of sulfonated polyol on the properties of the resultant aqueous polyurethane dispersions, *Colloids and Surfaces A: Physicochem. Eng. Aspects* 276 (2006) 176-185.
- [11] T. Calvo-Correas, M. D. Martin, A. Retegi, N. Gabilondo, M. A. Corcuera, A. Eceiza, Synthesis and characterization of polyurethanes with high renewable carbon content and tailored properties, *ACS Sustainable Chemistry and Engineering* 4 (2016) 5684-5692.
- [12] Y. Lu, R. C. Larock, Soybean-oil-based waterborne polyurethane dispersions: Effects of polyol functionality and hard segment content on properties, *Biomacromolecules* 9 (2008) 3332-3340.
- [13] S. M. Cakić, I. S. Ristić, M. M. Cincović, D. T. Stojiljković, J. K. Budinski-Simendić, Preparation and characterization of waterborne polyurethane/silica hybrid dispersions from castor oil polyols obtained by glycolysis poly(ethylene terephthalate) waste, *International Journal of Adhesion & Adhesives* 70 (2016) 329-341.
- [14] Z. Gao, J. Peng, T. Zhong, J. Sun, X. Wang, C. Yue, Biocompatible elastomer of waterborne polyurethane based on castor oil and polyethylene glycol with cellulose nanocrystals, *Carbohydrate Polymers* 87 (2012) 2068-2075.
- [15] G. A. Skarja, K. A. Woodhouse, Structure-property relationships of degradable polyurethane elastomers containing an amino, *Journal of Applied Polymer Science* 75 (2000) 1522-1534.

- [16] J. H. Silver, E. Karayianni, S. L. Cooper, Effect of polyol hydrophilicity on the structure and anticoagulant activity of water-soluble sulfonated polyurethanes, *Journal of Colloid and Interface Science* 178 (1996) 219-232.
- [17] F. M. B. Coutinho, M. C. Delpech, L. S. Alves, Anionic waterborne polyurethane dispersions based on hydroxyl-terminated polybutadiene and poly(propylene glycol): Synthesis and characterization, *Journal of Applied Polymer Science* 80 (2001) 566-572.
- [18] B. K. Kim, Aqueous polyurethane dispersions, *Colloid and Polymer Science* 274 (1996) 599-611.
- [19] A. Santamaría-Echart, A. Arbelaiz, A. Saralegi, B. Fernández-d'Arlas, A. Eceiza, M. A. Corcuera, Relationship between reagents molar ratio and dispersion stability and film properties of waterborne polyurethanes, *Colloids and Surfaces A: Physicochemical and Engineering Aspects* 482 (2015) 554-561.
- [20] M. S. Yen, S. C. Kuo, Effects of a soft segment component on the physical properties of synthesized waterborne polyurethanes by using triblock ester-ether copolydiol as the soft segment, *Journal of Polymer Research* 5 (1998) 121-131.
- [21] J. Mattia, P. Painter, A comparison of hydrogen bonding and order in a polyurethane and poly(urethane-urea) and their blends with poly(ethylene glycol), *Macromolecules* 40 (2007) 1546-1554.
- [22] S. M. Cakic, I. S. Ristic, M. Marinovic-Cincovic, M. Spirkova, The effects of the structure and molecular weight of the macrodiol on the properties polyurethane anionic adhesives, *International Journal of Adhesion & Adhesives* 41 (2013) 132-139.
- [23] M. Villani, J. Scheerder, R. A. T. M. Van Benthem, G. De With, Interfacial interactions of poly(urethane-urea) based primers with polypropylene, *European Polymer Journal* 56 (2014) 118-130.
- [24] L. Ugarte, B. Fernández-d'Arlas, A. Valea, M. L. González, M. A. Corcuera, A. Eceiza, Morphology-properties relationship in high-renewable content polyurethanes, *Polymer Engineering and Science* 47 (2007) 21-25.
- [25] S. M. Cakic, M. Spirková, I. S. Ristic, J. K. B. Simendic, M. M. Cincovic, R. Poreba, The waterborne polyurethane dispersions based on polycarbonate diol: Effect of ionic content, *Materials Chemistry and Physics* 138 (2013) 277-285.
- [26] J. M. Rubin-Preminger, J. Bernstein, Surprises in a 'simple' system: 2,4-diaminobenzenesulfonic acid, *Helvetica Chimica Acta* 86 (2003) 3037-3054.
- [27] R. W. Seymour, S. L. Cooper, Thermal analysis of polyurethane block polymers, *Macromolecules* 6 (1973) 48-53.
- [28] J. P. Sheth, D. B. Klinedinst, G. L. Wilkes, I. Yilgor, E. Yilgor, Role of chain symmetry and hydrogen bonding in segmented copolymers with monodisperse hard segments, *Polymer* 46 (2005) 7317-7322.
- [29] D. J. Martin, G. F. Meijs, P. A. Gunatillake, S. J. McCarthy, G. M. Renwick, The effect of average soft segment length on morphology and properties of a series of polyurethane elastomers. II. SAXS-DSC annealing study, *Journal of Applied Polymer Science* 62 (1996) 1377-1386.
- [30] A. Eceiza, M. D. Martin, K. de la Caba, G. Kortaberria, N. Gabilondo, M. A. Corcuera, I. Mondragon, Thermoplastic polyurethane elastomers based on polycarbonate diols with different soft segment molecular weight and chemical structure: mechanical and thermal properties, *Polymer Engineering and Science* 48 (2008) 297-306.

- [31] G. N. Mahesh, P. Banu, G. Radhakrishnan, Investigations on polyurethane ionomers. II. 3,4-dihydroxycinnamic acid-based anionomers, *Journal of Applied Polymer Science* 65 (1997) 2105-2109.
- [32] O. Jaudouin, J. J. Robin, J. M. Lopez-Cuesta, D. Perrin, C. Imbert, Ionomer-based polyurethanes: a comparative study of properties and applications, *Polymer International* 61 (2012) 495-510.
- [33] B. S. Lee, B. C. Chun, Y. C. Chung, K. I. Sul, J. W. Cho, Structure and thermomechanical properties of polyurethane block copolymers with shape memory effect, *Macromolecules* 34 (2001) 6431-6437.
- [34] S. Mondal, J. L. Hu, Structural characterization and mass transfer properties of nonporous segmented polyurethane membrane: Influence of hydrophilic and carboxylic group, *Journal of Membrane Science* 274 (2006) 219-226.
- [35] J. T. Garrett, R. Xu, J. Cho, J. Runt, Phase separation of diamine chain-extended poly(urethane) copolymers: FTIR spectroscopy and phase transitions, *Polymer* 44 (2003) 2711-2719.
- [36] A. Eceiza, M. Larrañaga, K. de la Caba, G. Kortaberria, C. Marieta, M. A. Corcuera, I. Mondragon, Structure-property relationships of thermoplastic polyurethane elastomers based on polycarbonate diols, *Journal of Applied Polymer Science* 108 (2008) 3092-3103.
- [37] I. Yilgor, E. Yilgor, G. L. Wilkes, Critical parameters in designing segmented polyurethanes and their effect on morphology and properties: A comprehensive review, *Polymer* 58 (2015) A1-A36.
- [38] X. Jiang, J. Li, M. Ding, H. Tan, Q. Ling, Y. Zhong, Q. Fu, Synthesis and degradation of nontoxic biodegradable waterborne polyurethanes elastomer with poly(ϵ -caprolactone) and poly(ethylene glycol) as soft segment, *European Polymer Journal* 42 (2007) 1838-1846
- [39] J. Xia, Y. Xu, C. Gong, D. Gao, Design strategy for waterborne polyurethane with sodium sulfonate groups on the soft segments, *Journal of Applied Polymer Science* 131 (2014) 39657/1-39657/6.
- [40] A. Bahadur, A. Saeed, S. Iqbal, M. Shoaib, M. S. Rahman, M. I. Bashir, M. Asghar, M. A. Ali, T. Mahmood, Biocompatible waterborne polyurethane-urea elastomer as intelligent anticancer drug release matrix: A sustained drug release study, *Reactive and Functional Polymers* 119 (2017) 57-63.
- [41] X. Cao, X. Ge, H. Chen, W. Li, Effects of trimethylol propane and AAS salt on properties of waterborne polyurethane with low gloss, *Progress in Organic Coatings* 107 (2017) 5-13.

Chapter

4

"Anyone who doesn't make mistakes isn't trying hard enough."

(Wess Roberts)

Triblock copolymers as macrodiols for synthesis of waterborne poly(urethane-urea)s

4. Triblock copolymers as macrodiols for the synthesis of waterborne poly(urethane-urea)s

4.1. Chapter overview	79
4.2. Introduction	79
4.3. Synthesis of waterborne poly(urethane-urea)s based on triblock copolymers	80
4.3.1. Preparation of poly(urethane-urea) films	83
4.4. Characterization of waterborne poly(urethane-urea)s	83
4.4.1. Characterization of dispersions	83
4.4.2. Characterization of films	86
4.5. Conclusions	94
4.6. Selection of synthesized waterborne poly(urethane-urea)s for novel applications	95
4.7. References	97

4.1. Chapter overview

The objective of this Chapter is the synthesis and characterization of organic solvent-free waterborne poly(urethane-urea)s based on different triblock copolymers as macrodiols adapting the synthesis procedure established in the Chapter 3. The aim of this investigation is to study the effect of the soft segment composition on the final properties of both synthesized waterborne poly(urethane-urea) dispersions and films.

Triblock copolymers based on poly(ethylene oxide) and poly(propylene oxide) blocks, with different block architectures and molecular weights, were employed as macrodiols. PU0, synthesized and characterized in the Chapter 3, is used as reference in this investigation work.

4.2. Introduction

The influence of the soft segment on the final properties of polyurethanes and poly(urethane-urea)s has been widely studied¹⁻⁷. Nevertheless, only a few investigations involving block copolymers as macrodiols have been carried out. Among research on polyurethanes and poly(urethane-urea)s synthesized from a block copolymer precursor, Pergal et al.⁸ used α,ω -dihydroxy-poly(ϵ -caprolactone-*b*-dimethylsiloxane-*b*- ϵ -caprolactone) (PCL-*b*-PDMS-*b*-PCL) triblock copolymer, Rueda-Larraz et al.⁹ utilized poly(ϵ -caprolactone-*b*-tetrahydrofuran-*b*- ϵ -caprolactone) (PCL-*b*-PTHF-*b*-PCL), whereas poly(ethylene oxide-*b*-propylene oxide-*b*-ethylene oxide) (PEO-*b*-PPO-*b*-PEO) triblock copolymer was employed by Waletzko et al.¹⁰, Korley et al.¹¹ and Lan et al.¹². Regarding waterborne polyurethane and poly(urethane-urea) dispersions investigation on block copolymers based soft segment is even more scarce. In relation to those materials, Yen et al.^{13,14} prepared waterborne polyurethanes based on poly(ϵ -caprolactone-*b*-ethylene oxide-*b*- ϵ -caprolactone) (PCL-*b*-PEO-*b*-PCL). The main objectives when synthesizing these kind of polyurethanes and poly(urethane-urea)s are the study of the effect of the soft segment on the final properties^{10,11,14} and the design of materials with potential medical applications^{8,9,12}.

The interest of making use of triblock copolymers as macrodiols for the synthesis of polyurethanes and poly(urethane-urea)s relies on their self-assembly at the nanometric scale. They can arrange into different morphologies and form well-defined structures at the nanometric level thanks to covalent bonding between blocks which prevents the separation at the macroscopic level^{10,15,16}. As mentioned in the Chapter 1, in the case of the block copolymers employed in this investigation work, the hydrophilic character of PEO makes it possible to use it as a nonionic internal emulsifier in the synthesis of waterborne polyurethanes and poly(urethane-urea)s. It is for this reason that block copolymers formed by hydrophilic blocks, such as mentioned PEO, are particularly interesting. PEO-b-PPO-b-PEO and PPO-b-PEO-b-PPO belong to that category of block copolymers formed by PEO blocks, which makes them water soluble^{17,18}. Accordingly, these amphiphilic block copolymers, which arrange into core-corona micelles, looping shaped in the case of PPO-b-PEO-b-PPO, in water^{17,18}, are appealing macrodiols for the synthesis of waterborne poly(urethane-urea)s following the synthesis procedure detailed in the Chapter 3.

4.3. Synthesis of triblock copolymers based waterborne poly(urethane-urea)

The synthesis procedure detailed in the Chapter 3 was followed for the synthesis of different waterborne poly(urethane-urea)s based on triblock copolymers as macrodiols. Some variations were introduced in the procedure due to different reactivity between employed triblock copolymers and the diisocyanate (Figure 4.1). In the case of PEO-b-PPO-b-PPO triblock copolymers based waterborne poly(urethane-urea)s, the temperature for the synthesis of the prepolymer was maintained at 80 °C, while for PPO-b-PEO-b-PPO triblock copolymers based waterborne poly(urethane-urea)s the temperature was set at 60 °C. In all these cases, the time for the synthesis of the prepolymer was established to be 90 min after kinetic evaluation by DBBTM (see Figure A.3 in Annexes). For the reference, PU0 was synthesized following the procedure detailed in Figure 3.2, using a prepolymer synthesis time equal to 2 h.

Triblock copolymers as macrodiols for synthesis of waterborne poly(urethane-urea)s

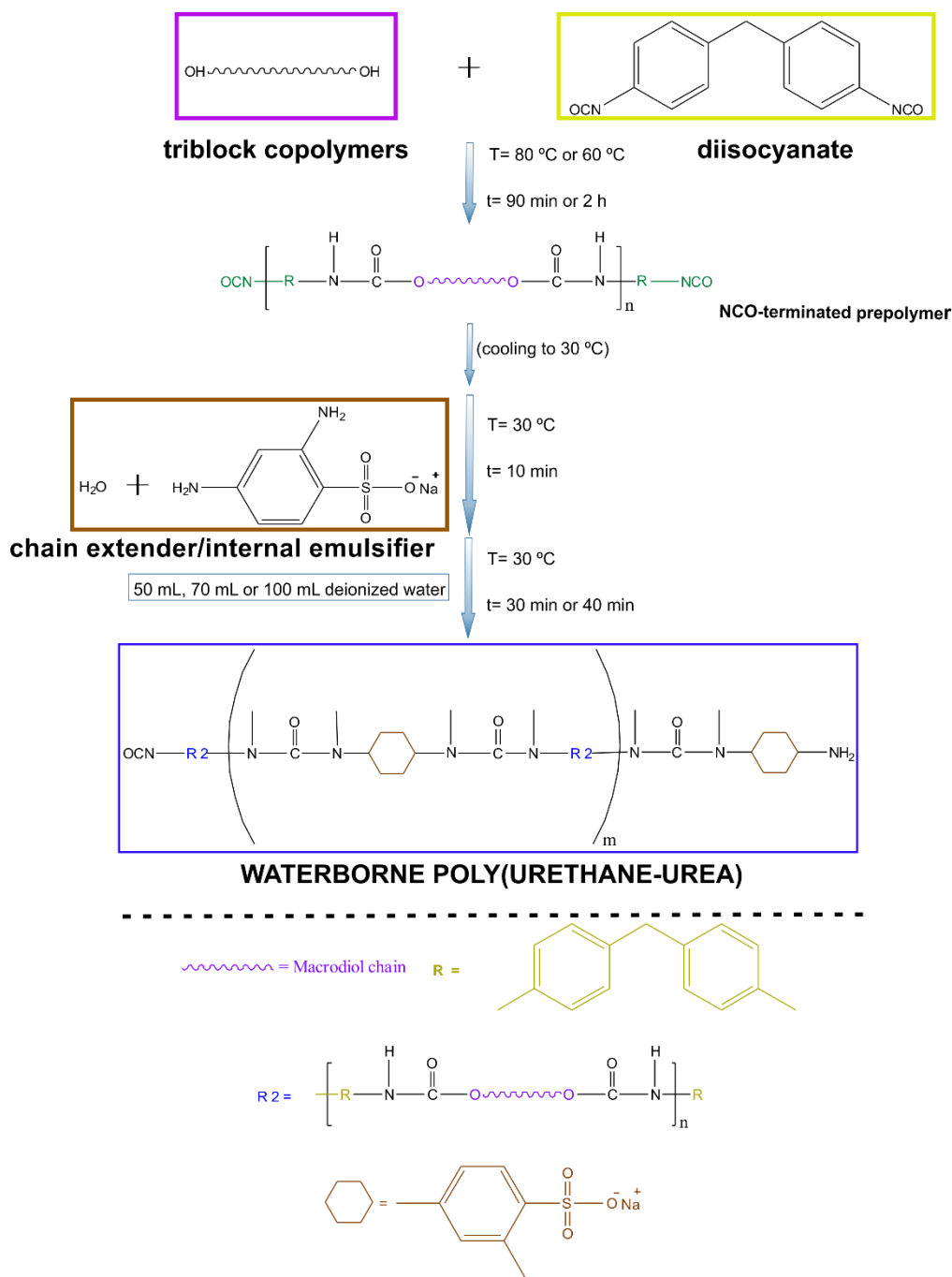


Figure 4.1. Schematic illustration of the synthesis of triblock copolymers based waterborne poly(urethane-urea)s.

The time for chain extension step was set at 10 min after evaluation. The time for chain extension was reduced to 10 min for the reference, PU0, which was a variation from the synthesis reported in the Chapter 3 section 3.3. Finally, different amounts of water were added in order to prepare dispersions with theoretical solid contents in the range of 25-27%. Water was added dropwise while vigorously stirring for 30-40

min, depending on the amount of water added in this last step. Samples were denoted as displayed in Table 4.1.

Table 4.1. Designation of samples, molar composition, MDI-SBBS segment content and acid group content of synthesized triblock copolymers based waterborne poly(urethane-urea)s and PEO based waterborne poly(urethane-urea).

Sample	Molar composition (mol)			MDI-SBBS ^a (wt%)	SO ₃ H _{tot} ^a (wt%)
	MDI	SBBS	Macrodiol		
PU0	2	1	1 (PEO 1000 g mol ⁻¹)	42.3	4.6
PUEPE19	2	1	1 (BCPEPE19 1900 g mol ⁻¹)	28.4	3.1
PUEPE29	2	1	1 (BCPEPE29 2900 g mol ⁻¹)	20.7	2.2
PUPEP20	2	1	1 (BCPPEP20 2000 g mol ⁻¹)	27.4	2.9
PUPEP27	2	1	1 (BCPPEP27 2700 g mol ⁻¹)	21.9	2.3

a) Theoretical stoichiometry values.

The obtained waterborne poly(urethane-urea) dispersions are shown in Figure 4.2.

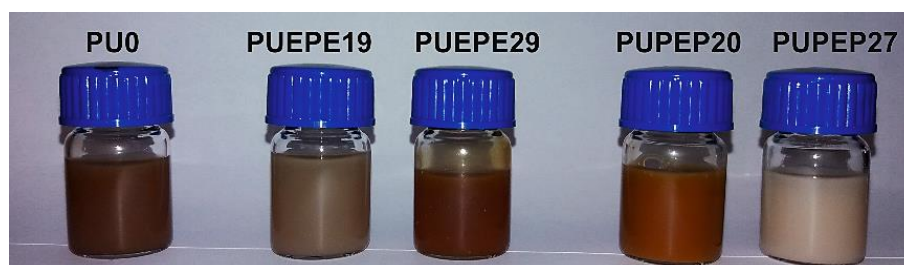


Figure 4.2. Visual appearance of synthesized triblock copolymers based waterborne poly(urethane-urea) dispersions. PU0 dispersion was added as reference.

4.3.1. Preparation of triblock copolymers based waterborne poly(urethane-urea) films

Films were prepared as detailed in Chapter 3. The visual aspect of the prepared waterborne poly(urethane-urea) films are shown in Figure 4.3. Synthesized waterborne poly(urethane-urea) films presented different colors, which makes them interesting for coating application.



Figure 4.3. Visual appearance of triblock copolymers based waterborne poly(urethane-urea) films. PU0 film was added for comparison purpose.

4.4. Characterization of triblock copolymers based waterborne poly(urethane-urea)s

4.4.1. Characterization of triblock copolymers based waterborne poly(urethane-urea) dispersions

The experimental solid contents of synthesized waterborne poly(urethane-urea) dispersions were close to the theoretical values (Table 4.2), indication of a proper reaction.

Table 4.2. Average particle size, experimental solid content and theoretical solid content of synthesized triblock copolymers based waterborne poly(urethane-urea) dispersions. PU0 dispersion was analyzed as reference.

Sample	Average particle size (nm)	Solid content (%)	Theoretical solid content (%)
PU0	2135 ± 199	24.10 ± 0.60	24.7
PUEPE19	1218 ± 34	24.66 ± 0.03	24.9
PUEPE29	935 ± 55	27.27 ± 0.07	27.5
PUPEP20	2692 ± 110	24.52 ± 0.07	25.6
PUPEP27	463 ± 16	25.87 ± 0.01	26.1

The average particle size of synthesized waterborne poly(urethane-urea) dispersions, displayed in Table 4.2, strongly depended on the macrodiol employed for the formation of the soft segment.

Regarding the differences observed in the average particle size, on the one hand, synthesized waterborne poly(urethane-urea) dispersions based on PEO-b-PPO-b-PEO triblock copolymers exhibited a decrease in the average particle size when the molecular weight of the macrodiol increased¹⁹⁻²¹. On the other hand, dispersions based on PPO-b-PEO-b-PPO triblock copolymers presented the highest average particle size of all synthesized waterborne poly(urethane-urea) dispersions, in the case of PUPEP20, and also the lowest average particle size, in the case of PUPEP27. The decrease in the average particle size observed from PUEPE19 to PUEPE29 and from PUPEP20 to PUPEP27 can be explained by the decrease on the PEO content (see Table 2.1). Taking into account that PEO block is the hydrophilic block, the higher its content the more extended the configuration of the formed particles as a result of interactions between PEO and water molecules^{19,22}. This decrease in the average particle size was also supported by the decrease in the molecular weight of synthesized waterborne poly(urethane-urea)s^{13,23} (Table 4.3 displayed in 4.2.2. Characterization of films).

If the average particle sizes of dispersions based on different triblock copolymers of similar molecular weights are compared, it can be appreciated that PUPEP20 showed a higher average particle size than PUEPE19. On the contrary, PUEPE29 exhibited a higher average particle size than PUPEP27. All this implied that the block formulation of triblock copolymers played a crucial role in the average particle size¹⁸.

As it has been reported, and previously mentioned, in order to form micelles in aqueous phase PPO-b-PEO-b-PPO triblock copolymer requires a chain loop since PEO blocks form the corona, in contact with water, and PPO blocks form the core^{17,18}. Taking this information into account, Figure 4.4 presents a proposed core-shell arrangement for the particles formed for synthesized triblock copolymers based waterborne poly(urethane-urea) dispersions.

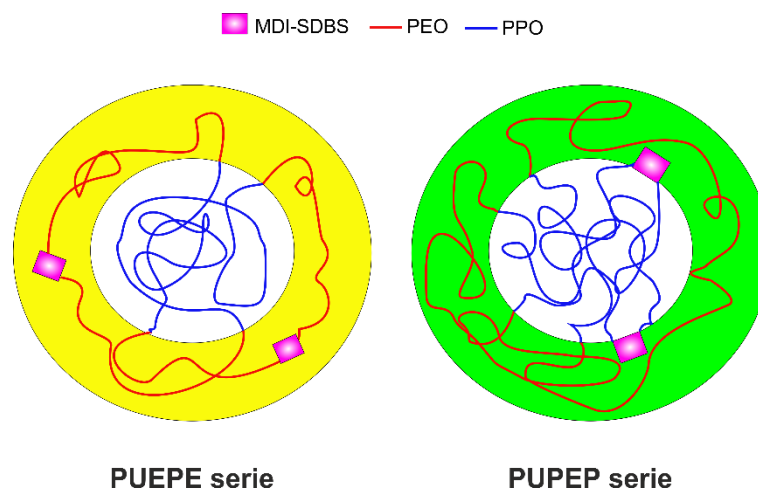


Figure 4.4. Proposed arrangements of core-shell particles of synthesized triblock copolymers based waterborne poly(urethane-urea) dispersions.

Regarding the viscosity of synthesized waterborne poly(urethane-urea) dispersions (Figure 4.5), it can be observed that PU0 was the most viscous dispersion. This was due to its soft segment formed just by PEO chains, which interacted with water molecules thanks to its hydrophilic character²². The $-CH_3$ side chains of PPO blocks favored the mobility of the MDI-SDBS segment. Therefore, leading to lower viscosities for dispersions based on triblock copolymers if compare to PU0^{24,25}. As clearly shown in Figure 4.5, synthesized waterborne poly(urethane-urea) dispersions based on PEO-b-PPO-b-PEO triblock copolymers possessed a higher viscosity than the ones based on PPO-b-PEO-b-PPO triblock copolymers. This can be the result of the different block formulations, since in PUEPE19 and PUEPEP29 the MDI-SDBS segment was directly linked to PEO block, whereas in the cases of PUPEP20 and PUPEP27 the MDI-SDBS segment was attached to PPO blocks. Accordingly, the effect of the $-CH_3$ side chain of PPO was more relevant when the MDI-SDBS was directly linked to PPO block. Moreover, waterborne poly(urethane-urea) dispersions based on PEO-b-PPO-b-PEO triblock can arrange easily hydrophilic PEO blocks on the particle surface, as show in Figure 4.4, that could interact more effectively with water, thus resulting in higher viscosity^{26,27}.

Comparing synthesized waterborne poly(urethane-urea) dispersions based on the same triblock copolymer formulation, with different molecular weight, it can be concluded that the viscosity was influenced by the average particle size. The viscosity

was higher for synthesized waterborne poly(urethane-urea) dispersions with the lowest average particle sizes²⁸.

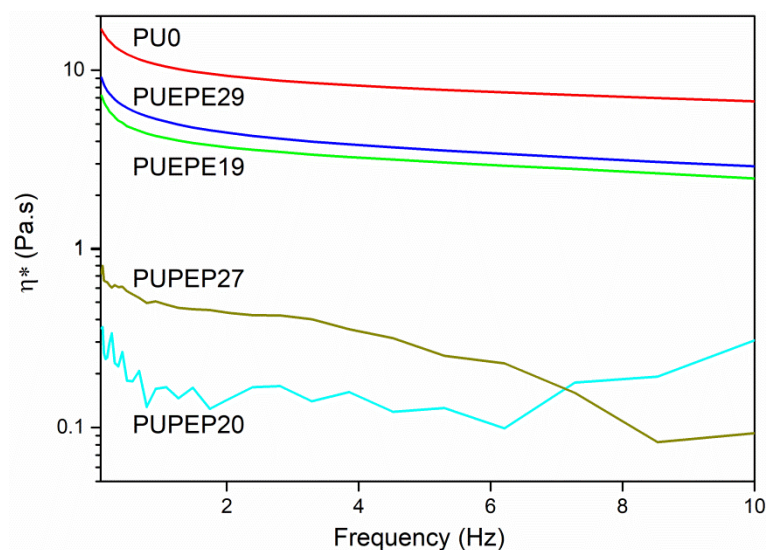


Figure 4.5. Dynamic viscosities of synthesized triblock copolymers based waterborne poly(urethane-urea) dispersions.

4.4.2. Characterization of triblock copolymers based waterborne poly(urethane-urea) films

FTIR analysis was performed to study the influence of employed different triblock copolymers on the chemical structure of synthesized waterborne poly(urethane-urea) films. Figure 4.6a shows the N–H stretching vibration bands at 3500–3200 cm^{-1} interval (Table 4.1). The absence of a band at 2270 cm^{-1} confirmed that the reaction proceeded completely²⁹.

The other interesting region in FTIR spectra was the amide I region, shown in detail in Figure 4.6b, in which bands are associated to carbonyl stretching vibrations, both from urea and urethane groups^{30,31}. Synthesized waterborne poly(urethane-urea) films, with the exception of PUPEP27, presented a less intense hydrogen bonded carbonyl group band than the band associated to the free carbonyl groups since the band above 1700 cm^{-1} , around 1730 cm^{-1} , was the most intense. In the case of PUPEP27, carbonyl groups likely tended to form hydrogen bonds between hard segments, as can be concluded from the more intense band at 1700 cm^{-1} than at 1730 cm^{-1} . This was also supported by the band that can be seen at 1640 cm^{-1} , that did not

appeared for the other investigated films, which was associated to hydrogen bonded urea carbonyl groups³¹⁻³⁴. This band probably showed up as a result of an inferior mixing between hard and soft segments consequence of increasing hydrogen bonding between hard segments³⁰.

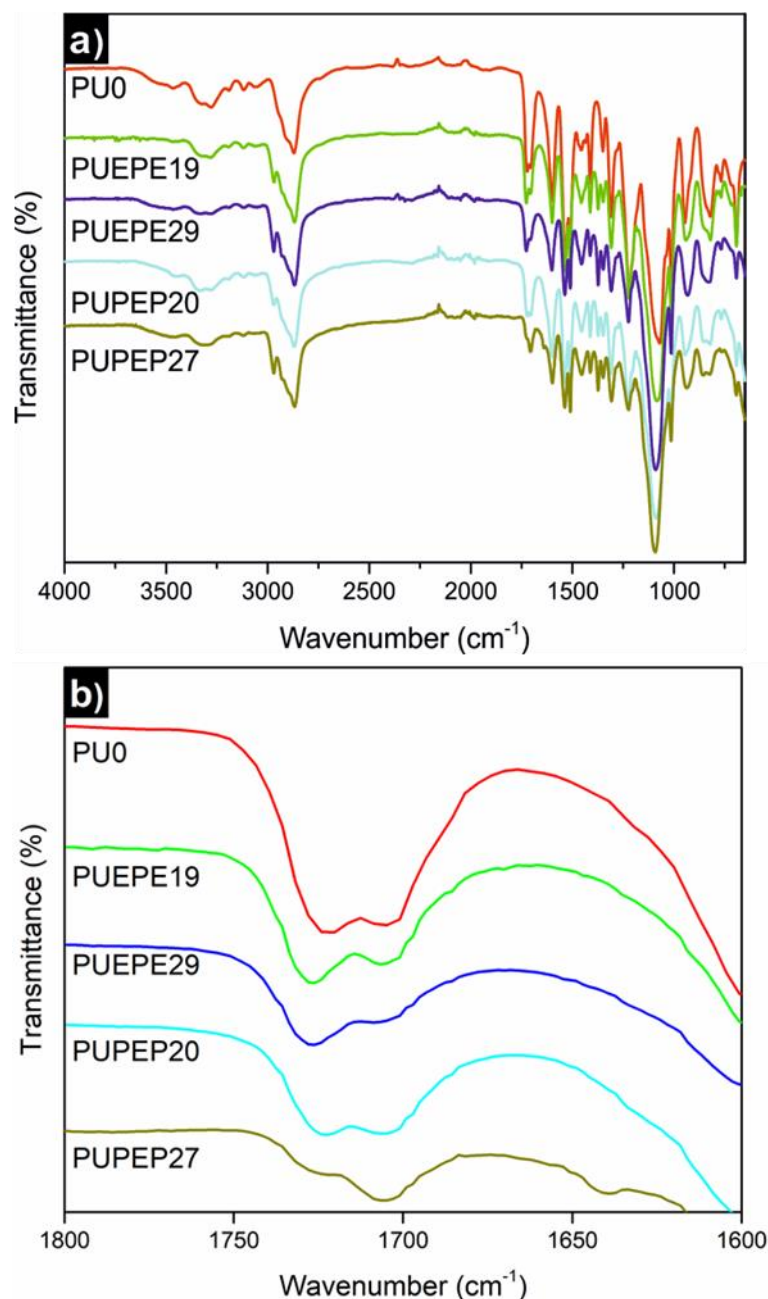


Figure 4.6. FTIR spectra of synthesized (a) triblock copolymers based waterborne poly(urethane-urea) films and (b) amplification of their carbonyl stretching region. FTIR spectra of PU0 was added for comparison.

For the other synthesized waterborne poly(urethane-urea) films, the lack of hydrogen bonding between hard segments pointed out in the direction of N–H groups forming

hydrogen bonds with the ether oxygen of C–O–C groups^{33,34}. These hydrogen bonds may have predominantly been formed with PEO rather than with PPO block, in the case of triblock copolymers based waterborne poly(urethane-urea)s, given the effect of the steric hindrance of –CH₃ side groups of PPO^{35,36}. The hydrogen bonding between N–H groups and ether oxygen of PEO would lead to an increase in the mixing of soft and hard segments³⁷. Herein, PU0, without PPO block, would exhibit the highest phase mixing from all synthesized waterborne poly(urethane-urea) films. The band at approximately 1100 cm⁻¹ was the one related to mentioned ether oxygen³⁸.

The \bar{M}_w values of synthesized waterborne poly(urethane-urea) films were determined by SEC (Figure A5 in Annexes) and are displayed in Table 4.3. PU0 was the film with the highest \bar{M}_w from all synthesized waterborne poly(urethane-urea)s.

Table 4.3. Average weight molecular weight (\bar{M}_w) and polydispersity index (IP) of synthesized triblock copolymers based waterborne poly(urethane-urea) films. PU0 film was added as reference.

Sample	\bar{M}_w	IP (\bar{M}_w/\bar{M}_n)
PU0	31,750	1.89
PUEPE19	26,740	1.79
PUEPE29	25,900	2.10
PUPEP20	16,250	2.36
PUPEP27	14,650	1.27

Regarding waterborne poly(urethane-urea)s based on triblock copolymers, for the same triblock copolymer formulation the \bar{M}_w of the resulting poly(urethane-urea) decreased when the \bar{M}_w of the triblock copolymer increased. This did not agree with the commonly reported increase of \bar{M}_w of poly(urethane-urea)s when increasing the \bar{M}_w of the macrodiol²³. Nonetheless, this is not a rule for all the cases³⁹. In the present case, the \bar{M}_w of synthesized waterborne poly(urethane-urea) films seemed to be related with the PEO content, since the macrodiols with the highest PEO content led to the waterborne poly(urethane-urea) films with the highest \bar{M}_w . Likely, PEO favored the access of the chain extender to the prepolymer during the chain extension step. Furthermore, the access of the chain extender to the prepolymer can be also promoted by the direct link of PEO block with MDI. This can be concluded since PEO-b-PPO-b-PEO triblock copolymers based waterborne poly(urethane-urea) films

presented higher \bar{M}_w values than PPO-b-PEO-b-PPO triblock copolymers based ones. This would suggest that during the chain extension the chains based on PPO-b-PEO-b-PPO triblock copolymer would be terminated faster resulting in shorter chains.

According to DSC curves (Figure 4.7), synthesized waterborne poly(urethane-urea) films based on triblock copolymers presented a single T_g , ranging from -66 to -42 °C (Table 4.4), which was related to the T_g of the soft segment^{11,40}. These values did not significantly vary from T_g values of the neat triblock copolymers when the soft segment was formed by the highest molecular weight triblock copolymers (those with molecular weights of 2700 and 2900 g mol⁻¹), indication of lower interaction between soft and hard segments, thus resulting in phase separation^{11,41,42}.

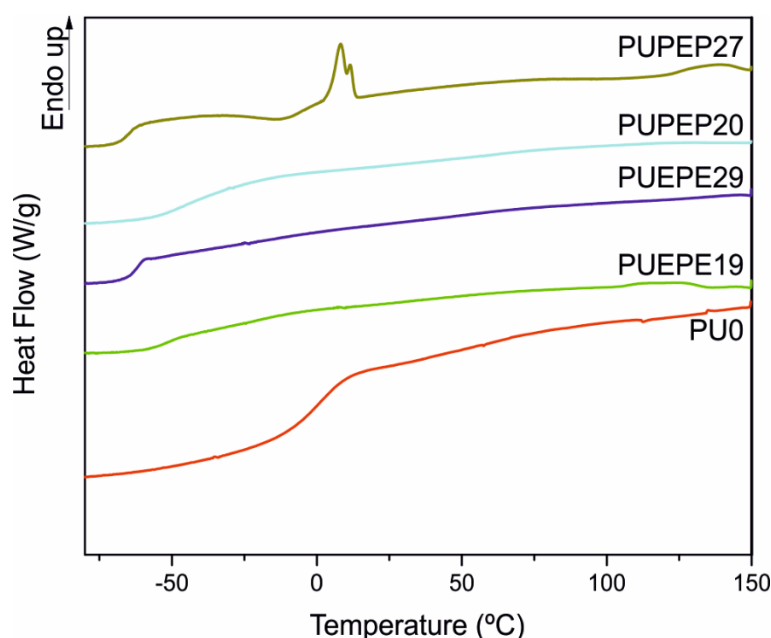


Figure 4.7. DSC heating scan curves of synthesized triblock copolymers based waterborne poly(urethane-urea) films. DSC curve of PU0 was added for comparison.

For PUEPE19 and PUPEP20, T_g values shifted 17 and 28 °C, respectively, to higher temperature if compare to the neat triblock copolymers, implying higher miscibility between segments. This can be the result of their shorter soft segment chain^{11,43}. PU0 also presented a single T_g , which was the highest of all synthesized waterborne poly(urethane-urea) films. This T_g could be the consequence of interaction between soft and hard segments. These interactions were favored since PEO homopolymer was the macrodiol with the lowest molecular weight, thus the shortest soft segment chains^{11,43}, and also due to the tendency to interaction between N-H groups and the

ether oxygen of PEO³⁴. All this resulted in lower mobility of chains and, accordingly, in a higher T_g ^{44,45}.

Table 4.4. Glass transition temperature of the soft segment (T_g), melting temperature (T_m) and melting enthalpy (ΔH_m) of synthesized triblock copolymers based waterborne poly(urethane-urea) films. PU0 film was added for comparison.

Sample	T_g (°C)	T_m (°C)	ΔH_m (J mol ⁻¹)
PU0	7	—	—
PUEPE19	-52	—	—
PUEPE29	-64	—	—
PUPEP20	-40	—	—
PUPEP27	-66	7, 11	30
PEO (1000 g mol ⁻¹)	—	28, 39	139
PEO-b-PPO-b-PEO (1900 g mol ⁻¹) ^a	-69	16	31
PEO-b-PPO-b-PEO (2900 g mol ⁻¹) ^a	-69	22	29
PPO-b-PEO-b-PPO (2000 g mol ⁻¹) ^a	-68	14	59
PPO-b-PEO-b-PPO (2700 g mol ⁻¹) ^a	-70	12	46

a) DSC curves displayed in Figure A.6 in Annexes.

The T_m was only observed for PUPEP27, which could be associated to the melting process of the soft segment, since it took place at similar temperatures to the T_m of PPO-b-PEO-b-PPO (2700 g mol⁻¹) triblock copolymer. The crystallization of the soft segment of PUPEP27 could be the result of the incompatibility between segments, supported by FTIR analysis, which was promoted by the higher molecular weight of the macrodiol⁴². Therefore, this triblock copolymer led to longer soft segment chains^{43,46}.

The morphology of synthesized waterborne poly(urethane-urea) films, analyzed by AFM, manifestly depended on the soft segment, as can be observed in Figure 4.8. On the one hand, in the case of PU0, there was not phase separation (Figure 4.8e), as was previously mentioned and discussed in the Chapter 3 section 3.4.2. On the other hand, synthesized triblock copolymers based waterborne poly(urethane-urea) films presented a microphase separated structure, particularly in the case of PUPEP27 (Figure 4.8d), in agreement with the previous results, which is a common effect of triblock copolymers, since they promote microtopographical surface separation⁴⁷.

Triblock copolymers as macrodiols for synthesis of waterborne poly(urethane-urea)s

Since the features that can be seen in Figure 4.8 were similar to the ones promoted by triblock copolymers^{15,48}, the impact of the soft segment formed by triblock copolymer on the final morphology is certain.

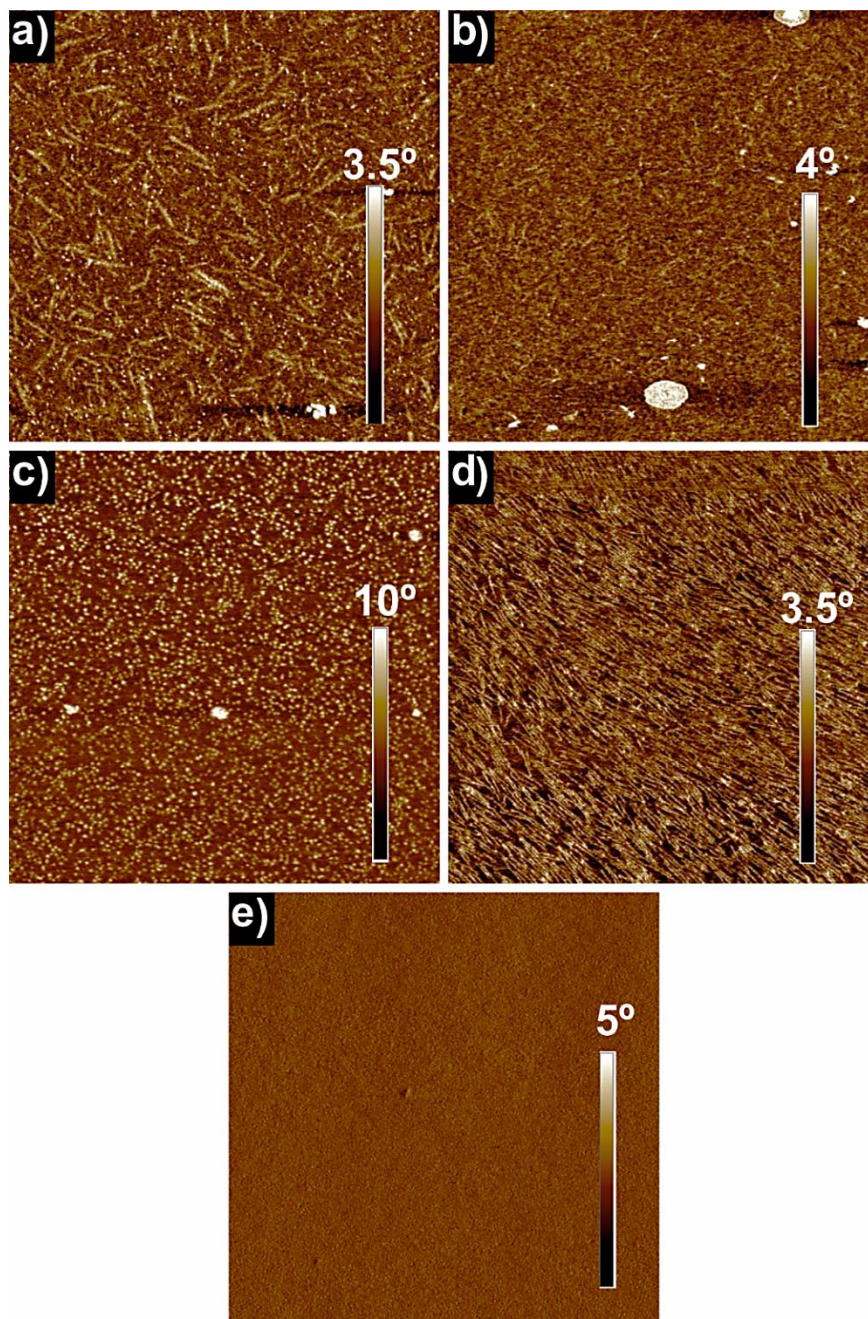


Figure 4.8. AFM phase images (3 μm x 3 μm) of (a) PUEPE19, (b) PUEPE29, (c) PUPEP20 and (d) PUPEP27 synthesized triblock copolymers based waterborne poly(urethane-urea) films. AFM phase images of (e) PU0 film was added for comparison.

The well-resolved boundaries between domains were the result of the thermodynamic incompatibility between PEO and PPO blocks limiting the large-scale interdomain hydrogen bonding contributing to microphase separation¹⁰. In

addition, the observed rod-like and spherical structures are typical for PEO and PPO based triblock copolymers, which tend to organize in those structures¹⁵.

The spherical structures appreciated for PUPEP20 can be formed thanks to the central PEO block. Yang et al.⁴⁹ observed similar spherical structures for a polyrotaxane modified with PPO-b-PEO-b-PPO triblock copolymer. In the case of PUPEP20, there could be a looping of micelles^{18,50} leading to spherical structures after water evaporation and coalescence of particles to form the film⁴⁹. PUPEP27 presented a different morphology as a consequence of a higher molecular weight and a lower PEO content of the triblock copolymer, leading to distinct interactions between segments⁵¹. This is in good agreement with FTIR results. Herein, the final morphology of each triblock copolymers based waterborne poly(urethane-urea) films was the result of the self-assembly of triblock copolymer formed soft segment in those structures and their interaction with the hard segment.

The mechanical properties of synthesized waterborne poly(urethane-urea) films obtained from the stress-strain curves (see Figure A.11 in Annexes) are shown in Table 4.5. Results of PUPEP20 are not presented since this material was excessively soft for tensile test. Firstly, as expected, PU0 exhibited the highest mechanical properties of all synthesized waterborne poly(urethane-urea) films. Triblock copolymers based soft segment led to an evident decrease in both modulus and stress at break. Nevertheless, values obtained for synthesized waterborne poly(urethane-urea) films were in the range of other similar systems, as it is the case of waterborne poly(urethane-urea)s synthesized by Meng et al.⁴, who employed PEO-b-PPO diblock copolymer as the soft segment. These values were the consequence of their low hard segment content⁵² and the steric hindrance caused by the side $-CH_3$ groups of PPO^{35,36} interfering with the formation of hydrogen bonds between segments. Furthermore, PEO based soft segment leads to low modulus and tensile strength^{52,53} and, additionally, polyurethanes formed by a rubbery soft segment (macrodiols with $T_g < T_m < T_{room}$) also exhibit low modulus as well as low values of stress at break⁵⁴. Taking all this into account, one can easily realized that the highest modulus and stress at break values among synthesized triblock copolymers based waterborne poly(urethane-urea) films corresponded to PUEPE19, which was the synthesized waterborne poly(urethane-urea) film with the highest hard segment content, as

Triblock copolymers as macrodiols for synthesis of waterborne poly(urethane-urea)s

detailed in Table 4.1. PUEPE19, with the highest T_g among the tested waterborne poly(urethane-urea)s, exhibited the highest value of stress at break, decreasing for PUEPE29 and shifting to an even lower value for PUPEP27. This decrease could be associated to the decrease of the T_g and the PEO content, displayed in Table 2.1, making them less deformable, as well as to the differences observed in their morphologies^{11,51}.

Table 4.5. Young's modulus (E), stress at break (σ_b) and deformation at break (ϵ_b) of synthesized triblock copolymers based waterborne poly(urethane-urea) films. PU0 film was added for comparison.

Sample	E (MPa)	σ_b (MPa)	ϵ_b (%)
PU0	5.8 ± 0.4	0.3 ± 0.10	573 ± 45
PUEPE19	1.0 ± 0.3	0.06 ± 0.01	360 ± 52
PUEPE29	0.4 ± 0.1	0.04 ± 0.01	265 ± 45
PUPEP27	0.5 ± 0.1	0.04 ± 0.01	170 ± 16

Figure 4.9 shows the UV-vis spectra of synthesized waterborne poly(urethane-urea) films, except for PUPEP20, which was not possible to handle in a proper way in order to perform the UV-vis analysis due to its softness.

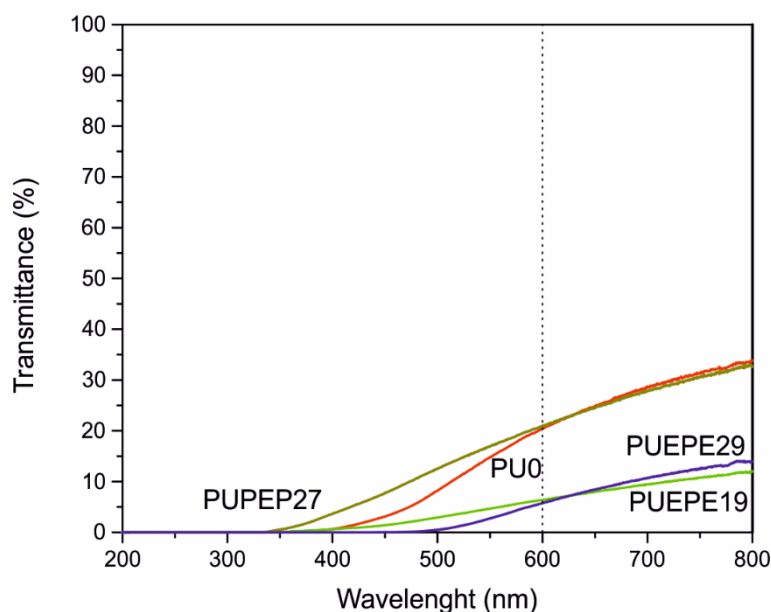


Figure 4.9. UV-visible spectra of synthesized triblock copolymers based waterborne poly(urethane-urea) films. PU0 was added for comparison.

PU0 and PUPEP27 exhibited similar transmittances, of 20 and 21%, respectively, at 600 nm wavelength. From this wavelength to lower ones the transmittance of PU0 decreased faster to 0%, approximately at 400 nm. The same occurred for synthesized PEO-b-PPO-b-PEO triblock copolymers based waterborne poly(urethane-urea) films, which displayed similar transmittances at 600 nm, ~6%. However, PUEPE29 reached 0% faster than PUEPE19. The latter one reached 0% transmittance at a similar wavelength to PU0, whereas the transmittance of PUEPE29 fell to 0% at 470 nm, meaning that it was opaque for violet and blue lights (380-490 nm).

Looking for an explanation for the transmittance of each synthesized waterborne poly(urethane-urea) film, there was a relation between their average particle size (Table 4.2) and their transmittance at 800 nm. The higher the average particle size the lower the transmittance at this wavelength^{55,56}. The fact that all investigated films presented 0% transmittance in the UV region makes them interesting materials for UV-shielding applications⁵⁷, particularly as coatings given the different colors they presented, as shown in Figure 4.3. These different colors were the result of the presence of chromophore groups in the structure of synthesized waterborne poly(urethane-urea)s, in fact the utilized chain-extender is frequently used as a precursor for the synthesis of azo-dyes⁵⁸.

4.5. Conclusions

According to the results obtained in the Chapter 4, the following conclusions can be extracted:

- Successful synthesis of organic solvent-free waterborne poly(urethane-urea)s consisting of PEO and PPO based triblock copolymers as macrodiols were carried out,
- The average particle size of investigated waterborne poly(urethane-urea) dispersions depended on the PEO block content,
- Different viscosities were obtained depending on the block formulation of the triblock copolymers,
- PPO-b-PEO-b-PPO triblock copolymers based waterborne poly(urethane-urea) dispersions presented lower viscosities due to the -CH₃ side groups

directly linked to MDI-SDBS segment. On the contrary, PEO-b-PPO-b-PEO triblock copolymers based waterborne poly(urethane-urea) dispersions displayed viscosities close to the one of PU0,

- PEO-b-PPO-b-PEO triblock copolymers based waterborne poly(urethane-urea) dispersions presented higher \bar{M}_w than PPO-b-PEO-b-PPO triblock copolymers based ones due to the favored accesibility of prepolymer based on PEO-b-PPO-b-PEO to the chain extender,
- Synthesized waterborne poly(urethane-urea) films based on triblock copolymers with lower molecular weights, which led to shorter soft segments, presented higher T_g values than the neat triblock copolymers,
- The morphology of synthesized triblock copolymers based wateborne poly(urethane-urea) films presented a well-defined microphase separation modulated by the thermodynamic incomopatibility between PEO and PPO blocks rather than hydrogen bonding interactions between domains,
- Mechanical properties of PEO-b-PPO-b-PEO triblock copolymers based waterborne poly(urethan-urea) films were higher than the ones of PPO-b-PEO-b-PPO triblock copolymers based waterborne poly(urethane-urea) films,
- The transmittance of investigated waterborne poly(urethane-urea) films depended on the average particle size. The transmittance at 800 nm wavelength was higher when the particle size was lower. All films possessed UV-shielding behavior,
- Synthesized waterborne poly(urethane-urea) films presented different colors, as a result of chromophore groups present in their structure, making them appealing for coating application.

4.6. Selection of synthesized waterborne poly(urethane-urea)s for novel applications

In the next Chapters, synthesized waterborne poly(urethane-urea)s were employed as matrices or basic components for prepared novel materials with different applications. Synthesized waterbone poly(urethane-urea)s used for each of these applications were selected taking the followed guidelines in consideration:

- Firstly, PU0 was selected as reference for all the novel applications,
- In the Chapter 5, one waterborne poly(urethane-urea) based on each of the two different triblock copolymer architectures (PEO-b-PPO-b-PEO and PPO-b-PEO-b-PPO) were selected for the preparation of nanocomposites for coating application. PUEPE19 and PUPEP27 triblock copolymers based waterborne poly(urethane-urea)s were the chosen ones since their presented better mechanical properties than PUEPE29 and PUPEP20,
- In the Chapter 7, hydrogels were prepared for application as biomaterials. PUEPE29 waterborne poly(urethane-urea) was selected due to its viscoelasticity,
- In the Chapter 8, application of synthesized waterborne poly(urethane-urea)s as adhesive is seek. After the evaluation of the adhesive performance of synthesized waterborne poly(urethane-urea)s, PU0 and PUEPE29 were employed for both blending and desiging of bilayer systems.

4.7. References

- [1] Y. Xiao, X. Fu, Y. Zhang, Z. Liu, L. Jiang, J. Lei, Preparation of waterborne polyurethanes based on the organic solvent-free process, *Green Chemistry* 18 (2016) 412-416.
- [2] M. J. O'Sickey, B. D. Lawrey, G. L. Wilkes, Structure-property relationships of poly(urethane urea)s with ultra-low monol content poly(propylene glycol) soft segments: I. Influence of soft segment molecular weight and hard segment content, *Journal of Applied Polymer Science* 84 (2002) 229-243.
- [3] O. Jaudouin, J. J. Robin, J. M. Lopez-Cuesta, D. Perrin, C. Imbert, Ionomer-based polyurethanes: a comparative study of properties and applications, *Polymer International* 61 (2012) 495-510.
- [4] Q. B. Meng, S. I. Lee, C. Nah, Y. S. Lee, Preparation of waterborne polyurethanes using an amphiphilic diol for breathable waterproof textile coatings, *Progress in Organic Coatings* 66 (2009) 382-386.
- [5] L. Ugarte, A. Saralegi, R. Fernández, L. Martín, M. A. Corcuera, A. Eceiza, Flexible polyurethane foams based on 100% renewably sourced polyols, *Industrial Crops and Products* 62 (2015) 545-551.
- [6] A. Noreen, K. M. Zia, M. Zuber, S. Tabasum, M. J. Saif, Recent trends in environmentally friendly water-borne polyurethane coatings: A review, *Korean Journal of Chemical Engineering* 33 (2016) 388-400.
- [7] J. O. Akindoyo, M. D. H. Beg, S. Ghazali, M. R. Islam, Polyurethane types, synthesis and applications - a review, *RSC Advances* 6 (2016) 114453-114482.
- [8] M. V. Pergal, Synthesis and characterization of novel urethane-siloxane copolymers with a high content of PCL-PDMS-PCL segments, *Journal of Applied Polymer Science* 122 (2011) 2715-2730.
- [9] L. Rueda-Larraz, B. F. d'Arlas, A. Tercjak, A. Ribes, I. Mondragon, A. Eceiza, Synthesis and microstructure-mechanical property relationships of segmented polyurethanes based on a PCL-PTHF-PCL block copolymer as soft segment, *European Polymer Journal* 45 (2009) 2096-2109.
- [10] R. S. Waletzko, L. S. T. James Korley, B. D. Pate, E. L. Thomas, P. T. Hammond, Role of increased crystallinity in deformation-induced structure of segmented thermoplastic polyurethane elastomers with PEO and PEO-PPO-PEO soft segments and HDI hard segments, *Macromolecules* 42 (2009) 2041-2053.
- [11] L. S. T. J. Korley, B. D. Pate, E. L. Thomas, P. T. Hammond, Effect of the degree of soft and hard segment ordering on the morphology and mechanical behavior of semicrystalline segmented polyurethanes, *Polymer* 47 (2006) 3073-3082.
- [12] P. N. Lan, S. Corneillie, E. Schacht, M. Davies, A. Shard, Synthesis and characterization of segmented polyurethanes based on amphiphilic polyether diols, *Biomaterials* 17 (1996) 2273-2280.
- [13] M. Yen, S. Kuo, PCL-PEG-PCL triblock ester-ether copolydiol-based waterborne polyurethane. II. Effect of NCO/OH mole ratio and DMPA content on the physical properties, *Journal of Applied Polymer Science* 67 (1997) 1301-1311.
- [14] M. Yen, S. Kuo, PCL-PEG-PCL triblock copolydiol-based waterborne polyurethane. I. Effects of the soft-segment composition, *Journal of Applied Polymer Science* 65 (1997) 883-892.
- [15] L. Cano, D. H. Builes, A. Tercjak, Morphological and mechanical study of nanostructured epoxy systems modified with amphiphilic poly(ethylene oxide-b-propylene oxide-b-ethylene oxide)triblock copolymer, *Polymer* 55 (2014) 738-745.

- [16] X. Liang, G. Mao, K. Y. S. Ng, Effect of chain lengths of PEO-PPO-PEO on small unilamellar liposome morphology and stability: An AFM investigation, *Journal of Colloid and Interface Science* 285 (2005) 360-372.
- [17] S. Liu, H. Bao, L. Li, Role of PPO-PEO-PPO triblock copolymers in phase transitions of a PEO-PPO-PEO triblock copolymer in aqueous solution, *European Polymer Journal* 71 (2015) 423-439.
- [18] S. Liu, L. Li, Molecular interactions between PEO-PPO-PEO and PPO-PEO-PPO triblock copolymers in aqueous solution, *Colloids and Surfaces A: Physicochemical and Engineering Aspects* 484 (2015) 485-497.
- [19] N. Liu, Y. Zhao, M. Kang, J. Wang, X. Wang, Y. Feng, N. Yin, Q. Li, The effects of the molecular weight and structure of polycarbonatediols on the properties of waterborne polyurethanes, *Progress in Organic Coatings* 82 (2015) 46-56.
- [20] V. García-Pacios, J.A. Jofre-Reche, V. Costa, M. Colera, J. M. Martín-Martínez, Coatings prepared from waterborne polyurethane dispersions obtained with polycarbonates of 1,6-hexanediol of different molecular weights, *Progress in Organic Coatings* 76 (2013) 1484-1493.
- [21] M. Yen, Effect of soft segment composition on the physical properties of nonionic aqueous polyurethane containing side chain PEGME, *Journal of Applied Polymer Science* 105 (2007) 1391-1399.
- [22] J. H. Silver, E. Karayianni, S. L. Cooper, Effect of polyol hydrophilicity on the structure and anticoagulant activity of water-soluble sulfonated polyurethanes, *Journal of Colloid and Interface Science* 178 (1996) 219-232.
- [23] D. K. Lee, H. B. Tsai, R. S. Tsai, Effect of composition on aqueous polyurethane dispersions derived from polycarbonatediols, *Journal of Applied Polymer Science* 102 (2006) 4419-4424.
- [24] S. L. Chang, T. L. Yu, C. C. Huang, W. C. Chen, K. Linliu, T. L. Lin, Effect of polyester side-chains on the phase segregation of polyurethanes using small-angle X-ray scattering, *Polymer* 39 (1998) 3479-3489.
- [25] X. Liu, K. Xu, H. Liu, H. Cai, J. Su, Z. Fu, Y. Guo, M. Chen, Preparation and properties of waterborne polyurethanes with natural dimer fatty acids based polyester polyol as soft segment, *Progress in Organic Coatings* 72 (2011) 612-620.
- [26] V. K. Syal, A. Chauhan, S. Chauhan, Ultrasonic velocity, viscosity and density studies of poly (ethylene glycols)(PEG-8,000, PEG-20,000) in acetonitrile (AN) and water (H₂O) mixtures at 25°C), *Journal of Pure and Applied Ultrasonics* 27 (2005) 61-69.
- [27] H. Lijie, D. Yongstao, Z. Zhiliang, S. Zhongsheng, S. Zhihua, Synergistic effect of anionic and nonionic monomers on the synthesis of high solid content waterborne polyurethane, *Colloids and Surfaces A: Physicochemical and Engineering Aspects* 467 (2015) 46-56.
- [28] V. García-Pacios, V. Costa, M. Colera, J. Miguel Martín-Martnez, Affect of polydispersity on the properties of waterborne polyurethane dispersions based on polycarbonate polyol, *International Journal of Adhesion and Adhesives* 30 (2010) 456-465.
- [29] A. Santamaría-Echart, A. Arbelaiz, A. Saralegi, B. Fernández-d'Arlas, A. Eceiza, M. A. Corcuera, Relationship between reagents molar ratio and dispersion stability and film properties of waterborne polyurethanes, *Colloids and Surfaces A: Physicochemical and Engineering Aspects* 482 (2015) 554-561.

- [30] S. M. Cakic, I. S. Ristic, M. Marinovic-Cincovic, M. Spirkova, The effects of the structure and molecular weight of the macrodiol on the properties polyurethane anionic adhesives, *International Journal of Adhesion and Adhesives* 41 (2013) 132-139.
- [31] S. Zhang, Z. Ren, S. He, Y. Zhu, C. Zhu, FTIR spectroscopic characterization of polyurethane-urea model hard segments (PUUMHS) based on three diamine chain extenders, *Spectrochimica Acta Part A: Molecular and Biomolecular Spectroscopy* 66 (2007) 188-193.
- [32] Z. Gao, J. Peng, T. Zhong, J. Sun, X. Wang, C. Yue, Biocompatible elastomer of waterborne polyurethane based on castor oil and polyethylene glycol with cellulose nanocrystals, *Carbohydrate Polymers* 87 (2012) 2068-2075.
- [33] M. Villani, J. Scheerder, R. A. T. M. Van Benthem, G. De With, Interfacial interactions of poly(urethane-urea) based primers with polypropylene, *European Polymer Journal* 56 (2014) 118-130.
- [34] J. Mattia, P. Painter, A comparison of hydrogen bonding and order in a polyurethane and poly(urethane-urea) and their blends with poly(ethylene glycol), *Macromolecules* 40 (2007) 1546-1554.
- [35] A. Pegoretti, L. Fambri, A. Penati, J. Kolarik, Hydrolytic resistance of model poly(ether urethane ureas) and poly(ester urethane ureas), *Journal of Applied Polymer Science* 70 (1998) 577-586.
- [36] D. J. Hourston, G. Williams, R. Satguru, J. D. Padget, D. Pears, Structure-property study of polyurethane anionomers based on various polyols and diisocyanates, *Journal of Applied Polymer Science* 66 (1997) 2035-2044.
- [37] S. M. Cakic M. Spirkova, I. S. Ristic, J. K. B. Simendic, M. M. Cincovic, R. Poreba, The waterborne polyurethane dispersions based on polycarbonate diol: Effect of ionic content, *Materials Chemistry and Physics* 138 (2013) 277-285.
- [38] L. Ugarte, B. Fernandez-d'Arlas, A. Valea, M. L. Gonzalez, M. A. Corcuera, A. Eceiza, Morphology-properties relationship in high-renewable content polyurethanes, *Polymer Engineering and Science* 47 (2007) 21-25.
- [39] Da-Kong Lee, H. B. Tsai, Z. D. Yang, R. S. Tsai, Polyurethane dispersions derived from polycarbonatediols by a solvent-free process, *Journal of Applied Polymer Science* 126 (2012) E275-E282.
- [40] A. Santamaria-Echart, I. Fernandes, L. Ugarte, F. Barreiro, A. Arbelaiz, M. A. Corcuera, A. Eceiza, Waterborne polyurethane-urea dispersion with chain extension step in homogeneous medium reinforced with cellulose nanocrystals, *Composites Part B: Engineering* 137 (2018) 31-38.
- [41] H. Liu, S. Cui, S. Shang, D. Wang, J. Song, Properties of rosin-based waterborne polyurethanes/cellulose nanocrystals composites, *Carbohydrate Polymers* 96 (2013) 510-515.
- [42] B. K. Kim, Y. M. Lee, Structure-property relationship of polyurethane ionomer, *Colloid and Polymer Science* 270 (1992) 956-961.
- [43] D. J. Martin, G. F. Meijs, G. M. Renwick, S. J. McCarthy, P. A. Gunatillake, The effect of average soft segment length on morphology and properties of a series of polyurethane elastomers. I. Characterization of the series, *Journal of Applied Polymer Science* 62 (1996) 1377-1386.
- [44] Y. Lu, R. C. Larock, Soybean-oil-based waterborne polyurethane dispersions: effects of polyol functionality and hard segment content on properties, *Biomacromolecules* 9 (2008) 3332-3340.

- [45] T. Calvo-Correas, M. D. Martin, A. Retegi, N. Gabilondo, M. A. Corcuera, A. Eceiza, Synthesis and characterization of polyurethanes with high renewable carbon content and tailored properties, *ACS Sustainable Chemistry and Engineering* 4 (2016) 5684-5692.
- [46] S. M. Cakić, I. S. Ristić, I. Krakovský, D. T. Stojiljković, P. Bělský, L. Kollová, Crystallization and thermal properties in waterborne polyurethane elastomers: Influence of mixed soft segment block, *Materials Chemistry and Physics* 144 (2014) 31-40.
- [47] P. Majumdar, D. C. Webster, Preparation of siloxane-urethane coatings having spontaneously formed stable biphasic microtopographical surfaces, *Macromolecules* 38 (2005) 5857-5859.
- [48] A. Karim, T. M. Slaweki, S. K. Kumar, J. F. Douglas, S. K. Satija, C. C. Han, T. P. Russell, Y. Liu, R. Overney, J. Sokolov, M. H. Rafailovich, Phase-separation-induced surface patterns in thin polymer blend films, *Macromolecules* 31 (1998) 857-862.
- [49] C. Yang, J. Li, Thermoresponsive behavior of cationic polyrotaxane composed of multiple pentaethylenhexamine-grafted α -cyclodextrins threaded on poly(propylene oxide)-poly(ethylene oxide)-poly(propylene oxide) triblock copolymer, *The Journal of Physical Chemistry B* 113 (2009) 682-690.
- [50] Q. Wang, L. Li, S. Jiang, Effects of a PPO-PEO-PPO triblock copolymer on micellization and gelation of a PEO-PPO-PEO triblock copolymer in aqueous solution, *Langmuir* 21 (2005) 9068-9075.
- [51] A. Ganguly, A. K. Bhowmick, Effect of polar modification on morphology and properties of styrene-(ethylene-co-butylene)-styrene triblock copolymer and its montmorillonite clay-based nanocomposites, *Journal of Materials Science* 44 (2009) 903-918.
- [52] A. Bahadur, A. Saeed, S. Iqbal, M. Shoaib, M. S. ur Rahman, M. I. Bashir, M. Asghar, M. A. Ali, T. Mahmood, Biocompatible waterborne polyurethane-urea elastomer as intelligent anticancer drug release matrix: A sustained drug release study, *Reactive and Functional Polymers* 119 (2017) 57-63.
- [53] X. Jiang, J. Li, M. Ding, H. Tan, Q. Ling, Y. Zhong, Q. Fu, Synthesis and degradation of nontoxic biodegradable waterborne polyurethanes elastomer with poly(ϵ -caprolactone) and poly(ethylene glycol) as soft segment, *European Polymer Journal* 42 (2007) 1838-1846.
- [54] B. Fernández-D'Arlas, J. A. Ramos, A. Saralegi, M. Corcuera, I. Mondragon, A. Eceiza, Molecular engineering of elastic and strong supertough polyurethanes, *Macromolecules* 45 (2012) 3436-3443.
- [55] J. L. Zhang, D. M. Wu, D. Y. Yang, F. X. Qiu, Environmentally friendly polyurethane composites: Preparation, characterization and mechanical properties, *Journal of Polymers and the Environment* 18 (2010) 128-134.
- [56] X. Cao, X. Ge, H. Chen, W. Li, Effects of trimethylol propane and AAS salt on properties of waterborne polyurethane with low gloss, *Progress in Organic Coatings* 107 (2017) 5-13.
- [57] B. Xu, H. Li, Y. Wang, G. Zhang, Q. Zhang, High strength nanocomposite hydrogels with outstanding UV-shielding property, *Polymer Composites* 37 (2016) 810-817.
- [58] G. H. Elgemeie, M. H. Helal, H. M. El-Sayed, Recent trends in synthesis and application of nitrogen heterocyclic azo dyes, *Pigment & Resin Technology* 30 (2001) 210-228.

Chapter

5

"It is only with the heart that one can see rightly; what is essential is invisible to the eye."

(Antoine de Saint-Exupery)

Nanocomposites prepared by incorporation of TiO₂ nanoparticles into waterborne poly(urethane-urea)s

5. Nanocomposites prepared by incorporation of TiO₂ nanoparticles to waterborne poly(urethane-urea)s

5.1. Chapter overview	105
5.2. Introduction	105
5.3. Preparation of nanocomposites by <i>ex-situ</i> addition of TiO₂ nanoparticles	106
5.4. Characterization of prepared nanocomposites	107
5.4.1. Nanocomposites by incorporation of TiO ₂ nanoparticle to PU0	107
5.4.2. Nanocomposites by incorporation of TiO ₂ nanoparticle to triblock copolymers based waterborne poly(urethane-urea)s	115
5.5. Conclusions	124
5.6. References	126

5.1. Chapter overview

The aim of this Chapter is to prepare different nanocomposites by *ex-situ* incorporation of TiO₂ nanoparticles into selected synthesized waterborne poly(urethane-urea)s developed in the Chapters 3 and 4. The main objective of the investigation work presented in this Chapter is to study the effect of the incorporation of inorganic nanoparticles on the final properties of designed nanocomposites.

In the first section, the preparation and characterization of the nanocomposites based on waterborne poly(urethane-urea)s synthesized using PEO homopolymer (PU0) are described. The second section is focused on the preparation and characterization of nanocomposites based on waterborne poly(urethane-urea)s synthesized using triblock copolymers (PUEPE19 and PUPEP27).

5.2. Introduction

Recently research on nanocomposite materials, in which fillers at the nanosize are dispersed in a polymer matrix¹, has attracted great attention as a consequence of their wide fields of applications, ranging from batteries, sensors, transistors and solar cells to biomedicine, gas separation and water purification, among others¹⁻³. The attractive properties of these materials are due to the synergistic effect that takes place between the nanofiller and the polymer matrix^{4,5}. The final properties of the nanocomposites essentially depend on both the nanofiller and the matrix⁶. It is for this reason that different nanofillers and matrices have been studied. Among polymer matrices, incorporation of nanofillers to waterborne polyurethanes and poly(urethane-urea)s is of considerable interest since, besides providing the polymeric matrix with novel properties, they can improve the commonly inferior properties^{5,7,8} of these polymeric matrices.

Some research has already been carried out on the incorporation of different kinds of nanofillers into waterborne polyurethanes, such as silica clays^{4,9,10}, graphene¹¹, Au¹², Ag⁸, CaCO₃¹³, Fe₃O₄¹⁴ and TiO₂¹⁵⁻¹⁷. These last ones are appealing considering that they are environmentally friendly, chemically inert and possess high photostability and photocatalytic activity^{14,15}. In addition, they can improve the mechanical

properties of waterborne polyurethanes and poly(urethane-urea)s at the same time that showing a higher resistance to UV radiation^{18,19}. TiO₂ nanoparticles, which are n-type semiconducting, can even provide the nanocomposite with electrical conductivity^{5,20}.

One of the main challenge in the process of designing new nanocomposites is the control of the dispersion of nanofillers in the polymer matrix. This problem arises as a consequence of the large surface area/particle size ratio^{13,15} and the high surface tension¹³ of the nanofiller. All this adds up to the incompatibility between the inorganic nanoparticles and the polymer matrix¹³. This all leads to the formation of agglomerations, or even clusters, as the result of the tendency of nanoparticles to aggregate^{13,15}. In order to overcome this and to obtain a proper dispersion, sol-gel process^{4,5} and dispersion by ultrasonication^{15,21} are the most commonly used methods. Nonetheless, from an industrial point of view, simpler procedures, as they are mechanical and magnetic stirring, would be desired¹⁷. This could be achieved conceiving a suitable strategy using the same solvent to disperse both the inorganic nanoparticles and the polymer matrix. This would favor the dispersion of nanoparticles within the polymer matrix just by mechanical or magnetic stirring.

5.3. Preparation of nanocomposites by *ex-situ* incorporation of TiO₂ nanoparticles

For the preparation of the nanocomposites, a commercial aqueous solution of TiO₂ nanoparticles (specified in the Chapter 2) was *ex-situ* physically mixed, by magnetic stirring, with synthesized waterborne poly(urethane-urea) dispersions. The density and the solid content of the commercial aqueous solution of TiO₂ nanoparticles as well as the solid content of synthesized waterborne poly(urethane-urea) dispersions were taken into account for the preparation of these nanocomposites. Three different TiO₂ weight content nanocomposites (10, 20 and 40 wt%) were prepared for each of the selected three waterborne poly(urethane-urea) matrices. The samples were denoted as PU0, PUEPE19 and PUPEP27, as in the Chapter 4, for the matrices without inorganic nanoparticles. Nanocomposites were denoted as XTiO₂-PU0, XTiO₂-PUEPE19 and XTiO₂-PUPEP27, where X can be correlated to the TiO₂ wt% content.

For the physical mixing of synthesized waterborne poly(urethane-urea) dispersions and the commercial aqueous solution of TiO₂ nanoparticles, a magnetic stir bar was used to keep the mixture stirring for 24 h at 500 rpm (Figure 5.1). White homogeneous dispersions were obtained.

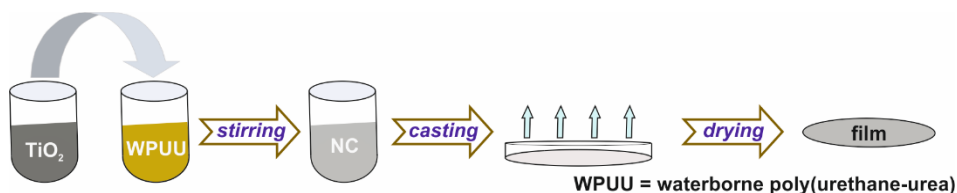


Figure 5.1. Schematic description of the procedure for the preparation of the nanocomposites.

5.4. Characterization of nanocomposites

5.4.1. Nanocomposites by incorporation of TiO₂ nanoparticles into PU0

The chemical structure, studied by FTIR, of TiO₂-PU0 nanocomposites was very similar to the one of the PU0, as shown in Figure 5.2. In the different spectra the characteristic absorbance bands that appeared at 3500-3000 cm⁻¹ corresponded to the stretching vibrations of N-H groups^{8,12,13,17}, either hydrogen bonded¹² or free¹³.

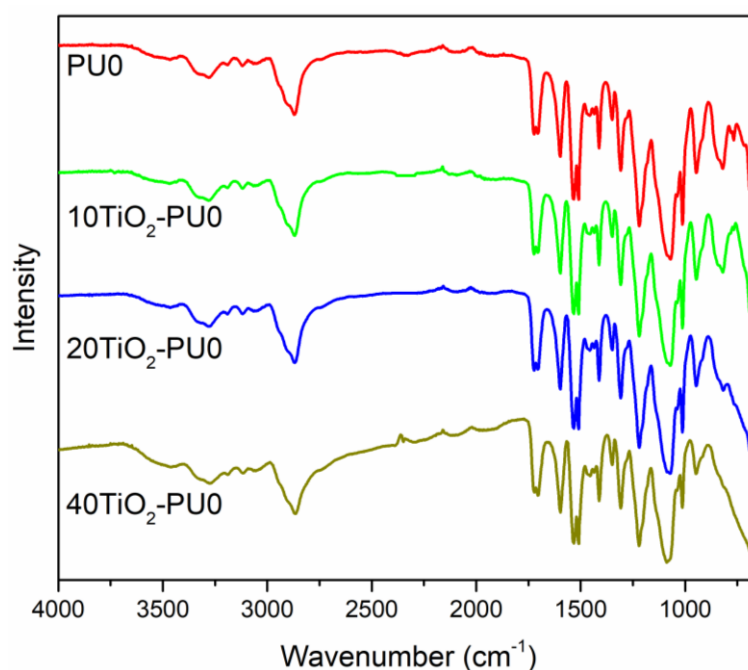


Figure 5.2. FTIR spectra of neat PU0 and TiO₂-PU0 nanocomposite films.

In the region of 1750-1650 cm^{-1} , the bands associated to the stretching vibrations of hydrogen bonded and free carbonyl groups²² from urea and urethane^{12,13,17} did not vary with the increase of the TiO_2 nanoparticles content. Nonetheless, in the case of 40 TiO_2 -PU0 an inversion between the intensities of hydrogen bonded and free carbonyl groups can be appreciated. This would suggest that increasing TiO_2 nanoparticles content resulted in an increase of the interactions between TiO_2 nanoparticles and hard segment. The absorbance band at 1100 cm^{-1} corresponded to the stretching vibration of the ether group of PEO^{13,17}.

As mentioned so far, FTIR spectra of TiO_2 -PU0 nanocomposites were almost identical to the one of PU0, however a change can be appreciated in the region under 800 cm^{-1} . The absorbance band at this wavelength was associated to Ti-O-Ti^{17,23,24}. This band broadened as the TiO_2 nanoparticles content increased, confirming their incorporation into the polymer matrix.

The T_g values of investigated TiO_2 -PU0 nanocomposite films, obtained from the DSC curves (Figure 5.3), are displayed in Table 5.1 and were under room temperature and below the one corresponding to neat PU0 film.

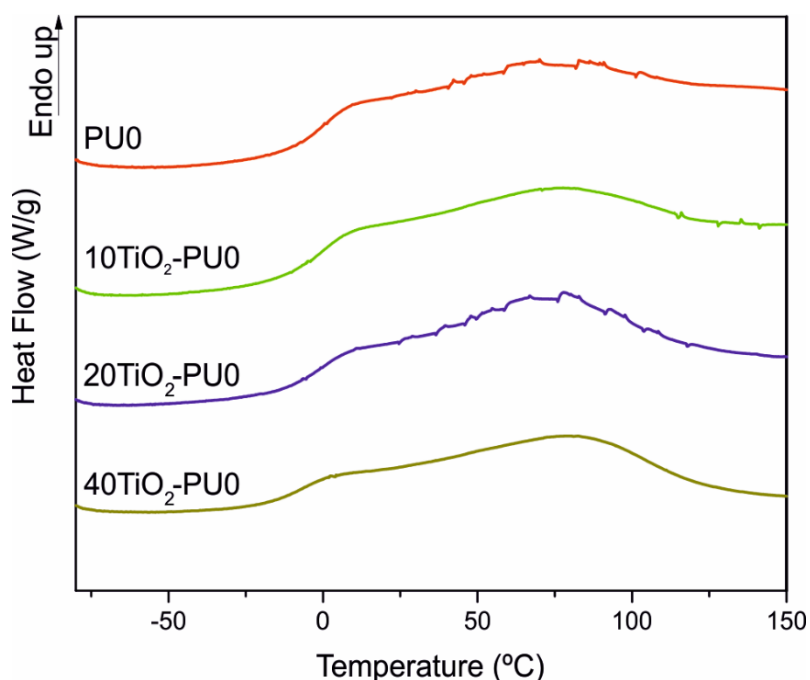


Figure 5.3. DSC curves of neat PU0 and TiO_2 -PU0 nanocomposite films.

The incorporation of TiO₂ nanoparticles led to a slight decrease in the T_g of TiO₂-PU0 nanocomposite films. This decrease was especially noticeable in the case of 40TiO₂-PU0 film, where T_g shifted 7 °C to lower temperature if compare to the T_g of 20TiO₂-PU0 film. This all pointed out to an increase in the mobility of the soft segment chains⁴, as the observed T_g is related to that segment. This increase in the mobility could arise from an increase in the interactions between TiO₂ nanoparticles and the polymer chains^{25,26}, particularly with the hard segment, reducing the interactions between the hard and the soft segment of PU0, herein increasing the mobility of the soft segment, in agreement with the FTIR analysis. In addition, the remarkable decrease in T_g that took place for 40TiO₂-PU0 film can be explained by increasing interactions between TiO₂ nanoparticles.

Table 5.1. Glass transition temperature (T_g) of neat PU0 and TiO₂-PU0 nanocomposite films.

Sample	T_g (°C)
PU0	7
10TiO₂-PU0	-1
20TiO₂-PU0	-1
40TiO₂-PU0	-8

Thermal stability of PU0 and TiO₂-PU0 nanocomposite films was studied by means of TGA. Figure 5.4 shows the TGA and dTGA curves and the information obtained from the curves is displayed in Table 5.2. As can be extracted from both Figure 5.4 and Table 5.2, the thermal stability decreased when TiO₂ nanoparticles were incorporated into PU0.

As can be observed in Figure 5.4, the degradation process of PU0 and TiO₂-PU0 nanocomposite films occurred in two steps. The first one, T₁, took place between 302 and 323 °C and corresponded to the degradation of the hard segment, whereas the second step, T₂, related to the soft segment¹⁴, happened between 394 and 406 °C. The decline in the thermal stability can be a consequence of interactions between TiO₂ nanoparticles²⁷, enhanced with the increase of TiO₂ nanoparticles content and the decrease of interactions between hard and soft segments, promoting particularly the decrease of T₂. The increase in the stability of T₁ from 20TiO₂-PU0 to 40TiO₂-PU0 can be the result of an increase in the interactions that took place between TiO₂

nanoparticles and the hard segment⁴, as previously observed by FTIR and DSC analysis.

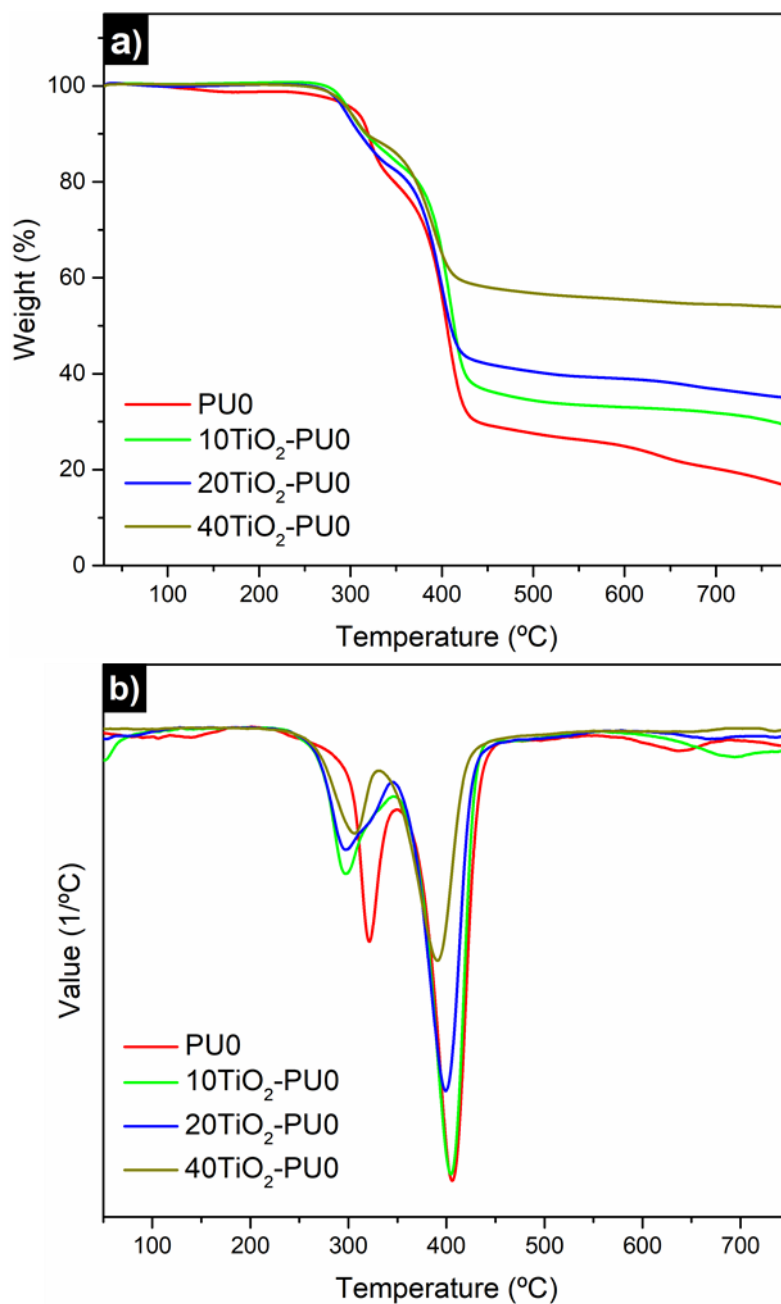


Figure 5.4. (a) Thermogravimetric analysis and (b) dTGA curves of neat PU0 and TiO₂-PU0 nanocomposite films.

Regarding the TiO₂ nanoparticles content, displayed in Table 5.2, it was calculated from the differences between residues of TiO₂-PU0 nanocomposite films and neat PU0 film.

Table 5.2. Decomposition temperatures of hard (T₁) and soft (T₂) segments as well as TiO₂ nanoparticles content of neat PU0 and TiO₂-PU0 nanocomposite films.

Sample	T ₁ ^a (°C)	T ₂ ^a (°C)	TiO ₂ nanoparticles content ^b (wt%)
PU0	323	406	0
10TiO ₂ -PU0	302	403	13
20TiO ₂ -PU0	302	402	18
40TiO ₂ -PU0	311	394	37

a) Temperature determined from dTGA curves (Figure 5.4b).

b) Calculated from residues of TGA curves (Figure 5.4a).

The morphology of PU0 and TiO₂-PU0 nanocomposite films was studied by AFM and is shown in Figure 5.5. OM micrographs of investigated films were also added to Figure 5.5 in order to confirm that TiO₂-PU0 nanocomposite films did not present any agglomeration of TiO₂ nanoparticles at the microscopic scale. The morphology obtained for the neat PU0 film was the same as the one obtained for PU0 batches discussed in the Chapters 3 and 4. Thus, any phase separation of soft and hard segments were detected.

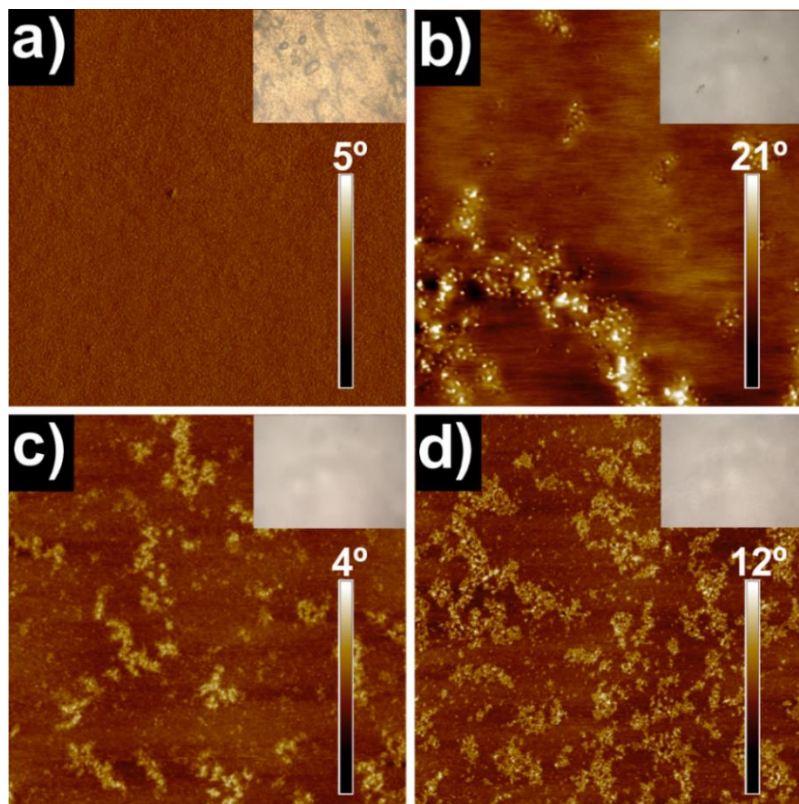


Figure 5.5. AFM phase images (3 μm x 3 μm) of investigated (a) PU0, (b) 10TiO₂-PU0, (c) 20TiO₂-PU0 and (d) 40TiO₂-PU0 films. The inset in each AFM image corresponds to OM micrograph.

The outcome of the observed lack of phase separation was that the polymer matrix acted as a homopolymer for TiO₂ nanoparticles, in agreement with the previously mentioned interactions between the hard segment and TiO₂ nanoparticles. Furthermore, TiO₂ nanoparticles were dispersed throughout the polymer matrix forming nanoclusters²⁸. This was the result of the tendency of TiO₂ nanoparticles to interact between each other¹⁵. This supports the conclusions drawn from the analysis of the thermal properties and thermal stability.

As can be clearly observed in AFM images, the number of nanoclusters increased with the increase in TiO₂ nanoparticles content. Nonetheless, even if nanoclusters were formed, neither OM nor AFM images showed agglomeration of TiO₂ nanoparticles. Some of the nanoclusters were interconnected²⁸, what could create a percolation path⁶ leading to conductivity at a macroscopic level given the electrical properties of TiO₂ nanoparticles.

EFM was used in order to investigate if TiO₂ nanoparticles maintained their electrical properties when embedded in the PU0 matrix. The obtained EFM images as well as the AFM images obtained at the same time are displayed in Figure 5.6. EFM is a practical qualitative technique to analyze the electric field gradient above investigated nanocomposite films, which allows distinguishing conductive areas of the sample by applying different positive and negative voltages^{29,30}. In all cases, a 0 V bias was applied to ensure that there was not influence of the topography of the surface. The noticed absence of charged domains confirmed that the conditions for EFM measurements were correctly selected^{30,31}. TiO₂ nanoparticles were the only conductive component in investigated TiO₂-PU0 nanocomposites³ and they were visualized when applying positive and negative bias of 6 and 9 V. The higher the voltage the higher the contrast between the locally charged TiO₂ nanoparticles and the nonconductive polymer matrix, as it is clearly visualized in the EFM phase images of each investigated sample.

In consideration of these results, it can be concluded that TiO₂ nanoparticles conserved their electrical properties when embedded in the PU0 matrix. Considering also the interconnected nanoclusters observed in AFM images, investigated TiO₂-PU0

nanocomposites may possess conductive behavior and they might be potential materials to be used in semiconductor applications⁶.

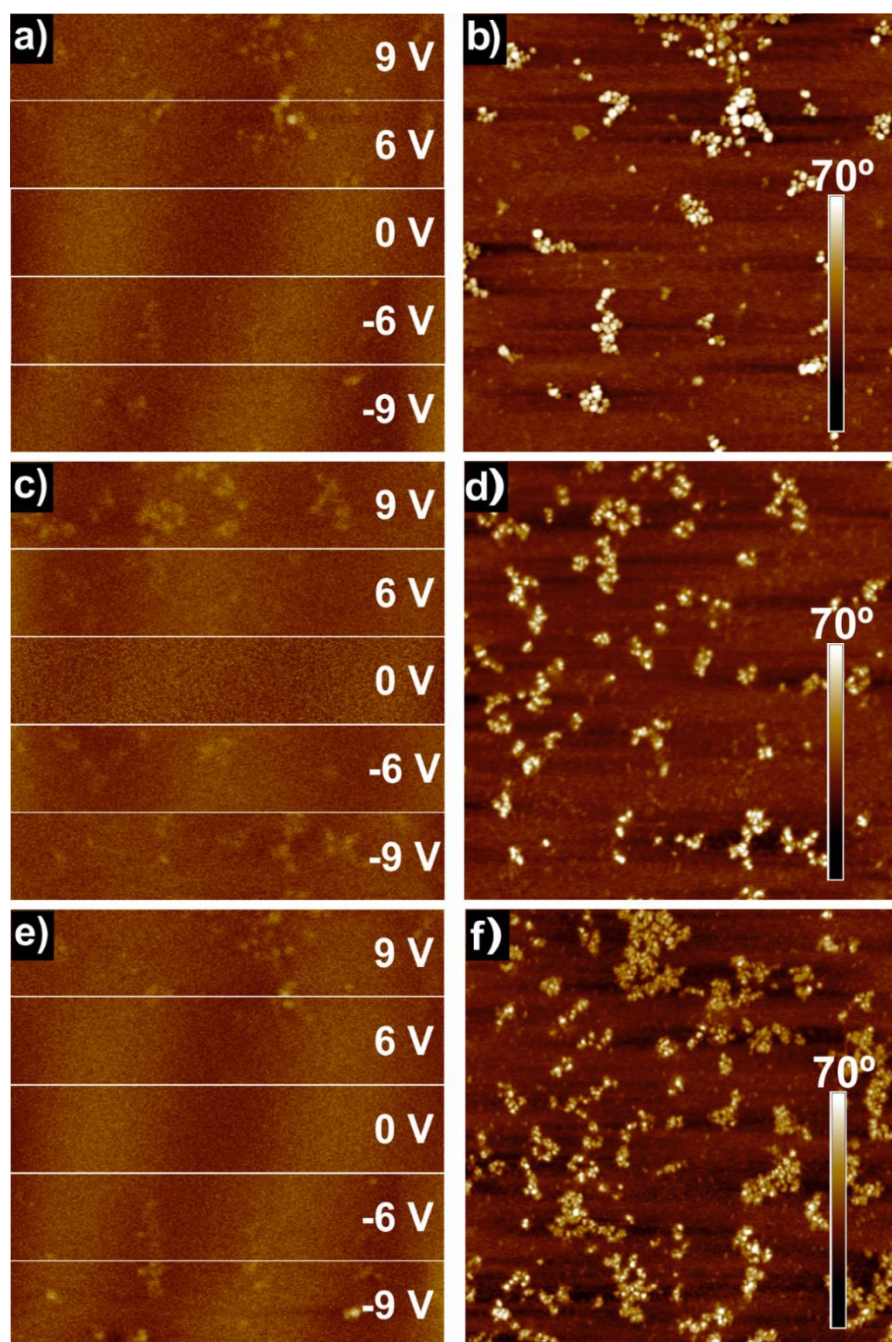


Figure 5.6. EFM phase images (3 μm x 3 μm) of investigated (a) 10TiO₂-PU0, (c) 20TiO₂-PU0, (e) 40TiO₂-PU0 films and their simultaneously obtained AFM phase images (3 μm x 3 μm).

The contact angles of investigated neat PU0 and TiO₂-PU0 nanocomposite films were determined by static WCA and are displayed in Table 5.3. The incorporation of TiO₂ nanoparticles led to a slight increase in the contact angle. It was expected that TiO₂-PU0 nanocomposite films showed a higher hydrophilicity than neat PU0 film taking

into account the hydrophilic nature of TiO₂ nanoparticles^{32,33}. Nevertheless, this hydrophilic nature of TiO₂ nanoparticles did not affect the hydrophilicity of the prepared nanocomposites until the addition of 40 wt% TiO₂ nanoparticles into PU0.

Table 5.3. Contact angle of investigated neat PU0 and TiO₂-PU0 nanocomposite films.

Sample	Contact angle (°)
PU0	62 ± 7
10TiO ₂ -PU0	66 ± 9
20TiO ₂ -PU0	66 ± 7
40TiO ₂ -PU0	56 ± 5

Finally, regarding neat PU0 and TiO₂-PU0 nanocomposite films, their mechanical properties were studied. For this purpose, tensile test was carried out and the values shown in Table 5.4 were determined from the obtained stress-strain curves.

Table 5.4. Young's modulus (E), tensile strength (σ_{max}), stress at break (σ_b), and deformation at break (ϵ_b) of investigated neat PU0 and TiO₂-PU0 nanocomposite films.

Sample	E (MPa)	σ_{max} (MPa)	σ_b (MPa)	ϵ_b (%)
PU0	6.2 ± 1.7	1.5 ± 0.2	0.7 ± 0.1	490 ± 90
10TiO ₂ -PU0	12.6 ± 2.2	1.6 ± 0.3	1.0 ± 0.2	289 ± 20
20TiO ₂ -PU0	25.0 ± 10.4	2.2 ± 0.3	1.3 ± 0.3	298 ± 50
40TiO ₂ -PU0	41.9 ± 9.1	2.6 ± 0.4	2.0 ± 0.6	200 ± 73

The increase of the TiO₂ nanoparticles content in nanocomposites provoked the increase in the modulus, tensile strength and stress at break. The increase in the Young's modulus was of almost 700% for 40TiO₂-PU0 nanocomposite film if compare to the Young's modulus of the neat PU0 film. This was thanks to TiO₂ nanoparticles acting as a reinforcement¹⁶. If compare to the neat PU0 film, the modulus increased a 100% in the case of 10TiO₂-PU0 film, further doubling for 20TiO₂-PU0 film. Notwithstanding, the incorporation of TiO₂ nanoparticles resulted in a diminishing of the deformation at break. Addition of 10 wt% of TiO₂ nanoparticles reduced the elongation at break by a noticeable 40%. A further increase in the TiO₂ nanoparticles content decreased slightly the deformation at break, reaching a deformation of 200% for 40TiO₂-PU0 film, being more than two times lower than the one of the neat PU0

film (~ 500%). These results meant that the incorporation of TiO₂ nanoparticles produced more rigid films than the neat PU0 film since incorporated TiO₂ nanoparticles, as mentioned before, acted as reinforcement for the polymer matrix¹⁶.

5.4.2. Nanocomposites by incorporation of TiO₂ nanoparticles to triblock copolymers based waterborne poly(urethane-urea)s

FTIR spectra of TiO₂-PUEPE19 and TiO₂-PUPEP27 nanocomposite films are shown in Figure 5.7.

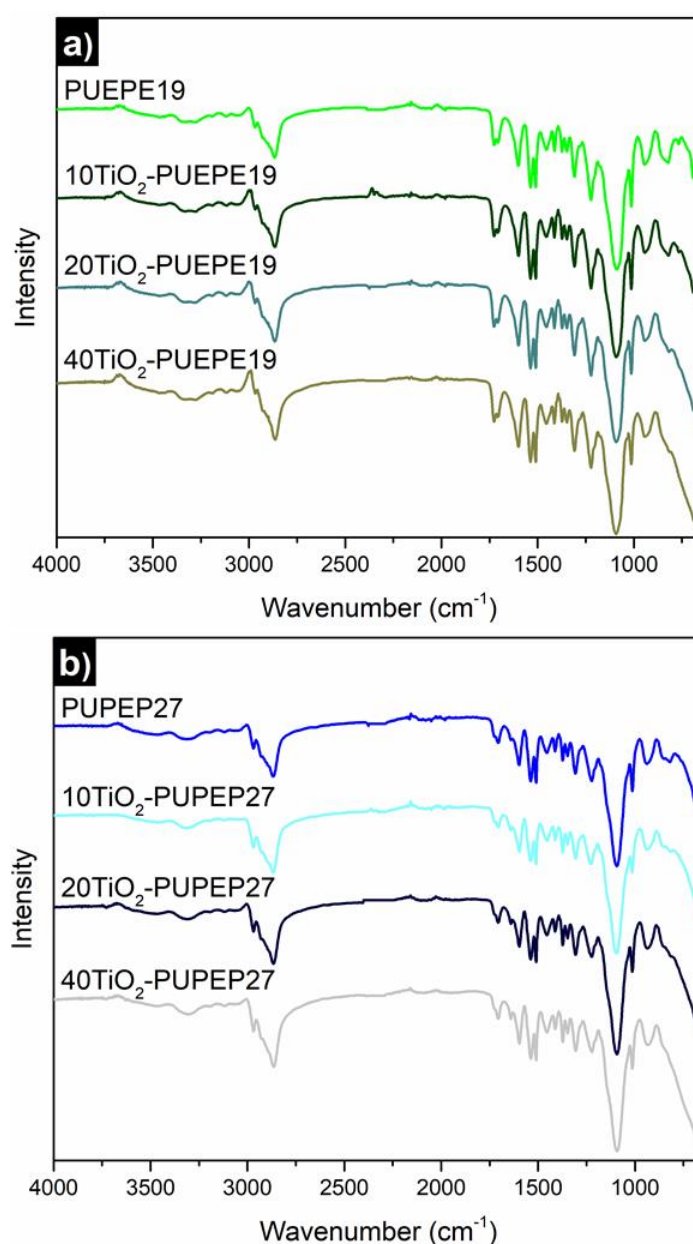


Figure 5.7. FTIR spectra of investigated (a) TiO₂-PUEPE19 and (b) TiO₂-PUPEP27 nanocomposite films. Neat PUEPE19 and PUPEP7 were added for comparison.

FTIR spectra of nanocomposite films did not present significant variations if compared to the FTIR spectra of neat PUEPE19 and PUPEP27 films, as in the case of FTIR spectra of TiO₂-PU0 nanocomposite films discussed previously.

Same bands mentioned in section 5.4.1 can be observed in FTIR spectra of TiO₂-PUEPE19 and TiO₂-PUPEP27 nanocomposite films. These were the ones related to the stretching vibrations of hydrogen and non-hydrogen bonded N-H groups^{8,12,13,17}, at 3500-3200 cm⁻¹, and the ones associated to the stretching vibrations of C=O groups^{12,13,17,22}, at 1700-1600 cm⁻¹. Around 1100 cm⁻¹ appeared the bands corresponding to the stretching vibrations of C-O-C groups^{13,17}, which were two in the case of the triblock copolymers, for both PEO and PPO blocks.

FTIR spectra of TiO₂-PUEPE19 and TiO₂-PUPEP27 nanocomposite films presented a band around 800 cm⁻¹ that widened with the increase of the TiO₂ nanoparticles content. This band was associated to Ti-O-Ti stretching vibrations^{17,23}.

In Figure 5.8, the DSC heating curves obtained for neat PUEPE19 and PUPEP27 as well as TiO₂-PUEPE19 and TiO₂-PUPEP27 nanocomposite films are shown, while the data obtained from the curves are displayed in Table 5.5.

First, it can be mentioned that T_g values of nanocomposite films were very similar to the ones corresponding to neat PUEPE19 and PUPEP27 films. Nevertheless, slight changes occurred when adding TiO₂ nanoparticles. Changes that were different depending on the waterborne poly(urethane-urea) used as the matrix. In the cases of TiO₂-PUEPE19 nanocomposite films, T_g slightly increased with the increase of the TiO₂ nanoparticles content. On the contrary, for TiO₂-PUPEP27 nanocomposite films an increase in the TiO₂ nanoparticles content led to a small decrease of T_g. Since an increase in T_g is commonly associated to a decrease in the mobility of the polymer chains^{34,35}, these results suggested that interactions of TiO₂ nanoparticles with the PUEPE19 matrix took place in a greater extent than with the PUPEP27 matrix^{25,26}. This was probably due to the differences in compatibility between TiO₂ nanoparticles and the matrices³⁶, result of the different block configurations of PEO and PPO blocks in each triblock copolymer (see the Chapter 4 for more details), which affected interaction of TiO₂ nanoparticles with these different matrices. This would suggest that for PUEPE19 interactions between TiO₂ nanoparticles and both the hard and the

soft segment were possible. On the contrary, -CH₃ side chains of PPO in the case of PPO-b-PEO-b-PPO triblock copolymer, which are directly linked to the hard segment, would hinder interactions between the soft segment and TiO₂ nanoparticles in the case of PUPEP27, thus promoting interactions between TiO₂ nanoparticles and the hard segment. This would have increased the mobility of the soft segment.

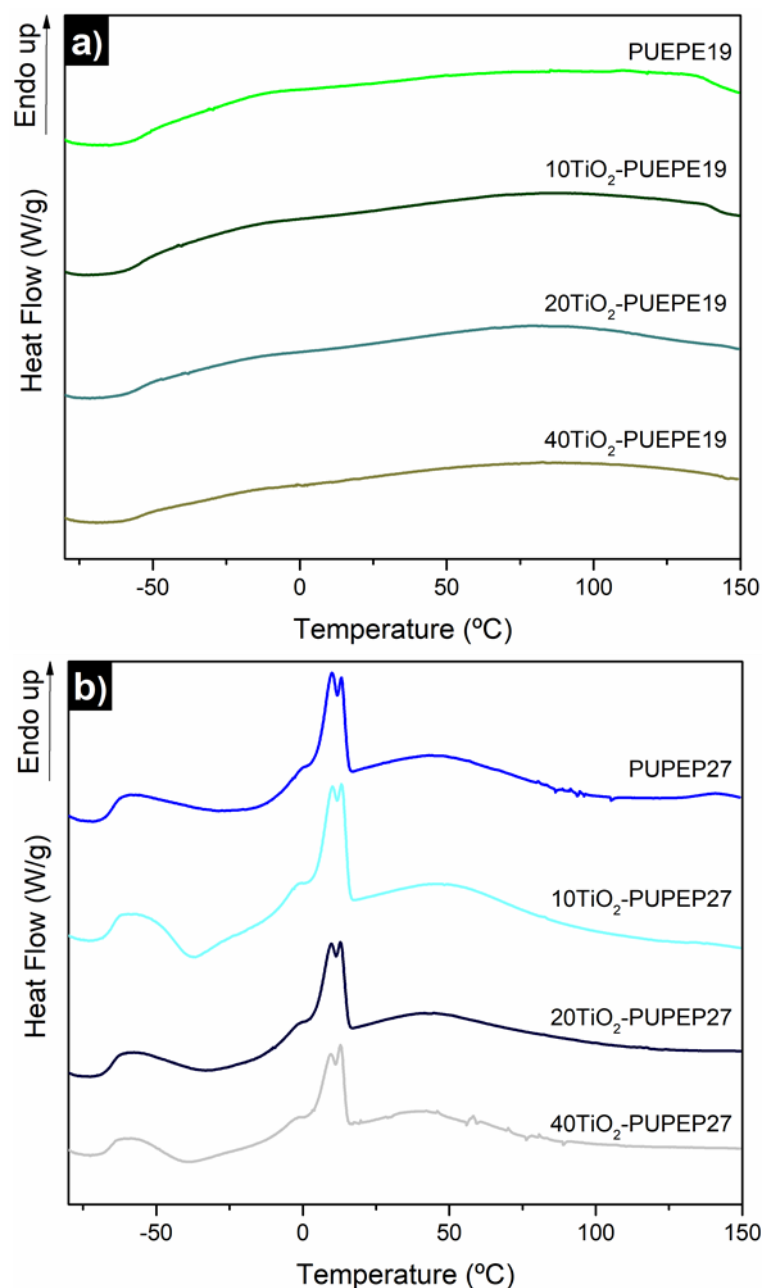


Figure 5.8. DSC curves of investigated (a) TiO₂-PUEPE19 and (b) TiO₂-PUPEP27 nanocomposite films. Neat PUEPE19 and PUPEP7 were added for comparison.

The most important difference between DSC curves of employed waterborne poly(urethane-urea)s and TiO₂-PUEPE19 and TiO₂-PUPEP27 nanocomposite films

consisted of the detection of the melting process for the PUPEP27 matrix and TiO₂-PUPEP27 nanocomposite films. This melting process was associated to the soft segment of PUPEP27, as discussed in the Chapter 4. Nonetheless, it was not significantly affected by the incorporation of TiO₂ nanoparticles.

Table 5.5. Glass transition temperature (T_g), melting temperature (T_m) and melting enthalpy (ΔH_m) of investigated TiO₂-PUEPE19 and TiO₂-PUPEP27 nanocomposite films. Neat PUEPE19 and PUPEP7 were added for comparison.

Sample	T_g (°C)	T_m peak (°C)	ΔH_m (J mol ⁻¹)
PUEPE19	-59	—	—
10TiO₂-PUEPE19	-58	—	—
20TiO₂-PUEPE19	-57	—	—
40TiO₂-PUEPE19	-57	—	—
PUPEP27	-65	10, 13	7
10TiO₂-PUPEP27	-66	10, 14	9
20TiO₂-PUPEP27	-67	10, 13	6
40TiO₂-PUPEP27	-67	9, 13	5

Degradation processes of neat PUEPE19 and PUPEP27 as well as their nanocomposites with TiO₂ nanoparticles were analyzed by TGA (Figure A.9 in Annexes). Figure 5.9 shows the corresponding dTGA curves. A main peak corresponding to triblock copolymer can be clearly observed, as well as a shoulder at lower temperatures, related to the hard segment.

In the case of TiO₂-PUEPE19 nanocomposite films, there were not significant variations in the degradation temperature with the increase of the TiO₂ nanoparticles content. Nevertheless, the incorporation of TiO₂ nanoparticles to PUPEP27 increased the thermal stability of the PUPEP27 matrix. It was remarkable the increase of 10 °C that took place with the incorporation of 20 wt% TiO₂ nanoparticles content. Interactions between TiO₂ nanoparticles and polymer chains would explain the increase in thermal stability³⁷. These differences indicate that TiO₂ nanoparticles interacted with both PUEPE19 and PUPEP27 polymer matrices but that the effect of the interaction was different, as concluded from DSC analysis. In the case of PUEPE19, TiO₂ nanoparticles interacted with the hard segment but also could interact with the soft segment. Meanwhile, in the case of PUPEP27 interactions with the soft segment

would be hindered. These interactions just with the hard segment would have promoted the increase in thermal stability for PUPEP27 matrix until a 20 wt% TiO₂ nanoparticles content. Nevertheless, a further increase of TiO₂ nanoparticles content resulted in a decrease of ~5 °C. This decrease in thermal stability can be due to an increase in interactions between TiO₂ nanoparticles²⁷. This would have reduced the interactions between TiO₂ nanoparticles and the hard segment producing the observed decrease in thermal stability⁴.

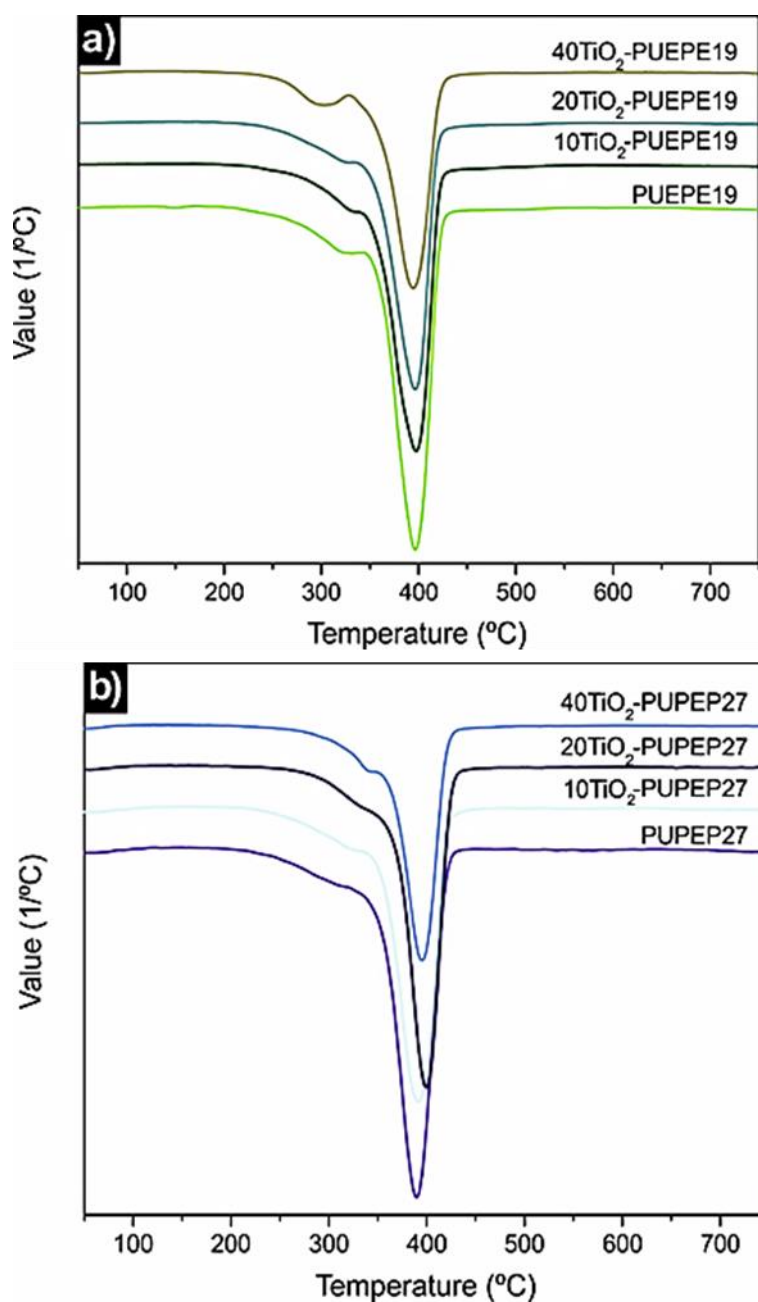


Figure 5.9. dTGA curves of investigated (a) neat PUEPE19 and TiO₂-PUEPE19 as well as (b) neat PUPEP27 and TiO₂-PUPEP27 nanocomposite films.

Table 5.6. Decomposition temperatures of (T_1) as well as TiO_2 nanoparticles content of neat PUEPE19 and PUPEP27 and TiO_2 -PUEPE19 and TiO_2 -PUPEP27 nanocomposite films.

Sample	T_1^a (°C)	TiO_2 nanoparticles content ^b (wt%)
PUEPE19	397	0
10TiO₂-PUEPE19	398	11
20TiO₂-PUEPE19	397	18
40TiO₂-PUEPE19	396	30
PUPEP27	390	0
10TiO₂-PUPEP27	392	11
20TiO₂-PUPEP27	400	18
40TiO₂-PUPEP27	395	36

a) Temperature determined from dTGA curves (Figure 5.9).

b) Calculated from residues of TGA curves shown in Figure A.9 in Annexes.

The morphology of TiO_2 -PUEPE19 and TiO_2 -PUPEP27 nanocomposite films was studied by AFM, as shown in Figure 5.10 and Figure 5.11, respectively. The most interesting morphology was the one corresponding to TiO_2 -PUEPE19 nanocomposite films (Figure 5.10), which exhibited a different morphology that of the neat PUEPE19 film. PUEPE19 film displayed a rod-like microphase separated structure (Figure 5.10a), as was also reported in the Chapter 4, whereas the incorporation of TiO_2 nanoparticles resulted in an interesting change if compared to the morphology of the neat PUEPE19 film. This change can be linked to the increase in the T_g since TiO_2 nanoparticles interacted in a relevant way with the matrix limiting the mobility of the polymer chains, supporting the mentioned interactions between TiO_2 nanoparticles and both the soft and the hard segment.

The morphology varied from a rod-like to a spherical one (Figure 5.10b-d). As the TiO_2 nanoparticles content increased, the rod-like structures disappeared and the spherical structures became more prominent. The diameter of these spherical structures decreased from 300-400 nm for 10 TiO_2 -PUEPE19 film to 100-200 nm for both 20 TiO_2 -PUEPE19 and 40 TiO_2 -PUEPE19 films. This change in the morphology was probably the result of interactions taking place between TiO_2 nanoparticles and the PEO-b-PPO-b-PEO triblock copolymer that formed the soft segment of neat PUEPE19 film³.

Looking more deeply at Figure 5.10b-d, one can easily distinguish bright small ~20 nm in diameter spherical spots, which can correspond to TiO₂ nanoparticles. These spots were preferentially located in the separated spherical domains or in the interphase between these domains and the polymer matrix. Similar distribution of nanoparticles have been already reported by Zheng et al.³⁸ in the case of ZnO in polyurethane matrix, Gutierrez et al.³⁹ for TiO₂ in PS-b-PEO and by Yeh et al.⁴⁰ for CdS nanoparticles dispersed in PS-b-PEO.

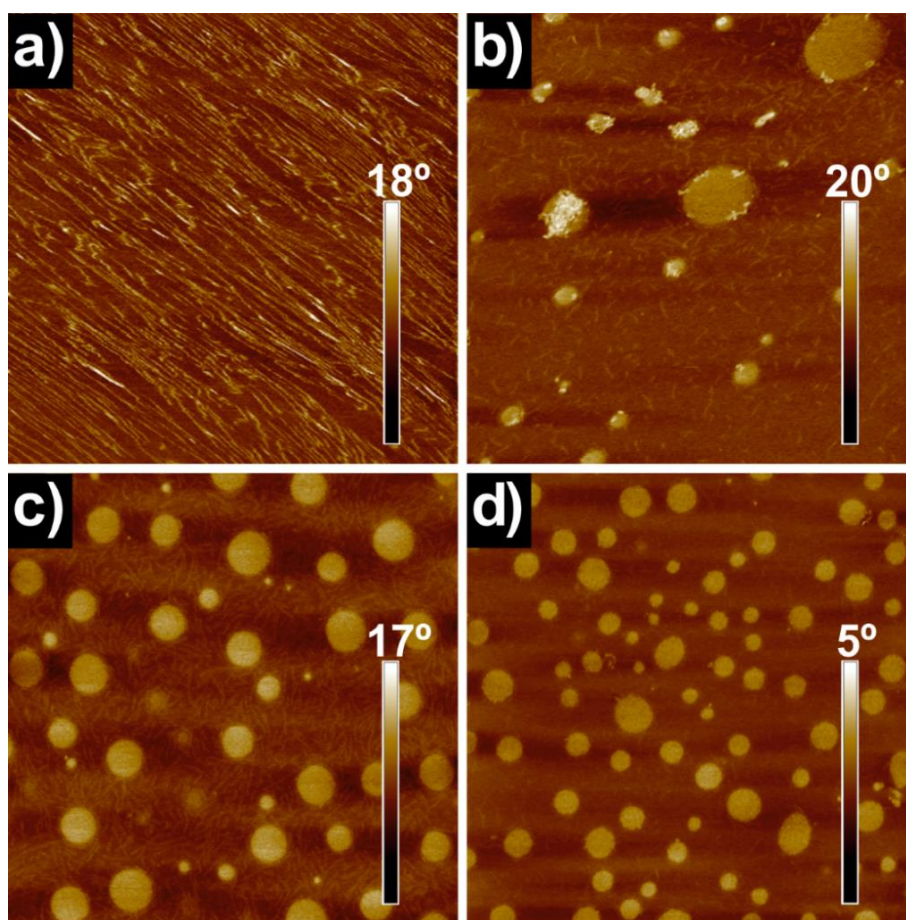


Figure 5.10. AFM phase images (3 μm x 3 μm) of investigated (a) neat PUEPE19, (b) 10TiO₂-PUEPE19, (c) 20TiO₂-PUEPE19 and (d) 40TiO₂-PUEPE19 nanocomposite films.

On the contrary to the changes in morphology observed for TiO₂-PUEPE19 nanocomposite films, the rod-like microphase separated structure of neat PUPEP27 film was unchanged when TiO₂ nanoparticles were incorporated (Figure 5.11).

Likewise to TiO₂-PUEPE19 nanocomposite films, bright small spherical spots with diameters of approximately 20 nm, corresponding as previously mentioned to TiO₂ nanoparticles, appeared and became more abundant with the increase of the TiO₂

nanoparticles content. In the case of TiO₂-PUPEP27 nanocomposite films, these small spherical spots were located throughout the matrix, preferentially within the rod-like microphase separated domains or in the interphase. This lack of morphology modification contrasting with what occurred to TiO₂-PUEPE19 nanocomposites can explain the previously reported slight decrease in the T_g. Interactions between TiO₂ nanoparticles and the polymer matrix cannot be significant enough to limit the mobility of the polymer chains since interactions between TiO₂ nanoparticles and the soft segment would be hindered.

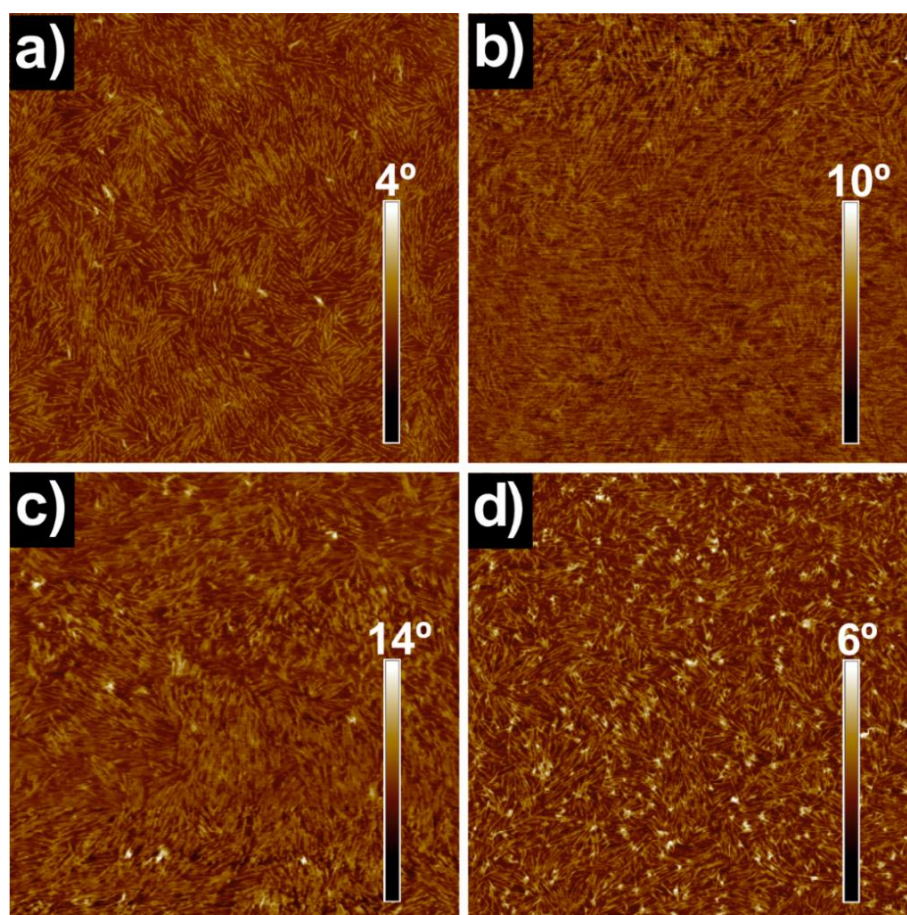


Figure 5.11. AFM phase images (3 μm x 3 μm) of investigated (a) neat PUPEP27, (b) 10TiO₂-PUPEP27, (c) 20TiO₂-PUPEP27 and (d) 40TiO₂-PUPEP27 nanocomposite films.

The observed differences in morphologies support the mentioned hypothesis that TiO₂ nanoparticles interacted in a different way depending on the polymer matrix, which resulted in different effects regarding the T_g values and thermal stability of the nanocomposite films.

EFM images obtained for 20TiO₂-PUEPE19, 40TiO₂-PUEPE19, 20TiO₂-PUPEP27 and 40TiO₂-PUPEP27 nanocomposite films are shown in Figure 5.12. Firstly, it can be noted that when a bias of 0 V was applied there were no charged domains observed. This confirmed that the topography of the surface did not influence the measurements and that the conditions were appropriately chosen.

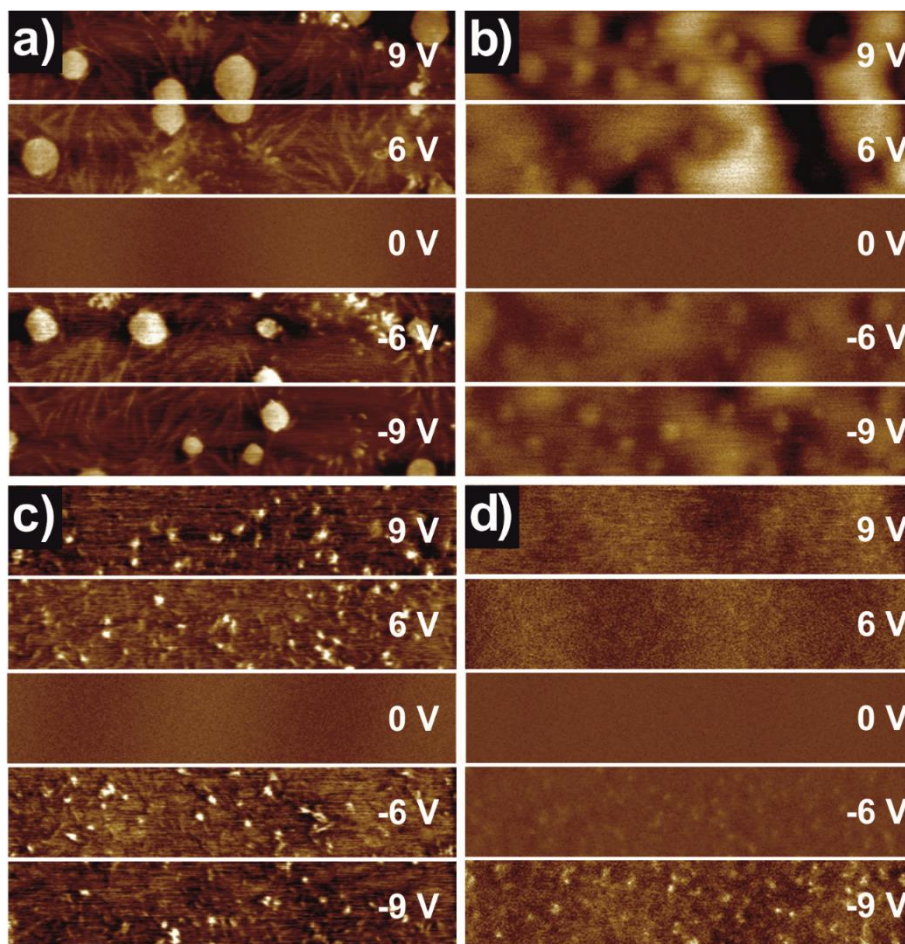


Figure 5.12. EFM phase images (3 μm × 3 μm) of investigated (a) 20TiO₂-PUEPE19 (b) 40TiO₂-PUEPE19, (c) 20TiO₂-PUPEP27 and (d) 40TiO₂-PUPEP27 nanocomposite films.

Locally charged TiO₂ nanoparticles, the only material with electric properties in investigated nanocomposites³, were detected when positive and negative bias of 6 and 9 V, independently of the sign, were applied. The contrast between the locally charged TiO₂ nanoparticles and the uncharged areas of the matrix increased when the applied voltage increased. These results confirmed that TiO₂ nanoparticles maintained their electrical properties even if embedded in PUEPE19 and PUPEP27 matrices.

It is worth mentioning that TiO₂ nanoparticles seemed to be covered by the matrix in the case of 40TiO₂-PUEPE19 (Figure 5.12b), making it more difficult to distinguish them by EFM measurement.

Finally, WCA measurements were carried out and obtained results are displayed in Table 5.7.

Table 5.7. Contact angle of investigated TiO₂-PUEPE19 and TiO₂-PUPEP27 nanocomposite films. Neat PUEPE19 and PUPEP27 were added for comparison.

Sample	Contact angle (°)
PUEPE19	37 ± 6
10TiO₂-PUEPE19	37 ± 3
20TiO₂-PUEPE19	35 ± 4
40TiO₂-PUEPE19	24 ± 4
PUPEP27	40 ± 3
10TiO₂-PUPEP27	41 ± 6
20TiO₂-PUPEP27	39 ± 6
40TiO₂-PUPEP27	23 ± 4

Neither the contact angle of TiO₂-PUEPE19 nanocomposite films nor the contact angle of TiO₂-PUPEP27 nanocomposite films varied until the TiO₂ nanoparticles content was higher than 20 wt%. The decreases in the contact angle for 40TiO₂-PUEPE19 and 40TiO₂-PUPEP27 nanocomposite films were remarkable. This meant that the hydrophilic nature of TiO₂ nanoparticles^{32,33} influenced the nanocomposite films making them more hydrophilic than neat PUEPE19 and PUPEP27 films. This was more noticeable considering that, as previously discussed, the hydrophilicity of 40TiO₂-PU0 film slightly varied from that of neat PU0 film. This suggested that the triblock copolymers had an effect on the increase in hydrophilicity that took place for 40TiO₂-PUEPE19 and 40TiO₂-PUPEP27 nanocomposite films due to different interactions if compare to TiO₂-PU0 nanocomposite films.

5.5. Conclusions

From the results discussed in this Chapter, the following conclusions were obtained:

- Nanocomposites based on synthesized waterborne poly(urethane-urea)s were successfully designed by incorporation of TiO₂ nanoparticles, up to a content of 40 wt%, just by *ex-situ* physically mixing,
- The characteristic FTIR spectra bands of neat PU0, PUEPE19 and PUPEP27 were not affected by the incorporation of TiO₂ nanoparticles. The appearance of a band at wavenumber lower than 800 cm⁻¹ confirmed the successful incorporation of TiO₂ nanoparticles,
- The T_g value of 40TiO₂-PU0 nanocomposite film clearly decreased after incorporation of TiO₂ nanoparticles. Meanwhile, TiO₂ nanoparticles affected T_g values of TiO₂-PUEPE19 and TiO₂-PUPEP27 nanocomposite films in a different way due to different block configurations of PEO and PPO blocks,
- The thermal stability of TiO₂-PU0 nanocomposite films decreased with the incorporation of TiO₂ nanoparticles if compare to neat PU0 film. In contraposition, thermal stability of TiO₂-PUEPE19 and TiO₂-PUPEP27 nanocomposite films increased if compared to neat PUEPE19 and PUPEP27 films,
- In the cases of TiO₂-PU0 and TiO₂-PUPEP27 nanocomposite films, the morphology did not vary if compare to neat PU0 and PUPEP27 film,
- In the case of TiO₂-PUPEP27 nanocomposite films, TiO₂ nanoparticles tended to locate in the rod-like microphase separated structures, while they were not located in any particular domain in the case of TiO₂-PU0 since there was not microphase separation,
- The morphology of TiO₂-PUEPE19 nanocomposite films varied from a rod-like structure for neat PUEPE19 film to a spherical one for nanocomposites films,
- TiO₂ nanoparticles maintained their electrical properties when embedded in all investigated polymer matrices,
- Contact angle of investigated nanocomposite films decreased for TiO₂ nanoparticles content higher than 20 wt%.

5.6. References

- [1] F. Huang, W. Zheng, A. Tahmasbi Rad, M. P. Nieh, C. J. Cornelius, SiO₂-TiO₂-PBC nanocomposite film morphology, solvent swelling, estimated χ parameter, and liquid transport, *Polymer* 123 (2017) 247-257.
- [2] L. Zhao, J. Yu, Controlled synthesis of highly dispersed TiO₂ nanoparticles using SBA-15 as hard template, *Journal of Colloid and Interface Science* 304 (2006) 84-91.
- [3] J. Gutierrez, A. Tercjak, I. Mondragon, Conductive behavior of high TiO₂ nanoparticle content of inorganic/organic nanostructured composites, *Journal of the American Chemical Society* 132 (2010) 873-878.
- [4] C. H. Yang, F. J. Liu, Y. P. Liu, W. T. Liao, Hybrids of colloidal silica and waterborne polyurethane, *Journal of Colloid and Interface Science* 302 (2006) 123-132.
- [5] L. Zhai, Y. Wang, F. Peng, Z. Xiong, R. Liu, J. Yuan, Y. Lan, Synthesis of TiO₂-SiO₂/waterborne polyurethane hybrid with amino-siloxane terminated via a sol-gel process, *Materials Letters* 89 (2012) 81-85.
- [6] L. Cano, A. Evelyn, D. Mauro, M. Striccoli, M. L. Curri, A. Tercjak, Optical and conductive properties of as-synthesized organic-capped TiO₂ nanorods highly dispersible in polystyrene-block-poly(methyl methacrylate) diblock copolymer. *ACS Applied Materials & Interfaces* 6 (2014) 11805-11814.
- [7] X. Y. Ma, W. D. Zhang, Effects of flower-like ZnO nanowhiskers on the mechanical, thermal and antibacterial properties of waterborne polyurethane, *Polymer Degradation and Stability* 94 (2009) 1103-1109.
- [8] Z. Zhong, S. Luo, K. Yang, X. Wu, T. Ren, High-performance anionic waterborne polyurethane/Ag nanocomposites with excellent antibacterial property via in situ synthesis of Ag nanoparticles, *RSC Advances* 7 (2017) 42296-42304.
- [9] S. M. Cakić, I. S. Ristić, M. M. Cincović, D. T. Stojiljković, J. B. Simendić, Preparation and characterization of waterborne polyurethane/silica hybrid dispersions from castor oil polyols obtained by glycolysis poly(ethylene terephthalate) waste, *International Journal of Adhesion and Adhesives* 70 (2016) 329-341.
- [10] S. Hendessi, E. B. Sevinis, S. Unal, F. C. Cebeci, Y. Z. Menciloglu, H. Unal, Antibacterial sustained-release coatings from halloysite nanotubes/waterborne polyurethanes, *Progress in Organic Coatings* 101 (2016) 253-261.
- [11] L. Hu, P. Jiang, P. Zhang, G. Bian, S. Sheng, M. Huang, Y. Bao, J. Xia, Amine-graphene oxide/waterborne polyurethane nanocomposites: effects of different amine modifiers on physical properties, *Journal of Materials Science* 51 (2016) 8296-8309.
- [12] J. G. Han, Y. Q. Xiang, Y. Zhu, New antibacterial composites: waterborne polyurethane/gold nanocomposites synthesized via self-emulsifying method, *Journal of Inorganic and Organometallic Polymers and Materials* 24 (2014) 283-290.
- [13] X. Gao, Y. Zhu, S. Zhou, W. Gao, Z. Wang, B. Zhou, Preparation and characterization of well-dispersed waterborne polyurethane/CaCO₃ nanocomposites, *Colloids and Surfaces A: Physicochemical and Engineering Aspects* 377 (2011) 312-317.

- [14] S. Zhang, Y. Li, L. Peng, Q. Li, S. Chen, K. Hou, Synthesis and characterization of novel waterborne polyurethane nanocomposites with magnetic and electrical properties, *Composites Part A: Applied Science and Manufacturing* 55 (2013) 94-101.
- [15] P. A. Charpentier, K. Burgess, L. Wang, R. R. Chowdhury, A. F. Lotus, G. Moula, Nano-TiO₂/polyurethane composites for antibacterial and self-cleaning coatings, *Nanotechnology* 23 (2012).
- [16] K. Li, J. Peng, M. Zhang, J. Heng, D. Li, C. Mu, Comparative study of the effects of anatase and rutile titanium dioxide nanoparticles on the structure and properties of waterborne polyurethane, *Colloids and Surfaces A: Physicochemical and Engineering Aspects* 470 (2015) 92-99.
- [17] H. Behniafar, M. Alimohammadi, K. Malekshahinezhad, Transparent and flexible films of new segmented polyurethane nanocomposites incorporated by NH₂-functionalized TiO₂ nanoparticles, *Progress in Organic Coatings* 88 (2015) 150-154.
- [18] X. D. Chen, Z. Wang, Z. F. Liao, Y. L. Mai, M. Q. Zhang, Roles of anatase and rutile TiO₂ nanoparticles in photooxidation of polyurethane, *Polymer Testing* 26 (2007) 202-208.
- [19] A. Abdal-hay, H. M. Mousa, A. Khan, P. Vanegas, J. H. Lim, TiO₂ nanorods coated onto nylon 6 nanofibers using hydrothermal treatment with improved mechanical properties, *Colloids and Surfaces A: Physicochemical and Engineering Aspects* 457 (2014) 275-281.
- [20] A. Fujishima, K. Honda, Electrochemical photolysis of water at a semiconductor electrode, *Nature* 238 (1972) 37-38.
- [21] J. Kirschner, J. Will, T. J. Rejek, L. Portilla, M. Berlinghof, P. Schweizer, E. Spiecker, H. Steinrück, T. Unruh, M. Halik, Memory effect of self-assembled PS-b-PEO block copolymer films with selectively embedded functionalized TiO₂ nanoparticles, *Advanced Materials Interfaces*. 4 (2017) 1700230/1-1700230/8.
- [22] S. Zhang, Z. Ren, S. He, Y. Zhu, C. Zhu, FTIR spectroscopic characterization of polyurethane-urea model hard segments (PUUMHS) based on three diamine chain extenders, *Spectrochimica Acta Part A: Molecular and Biomolecular Spectroscopy* 66 (2007) 188-193.
- [23] K. Schrijnemakers, N. R. E. N. Impens, E. F. Vansant, Deposition of a titania coating on silica by means of the chemical surface coating, *Langmuir* 15 (1999) 5807-5813.
- [24] M. Zhang, T. Chen, Y. Wang, Insights into TiO₂ polymorphs: highly selective synthesis, phase transition, and their polymorph-dependent properties, *RSC Advances* 7 (2017) 52755-52761.
- [25] L. S. Schadler, L. C. Brinson, W. G. Sawyer, Polymer nanocomposites: A small part of the story, *JOM* 59 (2007) 53-60.
- [26] B. J. Ash, L. S. Schadler, R. W. Siegel, Glass transition behavior of alumina/polymethylmethacrylate nanocomposites, *Materials Letters* 55 (2002) 83-87.
- [27] H. Mahfuz, V. K. Rangari, M. S. Islam, S. Jeelani, Fabrication, synthesis and mechanical characterization of nanoparticles infused polyurethane foams, *Composites Part A: Applied Science and Manufacturing* 35 (2004) 453-460.
- [28] A. Ramar, R. Saraswathi, M. Rajkumar, S. M. Chen, Influence of poly(N-vinylcarbazole) as a photoanode component in enhancing the performance of a dye-sensitized solar cell, *The Journal of Physical Chemistry C* 119 (2015) 23830-23838.
- [29] R. M. Nyffenegger, R. M. Penner, R. Schierle, Electrostatic force microscopy of silver nanocrystals with nanometer-scale resolution, *Applied Physics Letters* 71 (1997) 1878-1880.

- [30] A. Tercjak, J. Gutierrez, G. Mondragon, I. Mondragon, Cellulose nanocrystals and Au nanoparticles well-dispersed in a poly(styrene- b -ethylene oxide) block copolymer matrix, *The Journal of Physical Chemistry C* 115 (2011) 22180-22185.
- [31] A. Tercjak, I. Garcia, I. Mondragon, Liquid crystal alignment in electro-responsive nanostructured thermosetting materials based on block copolymer dispersed liquid crystal, *Nanotechnology* 19 (2008) 275701/1-275701/5.
- [32] J. Gutierrez, A. Tercjak, L. Peponi, I. Mondragon, Conductive properties of inorganic and organic TiO₂/polystyrene-block-poly(ethylene oxide) nanocomposites, *The Journal of Physical Chemistry C* 113 (2009) 8601-8605.
- [33] Z. Sun, M. Wolkenhauer, G. Bumbu, D. H. Kim, J. S. Å. Gutmann, GISAXS investigation of TiO₂ nanoparticles in PS-b-PEO block-copolymer films, *Physica B: Condensed Matter* 357 (2005) 141-143.
- [34] Y. Lu, R. C. Larock, Soybean-oil-based waterborne polyurethane dispersions: Effects of polyol functionality and hard segment content on properties, *Biomacromolecules* 9 (2008) 3332-3340.
- [35] T. Calvo-Correas, M. D. Martin, A. Retegi, N. Gabilondo, M. A. Corcuera, A. Eceiza, Synthesis and characterization of polyurethanes with high renewable carbon content and tailored properties, *ACS Sustainable Chemistry & Engineering* 4 (2016) 5684-5692.
- [36] Y. G. Hsu, F. J. Lin, Organic-inorganic composite materials from acrylonitrile-butadiene-styrene copolymers (ABS) and silica through an in situ sol-gel process, *Journal of Applied Polymer Science* (1999) 275-283.
- [37] Z. Gao, J. Peng, T. Zhong, J. Sun, X. Wang, C. Yue, Biocompatible elastomer of waterborne polyurethane based on castor oil and polyethylene glycol with cellulose nanocrystals, *Carbohydrate Polymers* 87 (2012) 2068-2075.
- [38] J. Zheng, R. Ozisik, R. W. Siegel, Disruption of self-assembly and altered mechanical behavior in polyurethane/zinc oxide nanocomposites, *Polymer* 46 (2005) 10873-10882.
- [39] J. Gutierrez, I. Mondragon, A. Tercjak, Morphological and optical behavior of thermoset matrix composites varying both polystyrene-block-poly(ethylene oxide) and TiO₂ nanoparticle content, *Polymer* 52 (2011) 5699-5707.
- [40] S. W. Yeh, Y. T. Chang, C. H. Chou, K. H. Wei, Effect of surface-hydroxylated CdS nanoparticles on the morphological transformation of polystyrene-block-poly(ethylene oxide) thin films, *Macromolecular Rapid Communications* 25 (2004) 1679-1686.

Chapter

6

“Some lessons are best taught, not by others’ scars, but by our own wounds.”

(Mokokoma Mokhonoana)

Self-healing ability of synthesized waterborne poly(urethane-urea)s and their nanocomposites

6. Self-healing ability of synthesized waterborne poly(urethane-urea)s and their nanocomposites

6.1. Chapter overview	133
6.2. Introduction	133
6.3. Materials and characterization techniques	134
6.3.1. Materials	134
6.3.2. Characterization techniques for self-healing study	134
6.4. Study of the self-healing ability of PU0 waterborne poly(urethane-urea) and TiO₂-PU0 nanocomposites	136
6.5. Study of the self-healing ability of PUEPE19 and PUPEP27 waterborne poly(urethane-urea)s and of TiO₂-PUEPE19 and TiO₂-PUPEP27 nanocomposites	139
6.6. Conclusions	142
6.7. References	144

6.1. Chapter overview

In this Chapter self-healing ability of synthesized waterborne poly(urethane-urea)s and their nanocomposites film is studied taking into account that highly hydrophilic waterborne poly(urethane-urea)s can exhibit this ability.

In the case of neat PU0 and TiO₂-PU0 nanocomposites films, their self-healing efficiency is analyzed by means of mechanical properties for three cut/recovery cycles. For PUEPE19 and PUPEP27 waterborne poly(urethane-urea) films, as well as their nanocomposites with TiO₂ nanoparticles, the self-healing ability is analyzed by OM. This Chapter reports the different self-healing performances of synthesized waterborne poly(urethane-urea) and their nanocomposite films, including the effect played by TiO₂ nanoparticles.

6.2. Introduction

Polyurethanes and poly(urethane-urea)s are polymers that can display self-healing ability. This can be achieved either by the addition of healing agents embedded in microcapsules, extrinsic healing, or by modifying the polymer backbone incorporating a moiety that works as healing element, intrinsic healing¹⁻⁸. Among these latter ones, self-healable polymers based on hydrogen bonding and ionic interactions can be found^{1,3,6,7,9}.

The vast number of applications of polyurethanes and poly(urethane-urea)s make them widely used polymers. During their lifetime, they may suffer different physical damages, which result in scratches, microcracks, larger cracks and even in catastrophic rupture⁴. Consequently, reducing their waste and maintenance costs by extending their life of use is of great interest. This can be achieved by designing self-healable polyurethanes and poly(urethane-urea)s that recover their original properties, therefore extending their lifespan^{4,6,8-10}.

Taking above into account, research on self-healable polyurethanes and poly(urethane-urea)s has increased. Different strategies have been successfully proved in order to provide polymers with self-healing ability. Some of the followed

strategies are based on reversible interactions thanks to Diels-Alder reaction¹¹⁻¹³, alkoxyamines¹, disulfide bonds^{4,5}, π - π stacking¹⁴, ionic forces¹⁰ and hydrogen bonding^{9,10}. Moreover, preparation of nanocomposites by incorporation of different nanofillers to self-healable polyurethanes and poly(urethane-urea)s, such as Cu nanowires¹¹, carbon nanotubes¹⁵, SiO₂¹⁶, neat graphene oxide^{17,18} as well as graphene oxide together with ferric and ferrous ions¹⁹, sulfur nanoparticles²⁰ or Ag²¹, has also been carried out. Near-infrared, microwave or sunlight radiation induced self-healing on some of these nanocomposites^{15,18-20}. The healing efficiency of reported graphene-based nanocomposites was high and was almost invariable after five recovery cycles^{19,20}. However, it has been reported that the healing efficiency decreased with the increase of SiO₂ nanoparticles content¹⁶. Meanwhile, Cu nanowires based nanocomposites exhibited electrical conductivity¹¹.

Notwithstanding, research on self-healable waterborne polyurethanes and poly(urethane-urea)s and, in fact, on any poly(urethane-urea) system, is scarce. Furthermore, study on the effect of the incorporation of nanofillers on the self-healing ability is also scarce. Taking all this into account, research on self-healing ability of synthesized waterborne poly(urethane-urea)s and their nanocomposites prepared by *ex-situ* addition of TiO₂ nanoparticles can allow to better understand their self-healing process.

6.3. Materials and characterization techniques

6.3.1. Materials

Synthesized waterborne poly(urethane-urea) and their nanocomposite films, reported in the Chapters 4 and 5, were evaluated regarding their self-healing ability.

6.3.2. Characterization techniques

6.3.2.1. Mechanical testing

The self-healing ability of neat PU0 and TiO₂-PU0 nanocomposite films, with the exception of 40TiO₂-PU0, was study by means of their mechanical properties. Three

cut/recovery cycles were carried out. For the first cycle, specimens were cut by half. For the second cycle, they were cut from upper left to lower right, while the third cut was carried out from upper right to lower left (Figure 6.1). After each cut the two halves of each specimen were put into contact and left healing for 23 h at room temperature, after evaluation of the optimal conditions for the analysis. Before measurement, and in order to handle specimens properly, they were kept in vacuum for 1 h at 60 °C. Six specimens (10 mm x 4.5 mm x 0.3 mm) of each composition were tested for each cut/recovery cycle.

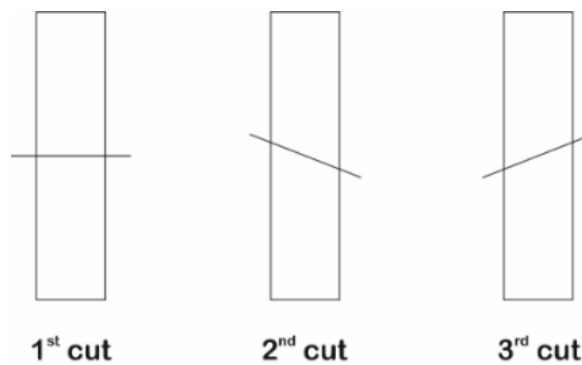


Figure 6.1. Schematic description of how specimens were cut in half for each cut/recovery cycle.

From obtained stress-strain curves of original and self-healed films E , σ_{max} , σ_b and ϵ_b were determined. The healing efficiency was considered as the ratio between each mechanical property after self-healing to that of the same mechanical property of the original film (Equation 6.1).

$$\text{Healing efficiency}(\%) = \frac{\text{mechanical property}_{\text{healed}}}{\text{mechanical property}_{\text{original}}} \quad (6.1)$$

6.3.2.2. Contact angle

It was also studied by WCA if neat PU0 and TiO₂-PU0 nanocomposite films, with the exception of 40TiO₂-PU0, preserved their hydrophilicity after self-healing. Measurements were carried out for original and self-healed (one, two and three cut/recovery cycles) films at room temperature using deionized water. Drops were deposited in the repaired area of the self-healed films.

6.3.2.3. Optical microscopy

The self-healing process of synthesized triblock copolymers based PUEPE19 and PUPEP27 waterborne poly(urethane-urea) films and of their nanocomposites with TiO₂ nanoparticles was analyzed by means of OM.

Due to the softness and tackiness exhibited by neat PUEPE19 and PUPEP27 films, the healing process was qualitatively analyzed. For this, the reparation of a produced scratch on each film, which were of ~0.3 mm in thickness, was studied by OM. Square samples of each film were scratched with a blade. The healing process was observed capturing images at ½, 1, 4 and 24 h with the x5 objective of a Nikon Eclipse E600 microscope.

6.4. Study of the self-healing ability of PU0 waterborne poly(urethane-urea) and their TiO₂-PU0 nanocomposites

Synthesized PU0 waterborne poly(urethane-urea) and prepared TiO₂-PU0 nanocomposite films exhibited intrinsic self-healing. This was the result of hydrogen bonding, which took place between urea and urethane groups^{7,10} as well as with the ether oxygen of PEO²² (Figure 6.2.), and also consequence of ionic interactions thanks to sulphonate groups¹⁰.

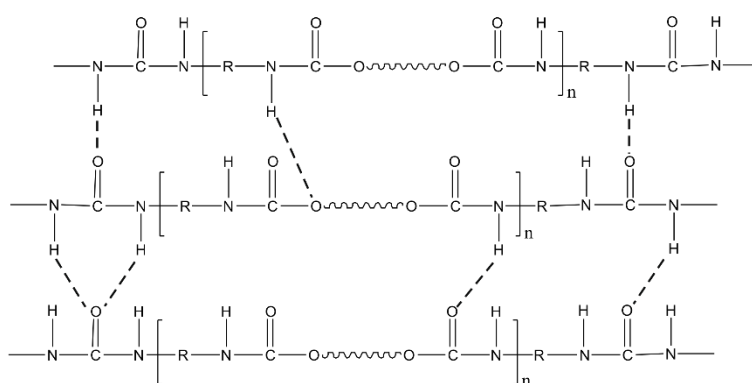


Figure 6.2. Schematic representation of the hydrogen bonds formed in the poly(urethane-urea) network.

In Figure 6.3, digital images in order to observe the visual aspect of each specimen after each cut/recovery cycle are shown.

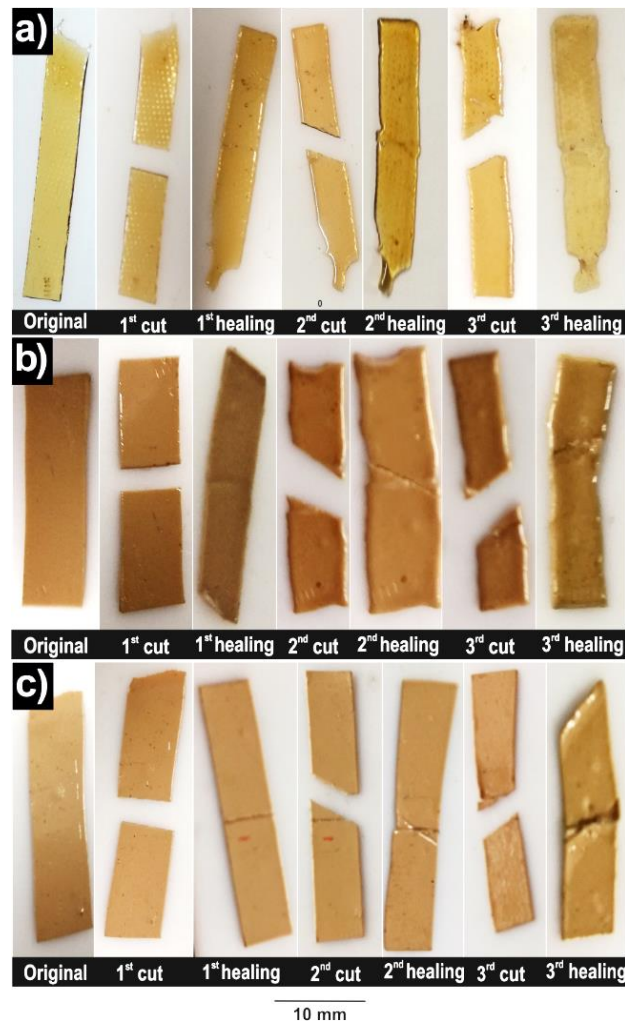


Figure 6.3. Digital images of the original and self-healed samples of (a) neat PU0, (b) 10TiO₂-PU0 and (c) 20TiO₂-PU0 films.

In addition to the presence of hydrogen bonds and sulphonate groups in their structure, neat PU0 film and TiO₂-PU0 nanocomposite films showed a low T_g below room temperature, which means that they can flow in order to ensure that damage areas get repaired⁷.

Figure 6.4 shows the healing efficiency of neat PU0 film and TiO₂-PU0 nanocomposite films by means of mechanical properties (strain-stress curves are presented in Figure A.12 in Annexes). Neat PU0 film possessed a higher healing efficiency than their nanocomposites for deformation at break. It is remarkable that 20TiO₂-PU0 film displayed a low healing efficiency for deformation at break just after one cut/recovery cycle. Nonetheless, the healing efficiencies of TiO₂-PU0 nanocomposite films were higher to that of neat PU0 film if mechanical properties such as modulus, tensile strength and stress at break are taken into consideration.

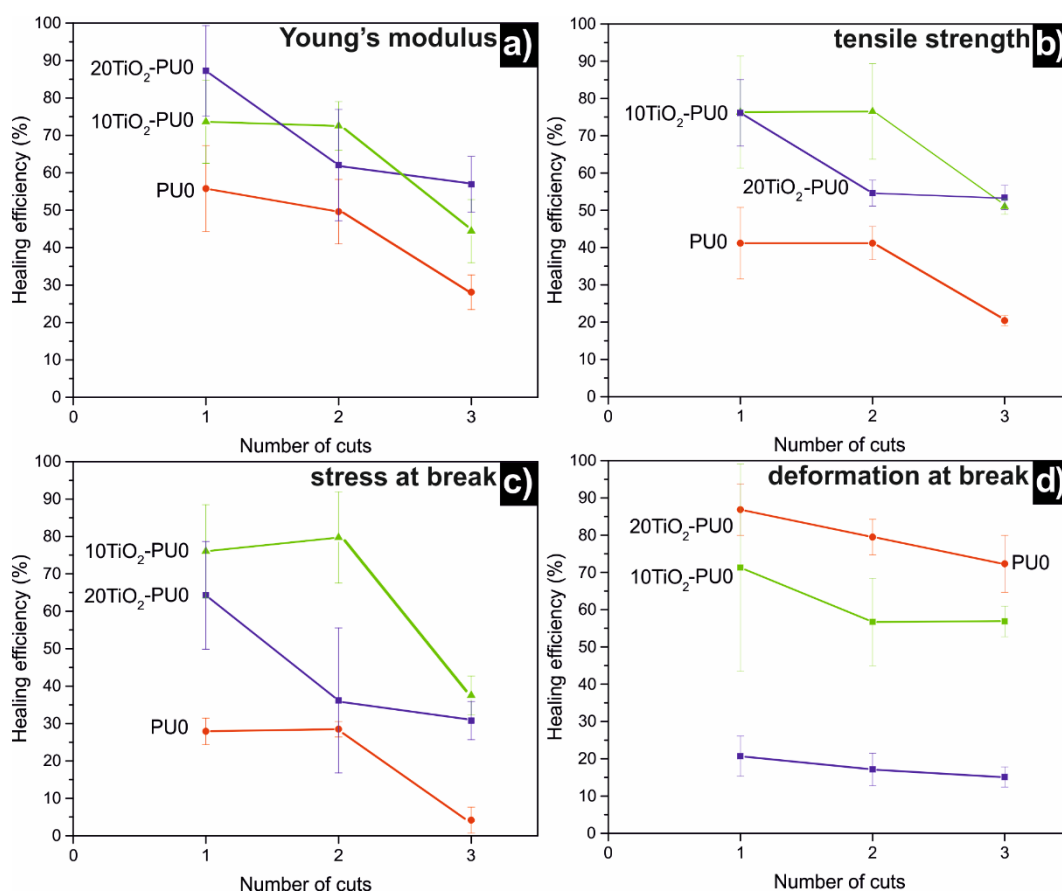


Figure 6.4. The healing efficiency of investigated neat PU0, 10TiO₂-PU0 and 20TiO₂-PU0 films determined from stress-strain curves for (a) Young's modulus, (b) tensile strength, (c) stress at break and (d) deformation at break.

10TiO₂-PU0 film presented the highest healing efficiency for stress at break, whereas the healing efficiencies of both 10TiO₂-PU0 and 20TiO₂-PU0 films were similar for modulus and tensile strength. The self-healing efficiencies of 20TiO₂-PU0 film for these latter mechanical properties were the highest after one and three cut/recovery cycle, whereas they were the highest for 10TiO₂-PU0 film after two cut/recovery cycles. Considering these results, and as mentioned in the Chapter 4, TiO₂ nanoparticles acted as a reinforcement of the modulus but diminished the deformation at break. This means that obtained healing efficiencies made sense since, in consideration of analyzed mechanical properties, TiO₂-PU0 nanocomposite films presented lower values than neat PU0 film for deformation at break and higher values for modulus, tensile strength and stress at break.

The decrease in the healing efficiency after successive cut/recovery cycles that occurred for all investigated films is a common and known effect²³. One of the reasons

reported with the aim of giving an explanation to this effect is the difficulty to keep the cut halves of the specimen in proper contact¹. In the cases of synthesized neat PU0 film and TiO₂-PU0 nanocomposite films analyzed in this investigation work this was a very likely reason given the softness of the samples.

Another measured parameter after healing of each film was their hydrophilic character by means of WCA. Table 6.1 displays the results obtained for the contact angles of neat PU0 film and TiO₂-PU0 nanocomposite films.

Table 6.1. Contact angle of original investigated neat PU0 and TiO₂-PU0 nanocomposite films and of the healed films.

Sample	Original (°)	1st healing (°)	2nd healing (°)	3rd healing (°)
PU0	62 ± 7	61 ± 8	54 ± 3	57 ± 9
10TiO₂-PU0	66 ± 9	50 ± 6	55 ± 4	57 ± 5
20TiO₂-PU0	66 ± 7	58 ± 3	58 ± 2	59 ± 3

As reported in the Chapter 4, TiO₂ nanoparticles did not influence the contact angle until a content higher than 20 wt%. Nevertheless, it was noticeable that the contact angles of TiO₂-PU0 nanocomposite films changed after one cut/recovery cycle, while the one of neat PU0 film stayed invariable. The contact angle of neat PU0 film decreased after the second cut/recovery cycle, whereas the values of investigated TiO₂-PU0 nanocomposite films were not affected. The third cut/recovery cycle did not vary the contact angle of any of investigated films. It has to be mentioned that, even if the contact angles decreased, these reductions were small and did not exceed 15°.

6.5. Study of the self-healing ability of PUEPE19 and PUPEP27 waterborne poly(urethane-urea)s and of their nanocomposites

Due to the softness of synthesized triblock copolymers based waterborne poly(urethane-urea) films and their nanocomposites with TiO₂ nanoparticles, their self-healing ability was analyzed by OM.

As shown in Figure 6.5a, neat PUEPE19 film exhibited a relatively fast intrinsic self-healing ability at room temperature, without any stimuli. After 1 h, the produced scratch was completely repaired. Nevertheless, incorporation of TiO_2 nanoparticles resulted in a decrease of the self-healing ability. 10TiO_2 -PUEPE19 and 20TiO_2 -PUEPE19 nanocomposite films still possessed self-healing ability, however they required longer times than neat PUEPE19 film for total recovery (Figure 6.5b-c). In the case of 10TiO_2 -PUEPE19 film, recovery was almost complete after 4 h and total recovery was achieved after 24 h. Nevertheless, for 20TiO_2 -PUEPE19 film, 4 h were not enough to get close to full repair and this film was not totally recovered even after one day. However, it was close to total recovery.

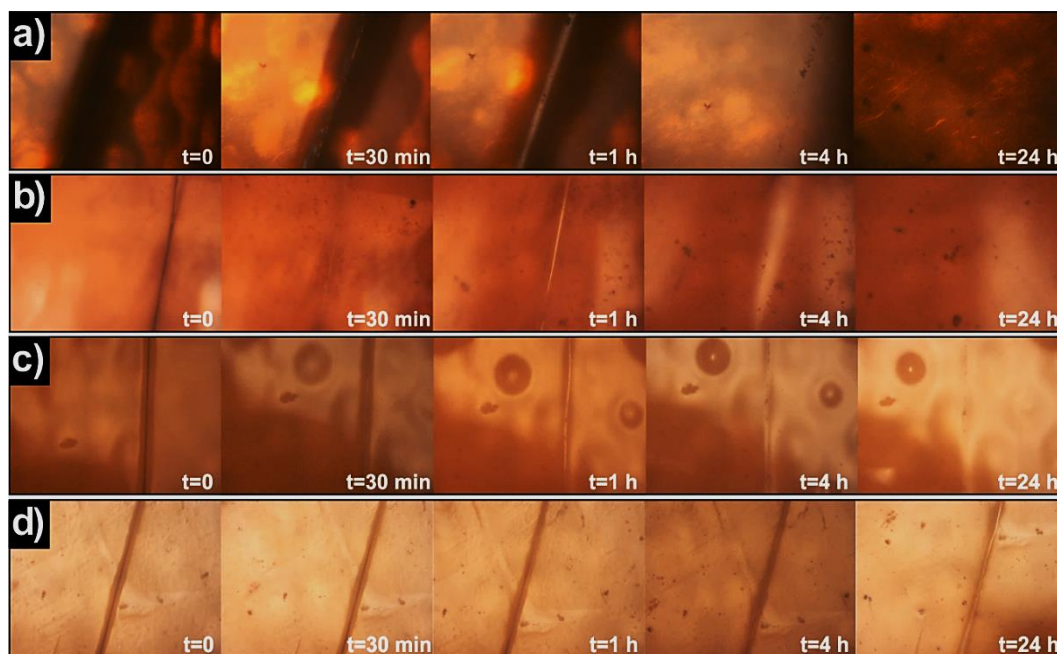


Figure 6.5. OM micrographs during self-healing process for investigated (a) neat PUEPE19, (b) 10TiO_2 -PUEPE19, (c) 20TiO_2 -PUEPE19 and (d) 40TiO_2 -PUEPE19 films.

The nanocomposite films prepared by the incorporation of 40 wt% content of TiO_2 nanoparticles lost self-healing ability (Figure 6.5d). 40TiO_2 -PUEPE19 film was observed for a week time and was not repaired even after that time.

The decrease in the self-healing ability that occurred when increasing the TiO_2 nanoparticles content can be caused by the disruption of hydrogen bonding and ionic interactions between soft and hard segments of waterborne poly(urethane-urea)s¹⁰. This can cause the loss of the self-healing ability of the matrix.

In Figure 6.6, the self-healing process followed by OM of neat PUPEP27 film and TiO₂-PUPEP27 nanocomposite films is observed. First, it is remarkable that both PUPEP27 and 10TiO₂-PUPEP27 films were completely repaired after 4 h at room temperature (Figure 6.6a-b). Comparing these results with the ones for neat PUEPE19 and TiO₂-PUEPE19 nanocomposite films, it was evident that incorporation of 10 wt% TiO₂ nanoparticles content to the PUPEP27 matrix did not affect the self-healing ability as much as it was observed for the PUEPE19 matrix. The lack of interactions between TiO₂ nanoparticles and the soft segment in the case of PUPEP27, as concluded in the Chapter 5, would be the responsible for this difference. Anyway, in the case of 20TiO₂-PUPEP27 film (Figure 6.6c) the self-healing ability decreased since it required one day in order to get close to total recovery of the produced scratch, similarly to 20TiO₂-PUEPE19 film. This was the result of increasing interactions between TiO₂ nanoparticles and the polymer matrix with the increase of the TiO₂ nanoparticles content, regardless of with which segment TiO₂ nanoparticles interacted.

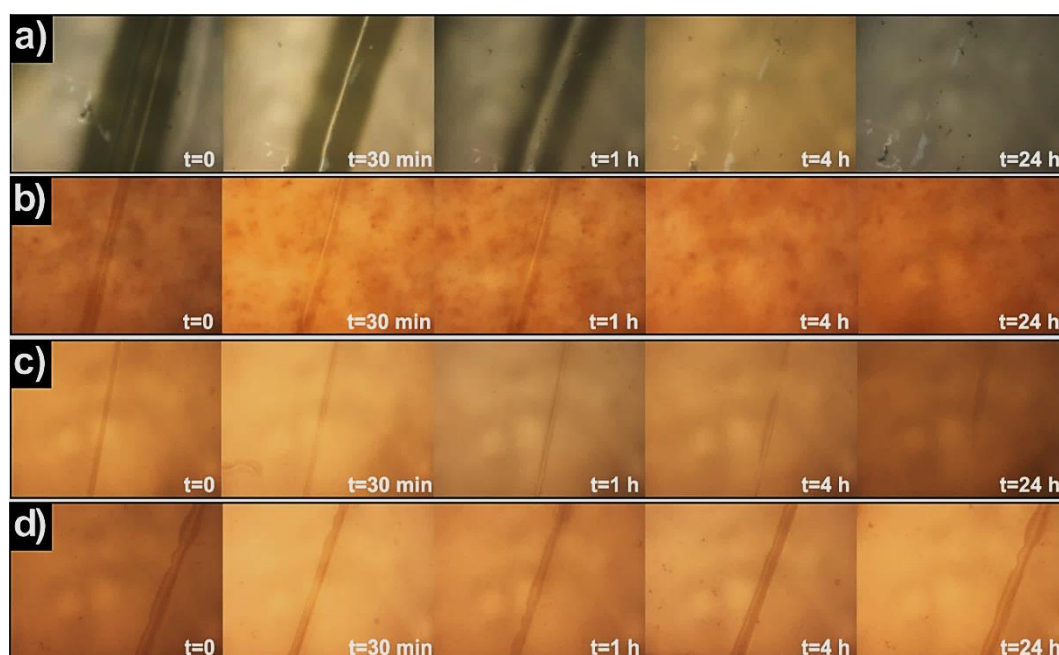


Figure 6.6. OM micrographs during self-healing process for investigated (a) neat PUPEP27, (b) 10TiO₂-PUPEP27, (c) 20TiO₂-PUPEP27 and (d) 40TiO₂-PUPEP27 films.

The self-healing ability exhibited by neat PUPEP27 film vanished when 40 wt% TiO₂ nanoparticles content was incorporated (Figure 6.6d), likewise to 40TiO₂-PUEPE19 film. The reparation process was followed for one week without observing any further healing. This decrease can be explained, as for TiO₂-PUEPEP19 nanocomposite films, by the disruption of hydrogen bonding and ionic interactions of waterborne

poly(urethane-urea)s that occurred as the TiO₂ nanoparticles content increased¹⁰. In addition, since they were located throughout the matrix, as mentioned in the Chapter 5, they can limit the interface contact after damage, apart from reducing the kinetic of diffusion¹⁷, which is a crucial parameter for an optimal self-healing efficiency⁹.

6.6. Conclusions

The effect of the incorporation of TiO₂ nanoparticles into synthesized waterborne poly(urethane-urea) films on the self-healing ability was investigated in this Chapter, getting to the next conclusions:

- It was proved that synthesized waterborne poly(urethane-urea) films and their nanocomposites with TiO₂ nanoparticles possess self-healing ability,
- Synthesized waterborne poly(urethane-urea) films exhibited intrinsic self-healing ability at room temperature without any external stimuli,
- Neat PU0 film showed a higher healing efficiency than TiO₂-PU0 nanocomposite films for deformation at break,
- 10TiO₂-PU0 and 20TiO₂-PU0 nanocomposite films exhibited higher healing efficiencies than neat PU0 film regardless of the number of cuts and of the mechanical property, except for the deformation at break,
- The WCA of neat PU0 film was not affected after the first cut/recovery cycle, while the contact angles of TiO₂-PU0 nanocomposite films were reduced from the first cut/recovery cycle. The contact angle of neat PU0 film decreased after the second cut/recovery cycle. Any change in contact angle were observed for investigated films after the third cut/recovery cycle,
- 40TiO₂-PU0 film did not possess self-healing ability, meaning that for a 40 wt% TiO₂ nanoparticles content the self-healing ability of the matrix disappeared.
- Both neat PUEPE19 and PUPEP27 films required shorter times than TiO₂-PUEPE19 and TiO₂-PUPEP27 nanocomposite films to completely repair the produced scratch,
- Neat PUEPE19 and PUPEP27 as well as 10TiO₂-PUEPE19 and 10TiO₂-PUPEP27 films were fully healed after 4 h,
- Increasing the TiO₂ nanoparticles content in TiO₂-PUEPE19 and TiO₂-PUPEP27 nanocomposite films resulted in a reduction of the self-healing

ability. This ability disappeared for 40TiO₂-PUEPE19 and 40TiO₂-PUPEP27 nanocomposite films.

6.7. References

- [1] C. Yuan, M. Z. Rong, M. Q. Zhang, Self-healing polyurethane elastomer with thermally reversible alkoxyamines as crosslinkages, *Polymer* 55 (2014) 1782-1791.
- [2] N. Roy, B. Bruchmann, J. M. Lehn, Dynamers: dynamic polymers as self-healing materials, *Chemical Society Reviews* 44 (2015) 3786-3807.
- [3] A. Faghihnejad, K. E. Feldman, J. Yu, M. V. Tirrell, J. N. Israelachvili, C. J. Hawker, E. J. Kramer, H. Zeng, Adhesion and surface interactions of a self-healing polymer with multiple hydrogen-bonding groups, *Advanced Functional Materials* 24 (2014) 2322-2333.
- [4] T. Wan, D. Chen, Synthesis and properties of self-healing waterborne polyurethanes containing disulfide bonds in the main chain, *Journal of Materials Science* 52 (2017) 197-207.
- [5] Y. Xu, D. Chen, A novel self-healing polyurethane based on disulfide bonds, *Macromolecular Chemistry and Physics* 217 (2016) 1191-1196.
- [6] D. G. Bekas, K. Tsirka, D. Baltzis, A. S. Paipetis, Self-healing materials: A review of advances in materials, evaluation, characterization and monitoring techniques, *Composites Part B: Engineering* 87 (2016) 92-119.
- [7] S. J. Garcia, Effect of polymer architecture on the intrinsic self-healing character of polymers, *European Polymer Journal* 53 (2014) 118-125.
- [8] J. Li, Q. Feng, J. Cui, Q. Yuan, H. Qiu, S. Gao, J. Yang, Self-assembled graphene oxide microcapsules in Pickering emulsions for self-healing waterborne polyurethane coatings, *Composites Science and Technology* 151 (2017) 282-290.
- [9] Y. J. Kim, P. H. Huh, B. K. Kim, Synthesis of self-healing polyurethane urea-based supramolecular materials, *Journal of Polymer Science Part B: Polymer Physics* 53 (2015) 468-474.
- [10] Y. Xiao, H. Huang, X. Peng, Synthesis of self-healing waterborne polyurethanes containing sulphonate groups, *RSC Advances* 7 (2017) 20093-20100.
- [11] X. Zhang, Z. Tang, D. Tian, K. Liu, W. Wu, A self-healing flexible transparent conductor made of copper nanowires and polyurethane, *Materials Research Bulletin* 90 (2017) 175-181.
- [12] Y. Fang, X. Du, Y. Jiang, Z. Du, P. Pan, X. Cheng, H. Wang, Thermal-driven self-healing and recyclable waterborne polyurethane films based on reversible covalent interaction, *ACS Sustainable Chemistry & Engineering* 6 (2018) 14490-14500.
- [13] J. Aizpurua, L. Martin, E. Formoso, A. González, L. Irusta, One pot stimuli-responsive linear waterborne polyurethanes via Diels-Alder reaction, *Progress in Organic Coatings* 130 (2019) 31-43.
- [14] A. Feula, A. Pethybridge, I. Giannakopoulos, X. Tang, A. Chippindale, C. R. Siviour, C. P. Buckley, I. W. Hamley, W. Hayes, A thermoreversible supramolecular polyurethane with excellent healing ability at 45 °C, *Macromolecules* 48 (2015) 6132-6141.

- [15] Q. Zheng, Z. Ma, S. Gong, Multi-stimuli-responsive self-healing metallo-supramolecular polymer nanocomposites, *Journal of Materials Chemistry A* 4 (2016) 3324-3334.
- [16] X. Yu, P. Yang, Z. Zhang, L. Wang, L. Liu, Y. Wang, Self-healing polyurethane nanocomposite films with recoverable surface hydrophobicity, *Journal of Applied Polymer Journal* 135 (2018) 46421/1-46421/10.
- [17] T. Wan, D. Chen, Mechanical enhancement of self-healing waterborne polyurethane by graphene oxide, *Progress in Organic Coatings* 121 (2018) 73-79.
- [18] J. T. Kim, B. K. Kim, E. Y. Kim, S. H. Kwon, H. M. Jeong, Synthesis and properties of near IR induced self-healable polyurethane/graphene nanocomposites, *European Polymer Journal* 49 (2013) 3889-3896.
- [19] S. Thakur, N. Karak, A tough, smart elastomeric bio-based hyperbranched polyurethane nanocomposite, *New Journal of Chemistry* 39 (2015) 2146-2154.
- [20] S. Thakur, S. Barua, N. Karak, Self-healable castor oil based tough smart hyperbranched polyurethane nanocomposite with antimicrobial attributes, *RSC Advances* 5 (2015) 2167-2176.
- [21] R. Duarah, N. Karak, High performing smart hyperbranched polyurethane nanocomposites with efficient self-healing, self-cleaning and photocatalytic attributes, *New Journal of Chemistry* (2018) 2167-2179.
- [22] J. Mattia, P. Painter, A comparison of hydrogen bonding and order in a polyurethane and poly(urethane-urea) and their blends with poly(ethylene glycol), *Macromolecules* 40 (2007) 1546-1554.
- [23] N. Kuhl, S. Bode, M. D. Hager, U. S. Schubert, Self-healing polymers based on reversible covalent bonds, *Advances in Polymer Science* 273 (2016) 1-58.

Chapter



"None of us is as good as all of us."

(Ray Kroc)

Development of hydrogels by incorporation of sodium alginate

7. Development of hydrogels by incorporation of sodium alginate

7.1. Chapter overview	151
7.2. Introduction	151
7.3. Preparation of hydrogels by incorporation of sodium alginate	152
7.4. Characterization of hydrogels	154
7.4.1. Rheology	154
7.4.2. Chemical structure, thermal properties and thermal degradation	156
7.4.3. Morphology	162
7.4.4. Mechanical properties	164
7.4.5. Swelling degree	165
7.4.6. Cell proliferation	167
7.5. Conclusions	168
7.6. References	170

7.1. Chapter overview

This Chapter deals with the design and characterization of hydrogels. This is achieved by the introduction of sodium alginate into synthesized waterborne poly(urethane-urea)s and forming after a cross-linked network employing calcium chloride.

For designed hydrogels, further characterization beyond chemical, thermal and mechanical properties is carried out. This additional characterization is focused on analyzing their cross-linking density by rheological measurements, observing their porous network by SEM and studying their swelling ability in acid medium. Furthermore, an *in vitro* cell proliferation study is carried out using Human Fibroblasts Cells.

7.2. Introduction

Sodium alginate (SA) is a natural polysaccharide formed by β -D-mannuronate (M) and α -L-guluronate (G) units¹⁻⁴. These blocks are disposed in different arrangements, as they are repeating (MM or GG) and alternating (MG or GM) blocks¹⁻⁴. The network of SA can be easily achieved by the incorporation of a divalent cation, leading to physical cross-linking^{5,6}. Different divalent cations can be employed in order to obtain a cross-linked network, such as Ba^{2+} , Mg^{2+} , Mn^{2+} , Sr^{2+} and Ca^{2+} , among others^{1,3-5,7-11}. Interactions taking place between divalent cations and the network of SA were explained by Grant et al¹⁰. They proposed what they denominated egg-box model (Figure 7.1), expounding that divalent cations form a chelated structure with guluronate blocks (GG) of the structure of SA by cooperatively binding to them^{1,4,7,10,12}. It has been concluded that Ca^{2+} is the optimal divalent cation among all which have been investigated^{1,4}.

Focusing on applying this strategy for the preparation of hydrogels based on polyurethanes and poly(urethane-urea)s, Travinskaya et al.^{9,11} have reported interesting results on waterborne polyurethanes. Nevertheless, poly(urethane-urea)s have not been a subject of study regarding the strategy of incorporation of SA and further cross-linking with CaCl_2 , even if blends with SA have been reported¹³.

Consequently, it is worth studying hydrogels based on poly(urethane-urea)s, especially waterborne ones, as they are more environmentally friendly. The preparation of hydrogels can extend the range of applications of these materials. It has been reported that the incorporation of magnetic nanoparticles, such as CoFe_2O_4 and Fe_3O_4 , allowed to control the location in the body of hydrogels for drug delivery by an external magnetic force^{14,15}. The addition of Au nanoparticles is carried out for application in bioprinting for tissue engineering¹⁶, whereas the incorporation of TiO_2 nanoparticles led to hydrogels with the ability to absorb and, thus, remove arsenic and other heavy metal ions from water^{17,18}. Therefore, these kind of hydrogels can be used for tissue engineering^{2,19}, wound dressing^{5,20}, drug delivery^{2,7,19}, among other applications.

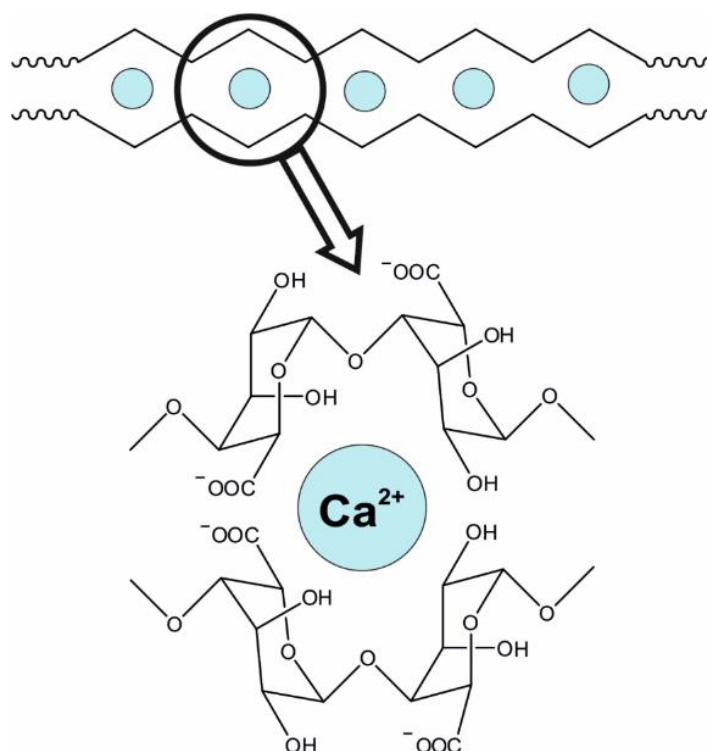


Figure 7.1. Schematic illustration of the egg-box model in which Ca^{2+} cations are accommodated between α -L-guluronate blocks of the alginate chains.

7.3. Preparation of hydrogels by incorporation of sodium alginate

PU0 and PUEPE29, which synthesis is described in Chapter 4, were the selected waterborne poly(urethane-urea)s for the preparation of hydrogels. First, equals

volumes of these dispersions, since their solid contents were similar (~25 wt%), were magnetically mixed with different volumes of SA (4 wt% in water) by stirring at 300 rpm for 24 h. In all cases, 2.6 g of waterborne poly(urethane-urea)s were employed. Once homogeneous mixtures were obtained, 3 mL of each mixture were poured into plastic vessels with a diameter of 25 mm. Finally, 5 mL of 5 wt% CaCl₂ were added to each vessel. After 48 h, CaCl₂ was removed and hydrogels were gently washed with distilled water. In the case of nanocomposite hydrogels, TiO₂ nanoparticles (33-37 wt% in water) and waterborne poly(urethane-urea) dispersion were magnetically mixed for 5 h at room temperature before addition of SA, then the process followed was the same as the described one. The followed procedure for hydrogels preparation, as well as the unsuccessful direct incorporation of CaCl₂ to the waterborne poly(urethane-urea)s, are presented in Figure 7.2.

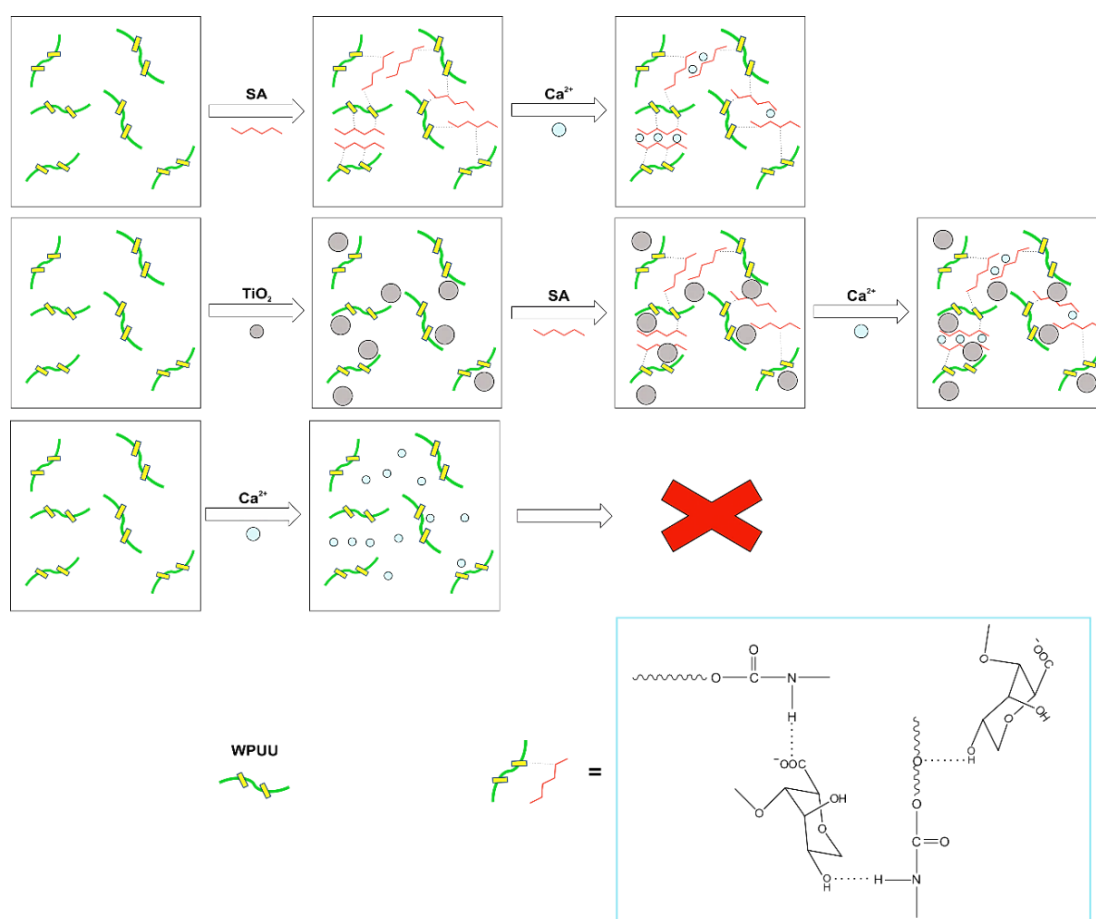


Figure 7.2. Schematic description of the protocol followed for the preparation of hydrogels, as well as the proposed hydrogen bonding between SA and waterborne poly(urethane-urea)s.

The designation of the prepared hydrogels, as well as the content of their constituents are summarized in Table 7.1.

Table 7.1. Designation of prepared hydrogels and content of PU0, PUEPE29, SA and TiO₂ nanoparticles in prepared hydrogels.

Sample	PU0 (wt%)	PUEPE29 (wt%)	SA (wt%)	TiO ₂ (wt%)
20SA-PU0	80	0	20	0
30SA-PU0	70	0	30	0
TiO ₂ -SA-PU0	65	0	27	8
20SA-PUEPE29	0	20	20	0
30SA-PUEPE29	0	30	30	0
TiO ₂ -SA-PUEPE29	0	65	27	8

The visual aspects of the prepared hydrogels are shown in Figure 7.3.

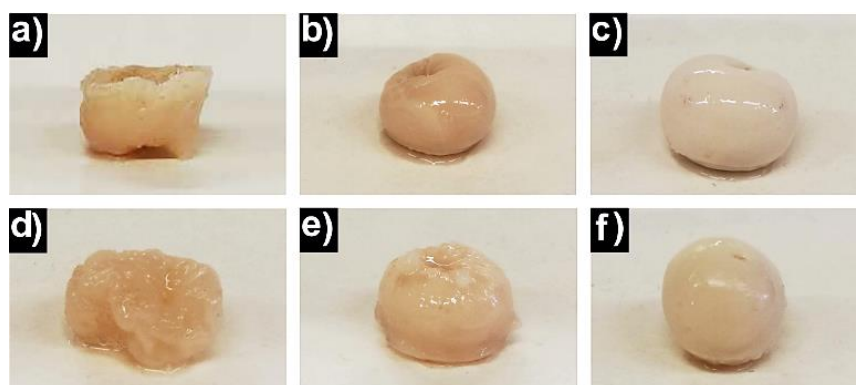


Figure 7.3. Visual aspect of prepared hydrogels based on synthesized waterborne poly(urethane-urea)s. (a) 20SA-PU0, (b) 30SA-PU0, (c) TiO₂-SA-PU0, (d) 20SA-PUEPE29, (e) 30SA-PUEPE29 and (f) TiO₂-SA-PUEPE29.

Hydrogels were freeze-dried before each measurement, except for rheological characterization.

7.4. Characterization of hydrogels

7.4.1. Rheology

The study of the viscoelastic properties by dynamic rheological analysis allowed confirming cross-linking and gelling formation for all designed hydrogels. As can be observed in Figure 7.4, all designed hydrogels exhibited a higher storage modulus (G') than loss modulus (G''). These results corroborated the successful physical cross-linking of prepared hydrogels since $G' > G''$ is an indication of gel formation²¹⁻²⁴.

Obtained values for G' and G'' were higher than for other reported polyurethane and waterborne polyurethane based gels^{25,26}, and in the order of gels based on alginate²⁷. As it can be observed, both G' and G'' decreased with the increase of SA content as well as with the incorporation of TiO_2 nanoparticles. Nonetheless, cross-linking is related to $\tan \delta$, as a lower value of $\tan \delta$ indicates a higher cross-linking density^{19,28}.

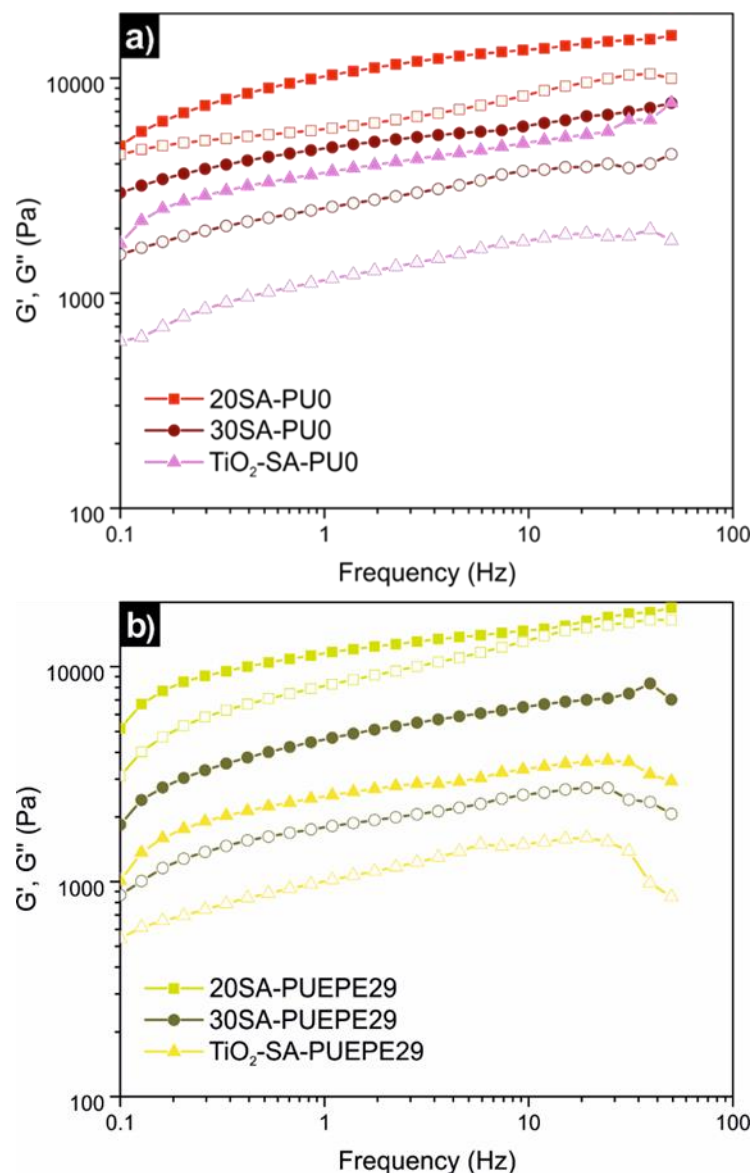


Figure 7.4. Frequency dependence of G' (solid symbols) and G'' (open symbols) of prepared hydrogels based on (a) PU0 and (b) PUEPE29 waterborne poly(urethane-urea)s.

In designed hydrogels, $\tan \delta$ values for 20 wt% SA content were of 0.63 ± 0.07 and 0.77 ± 0.12 for 20SA-PU0 and 20SA-PUEPE29, respectively. These values suggested that for 20 wt% SA content the cross-linking density was similar regardless of the waterborne poly(urethane-urea). Nonetheless, $\tan \delta$ values decreased when the SA content increased to 30 wt%, resulting in 0.55 ± 0.04 and 0.39 ± 0.03 for 30SA-PU0 and

30SA-PUEPE29, respectively. These different $\tan \delta$ values suggested that the soft segment structure of employed waterborne poly(urethane-urea)s modulated the cross-linking ability. The lower decrease in $\tan \delta$ observed for 30SA-PU0 in comparison to 30SA-PUEPE29 points out to more interactions taking place between SA and ether oxygen of soft segment of PU0¹². The result of this was less chelation points available for cross-linking. The explanation for this was the higher PEO content in PU0 than in PUEPE29. There was a higher tendency of ether oxygen of PEO to form the hydrogen bonds in comparison to PPO block as a consequence of the steric hindrance effect of its $-\text{CH}_3$ side chains^{29,30}. At this point, it must be bring up, as previously mentioned, that cross-linking is consequence of chelation between Ca^{2+} and SA, whereas waterborne poly(urethane-urea) did not participate in cross-linking (see Figure 7.2).

Incorporation of TiO_2 nanoparticles led to $\tan \delta$ values of 0.33 ± 0.05 and 0.43 ± 0.04 for TiO_2 -SA-PU0 and TiO_2 -SA-PUEPE29, respectively. TiO_2 nanoparticles affected the cross-linking density of TiO_2 -SA-PU0, increasing it if compared to the cross-linking of 30SA-PU0. This increase can be related to the incorporation of TiO_2 nanoparticles, which interacted predominately with the hard segment, as concluded in the Chapter 5, restricting hydrogen bonding between SA and PU0. This can result in more chelation points available, hence higher cross-linking density if compared to 30SA-PU0 for a similar SA content. This effect can be explained assuming that TiO_2 nanoparticles present OH groups in their surface formed after dissociative chemisorption of water³¹. Therefore, TiO_2 nanoparticles, incorporated to the waterborne poly(urethane-urea) before addition of SA, can form hydrogen bonds with the waterborne poly(urethane-urea) structure³²⁻³⁴, particularly with the ether oxygen of PEO³², given the steric hindrance of $-\text{CH}_3$ side chains of PPO block^{29,30}, and with the hard segment. Accordingly, since the SA content in TiO_2 -SA-PUEPE29 was equal to 27 wt%, the cross-linking density was quite similar to that for 30SA-PUEPE29.

7.4.2. Chemical structure, thermal properties and thermal degradation

FTIR spectra of investigated hydrogels are shown in Figure 7.5 and FTIR spectra of the basic components are displayed in Figure A.8 in Annexes.

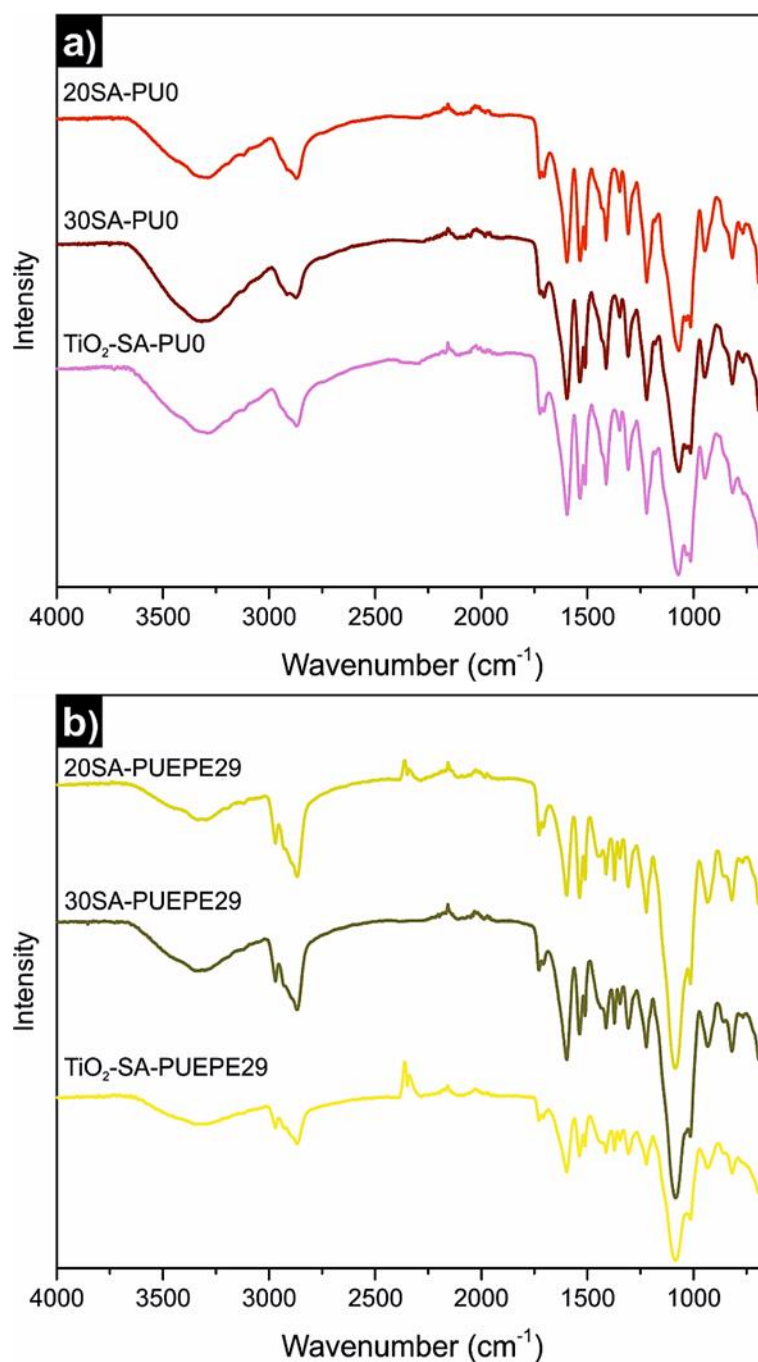


Figure 7.5. FTIR spectra of designed hydrogels based on (a) PU0 and (b) PUEPE29 waterborne poly(urethane-urea)s.

The broad absorption bands at 3500-3200 cm⁻¹ confirmed the incorporation of SA to the structure of the hydrogels since that broad band was similar to the one observed for SA (Figure A.8). It was the result of the multiple hydrogen bonding of its structure^{12,35}. Stretching vibration of N-H groups of poly(urethane-urea) structure also appeared in that region¹² but they were overlapped by the intense band of O-H groups of alginate. The presence of poly(urethane-urea) chains in designed hydrogel was confirmed by bands at 3000-2700 cm⁻¹, corresponding predominantly to the

stretching vibrations of C–H groups within the structure of poly(urethane-urea)s^{12,35}. The band at 1200-1000 cm^{-1} were related to the stretching vibration of ether groups^{12,35} of both structures of poly(urethane-urea) and SA. Incorporation of TiO_2 nanoparticles was confirmed by the increase in intensity observed below 800 cm^{-1} , which is associated to stretching vibrations of Ti–O–Ti³⁶. TiO_2 nanoparticles content was the same for both TiO_2 -SA-PU0 and TiO_2 -SA-PUEPE29.

Figure 7.6 shows the DSC thermograms of designed hydrogels.

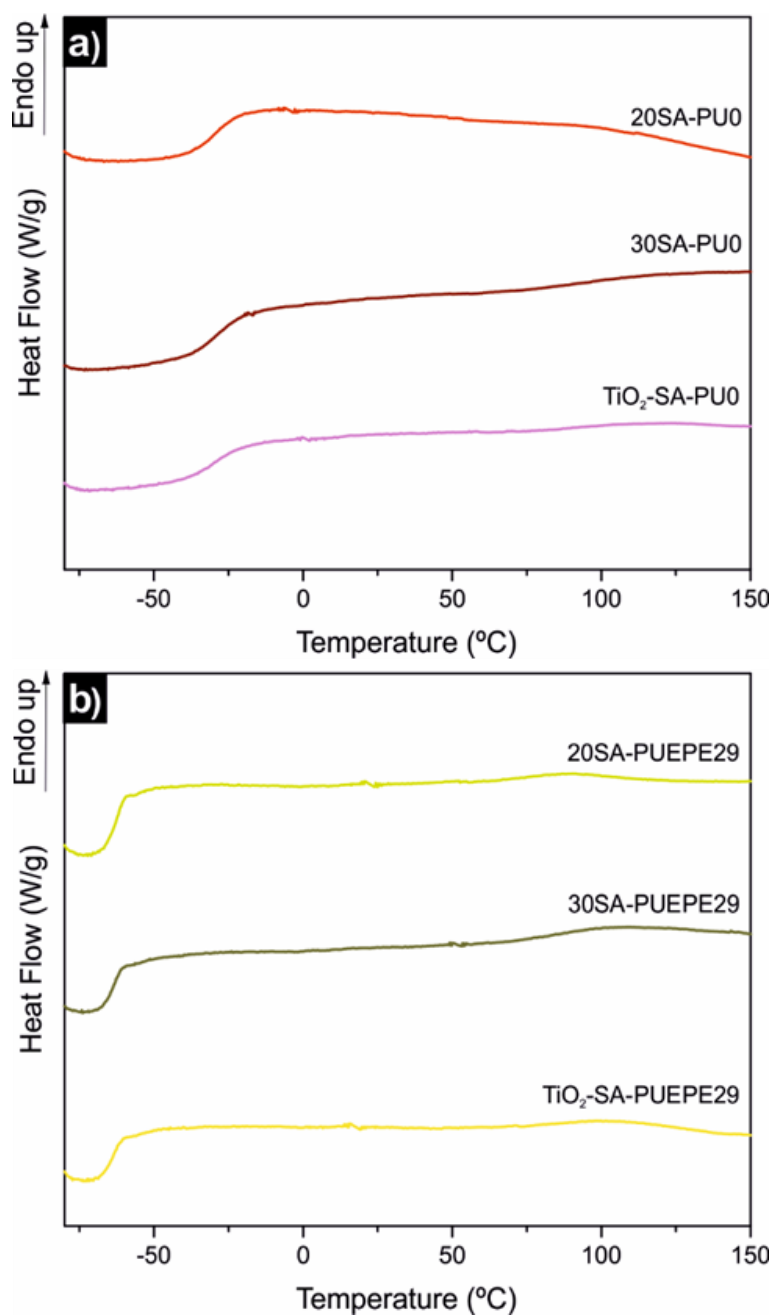


Figure 7.6. DSC curves of hydrogels based on (a) PU0 and (b) PUEPE29 waterborne poly(urethane-urea)s.

The T_g values of SA-PU0 serie were lower if compared to neat PU0 (Table 7.2). The decrease of T_g values observed for SA-PU0 serie in comparison to neat PU0 can be result of the interaction between SA and PU0. The formation of hydrogen bonds between SA and PU0 probably restricted intramolecular hydrogen bonding between soft and hard segments of PU0. Therefore, observed decrease in the T_g associated with the soft segment was caused by the increase in the mobility of the polymer chains^{22,37}. T_g almost did not vary with the increase in the content of SA and the incorporation of TiO₂ nanoparticles.

In the case of SA-PUEPE29 serie, the T_g barely change with the incorporation of SA and TiO₂ nanoparticles. This can be the result of the inferior intramolecular hydrogen bonding between soft and hard segments that PUEPE29 waterborne poly(urethane-urea) presents, consequence of the, as previously mentioned, steric hindrance of -CH₃ side chains of PPO blocks^{29,30}. Therefore, the incorporation of SA did not affect the mobility of the poly(urethane-urea) chains in a great extent, thus T_g was almost invariable.

Table 7.2. Glass transition temperatures of neat waterborne poly(urethane-urea)s and of the prepared hydrogels.

Sample	T_g (°C)
PU0^a	6
20SA-PU0	-29
30SA-PU0	-28
TiO₂-SA-PU0	-31
PUEPE29^a	-62
20SA-PUEPE29	-63
30SA-PUEPE29	-64
TiO₂-SA-PUEPE29	-65

a) Determined from DSC curves displayed in Figure A.7 in Annexes.

Derivative thermogravimetric analysis (dTGA) curves of designed hydrogels are plotted in Figure 7.7. Temperatures for the different peaks observed in dTGA curves of hydrogel components and designed hydrogels are displayed in Table 7.3. dTGA curves of SA, PU0, PUEPE29 and TiO₂ nanoparticles employed for the preparation of designed hydrogels are shown in Figure A.10 in Annexes.

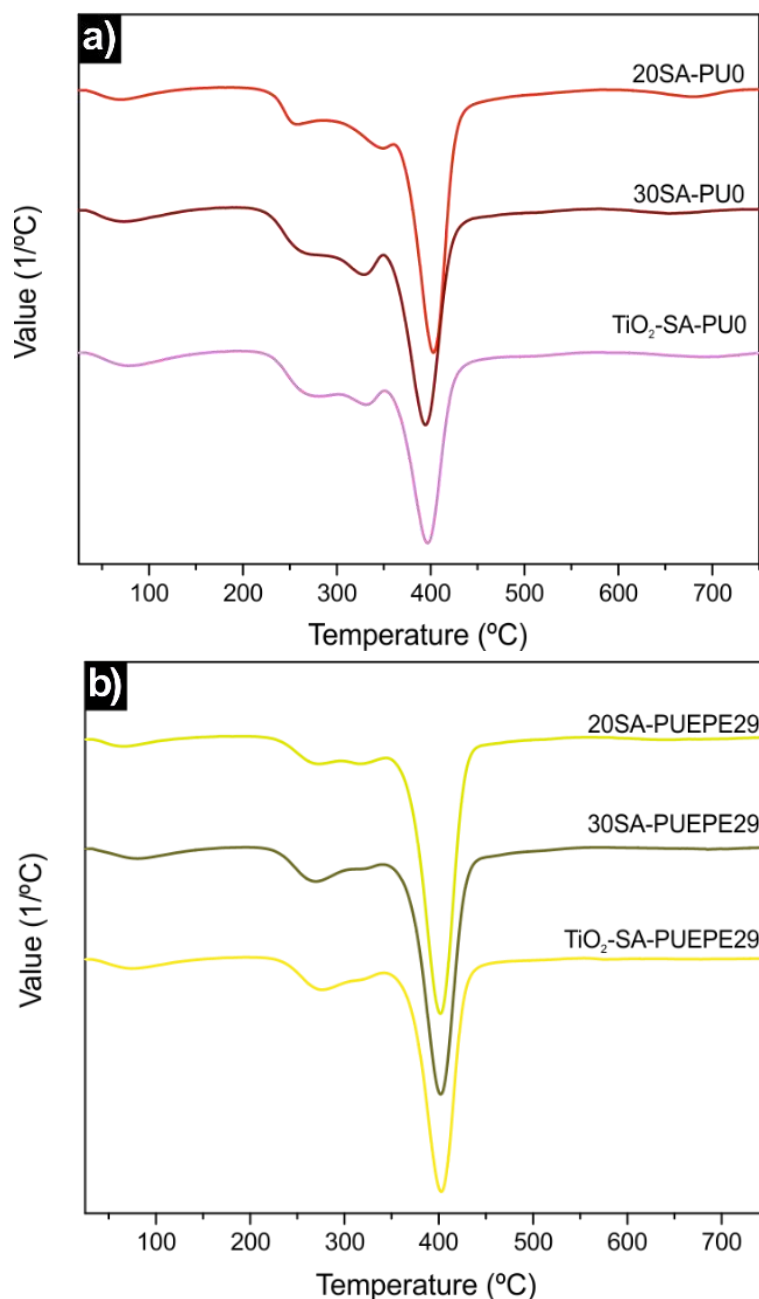


Figure 7.7. dTGA curves of designed hydrogels based on (a) PU0 and (b) PUEPE29 waterborne poly(urethane-urea)s.

The peak observed below 100 °C corresponded to the water evaporation. The first peak in dTGA curves (T_{SA}), taking place between 258 and 282 °C, depending on the hydrogel, corresponded to the degradation of SA. Taking into account that the degradation of neat SA occurred at 233 °C, it can be concluded that the interactions of SA with Ca^{2+} and waterborne poly(urethane-urea)s led to an increase in the thermal stability of SA³⁸. The second peak (T_1) for each designed hydrogel corresponded to the degradation of the hard segment of either PU0 or PUEPE29. Meanwhile, the third

peak (T_2) was associated to the degradation of the soft segment of synthesized waterborne poly(urethane-urea)s³⁹.

T_1 and T_2 slightly varied for hydrogels of SA-PU0 serie. These degradations took place at similar temperatures regardless of the SA and TiO₂ nanoparticles contents in the case of designed hydrogels of SA-PUEPE29 serie. This can be explained by the previously discussed less favored interactions between SA and PUEPE29 if compare to interactions between SA and PU0.

Table 7.3. Decomposition temperatures of neat SA and waterborne poly(urethane-urea)s as well as of the designed hydrogels. Decomposition temperatures were related to SA (T_{SA}), the hard segment (T_1) and the soft segment (T_2) of waterborne poly(urethane-urea)s.

Sample	T_{SA} (°C)	T_1 (°C)	T_2 (°C)
Alginate^b	233	—	—
PU0^b	—	335	412
20SA-PU0^a	258	349	403
30SA-PU0^a	263	329	395
TiO₂-SA-PU0^a	282	332	397
PUEPE29^b	—	352	395
20SA-PUEPE29^a	273	316	402
30SA-PUEPE29^a	270	319	402
TiO₂-SA-PUEPE29^a	276	317	403

a) Determined from dTGA curve (Figure 7.7).

b) Determined from dTGA curve which is presented in Figure A.10 in Annexes.

In consideration of all the results and conclusions discussed so far, Figure 7.8 presents an schematic representation of the proposed effect of the incorporation of SA and TiO₂ to synthesized waterborne poly(urethane-urea)s. It can be appreciated the higher amount of intramolecular hydrogen bonding between segments of PU0 than of PUEPE29.

The incorporation of SA led to disruption of interactions within the waterborne poly(urethane-urea) structure and the formation of hydrogen bonds between waterborne poly(urethane-urea) and SA. These latter ones could be more favored in the case of PU0 than in the case of PUEPE29 consequence of the PPO block, as mentioned before. Interaction of TiO₂ nanoparticles with PU0 could be more favored

than with PUEPE29. These interactions taking place between the inorganic nanoparticles and predominately the hard segment, in an inferior extent with the PEO block of the soft segment, can be more restricted in the case of PUEPE29 due to the effect of PPO blocks.

Summing up, and as it is described in Figure 7.8, depending on the mentioned hydrogen bonding interactions, SA exhibited different ability for chelation with Ca^{2+} since the number of available chelation points varied. This led to the observed differences in the final properties of designed hydrogels.

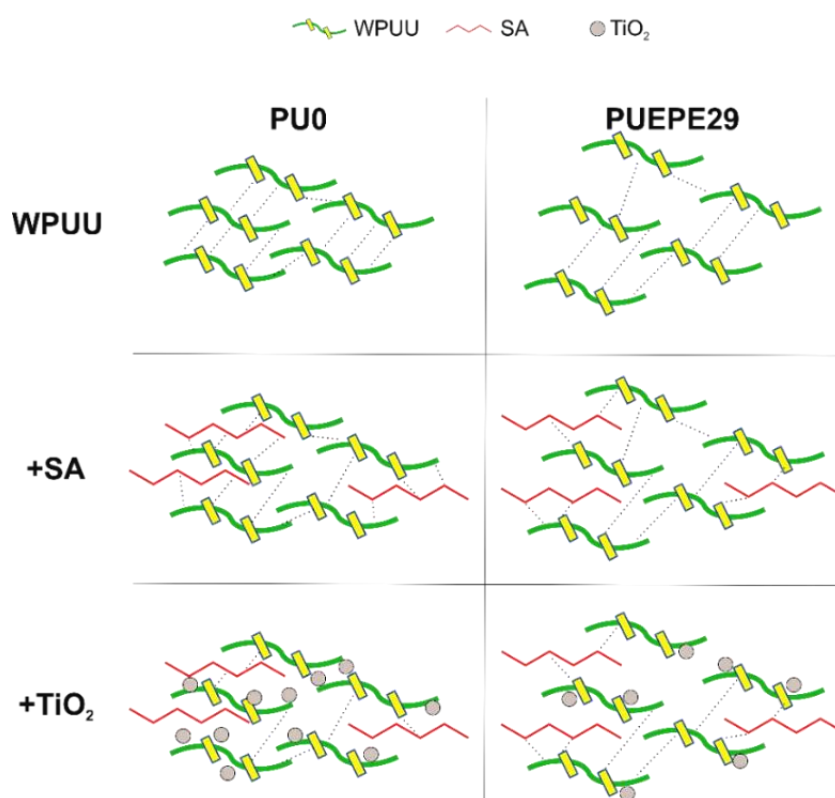


Figure 7.8. Proposed hydrogen bonding interactions between SA, TiO_2 nanoparticles and both PU0 and PUEPE29 waterborne poly(urethane-urea)s regarding their different soft segment compositions.

7.4.3. Morphology

The morphology of designed hydrogels was studied by means of SEM. As shown in Figure 7.9, designed hydrogels presented a heterogeneous interconnected porous network. At first sight, it can be appreciated that the morphology of SA-PU0 serie was smoother than the one of SA-PUEPE29 serie. 20SA-PU0 presented a higher amount of open areas than 30SA-PU0 and TiO_2 -SA-PU0. Considering that an increase in size

regularity and compactness is associated to an increase in the cross-linking density^{22,40,41}, it can be concluded that the cross-linking density increased when increasing SA content. Likewise, SA-PUEPE29 serie hydrogels presented a similar structure to that of hydrogels based on PU0.

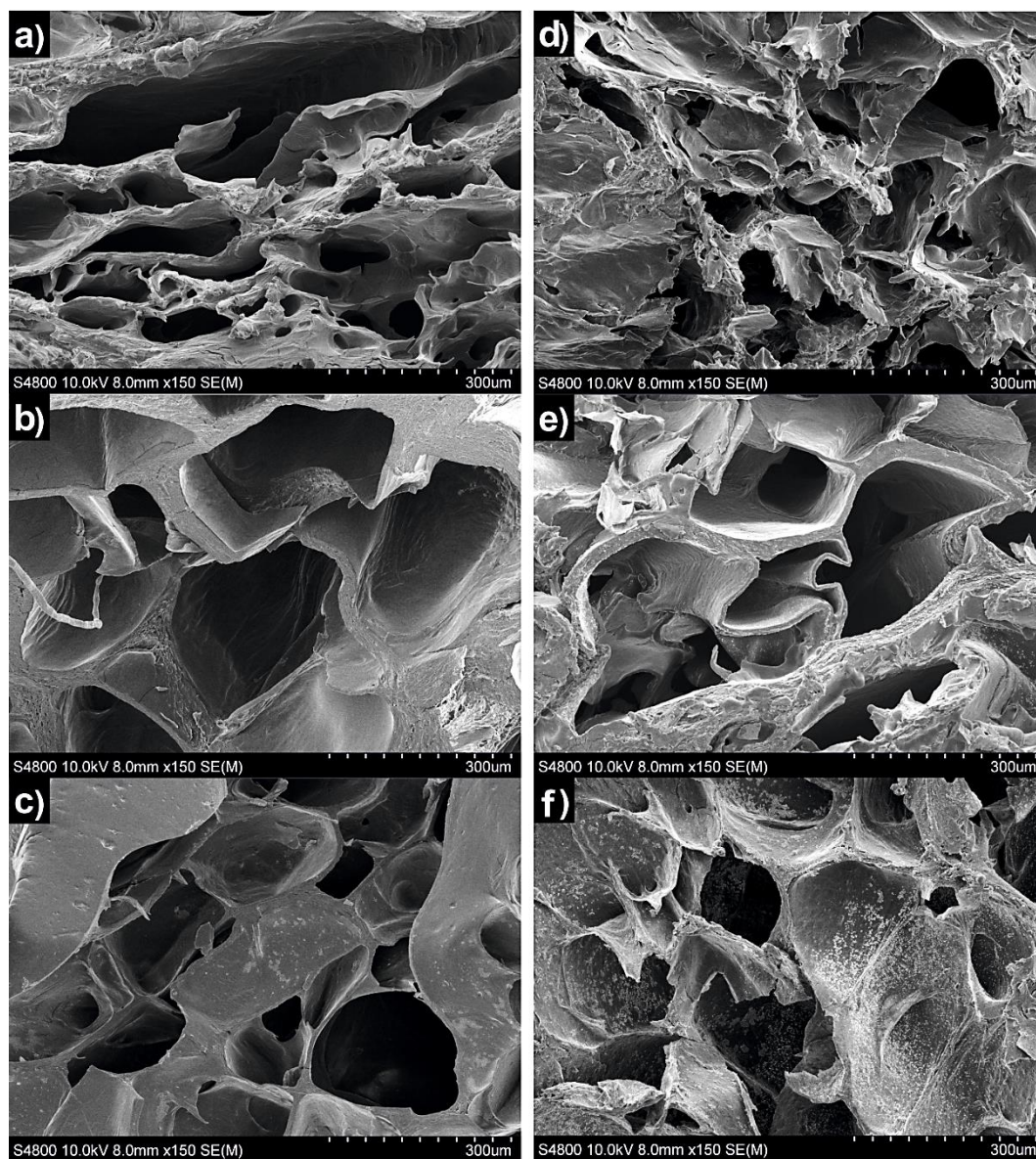


Figure 7.9. SEM images of cross-section of (a) 20SA-PU0, (b) 30SA-PU0, (c) TiO₂-SA-PU0, (d) 20SA-PUEPE29, (e) 30SA-PUEPE29 and (f) TiO₂-SA-PUEPE29.

In Figure 7.9c and Figure 7.9f the effect of the incorporation of TiO₂ nanoparticles on SA-PU0 and SA-PUEPE29 structures can be observed. Although both hydrogels contained the same amount of TiO₂ nanoparticles, these nanoparticles dispersed throughout the hydrogel network were more distinguishable for TiO₂-SA-PUEPE29. On the one hand, as explained in the Chapter 5 and evaluated by AFM, triblock

copolymers based waterborne poly(urethane-urea)s, as it is the case of PUEPE29, displayed a microphase separated morphology consequence of the thermodynamically incompatible PEO and PPO blocks. On the other hand, PU0, with a soft segment formed just by PEO homopolymer, did not present phase separation, as observed in both the Chapters 3 and 5, and as a result TiO₂ nanoparticles were dispersed throughout the polymer matrix.

7.4.4. Mechanical properties

Compressive modulus and stress, at strains of 60 and 70%, of prepared hydrogels investigated by means of compression test are listed in Table 7.4. In the cases of both SA-PU0 and SA-PUEPE29 hydrogel series, the compressive modulus increased with the increase of the SA content. This increase was particularly remarkable for 30SA-PUEPE29, presenting a compressive modulus 2.5 MPa higher than that of 20SA-PUEPE29. These results were in concordance with the conclusions from previously analyzed data, from which it was concluded that the cross-linking density of 30SA-PUEPE29 and 30SA-PU0 were higher than the one of 20SA-PUEPE29 and 20SA-PU0.

Table 7.4. Compressive modulus and compressive stress, at different strains, of designed hydrogels.

Sample	Compressive modulus (MPa)	Compressive stress (MPa)	
		Strain 60%	Strain 70%
20SA-PU0	4.9 ± 1.1	0.13 ± 0.03	0.27 ± 0.07
30SA-PU0	5.1 ± 0.9	0.22 ± 0.07	0.46 ± 0.20
TiO₂-SA-PU0	6.3 ± 0.5	0.20 ± 0.10	0.41 ± 0.10
20SA-PUEPE29	3.9 ± 0.3	0.15 ± 0.07	0.33 ± 0.09
30SA-PUEPE29	6.4 ± 1.1	0.19 ± 0.02	0.39 ± 0.04
TiO₂-SA-PUEPE29	4.7 ± 0.4	0.19 ± 0.07	0.40 ± 0.18

The incorporation of TiO₂ nanoparticles clearly increased the compressive modulus for TiO₂-SA-PU0, since it was 1.2 MPa higher than that of 30SA-PU0 hydrogel. Nonetheless, the compressive modulus of TiO₂-SA-PUEPE29 was 1.7 MPa lower than the compressive modulus of 30SA-PUEPE29. These results agreed with the

rheological results and proved the commented relevance of different interactions of TiO₂ nanoparticles depending on the soft segment of employed waterborne poly(urethane-urea)s, since interactions were more favored with PU0 than with PUEPE29.

Regarding compressive stress values, there were not appreciated great differences neither at 60% of strain nor at 70% of strain. Nonetheless, slight increases were observed when the SA content was increased from 20 to 30%, whereas the hydrogels based on nanocomposites showed similar values to the observed for those containing 30% of SA. The obtained results also agreed with the observed rheological behavior.

From compressive test results, it can be concluded that mechanical properties were improved when SA content was increased and when TiO₂ nanoparticles were added. This was something expected taking into account that SA interacts with Ca²⁺ cations^{7,10,27}, what leads to higher cross-linking density with the increase of SA content, and also in contemplation that TiO₂ nanoparticles are commonly used as reinforcement^{42,43}.

7.4.5. Swelling degree

Swelling degree curves for acid medium are shown in Figure 7.10. Study of the swelling degree in basic medium was not carried out due to hydrogels breaking down and losing their integrity immediately when they were submerged in this medium, while in neutral medium, just water, they also lost their integrity after 2 h. This was an expected result since the pKa of the carboxyl groups within alginate structure ranges from 3.4 to 4.4, meaning that the physical cross-linked network remains in acid conditions breaking down as the pH increases^{3,20}. The mass evolution during the swelling test for each measured sample was determined by comparison of the weight before and after carrying out the swelling test.

Designed hydrogels reached swelling equilibrium after 2 h in 0.1 M citric acid solution. Equilibrium swelling degrees within each hydrogel serie were quite similar. Nonetheless, equilibrium swelling degrees of hydrogels of SA-PUEPE29 serie were higher if compare to those of hydrogels of SA-PU0 serie. In the case of SA-PU0 serie, equilibrium swelling degrees ranged from 330±2 to 357±31%. All three hydrogels

maintained their integrity and their mass loss was low (~10-20%). Regarding SA-PUEPE29 serie, designed hydrogels presented equilibrium swelling degrees higher than those of SA-PU0 serie, ranging from 426 ± 54 to $462\% \pm 56$. Their mass loss was also small (~12-21%).

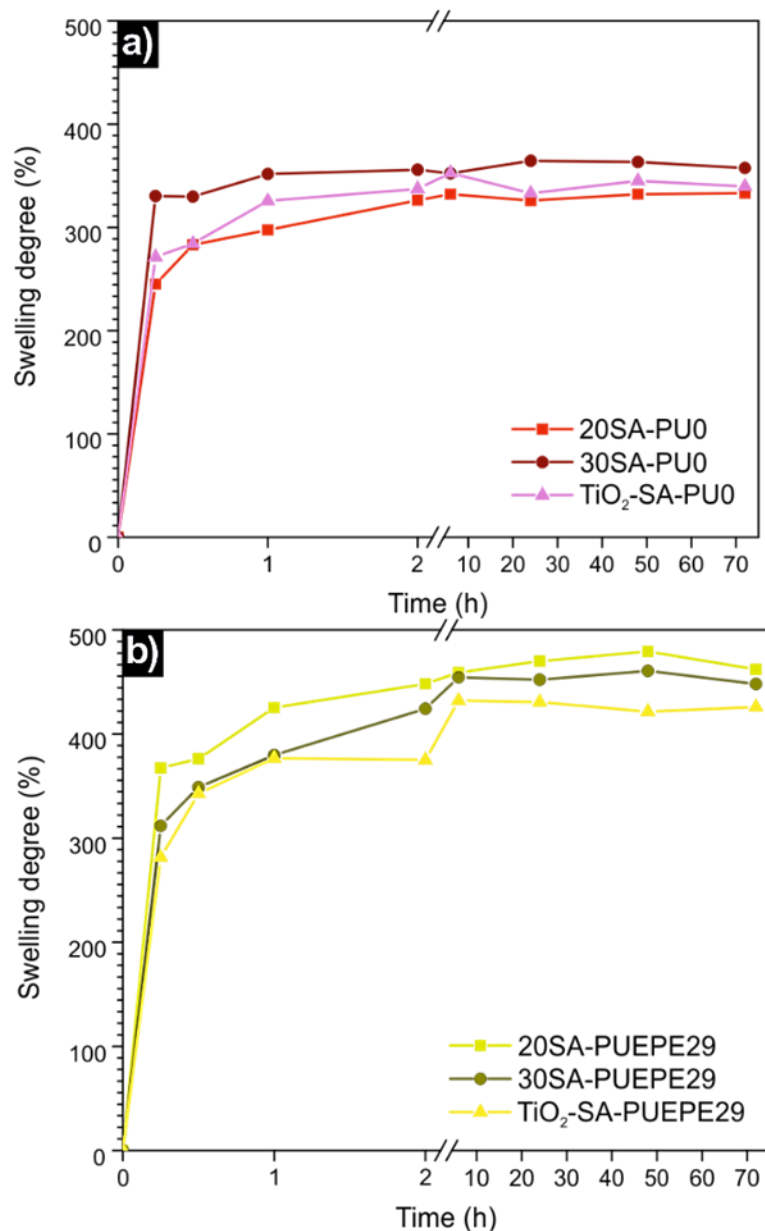


Figure 7.10. Swelling degree of prepared hydrogels based on (a) PU0 and (b) PUEPE29 waterborne poly(urethane-urea)s in acidic pH (solid symbols).

The swelling degree in aqueous solutions strongly depends on the cross-linking density, since the part of hydrogels which shows higher swelling ability is related to the non-cross-linked segments, while the cross-linked regions obstruct the solution from entering the hydrogel^{5,22,24,40}. Nonetheless, there were not significant differences

in equilibrium degree values within each series, regardless of the SA and TiO₂ nanoparticles contents. From these results, it can be concluded that in designed hydrogels the cross-linking density did not play a key role. On the contrary, there were differences in equilibrium degree values between SA-PU0 and SA-PUEPE29 hydrogel series. These differences can be related with the availability of hydrophilic sites of the hydrogel, and thus related to the previously commented interactions between SA and waterborne poly(urethane-urea)s. As discussed, interactions of SA with PU0 were more favored than with PUEPE29. The consequence of this effect was that there were more SA molecules that could not interact with the waterborne poly(urethane-urea) structure in the case of PUEPE29, thus available to interact with water molecules, resulting in a higher swelling ability.

7.4.6. Cell proliferation

Since synthesized hydrogels can find applications as biomaterials in medicine, it was necessary to verify the absence of cytotoxicity in these hydrogels. Figure 7.11 presents *in vitro* cell proliferation of investigated hydrogels in comparison with the control group, where the absorbance of the negative control (Control) and of the investigated samples cells are shown.

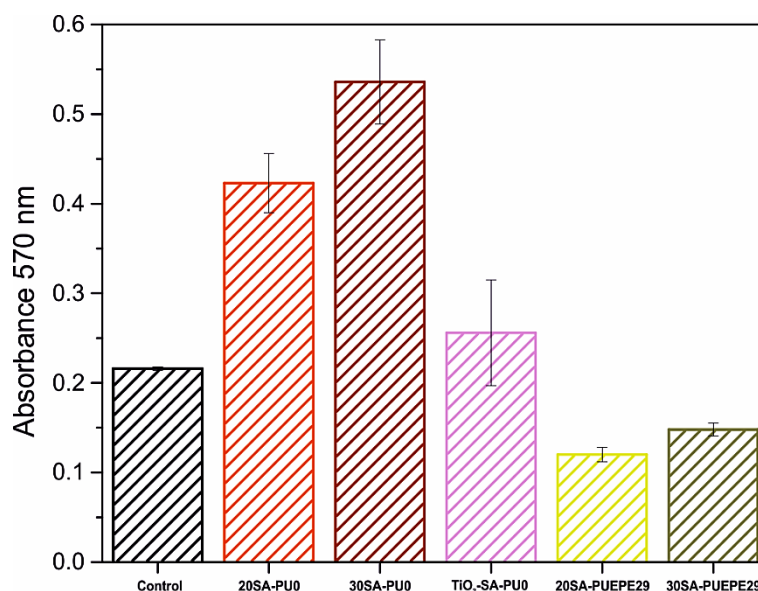


Figure 7.11. *In vitro* cell proliferation (MTT method) of prepared hydrogels after Human Fibroblast cell culture (48 h) in the presence or not of different treated materials. (Control x 20SA-PU0 $p < 0.0006$, Control x 30SA-PU0 $p < 0.0003$, Control x 20SA-PUEPE29 $p < 0.0008$, Control x 30SA-PUEPE29 $p < 0.0002$).

In general, the hydrogels based on PU0 showed no cytotoxicity if compare to hydrogels based on PUEPE29 which were not efficient in maintaining the cell growth indicating their cytotoxic effect. 20SA-PU0 and 30SA-PU0 hydrogels showed the highest cell growth if compared with control group suggesting that these materials can behave as promoters of cellular growth. The cell proliferation was even higher than the one observed for the Control after the incubation period. This means that these hydrogels had the effect of inducing cell proliferation⁴⁴. Especially taken into account that the cell viability of these hydrogels is two times higher that this of the control group. In the case of 20SA-PU0, cell viability value was almost 200%, whereas it was almost of 250% for 30SA-PU0. As can be clearly observed, the addition of the TiO₂ nanoparticles into SA-PU0 hydrogel decreased the cell growth even if the system was still no cytotoxic. This makes sense since some kind of toxicity of TiO₂ nanoparticles caused by dermal exposure has been reported⁴⁵. Nevertheless, the doses employed in these studies are commonly too high if compared to a normal dose to which a person can be exposed on a daily basis⁴⁵. In contemplation of these results, TiO₂ nanoparticles could be utilized in order to modulate the cell proliferation of the hydrogels.

Regarding PUEPE29 based hydrogels, it was not possible to perform *in vitro* cell proliferation test in TiO₂-SA-PUEPE29 hydrogel. In the cases of 20SA-PUEPE29 and 30SA-PUEPE29, their cell viability values were under 70%, meaning that they had a cytotoxic effect.

7.5. Conclusions

In this Chapter it was proved that hydrogels based on synthesized waterborne poly(urethane-urea)s can be successfully designed concluding that:

- Interactions of SA and TiO₂ nanoparticles with the hard segment and PEO block of waterborne poly(urethane-urea)s controlled the cross-linking density and, therefore, final properties of designed hydrogels,
- Increasing the SA content led to an increase of the cross-linking density of the hydrogel network. Furthermore, incorporation of TiO₂ nanoparticles

contributed to increase the cross-linking density in the case of hydrogels based on PU0,

- The incorporation of SA affected the T_g of designed hydrogels based on PU0. A decrease of the T_g was observed for SA-PU0 hydrogels if compared to the T_g of the neat PU0,
- The incorporation of SA and TiO₂ nanoparticles did not significantly vary the thermal stability of designed hydrogels if compare to neat synthesized waterborne poly(urethane-urea)s,
- SEM images proved the effect of SA on the cross-linking density and the different distributions of TiO₂ nanoparticles in PU0 and PUEPE29 due to microphase separation of waterborne poly(urethane-urea) matrices,
- Designed hydrogels exhibited swelling ability when submerged in acid medium. SA-PUEPE29 serie hydrogels displayed higher swelling equilibriums than those of SA-PU0 serie hydrogels due to the higher availability of hydrophilic SA,
- The incorporation of TiO₂ nanoparticles led to the hydrogel with the highest compressive modulus in the case of SA-PU0 serie. In contrast, 30SA-PUEPE29 displayed the highest modulus for SA-PUEPE29 serie,
- 20SA-PU0 and 30SA-PU0 hydrogels presented higher *in vitro* cell proliferation than the control, what means that they can be utilized as promoters for cell proliferation. This proves that these hydrogels can find application as biomaterials for tissue engineering or wound dressing.

7.6. References

- [1] S. J. Khouri, V. Buss, Interaction of cationic cyanine dye with algal alginates: evidence for a polymer bound dye dimer, *Journal of Biophysical Chemistry* 2 (2011) 380-385.
- [2] J. Wang, X. Ying, X. Li, W. Zhang, Preparation, characterization and swelling behaviors of polyurethane-grafted calcium alginate hydrogels, *Materials Letters* 126 (2014) 263-266.
- [3] S. Oh, S. Kim, H. Jeong, J. Lee, J. W. Cho, J. Park, The mechanical properties of polyurethane foam wound dressing hybridized with alginate hydrogel and jute fiber, *Fibers and Polymers* 14 (2013) 173-181.
- [4] O. Smidsrod, Molecular basis for some physical properties of alginates in the gel state, *Fraday Discussion of the Chemical Society* 57(1973) 263-274.
- [5] A. S. Hoffman, Hydrogels for biomedical applications, *Advanced Drug Delivery Reviews* 54 (2002) 3-12.
- [6] W. Hu, Z. Wang, Y. Xiao, S. Zhang, J. Wang, Advances in crosslinking strategies of biomedical hydrogels, *Biomaterials Science* 7 (2019) 843-855.
- [7] S. K. Bajpai, S. Sharma, Investigation of swelling/degradation behaviour of alginate beads crosslinked with Ca^{2+} and Ba^{2+} ions, *Reactive & Functional Polymers* 59 (2004) 129-140.
- [8] Y. Huang, H. Yu, C. Xiao, Effects of Ca^{2+} crosslinking on structure and properties of waterborne polyurethane-carboxymethylated guar gum films, *Carbohydrate Polymers* 66 (2006) 500-513.
- [9] T. Travinskaya, Y. Savelyev, Aqueous polyurethane dispersions-sodium alginate based blends and hydrogels, *American Journal of Heterocyclic Chemistry* 2 (2017) 20-25.
- [10] G. T. Grant, E. R. Morris, D. A. Rees, Biological interactions between polysaccharides and divalent cations: the egg-box model, *FEBS Letters* 32 (1973) 195-198.
- [11] T. V. Travinskaya, Y. V. Savelyev, Aqueous polyurethane-alginate compositions: Peculiarities of behavior and performance, *European Polymer Journal* 42 (2006) 388-394.
- [12] H. Daemi, M. Barikani, M. Barmar, Compatible compositions based on aqueous polyurethane dispersions and sodium alginate, *Carbohydrate Polymers* 92 (2013) 490-496.
- [13] J. Yun, H. Yoo, H. Kim, Preparation and properties of waterborne polyurethane-urea/sodium alginate blends for high water vapor permeable coating materials, *Journal of Applied Polymer Science* 105 (2007) 1168-1176.
- [14] R. Barbucci, G. Giani, S. Fedi, S. Bottari, M. Casolaro, Biohydrogels with magnetic nanoparticles as crosslinker: Characteristics and potential use for controlled antitumor drug-delivery, *Acta Biomaterialia* 8 (2012) 4244-4252.
- [15] R. Messing, N. Frickel, L. Belkoura, R. Strey, H. Rahn, S. Odenbach, A. M. Schmidt, Cobalt ferrite nanoparticles as multifunctional cross-linkers in PAAm ferrohydrogels, *Macromolecules* 44 (2011) 2990-2999.
- [16] B. A. Skardal, J. Zhang, L. Mccoard, S. Oottamasathien, G. D. Prestwich, Dynamically crosslinked gold nanoparticle-hyaluronan hydrogels, *Advanced Materials* 22 (2010) 4736-4740.
- [17] M. Luz, P. Ramos, J. A. González, S. G. Albornoz, C. J. Pérez, M. E. Villanueva, S. A. Giorgieri, G. J. Copello, Chitin hydrogel reinforced with TiO_2 nanoparticles as an arsenic sorbent, *Chemical Engineering Journal* 285 (2016) 581-587.

- [18] K. Yu, D. Wang, Q. Wang, Tough and self-healable nanocomposite hydrogels for repeatable water treatment, *Polymers* 10 (2018) 880/1-880/12.
- [19] C. Zhu, R. Yang, X. Hua, H. Chen, J. Xu, R. Wu, L. Cen, Highly stretchable HA/SA hydrogels for tissue engineering, *Journal of Biomaterials Science* 5063 (2018) 1-19.
- [20] B. Science, S. Oh, W. Kim, S. Kim, Y. Chung, J. Park, The preparation of polyurethane foam combined with ph-sensitive alginate/bentonite hydrogel for wound dressings, *Fibers and Polymers* 12 (2011) 159-165.
- [21] G. Palui, A. Garai, J. Nanda, A. K. Nandi, A. Banerjee, Organogels from different self-assembling new dendritic peptides: morphology, rheology, and structural investigations, *The Journal of Physical Chemistry B* 114 (2010) 1249-1256.
- [22] C. García-Astrain, A. Gandini, C. Peña, I. Algar, A. Eceiza, N. Gabilondo, Diels-Alder “click” chemistry for the cross-linking of furfuryl-gelatin-polyetheramine hydrogels, *RSC Advances* 4 (2014) 35578-35587.
- [23] S. Ikeda, K. Nishinari, “Weak gel”-type rheological properties of aqueous dispersions of nonaggregated K-carrageenan helices, *Journal of Agricultural and Food Chemistry* 49 (2001) 4436-4441.
- [24] K. González, T. Gurrea, O. Guaresti, I. Algar, A. Eceiza, N. Gabilondo, Maleimide-grafted cellulose nanocrystals as cross-linkers for bionanocomposite hydrogels, *Carbohydrate Polymers* 149 (2016) 94-101.
- [25] Y. Wang, A. Lue, L. Zhang, Rheological behavior of waterborne polyurethane/starch aqueous dispersions during cure, *Polymer* 50 (2009) 5474-5481.
- [26] Q. Zhang, X. Huang, X. Wang, X. Jia, K. Xi, Rheological study of the gelation of cross-linking polyhedral oligomeric silsesquioxanes (POSS)/PU composites, *Polymer* 55 (2014) 1282-1291.
- [27] Y. Nishio, A. Yamada, K. Ezaki, Y. Miyashita, Preparation and magnetometric characterization of iron oxide-containing alginate/poly(vinyl alcohol) networks, *Polymer* 45 (2004) 7129-7136.
- [28] C. Huang, S. Ravindran, Z. Yin, A. George, Biomaterials 3-D self-assembling leucine zipper hydrogel with tunable properties for tissue engineering, *Biomaterials* 35 (2014) 5316-5326.
- [29] A. Pegoretti, L. Fambri, A. Penati, J. Kolarik, Hydrolytic resistance of model poly(ether urethane ureas) and poly(ester urethane ureas), *Journal of Applied Polymer Science* 70 (1998) 577-586.
- [30] D. J. Hourston, G. Williams, R. Satguru, J. D. Padget, D. Pears, Structure-property study of polyurethane anionomers based on various polyols and diisocyanates, *Journal of Applied Polymer Science* 66 (1997) 2035-2044.
- [31] C. Liu, Q. Ma, H. He, G. He, J. Ma, Y. Liu, Y. Wu, Environmental science nano groups during NO₂ adsorption and transformation, *Environmental Science: Nano* 4 (2017) 2388-2394.
- [32] J. Gutierrez, A. Tercjak, I. Garcia, L. Peponi, I. Mondragon, Hybrid titanium dioxide/PS-b-PEO block copolymer nanocomposites based on sol-gel synthesis, *Nanotechnology* 19 (2008) 155607/1-155607/8.
- [33] K. Fischer, P. Schulz, I. Atanasov, A. A. Latif, I. Thomas, M. Kühnert, A. Prager, J. Griebel, A. Schulze, Synthesis of high crystalline TiO₂ nanoparticles on a polymer membrane to degrade pollutants from water, *Catalysts* 8 (2018) 376/1-376/16.
- [34] J. Gutierrez, A. Tercjak, I. Algar, A. Retegi, I. Mondragon, Conductive properties of TiO₂/bacterial cellulose hybrid fibres, *Journal of Colloid and Interface Science* 377 (2012) 88-93.

- [35] A. Bhattacharyya, D. Mukherjee, R. Mishra, P. P. Kundu, Development of pH sensitive polyurethane-alginate nanoparticles for safe and efficient oral insulin delivery in animal models, *RSC Advances* 6 (2016) 41835-41846.
- [36] H. Behniafar, M. Alimohammadi, K. Malekshahinezhad, Transparent and flexible films of new segmented polyurethane nanocomposites incorporated by NH₂-functionalized TiO₂ nanoparticles, *Progress in Organic Coatings* 88 (2015) 150-154.
- [37] H. Liu, S. Cui, S. Shang, D. Wang, J. Song, Properties of rosin-based waterborne polyurethanes/cellulose nanocrystals composites, *Carbohydrate Polymers* 96 (2013) 510-515.
- [38] Z. Tong, Y. Chen, Y. Liu, L. Tong, J. Chu, K. Xiao, Z. Zhou, Preparation, characterization and properties of alginate/poly(γ -glutamic acid) composite microparticles, *Marine Drugs* 15 (2017) 91/1-91/14.
- [39] S. Zhang, Y. Li, L. Peng, Q. Li, S. Chen, K. Hou, Synthesis and characterization of novel waterborne polyurethane nanocomposites with magnetic and electrical properties, *Composites Part A: Applied Science and Manufacturing* 55 (2013) 94-101.
- [40] O. Guaresti, C. García-Astrain, R. H. Aguirresarobe, A. Eceiza, N. Gabilondo, Synthesis of stimuli-responsive chitosan - based hydrogels by Diels-Alder cross-linking 'click' reaction as potential carriers for drug administration, *Carbohydrate Polymers* 183 (2018) 278-286.
- [41] R. Dash, M. Foston, A. J. Ragauskas, Improving the mechanical and thermal properties of gelatin hydrogels cross-linked by cellulose nanowhiskers, *Carbohydrate Polymers* 91 (2013) 638- 645.
- [42] K. Li, J. Peng, M. Zhang, J. Heng, D. Li, C. Mu, Comparative study of the effects of anatase and rutile titanium dioxide nanoparticles on the structure and properties of waterborne polyurethane, *Colloids and Surfaces A: Physicochemical and Engineering Aspects* 470 (2015) 92-99.
- [43] S. M. Mirabedini, M. Sabzi, J. Zohuriaan-Mehr, M. Atai, M. Behzadnasab, Weathering performance of the polyurethane nanocomposite coatings containing silane treated TiO₂ nanoparticles, *Applied Surface Science* 257 (2011) 4196-4203.
- [44] M. Singh, R. K. Singh, S. K. Singh, S. K. Mahto, N. Misra, In vitro biocompatibility analysis of functionalized poly(vinyl chloride)/layered double hydroxide nanocomposites, *RSC Advances* 8 (2018) 40611-40620.
- [45] M. Shakeel, F. Jabeen, S. Shabbir, M. S. Asghar, M. S. Khan, A. S. Chaudhry, Toxicity of nano-titanium dioxide (TiO₂-NP) through various routes of exposure: A review, *Biological Trace Element Research* 172 (2016) 1-36.

Chapter

8

"Remember that happiness is a way of travel, not a destination."

(Roy Goodman)

Adhesive performance of waterborne poly(urethane-urea)s

8. Adhesive performance of waterborne poly(urethane-urea)s

8.1. Chapter overview	177
8.2. Introduction	177
8.3. Preparation of bilayer systems	179
8.4. Preparation of blends	180
8.5. Preparation of sheets for 180° peel-off test	180
8.6. Probe-tack adhesion	180
8.6.1. Waterborne poly(urethane-urea) dispersions	180
8.6.2. Bilayer systems based on PU0 and PUEPE29	185
8.6.3. Blends of PU0/PUEPE29 blends	187
8.7. Comparison of probe-tack performances	188
8.7.1. Tensile strength, σ_{\max}	189
8.7.2. Debonding energy, W_{deb}	190
8.8. Application as adhesive tape	191
8.9. Conclusions	192
8.10. References	194

8.1. Chapter overview

In this Chapter adhesive properties of synthesized waterborne poly(urethane-urea)s are studied from the point of view of their potential application as pressure sensitive adhesive (PSA) in adhesive tapes.

Accordingly, firstly, the PSA adhesive performance determined by probe-tack measurements is discussed. Bilayer systems and blends based on selected synthesized waterborne poly(urethane-urea)s are prepared seeking an improvement on their adhesive performance.

Potential application as PSA adhesive tape is investigated by means of 180° peel-off test. For this matter, a bilayer system configuration is selected and prepared on different polymer surface sheets.

8.2. Introduction

Polyurethanes are an interesting family of polymers for application as adhesives¹ thanks to the high cohesive energy they exhibit. This is consequence of the hydrogen bonds formed between the urethane linkages within their structure². Polyurethanes are formed by two thermodynamically incompatible segments (soft and hard segment)³, this means that their final properties can be tailored designing polyurethanes with different soft and hard segments as well as different ratios between these segments. This implies different molecular architectures^{4,5} and molecular weights^{2,6,7}, which affect the mechanical² and viscoelastic^{2,4-7} properties and, in consequence, the adhesive performance.

So far, in order to reach PSA behavior cross-linked polyurethanes have been designed^{6,8}. This has proved to be a requirement for PSAs⁸⁻¹⁰ since noncross-linked polymers do not possess enough cohesive strength to form fibrils or to resist the shear stress for long periods of times without flowing^{9,11}. Nevertheless, as proved by Carelli et al.⁹, the adhesive performance of soft adhesives can be satisfactorily improved by preparation of a bilayer system with a gradient in the viscoelastic properties. In this case, one of the layers was more dissipative while the other one was more elastic. In

fact, this strategy has guided researchers into preparation of bioinspired layer systems trying to emulate the adhesion ability displayed by toe pads of both gecko and tree frog¹². Besides preparation of bilayer systems, blending of polymers seems to be also a good strategy for improvement of the adhesive performance^{13,14}. As a matter of fact, blends of triblock copolymers formed by thermodynamically incompatible blocks, which are capable of microphase separation, are employed as base for PSAs. This is due to the ability that endblocks can possess to self-organize into hard spherical domains leading to physical cross-linking¹¹. These physical entanglements can be broken and remake at high stress, resulting in formation of fibrils¹¹. In addition, these entanglements may prevent polymer from flowing⁹.

There is an increasing restriction on the use of VOCs promoted by a growing number of governments and organizations. At the same time, there is also an increasing awareness of companies and researchers concerning this issue^{2,6-8}. Therefore, development of more environmentally friendly adhesives is mandatory. Waterborne polymers are suitable candidates for the development of more environmentally friendly adhesives. In the case of waterborne polyurethanes and poly(urethane-urea)s, they combine the versatility and characteristics of conventional solvent-borne polyurethanes and poly(urethane-urea)s with a reduction in emissions of VOCs to the atmosphere¹⁵.

8.3. Preparation of bilayer systems

Bilayer systems were prepared by applying the first layer on a glass surface utilizing a 200 μm cube applicator and left drying for 24 h at room temperature. The waterborne poly(urethane-urea) dispersion for the second layer was applied directly on the flat and homogeneous film formed after the first layer was dried. For this second layer, and differently to the first layer, cube applicators with three different thicknesses (50, 100 and 200 μm) were employed with the aim of studying the effect of the thickness of the second layer on the adhesive performance.

Considering the probe-tack adhesion test results, PU0 and PUEPE29 were the selected waterborne poly(urethane-urea)s for the design of bilayer systems. The waterborne

poly(urethane-urea) of the two layers, as well as the thickness of the second layer were the modified parameters. Prepared samples are listed in Table 8.1.

Table 8.1. Sample denotation of designed bilayers systems based on PU0 and PUEPE29.

Sample	1 st layer		2 nd layer	
	Waterborne poly(urethane-urea)	Thickness of applicator (μm)	Waterborne poly(urethane-urea)	Thickness of applicator (μm)
Bilayer029-50	PU0	200	PUEPE29	50
Bilayer029-100	PU0	200	PUEPE29	100
Bilayer029-200	PU0	200	PUEPE29	200
Bilayer290-50	PUEPE29	200	PU0	50
Bilayer290-100	PUEPE29	200	PU0	100
Bilayer290-200	PUEPE29	200	PU0	200

They were denoted as BilayerXY-Z, where the X stands for the waterborne poly(urethane-urea) used for the first layer, the Y stands for the waterborne poly(urethane-urea) of the second layer (that will be in contact with the adherent), and the Z stands for the thickness of the cube applicator (in μm) employed for the application of the second layer. Here, it should be noted that, for dispersion with a solids content of ~25 wt%, the final film thickness was approximately 25% of the thickness of the applicator. Figure 8.1 shows a schematic illustration of the arrangement of designed bilayer systems.

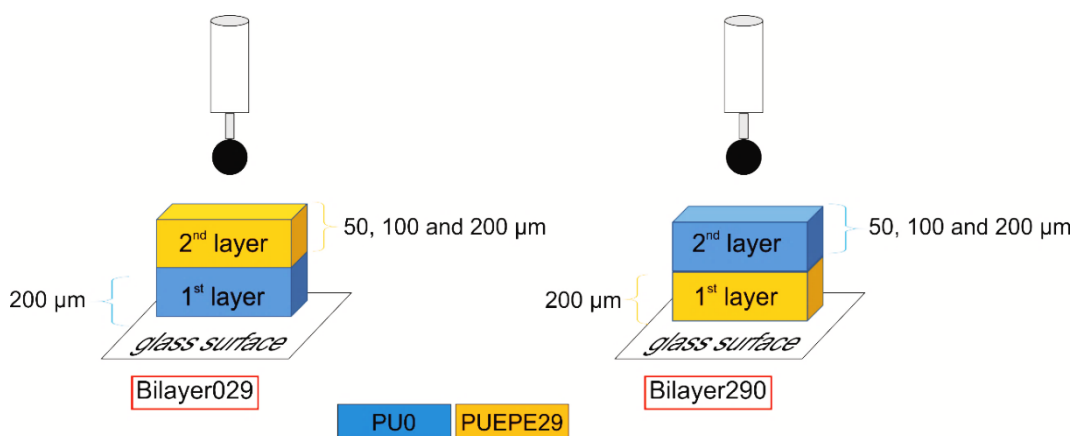


Figure 8.1. Schematic illustration of the arrangement of designed bilayer systems for probe-tack adhesion measurement. Thickness refers to the thickness of the applicator.

8.4. Preparation of blends

Likewise to bilayers systems, PU0 and PUEPE29 were also the selected waterborne poly(urethane-urea)s for preparation of blends. These two dispersions were blended in two different mass ratios (based on the initial dispersion mass) of PUEPE29/PU0, 1/1 and 2.3/1, denoted as Blend1 and Blend2.3, respectively.

Blending consisted on physically mixing PU0 and PUEPE29 waterborne poly(urethane-urea) dispersions using a mechanical stirrer at 500 rpm for 24 h at room temperature. Blends were casted on a glass surface as detailed previously for the first layer of the bilayer systems.

8.5. Preparation of strips for 180° peel-off test

Seeking potential applications for synthesized waterborne poly(urethane-urea)s as adhesives, 180° peel-off test was carried out. This test was performed for a bilayer system configuration based on Bilayer029-100 (denoted as Bilayer029-P). The designed bilayer system was prepared onto PET and PP polymer sheets. These polymer sheets were subjected to corona treatment, which increased their surface energy¹⁶ to facilitate the formation of film on them. For the preparation of testing strips, firstly, PU0 dispersion was cast on the polymer sheet using a 120 µm spiral bar applicator. It was left drying for 24 h at room conditions. Once the PU0 first layer dried and a homogeneous and flat film was formed, PUEPE29 dispersion, for the second layer, was directly applied onto the first layer using a 60 µm spiral bar applicator. It was left to dry for 24 h at room conditions. Finally, 25 mm wide long strips for testing were cut from the prepared sheets of PET and PP. These strips were adhered onto glass and aluminum surfaces to study their adhesive properties for different surfaces.

8.6. Probe-tack adhesion

8.6.1. Waterborne poly(urethane-urea) dispersions

A probe-tack curve, presented as stress versus strain, is rich in information^{8,17,18}. The gradient of the linear region at low strain is related to the elastic modulus of the

polymer in confinement. The stress reaches a maximum value, σ_{\max} , which indicates the point where debonding or cavitation commences, and then the stress falls. If a polymer has an elastic modulus that is too high, a type of interfacial failure (also known as brittle failure) follows, where the stress falls abruptly to zero without any further polymer deformation. Nonetheless, if a polymer possesses a good viscoelasticity balance, fibrillation will follow. This is observed as a stress plateau, followed by failure at a strain (ε_{\max}). The higher the fibrillation the higher the debonding energy (W_{deb}) as a consequence of the energy expended in the polymer deformation. A cross-linked polymer usually exhibits stress hardening during fibrillation, prior to clean detachment from the probe, without any cohesive failure.

As a general trend, σ_{\max} is influenced by the thermodynamic work of adhesion (W_{adh}), which is the surface free energy associated with the creation of new surfaces after debonding a joint. For the case of an adhesive poly(urethane-urea) debonding from a probe, thermodynamic work of adhesion (per unit area) can be calculated from the Dupré equation¹⁹:

$$W_{\text{adh}} = \gamma_{\text{PU}} + \gamma_{\text{P}} - \gamma_{\text{PUP}} \quad (8.1)$$

where γ_i represents the interfacial free energy between the PSA poly(urethane-urea) (PU) and air, the probe (P) and air, or between the poly(urethane-urea) and the probe (PUP). In concordance with the Dupré equation, the interfacial energy (γ_{PUP}) should be minimized to achieve a high W_{adh} . The equation also reveals the reason why the work of adhesion on low surface energy probes (or other adherends) tends to be lower. For good adhesion on a substrate (or probe) with a low surface energy the adhesive poly(urethane-urea) should have a high surface energy. Even if this may lead to a higher interfacial energy between the adhesive and the adherend probe¹⁶, W_{adh} would still be high. The energy of debonding is related to W_{adh} through the dissipation of the polymer (Φ) (Equation 8.2). The viscoelastic properties of the polymer determine the value of Φ for a particular PSA.

$$W_{\text{deb}} = W_{\text{adh}} (1 + \Phi) \quad (8.2)$$

Finding a suitable adhesive for low surface energy materials is still such a challenge, since most polymers employed as adhesives possess a similar low surface energy, and hence W_{adh} is low. For instance, the surface energy of PPO is in the range of 28 to 34 mJ m^{-2} at room temperature^{20,21}, which is close to the value for the PP probe ($\sim 27 \text{ mJ m}^{-2}$)²². By comparison, the surface energy of PEO is higher (41 to 44 mJ m^{-2})^{21,23}. Therefore, the inclusion of PEO in a polymer could be advantageous to adhesion. Other polymers typically used in PSAs, such as poly(butyl acrylate)²⁴ and poly(ethyl hexyl acrylate)²⁵, likewise have a low surface energy (30–31 mJ m^{-2}), and consequently they typically show poorer adhesion on PP, polyethylene (PE) and other low energy surfaces²⁶. Kowalski et al.²⁷ measured a surface energy of 30 mJ m^{-2} for a model acrylic PSA (Table 8.2).

A value of γ_{PU} was estimated by using the surface energy values for PEO, PPO and the probes (steel or PP) that are available in literature^{22,23,28}, via the equation¹⁹:

$$\gamma_{PUP} = \left(\sqrt{\gamma_{PU}} + \sqrt{\gamma_P} \right)^2 \quad (8.3)$$

In this simple calculation, both separate polar and dispersive components and the use of the total surface energy were ignored. Moreover, these calculations did not consider the effect of the hard segment on the surface and interfacial energies.

Table 8.2 presents calculated values of γ_{PUP} for both steel and PP probes for each of synthesized waterborne poly(urethane-urea)s. For comparison, values for a model acrylic PSA measured by Kowalski et al.²⁷ are displayed. γ_{PU} values for synthesized waterborne poly(urethane-urea)s were calculated taking into account the proportion of PEO and PPO blocks in the triblock copolymers used as macrodiols (see the Chapter 2). The value for the surface energy of PEO presented in Table 8.2 (42.8 mJ m^{-2}) was reported by Roe et al.²³, while the one for PPO (31.7 mJ m^{-2}) was reported by Kasemura et al.²⁸. Considering that PEO has a higher surface energy than PPO, the increment in the content of PEO in the soft segment has the benefit of increasing W_{adh} with the PP probe. Therefore, PU0 presented the highest calculated values of W_{adh} of all investigated waterborne poly(urethane-urea)s with values of 87 mJ m^{-2} for steel and 74 mJ m^{-2} for PP. In contrast, the model acrylic PSA had the lowest values for steel and PP (73 and 62 mJ m^{-2} , respectively). Synthesized triblock copolymers based

waterborne poly(urethane-urea)s presented values that were intermediate between PU0 and the model acrylic PSA. Although W_{adh} for synthesized triblock copolymers based waterborne poly(urethane-urea)s was calculated to be higher for the stainless steel probe than for the PP probe, the estimated values for PP were more favorable for adhesion in comparison to the model acrylic PSA.

Table 8.2. Surface energy (γ_{PU}), calculated interfacial energy (γ_{PUP}) and thermodynamic work of adhesion (W_{adh}) of synthesized waterborne poly(urethane-urea)s.

Sample	γ_{PU} (mJ m⁻²)	γ_{PUP} for PP (mJ m⁻²)	γ_{PUP} for steel (mJ m⁻²)	W_{adh} on PP (mJ m⁻²)	W_{adh} on steel (mJ m⁻²)
PU0	42.8	0.8	0.02	74	87
PUEPE19	37.2	0.2	0.3	69	81
PUEPE29	36.1	0.1	0.4	68	80
PUPEP27	36.1	0.1	0.4	68	80
Model PSA	30	0.03	1.4	62	73

The probe-tack curves obtained for investigated waterborne poly(urethane-urea)s are presented in Figure 8.2. PU0 and PUPEP27 displayed the lowest adhesive performance (smallest ϵ_{max} and no fibrillation). Nevertheless, in the case of PUPEP27, the stress did not fall abruptly to zero after reaching σ_{max} , instead it fell gradually due to a cohesive debonding, leaving residue on the probe afterward²⁹. In the case of PU0, for both probes, and of PUEPE19 for the steel probe, a sudden decline of the stress to zero at ϵ_{max} occurred. This can be related to a clean interfacial detachment of the probe from the film, what was indicative of a brittle failure²⁹. For the steel probe, both PUEPE29 and PUPUP27 exhibited a gradual decrease of the stress, which corresponded to a liquid-like cohesive debonding^{2,29}. However, for the low surface energy PP probe, as can be seen in Figure 8.2b, two of the investigated waterborne poly(urethane-urea)s (PUEPE19 and PUEPE29) presented a short plateau-like segments in their probe-tack curves, which can be the result of physical entanglements formed thanks to the triblock copolymers¹¹. This observation suggested some partial fibrillation or at least some extension of the poly(urethane-urea) film, which resulted in the greatest ϵ_{max} . Nevertheless, these waterborne poly(urethane-urea)s still exhibited a cohesive failure and left residue on the probe,

probably as a consequence of the absence of cross-linking and associated strain hardening⁹.

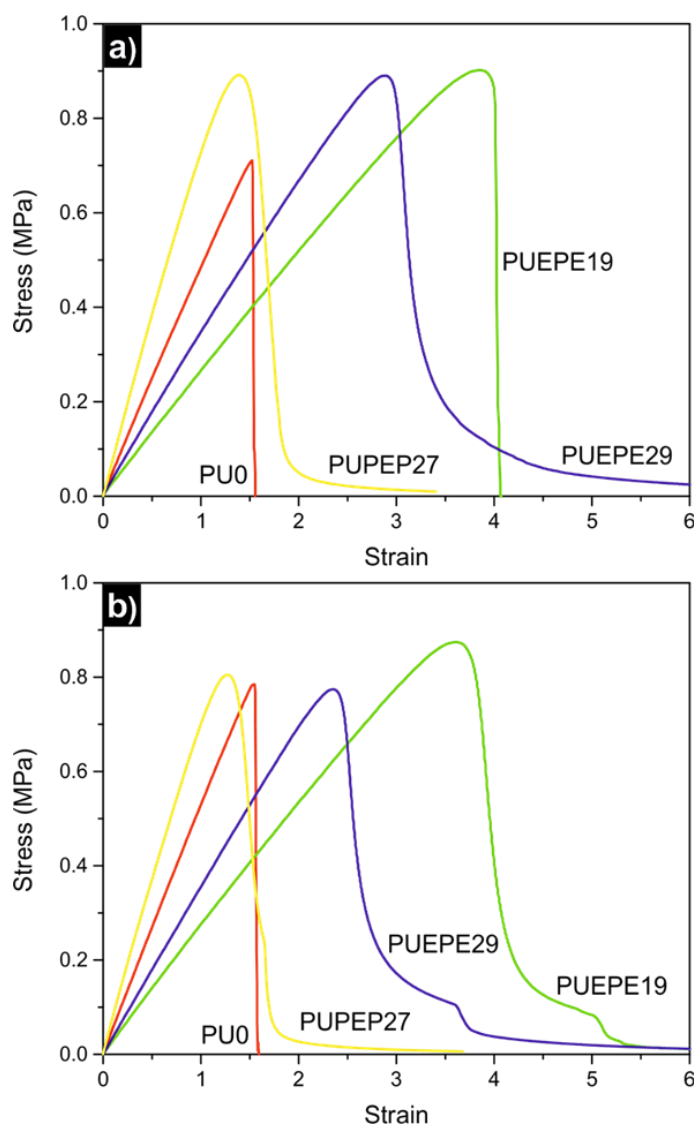


Figure 8.2. Representative probe-tack curves of synthesized waterborne poly(urethane-urea)s for measurements carried out with both (a) steel and (b) PP probes.

All three triblock copolymers based waterborne poly(urethane-urea)s exhibited a better probe-tack adhesion than PU0, which is based on PEO only. These results can be explained by the relatively high elastic modulus of PU0 (see the Chapters 3 and 4), which is far above the acceptable range of 0.1 MPa, according to the Dahlquist criterion, for PSAs²⁹⁻³¹. The two synthesized waterborne poly(urethane-urea)s based on PEO-*b*-PPO-*b*-PEO triblock copolymers (PUEPE19 and PUEPE29) displayed a lower slope at low strain, evidencing an inferior elastic modulus in confinement between the probe and the substrate in comparison to PPO-*b*-PEO-*b*-PPO triblock copolymer based PUPEP27. The differences in the adhesive performance were

ascribed to the differences in their soft segments and viscoelasticity, which determines Φ , rather than to the influence of W_{adh} . The surface energy effects are more likely to influence σ_{max} . The surface energies of all investigated waterborne poly(urethane-urea) films were similar for a given probe, and the resulting σ_{max} was likewise similar.

In short, none of the investigated waterborne poly(urethane-urea)s behaved as high performing PSA, which shows extensive fibrillation during debonding¹⁴. Nonetheless, they presented some measurable tackiness. Furthermore, it was remarkable that investigated waterborne poly(urethane-urea)s exhibited relatively good adhesive performance on a low surface energy material, as it was the PP probe. This observation indicated that, after optimization, they can potentially be used as soft adhesives for substrates with a low surface energy, such as packaging material. Hereafter, we evaluate how the adhesive performance of synthesized waterborne poly(urethane-urea)s can be improved via a bilayer system design.

8.6.2. Bilayer systems based on PU0 and PUEPE29

Carelli et al.⁹ proved that the adhesive performance can be optimized by the preparation of bilayer systems with layers that present different elastic and viscous properties in order to create a gradient in the viscoelastic properties. Considering the probe-tack results of investigated waterborne poly(urethane-urea)s (Figure 8.2), two of them, which presented distinct properties, were selected to be used in the design of bilayer systems. The selected waterborne poly(urethane-urea)s were PU0, which was more solid-like and had a high elastic modulus, and PUEPE29, which was more liquid-like, presented the highest ϵ_{max} of all investigated waterborne poly(urethane-urea)s and exhibited a short plateau in the PP probe-tack tests (Figure 8.2b).

Table 8.1 lists the geometries of investigated samples. Figure 8.3a and 8.3b show the probe-tack curves obtained for the bilayer systems in which PUEPE29 was cast on the glass substrate and PU0 was cast on top of that first layer, so it was in direct contact with the probe. These results indicated that the interfacial failure of PU0 (Figure 8.2) prevailed regardless of the thicknesses of the second layer of designed Bilayer290 systems. There was not polymer extension or fibrillation during the debonding

process. In the case of the steel probe, ϵ_{\max} values were higher to those found previously for PU0, but lower than those of PUEPE29. The curves for the PP probe showed inferior adhesion for all three designed Bilayer290 systems in comparison to single PU0 and PUEPE29 waterborne poly(urethane-urea)s. The debonding process was dominated by the solid-like PU0 film, which was the one in direct contact with the probe. This meant that interfacial failure at relatively low strains occurred. There was not any benefit obtained from the preparation of Bilayer290 systems.

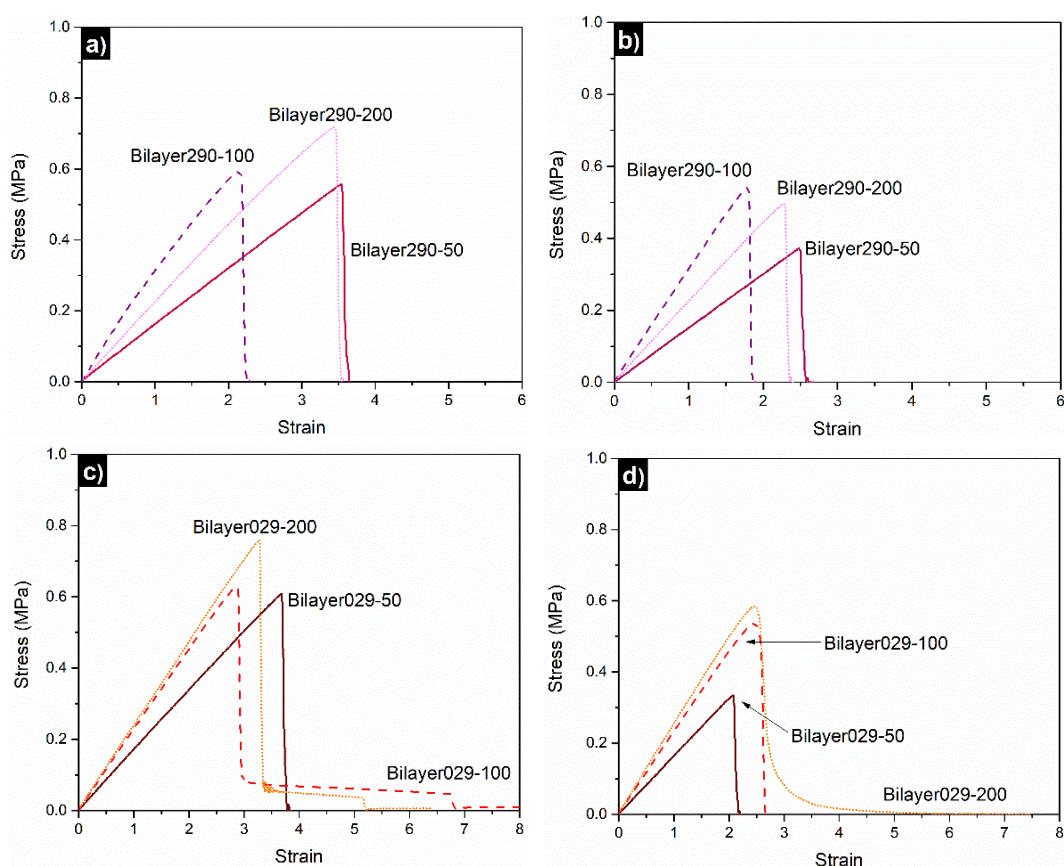


Figure 8.3. Representative probe-tack curves of designed different thickness top layer bilayer systems measured with (a) (c) steel and (b) (d) PP probes. The sample names are defined in Table 2.

In contrast, there was some benefit appreciated for designed Bilayers029 systems. In these bilayer systems, PUEPE29 layer was on top and in direct contact with the probe, whereas PU0 formed the first layer. For the steel probe, the adhesive performance clearly improved for thicker PUEPE29 layers. This improvement can be seen in Figure 8.3c, where a plateau appeared for Bilayer029-100 and Bilayer029-200, which was similar to standard PSAs^{2,9,32} with fibrillation and an adhesive debonding (not cohesive failure)²⁹. Bilayer029-100 presented a longer plateau than Bilayer029-200. This was likely due to a decrease in the synergistic effect between the two layers for

Bilayer029-200. From comparison of curves reported in Figure 8.3c, it can be concluded that the PUEPE29 layer required to be thick enough in order to achieve an improvement in the adhesive performance. This need for a thick enough second layer was also reported by Carelli et al.⁹.

For the PP probe, designed Bilayer029 systems were less effective. However, in the case of Bilayer029-200, the observed detachment exhibited a cohesive liquid-like debonding²⁹ where the adhesive material left residue on the PP probe. This phenomenon can be better understood considering the liquid-like character of the PUEPE29 top layer as well as its thickness.

These results suggested that the adhesive performance can be tailored and adjusted for different applications just by preparing bilayers systems with a gradient in the viscoelastic properties. PSA-like performance was observed when the softer polymer, supported by a harder polymer, was in direct contact with the steel surface.

8.6.3. Blends of PUEPE29/PU0 blends

Improved adhesion can be achieved by polymer blending^{7,14}. In particle mixtures, glassy (or hard) particles increase the elastic modulus but with the drawback of leading to brittleness. Meanwhile, soft particles add energy dissipation and raise the extensibility. In the prepared bilayer systems, PU0 waterborne poly(urethane-urea) dispersion, which was more solid-like (hard), was used in combination with PUEPE29 waterborne poly(urethane-urea) dispersion, which was more liquid-like (soft). This brings in the question as to whether the mixing of these two waterborne poly(urethane-urea)s would prove as beneficial as their use in a bilayer system. Experiments were performed to answer this question.

The probe tack analysis for blends of PU0 and PUEPE29 waterborne poly(urethane-urea) dispersions is shown in Figure 8.4. Prepared two blends presented a higher strain at failure for the steel probe than for the PP probe. Blend1 displayed brittle fracture on both probes as a consequence of its solid-like behavior. It exhibited higher stress and strain for the steel probe. Its adhesive performance was in between the ones observed for neat PU0 and PUEPE29 (Figure8.2a).

Regarding Blend2.3, the adhesive performance on both probes during debonding was very similar. There was a gradual drop in the stress, a sign of cohesive failure.

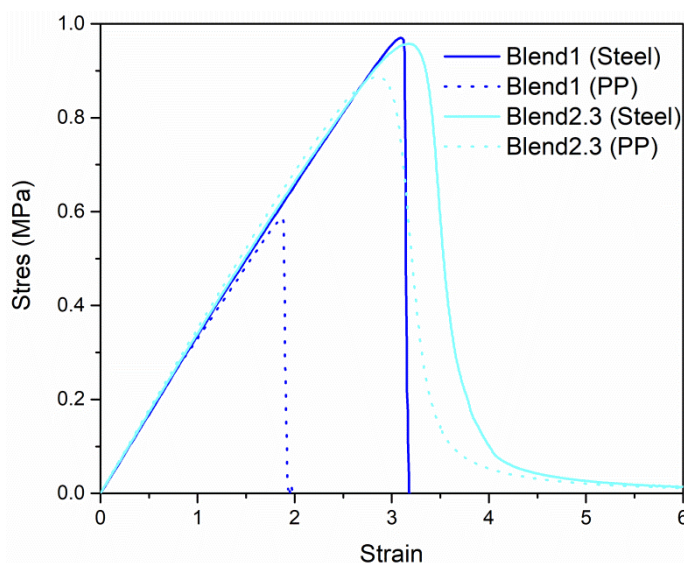


Figure 8.4. Representative probe-tack curves of the prepared PUEPE29/PU0 blends using both steel and PP probes.

Blend1 behaved more similarly to PU0 (Figure8.2), whereas the curves for Blend2.3 were more similar to that of PUEPE29 (Figure8.2). Nonetheless, neither of the prepared blends improved the adhesive performance of neat synthesized waterborne poly(urethane-urea)s. Furthermore, the adhesive performances of the blends were inferior to those of neat synthesized waterborne poly(urethane-urea)s, even causing the disappearance of the small plateau observed in the case of PUEPE29 for the PP probe (Figure 8.2b). This all indicates that the adhesive performance of synthesized waterborne poly(urethane-urea)s can be better optimized by the designing of bilayer systems.

8.7. Comparison of probe-tack performances

Once probe-tack tests were performed, and in order to draw conclusions, the adhesive properties of synthesized waterborne poly(urethane-urea)s are compared with those of designed Bilayer029 systems and prepared blends. The trends in the maximum tack stress (Figure 8.5) and in the debonding energy (Figure 8.6) are the ones analyzed.

8.7.1. Maximum tack stress, σ_{\max}

The maximum tack stress (Figure 8.5) is influenced by the thermodynamic work of adhesion. The differences in σ_{\max} were not significant regardless of the composition of the soft segment of synthesized waterborne poly(urethane-urea)s.

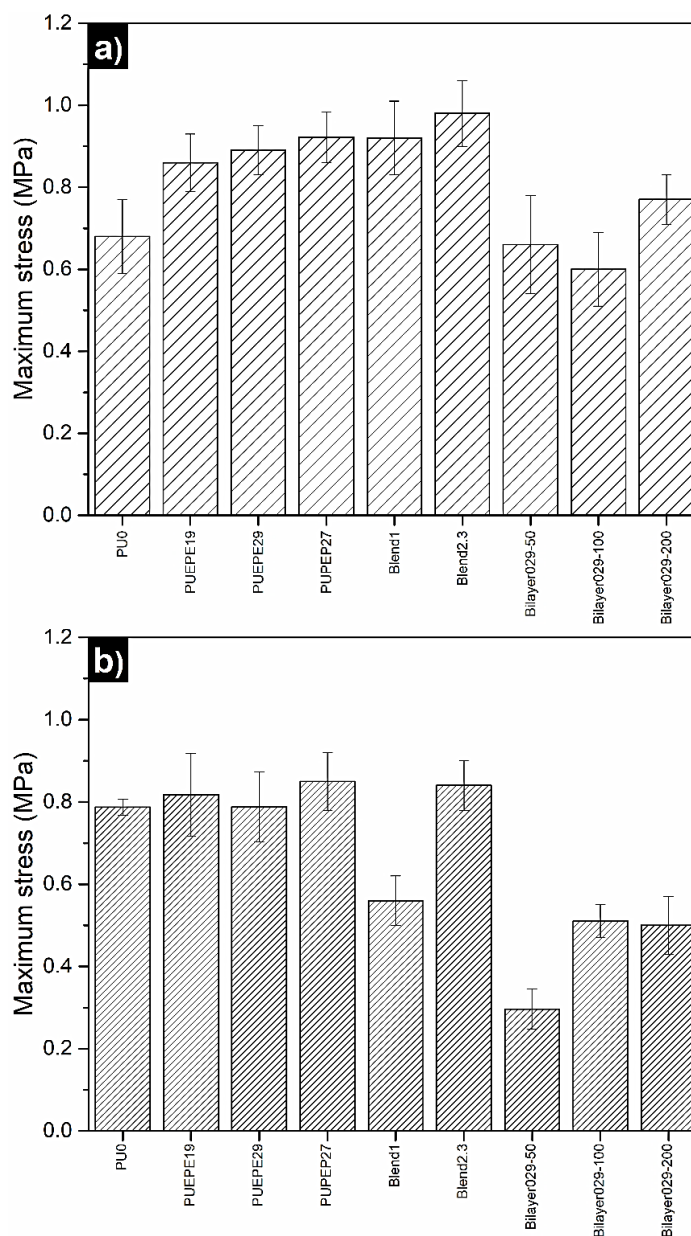


Figure 8.5. Maximum tack stress of synthesized waterborne poly(urethane-urea)s, prepared blends, and designed Bilayer029 systems for both (a) steel and (b) PP probes.

As it was previously discussed, surface energies of synthesized waterborne poly(urethane-urea)s were very similar, what would explain the lack of significant differences in σ_{\max} . Blends exhibited similar σ_{\max} . In contrast, Bilayer029 systems

presented lower σ_{\max} than synthesized waterborne poly(urethane-urea)s and prepared blends. This was probably the result of the effect of casting layers of different synthesized waterborne poly(urethane-urea)s one onto the other.

8.7.2. Debonding energy, W_{deb}

The debonding energy, calculated from the area under the stress-strain curve is presented in Figure 8.6.

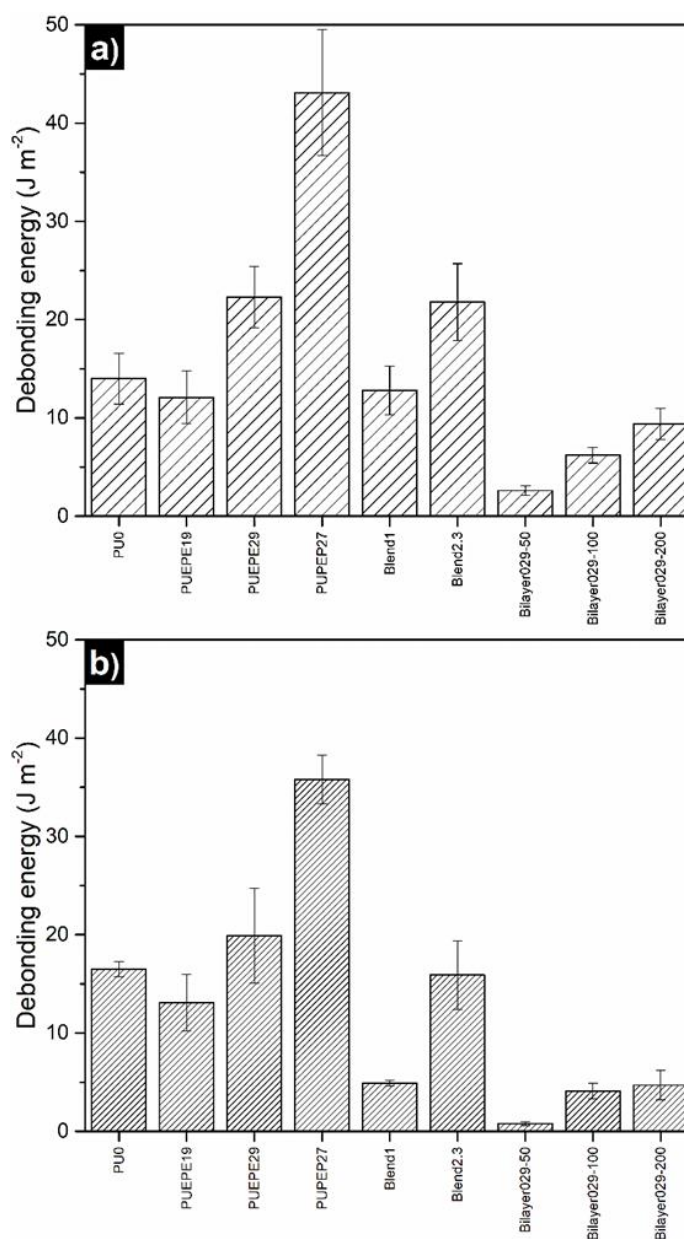


Figure 8.6. Debonding energy calculated from the area under the probe-tack curves of synthesized waterborne poly(urethane-urea)s, prepared blends, and designed Bilayer029 systems for both (a) steel and (b) PP probes.

W_{deb} is a function of the maximum tack force, stress in the plateau region and the extent of fibrillation (which affects ϵ_{max}). Therefore, it is a good barometer of the overall adhesive performance.

The trends in W_{deb} of investigated waterborne poly(urethane-urea)s, shown in Figure 8.6, were fairly similar regardless of the probe. PUPEP27 exhibited the highest value for W_{deb} for both steel and PP probes despite its lower ϵ_{max} since it was the thickest film of all. The lowest values for both probes were displayed by Bilayer029-50. In the case of the designed Bilayer029 systems, it was evident that the increase of the thickness of the top PUEPE29 layer led to an increase in the W_{deb} . This was the result of a higher volume of extensible material. Moreover, the positive effect of adding PUEPE29 was also observed in Blend2.3, with a W_{deb} higher than that of Blend1, regardless of the probe.

8.8. Application as adhesive tape

For evaluation of the potential application of designed Bilayer029 system configuration as adhesive tape (Bilayer029-P), 180° peel test was carried out in tensile mode. The plateau-like zone of obtained curves was considered as the peel force. A commercial domestic tape (Tape) was used for comparison purpose.

The first conclusion that can be extracted from the results presented in Figure 8.7 is that PET was not a satisfactory backing layer for the preparation of adhesive tapes based on Bilayer029-P. A fast detachment from the PET backing layer under a low applied force took place. Nevertheless, Bilayer029-P applied on PP backing layer was suitable for adhesive tapes. This was an unexpected effect considering that the surface energy of PET is higher than the one of PP³³. Nonetheless, even if after the corona treatment the surface energy of PET is higher than for PP³³ due to the inferior amount or lack of polar groups in the structure of polyolefins, the increase produced by the corona treatment in the surface energy of PP is more pronounced³³. Moreover, how corona treatment is applied as well as the storage of the film sheet has a strong influence on the surface energy³³.

The peel force of Bilayer029-P on glass surface was lower than the one of the commercial domestic adhesive tape. Despite this, and satisfactorily, when the adhesive tape was fabricated by applying Bilayer029-P on PP backing, the achieved peel force on an aluminum surface was slightly superior to that of the commercial domestic adhesive tape. However, it is important to remark that the adhesive layer of the commercial domestic adhesive tape was significantly thinner than that of the designed Bilayer029-P. Thicker films can dissipate more energy during debonding, thus their adhesion energy is higher.

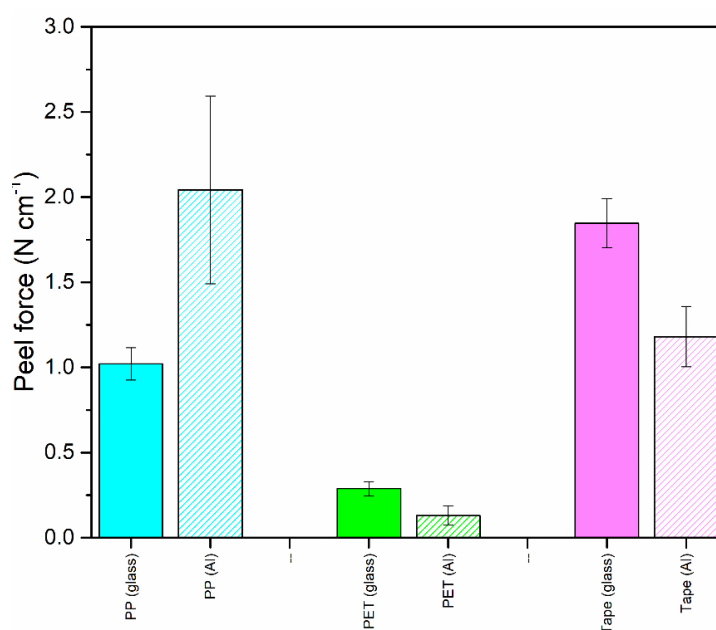


Figure 8.7. Peel force determined for the designed Bilayer029-P system by 180° peel-off test on glass (solid bars) and aluminum (striped bars) surfaces with either PP (blue) or PET (green) backing layer. Results of a commercial tape (purple) are also presented for comparison purpose.

In consideration of the obtained results for the fabricated adhesive tapes, application of synthesized PU0 and PUEPE29 waterborne poly(urethane-urea) dispersions on a PP surface creating a gradient in viscoelasticity, Bilayer029 configuration, can potentially be employed for adhesive tape application.

8.9. Conclusions

The evaluation of the adhesive performance of synthesized waterborne poly(urethane-urea)s, prepared blends and designed bilayer systems was carried out obtaining the next conclusions:

- Synthesized waterborne poly(urethane-urea)s exhibited tackiness,
- The adhesive performance of synthesized waterborne poly(urethane-urea)s was relatively good, however not similar to the one of PSAs,
- The adhesive performance exhibited by designed Bilayer029 systems was more similar to the one of classical PSAs, presenting a plateau in the probe-tack curves,
- Synthesized waterborne poly(urethane-urea)s presented similar σ_{\max} and W_{deb} ,
- In the case of Bilayer029 systems, the thicker the PUEPE29 top layer the higher they were both σ_{\max} and W_{deb} . The same beneficial effect of increasing the amount of PUEPE29 was also observed when comparing Blend1 and Blend2.3.
- Designed Bilayer029 systems can be used as base for PSAs,
- It was proved that fabricated adhesive tape based on Bilayer029-P system applied on PP backing layer can be employed as adhesive tape for glass and aluminum surfaces.

8.10. References

- [1] G. Malucelli, A. Priola, F. Ferrero, A. Quaglia, M. Frigione, C. Carfagna, Polyurethane resin-based adhesives: curing reaction and properties of cured systems, *International Journal of Adhesion and Adhesives* 25 (2005) 87-91.
- [2] N. Akram, R. S. Gurney, M. Zuber, M. Ishaq, J. L. Keddie, Influence of polyol molecular weight and type on the tack and peel properties of waterborne polyurethane pressure-sensitive adhesives, *Macromolecular Reaction Engineering* 7 (2013) 493-503.
- [3] A. Saralegi, L. Rueda, B. Fernández-D'Arilas, I. Mondragon, A. Eceiza, M. A. Corcuera, Thermoplastic polyurethanes from renewable resources: Effect of soft segment chemical structure and molecular weight on morphology and final properties, *Polymer International* 62 (2013) 106-115.
- [4] A. Barona, J. Rodriguez-Hernandez, E. Ibarbourea, C. Derailb, E. Papon, Adhesives based on polyurethane graft multiblock copolymers: Tack, rheology and first morphological analyses, *International Journal of Adhesion & Adhesives* 29 (2009) 1-8.
- [5] A. Falsafi, F. S. Bates, M. Tirrell, Role of chain architecture in the adhesion of block copolymers, *Macromolecules* 34 (2001) 1323-1327.
- [6] A. Lopez, E. Degrandi-Contraires, E. Canetta, C. Creton, J. L. Keddie, M. Asua, Waterborne polyurethane - acrylic hybrid nanoparticles by miniemulsion polymerization: applications in pressure-sensitive adhesives, *Langmuir* 27 (2011) 3878-3888.
- [7] A. Bellamine, E. Degrandi, M. Gerst, C. Beyers, C. Creton, Design of nanostructured waterborne adhesives with improved shear resistance, *Macromolecular Materials and Engineering* 296 (2011) 31-41.
- [8] E. Degrandi-Contraires, R. Udagama, E. Bourgeat-Lami, T. Mckenna, K. Ouzineb, C. Creton, Mechanical properties of adhesive films obtained from PU-acrylic hybrid particles, *Macromolecules* 44 (2011) 2643-2652.
- [9] C. Carelli, F. Déplacé, L. Boissonent, C. Creton, Effect of a gradient in viscoelastic properties on the debonding mechanisms of soft adhesives, *The Journal of Adhesion* 83 (2007) 491-505.
- [10] J. Courtois, I. Baroudi, N. Nouvel, E. Degrandi, L. Bouteiller, S. Pensec, G. Ducouret, C. Chane, C. Creton, Supramolecular soft adhesive materials, *Advanced Functional Materials* 20 (2010) 1803-1811.
- [11] C. Creton, P. Fabre, *The Mechanics of Adhesion*, 1st Ed., Elsevier, 2002, p. 535-576.
- [12] H. Shahsavan, B. Zhao, Bioinspired functionally graded adhesive materials: synergetic interplay of top viscous-elastic layers with base micropillars, *Macromolecules* 47 (2014) 353-364.
- [13] M. M. Feldstein, P. E. Kireeva, T. I. Kiseleva, B. E. Gdalin, M. B. Novikov, G. A. Shandryuk, P. Singh, G. W. Cleary, A new class of pressure sensitive adhesives based on interpolymer and polymer-oligomer complexes, *Polymer Science Series A* 51 (2009) 799-814.
- [14] M. M. Feldstein, E. E. Dormidontova, A. R. Khokhlov, Pressure sensitive adhesives based on interpolymer complexes, *Progress in Polymer Science* 42 (2015) 79-153.

- [15] S. Gogoi, N. Karak, Biobased biodegradable waterborne hyperbranched polyurethane as an ecofriendly sustainable material, *ACS Sustainable Chemistry and Engineering* 2 (2014) 2730-2738.
- [16] R. Dorai, M. J. Kushner, A model for plasma modification of polypropylene using atmospheric pressure discharges, *Journal of Physics D: Applied Physics* 36 (2003) 666-685.
- [17] F. Deplace, M. A. Rabjohns, T. Yamaguchi, A. B. Foster, C. Carelli, C. Lei, K. Ouzineb, J. L. Keddie, A. Lovell, C. Creton, Deformation and adhesion of a periodic soft - soft nanocomposite designed with structured polymer colloid particles, *Soft Matter* 7 (2009) 1440-1447.
- [18] A. Agirre, J. Nase, E. Degrandi, C. Creton, Improving adhesion of acrylic waterborne psas to low surface energy materials: introduction of stearyl acrylate, *Journal of Polymer Science Part A: Polymer Chemistry* 48 (2010) 5030-5039.
- [19] J. N. Israelachvili, *Intermolecular and Surface Forces*, 3rd Ed., Elsevier-Academic Press, 2011, p. 191-204.
- [20] R. A. Marcus, Theoretical relations among rate constants, barriers, and Broensted slopes of chemical reactions, *The Journal of Physical Chemistry* 72 (1968) 891-899.
- [21] K. E. Van Ness, Surface tension and surface entropy for polymer liquids, *Polymer Engineering and Science* 32 (1992) 122-129.
- [22] E. Occhiello, M. Morra G. Morini F. Garbassi D. Johnson, On oxygen plasma-treated polypropylene interfaces with air, water, and epoxy resins. II. Epoxy resins, *Journal of Applied Polymer Science* 42 (1991) 2045-2052
- [23] R. J. Roe, Surface tension of polymer liquids, *The Journal of Physical Chemistry* 72 (1968) 2013-2017.
- [24] D. Ahn, K. R. Shull, Effects of substrate modification on the interfacial adhesion of acrylic elastomers, *Langmuir* 14 (1998) 3646-3654.
- [25] S. Wu, *Polymer Handbook*, 3rd Ed., Wiley-Interscience, 1989, p. 414-426.
- [26] Y. Peykova, O. V Lebedeva, A. Diethert, M. Peter, N. Willenbacher, Adhesive properties of acrylate copolymers: Effect of the nature of the substrate and copolymer functionality, *International Journal of Adhesion and Adhesives* 34 (2012) 107-116.
- [27] A. Kowalski, Z. Czech, How does the surface free energy influence the tack of acrylic pressure-sensitive adhesives (PSAs)?, *Journal of Coatings Technology and Research* 10 (2013) 879-885.
- [28] T. Kasemura, T. Suzuki, K. Uzi, F., Kondo, T., Hata, Composition dependence of surface tension of ethylene oxide-propylene oxide copolymers, *Kobunshi Ronbunshu* 35 (1978) 779-786.
- [29] F. Deplace, C. Carelli, S. Mariot, H. Retsos, A. Chateaminois, K. Ouzineb, C. Creton, C. Carelli, S. Mariot, H. Retsos, A. Chateaminois, K. Ouzineb, Fine tuning the adhesive properties of a soft nanostructured adhesive with rheological measurements, *The Journal of Adhesion* 85 (2009) 18-54.

[30] B. E. Gdalin, E. V. Bermesheva, G. A. Shandryuk, M. Mikhail, G. A. Shandryuk, M. M. Feldstein, Effect of temperature on probe tack adhesion: Extension of the dahlquist criterion of tack extension of the dahlquist criterion of tack, *The Journal of Adhesion* 87 (2011) 111-138.

[31] A. Zosel, Adhesion and tack of polymers: Influence of mechanical properties and surface tensions, *Colloid and Polymer Science* 263 (1985) 541-553.

[32] R. S. Gurney, D. Dupin, J. S. Nunes, K. Ouzineb, E. Siband, J. M. Asua, S. P. Armes, J. L. Keddie, Switching off the tackiness of a nanocomposite adhesive in 30 s via infrared sintering, *ACS Applied Materials & Interfaces* 4 (2012) 5442-5452.

[33] M. Lindner, N. Rodler, M. Jesdinszki, M. Schmid, S. Sven, Surface energy of corona treated PP, PE and PET films, its alteration as function of storage time and the effect of various corona dosages on their bond strength after lamination, *Journal of Applied Polymer Science* 135 (2018) 45842/1-45842/9.

Chapter

9

"Life can only be understood backwards; but it must be lived forwards."

(Søren Aabye Kierkegaard)

**General conclusions, future works and
publications**

9. General conclusions, future works and publications

9.1. General conclusions	201
9.2. Future works	202
9.3. List of publications and communications	203
9.3.1. List of publications	203
9.3.2. List of communications	206
9.4. Research stages	210

9.1. General conclusions

An organic solvent-free synthesis procedure was proved successful for the synthesis of waterborne poly(urethane-urea)s based on different macrodiols. A bio-based macrodiol, P3MG, can form the soft segment of a poly(urethane-urea) together with PEO, as the solubilizing agent. The ratio of 80/20 (P3MG/PU0) was the best one in terms of final properties and amount of renewable content, since it presented the lowest particle size as well as the highest molecular weight and mechanical properties.

In addition to waterborne poly(urethane-urea)s based on a bio-based macrodiol, triblock copolymers containing PEO blocks were also used to form the soft segment. In this case, triblock copolymers with different molecular weights as well as PEO and PPO block arrangements were studied. The obtained triblock copolymers based waterborne poly(urethane-urea) films were softer and presented inferior molecular weights than the bio-based ones. Nevertheless, triblock copolymers based ones presented an organized microphase separated structure in their morphology, modulated by the triblock copolymer structure and composition, with well-defined boundaries between domains.

Preparation of nanocomposites based on synthesized waterborne poly(urethane-urea)s by *ex-situ* incorporation of TiO₂ nanoparticles was successful. These nanoparticles increased the mechanical properties of PU0 based nanocomposites, while increasing the thermal stability of nanocomposites based on waterborne poly(urethane-urea)s with soft segment formed by triblock copolymer. These last ones presented interesting features in their morphology, since depending on the arrangement of the PEO and PPO blocks the incorporation of TiO₂ nanoparticles led to a change in the morphology, from a rod-like one to a spherical one.

Synthesized waterborne poly(urethane-urea) films based on PEO homopolymer as well as on triblock copolymers, as well as the nanocomposites prepared from them, exhibited self-healing ability. In the case of PEO homopolymer based waterborne poly(urethane-urea) films, the incorporation of TiO₂ nanoparticles increased the healing efficiency for most of the mechanical properties, with the exception of the

deformation at break. Meanwhile, in the case of triblock copolymers based ones, the incorporation of TiO₂ nanoparticles resulted in a slower healing process, as proven by optical microscopy.

Structurally stable hydrogels based on synthesized waterborne poly(urethane-urea)s and designed nanocomposites were successfully prepared by the incorporation of SA and further cross-linking with CaCl₂. Regarding the influence of the SA content, an increase in its content resulted in an increase in the cross-linking density. This was proved by rheological measurements and SEM imaging. In the cases of the nanocomposite based hydrogels, SEM images showed the different distributions of TiO₂ nanoparticles in PU0 and PUEPE29 consequence of their different microphase separations. Designed hydrogels displayed swelling ability in acid medium. In addition these hydrogels can be used as promoters for cell proliferation, thus they can be employed as biomaterials for tissue engineering and wound dressing.

Finally, the adhesive performance of synthesized waterborne poly(urethane-urea)s was analyzed. All investigated waterborne poly(urethane-urea)s exhibited some kind of tackiness. Nonetheless, their adhesive performance was not the one of PSAs. For this reason, different strategies were tested in order to improve the adhesive performance. Bilayer systems in which the softer, more liquid-like and in contact with the surface, waterborne poly(urethane-urea) was supported by a harder, more solid-like, exhibited a PSA-like adhesive performance. Prepared bilayer systems could potentially be employed to fabricate adhesive tapes, as it was proved by 180° peel-off test.

9.2. Future works

With the aim of giving a continuity to the work here presented, and based on the obtained results, the following future works are proposed. These future works would complete the present work as well as open new research lines:

- On the one hand, in addition to the macrodiols presented in this work, it would be interesting to synthesize waterborne poly(urethane-urea)s from different bio-based precursors (macrodiols, diisocyanate and chain extender) following

the organic solvent-free process presented in this work. A process based on a water-soluble bio-based macrodiol and on a bio-based diisocyanate would make the employed synthesis more environmentally friendly,

- On the other hand, it is proposed to study the influence that the *in-situ* incorporation of TiO₂ nanoparticles to synthesized waterborne poly(urethane-urea)s would have on the final properties in comparison to the presented *ex-situ* process,
- In addition, it would be appealing to prepare a new class of hydrogels based on the freeze-thawing process by blending polyvinyl alcohol and synthesized waterborne poly(urethane-urea),
- A further study of synthesized waterborne poly(urethane-urea)s as adhesives would be appealing in order to design adhesive tapes which could find a place in the market.

9.3. List of publications and communications

9.3.1. List of publications

Authors	Iñigo Díez-García, Monica Rosas de Costa Lemma, Hernane S. Barud, Arantxa Eceiza, Agnieszka Tercjak
Title	Hydrogels based on waterborne poly(urethane-urea)s by physically cross-linking with sodium alginate and calcium chloride
Journal	Sent for publication
Year	2020
Authors	Iñigo Díez-García, Joseph L. Keddie, Arantxa Eceiza, Agnieszka Tercjak

Title Optimization of adhesive performance of waterborne poly(urethane-urea)s for adhesion on high and low surface energy surfaces

Journal Progress in Organic Coatings

Year 2020

Impact factor 3.420

15/71 Chemistry, Applied (JCR 2018)

2/20 Materials Science, Coatings and Films (JCR 2018)

Authors Iñigo Díez-García, Arantxa Eceiza, Agnieszka Tercjak

Title Self-healable nanocomposites with enhanced thermal stability by incorporation of TiO₂ nanoparticles to waterborne poly(urethane-urea) matrices based on amphiphilic triblock copolymers

Journal The Journal of Physical Chemistry C

Year 2019

Impact factor 4.309

60/293 Materials Science, Multidisciplinary (JCR 2018)

44/148 Chemistry, Physical (JCR 2018)

34/94 Nanoscience & Nanotechnology (JCR 2018)

Authors Iñigo Díez-García, Arantxa Eceiza, Agnieszka Tercjak

Title Improvement of mechanical properties and self-healing efficiency by ex-situ incorporation of TiO₂ nanoparticles to a waterborne poly(urethane-urea)

Journal Polymers

Year 2019

Impact factor 3.164

17/87 Polymer Science (JCR 2018)

Authors Iñigo Díez-García, Arantzazu Santamaría-Echart, Arantxa Eceiza, Agnieszka Tercjak

Title Triblock copolymers containing hydrophilic PEO blocks as effective polyols for organic solvent-free waterborne poly(urethane-urea)s

Journal Reactive and Functional Polymers

Year 2018

Impact factor 3.074

18/87 Polymer Science (JCR 2018)

19/71 Chemistry, Applied (JCR 2018)

43/138 Engineering, Chemical (JCR 2018)

Authors Iñigo Díez-García, Arantzazu Santamaría-Echart, Arantxa Eceiza, Agnieszka Tercjak

Title	Synthesis and characterization of environmentally-friendly waterborne poly(urethane-urea)s
Journal	European Polymer Journal
Year	2018
Impact factor	3.621
	14/87 Polymer Science (JCR 2018)

9.3.2. List of communications

Authors	Iñigo Díez-García, Arantxa Eceiza, Agnieszka Tercjak
Title	Preparation of nanocomposites by ex-situ incorporation of TiO ₂ nanoparticles to synthesized solvent-free waterborne poly(urethane-urea)s based on triblock copolymers
Congress	7th International Conference on Biobased and Biodegradable Polymers (BIOPOL 2019)
Participation	Oral communication
Year	2019
Place	Stockholm, Sweden
Authors	Iñigo Díez-García, Arantxa Eceiza, Agnieszka Tercjak
Title	Self-healable nanocomposites based on waterborne poly(urethane-urea)s modified with TiO ₂ nanoparticles
Congress	X Congreso de Jóvenes Investigadores en Polímeros (JIP2019)
Participation	Oral communication

General conclusions, future works and publications

Year	2019
Place	Burgos, Spain
Authors	Iñigo Díez-García, Arantzazu Santamaría-Echart, Arantxa Eceiza, Agnieszka Tercjak, Joseph L. Keddie
Title	Synthesis of solvent-free waterborne poly(urethane-urea) based on biocompatible and bio-based polyols
Congress	4th London Polymer Group Symposium
Participation	Poster
Year	2018
Place	London, United Kingdom
Authors	Iñigo Díez-García, Arantzazu Santamaría-Echart, Arantxa Eceiza, Agnieszka Tercjak
Title	Nanostructured waterborne poly(urethane-urea) with PEO containing triblock copolymers
Congress	AEM2018 Advanced Energy Materials
Participation	Oral communication
Year	2018
Place	Guildford, United Kingdom

Authors Iñigo Díez-García, Arantzazu Santamaría-Echart, Arantxa Eceiza, Agnieszka Tercjak

Title Waterborne poly(urethane-urea) synthesized from biobased polyol and triblock copolymers containing hydrophilic block

Congress 82nd Prague Meeting on Macromolecules - Polymer Networks
24th meeting of the International Polymer Networks Group

Participation Oral communication

Year 2018

Place Prague, Czech Republic

Authors Iñigo Díez-García, Arantzazu Santamaría-Echart, Arantxa Eceiza, Agnieszka Tercjak

Title Synthesis of solvent-free waterborne poly(urethane-urea) based on biocompatible and bio-based polyols

Congress International Conference on Materials & Energy (ICOME 2018)

Participation Poster and Oral communication

Year 2018

Place Donostia-San Sebastián, Spain

Authors Iñigo Díez-García, Arantzazu Santamaría-Echart, Arantxa Eceiza, Agnieszka Tercjak

Title Synthesis of organic solvent-free green waterborne poly(urethane-urea)s

Congress IX Congreso de Jóvenes Investigadores en Polímeros (JIP2017)

Participation Oral communication

Year 2017

Place La Pineda, Spain

Authors Iñigo Díez-García, Arantzazu Santamaría-Echart, Arantxa Eceiza, Agnieszka Tercjak

Title The role of microdomain structure on the properties of green waterborne poly(urethane-urea)s

Congress 24th International Symposium on Metastable, Amorphous and Nanostructured Materials (ISMANAM 2017)

Participation Poster

Year 2017

Place Donostia-San Sebastián, Spain

Collaborations

Authors Aitor Arbelaiz, Axier Domiguez, Ander Orue, Iñigo Díez-García, Marian Corcuera, Arantxa Eceiza

Title Preparation and characterization of composites based on PLA/PHBV matrix and lignocellulosic fibers

Congress	7th International Conference on Biobased and Biodegradable Polymers (BIOPOL 2019)
Participation	Poster
Year	2019
Place	Stockholm, Sweden

9.4. Research stages

Research	Study of the photocatalytic activity of synthesized waterborne poly(urethane-urea)s
Dates	10/07/2019-20/07/2019
University	University of Gdansk
Place	Gdansk, Poland
Founding	NAWA Polish National Agency for Academic Exchange
Research	Characterization of the adhesive performance of the synthesized waterborne poly(urethane-urea)s
Dates	30/08/2018-30/11/2018
University	University of Surrey
Place	Guildford, United Kingdom
Founding	Basque Government (EGONLABUR 2018)

Chapter



"He who is not everyday conquering some fear has not learned the secret of life."

(Ralph Waldo Emerson)

Annexes

A. Annexes

A.1. Additional information	215
A.2. List of tables	222
A.3. List of figures	225
A.4. List of abbreviations	232
A.5. List of symbols	235

A.1. Additional information

Hydroxyl index

Table A.1. Hydroxyl index of employed macrodiol as determined by ASTM D4274–99.

Macrodiol	OH index
PEO	105
P3MG	114
BCPEPE19	57
BCPEPE29	39
BCPPEP20	56
BCPPEP27	42

Proton nuclear magnetic resonance ($^1\text{H-NMR}$) of macrodiols

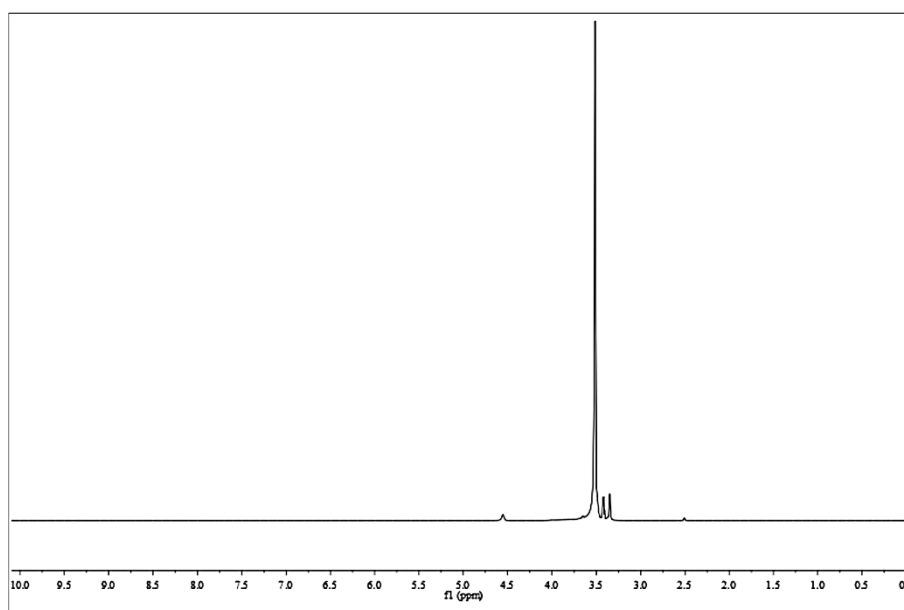


Figure A.1. $^1\text{H-NMR}$ spectra of PEO. (Liquid-state ^1H NMR measurements were carried out employing an Avance Bruker 500 spectrometer equipped with a BBO probe with gradient in Z axis, at a frequency of 500 MHz. Number of scans was 64, with spectral window of 5000 Hz and recovery delay of 1 s. Waterborne poly(urethane-urea)s films were dissolved in deuterated DMSO).

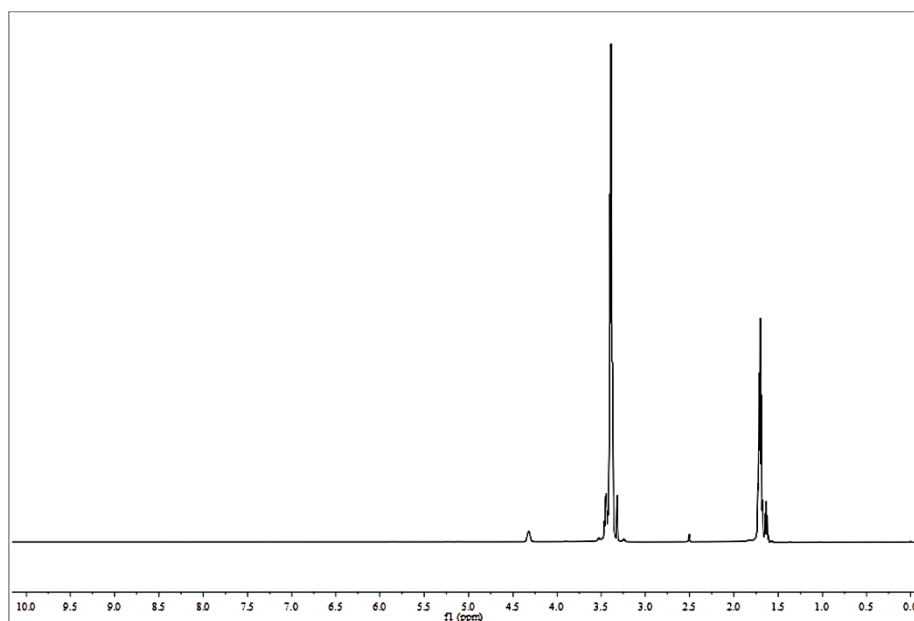


Figure A.2. ^1H -NMR spectra of P3MG. (Liquid-state ^1H NMR measurements were carried out employing an Avance Bruker 500 spectrometer equipped with a BBO probe with gradient in Z axis, at a frequency of 500 MHz. Number of scans was 64, with spectral window of 5000 Hz and recovery delay of 1 s. Waterborne poly(urethane-urea)s films were dissolved in deuterated DMSO).

NCO titration curves

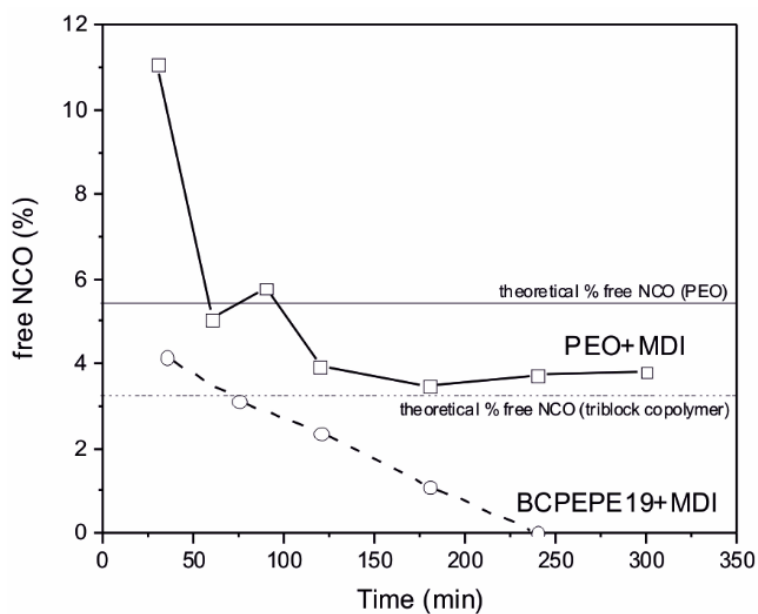


Figure A.3. Evolution of the amount of free NCO groups in the reaction between MDI and PEO, as well as of MDI and BCPEPE19. The values were determined by dibutylamine back titration method (DBBTM) according to ASTM D2572-97.

SEC Curves

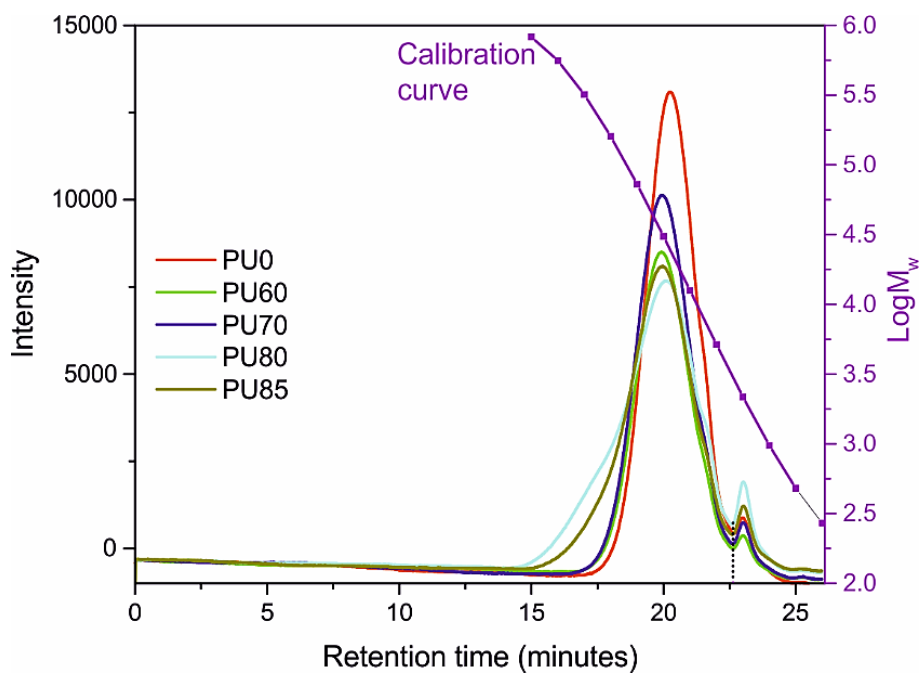


Figure A.4. SEC curves obtained from the PE0/P3MG based waterborne poly(urethane-urea) films dissolved in DMF at 0.5 wt%. LogMW axis, in purple, corresponds to the calibration curve. Integration of curves was considered until dash-dot line.

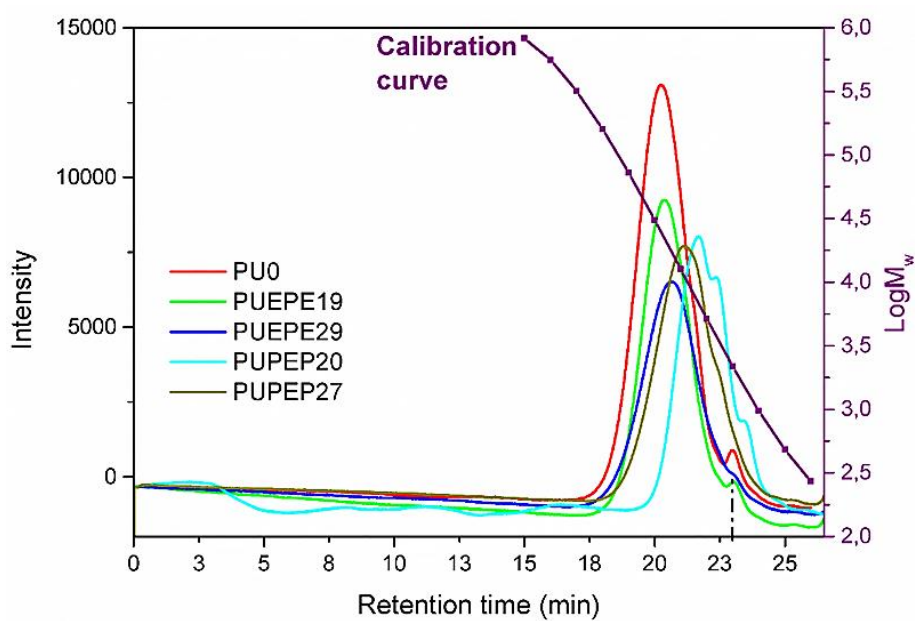


Figure A.5. SEC curves obtained from the triblock copolymers based waterborne poly(urethane-urea) films dissolved in DMF at 0.5 wt%. LogMW axis, in purple, corresponds to the calibration curve. Integration of curves was considered until dash-dot line.

DSC curves of triblock copolymers

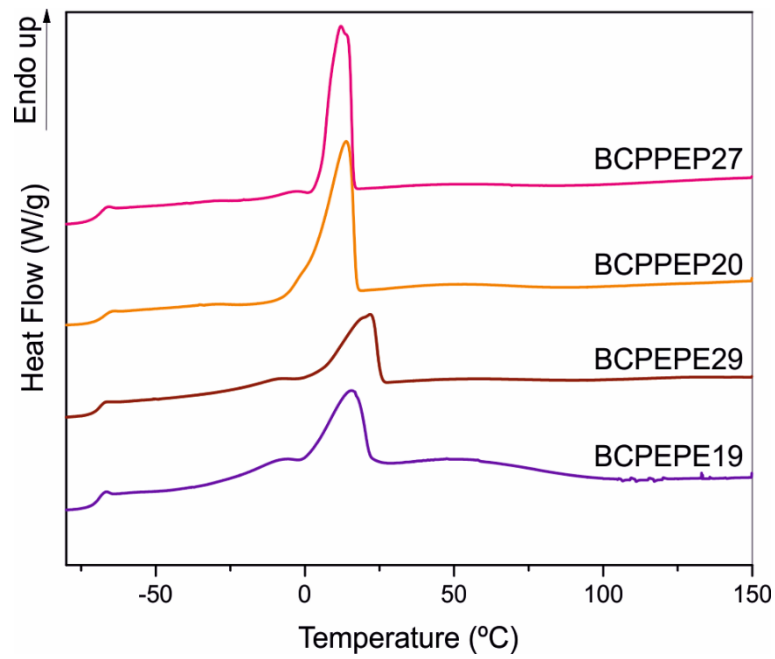


Figure A.6. DSC curves of triblock copolymers.

DSC of SA, PU0 and PUEPE29

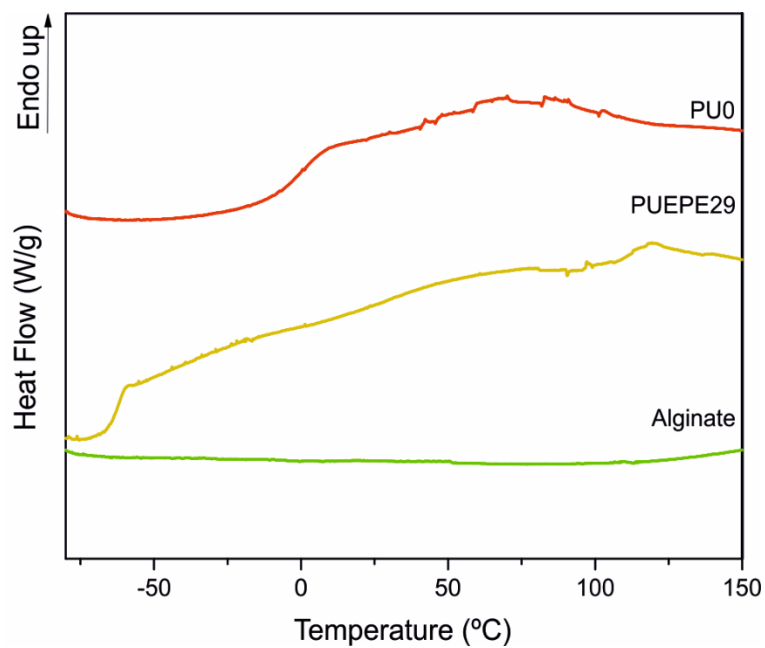


Figure A.7. DSC curves of SA, PU0 and PUEPE29 employed for the preparation of the hydrogels.

FTIR of SA, PU0 and PUEPE29

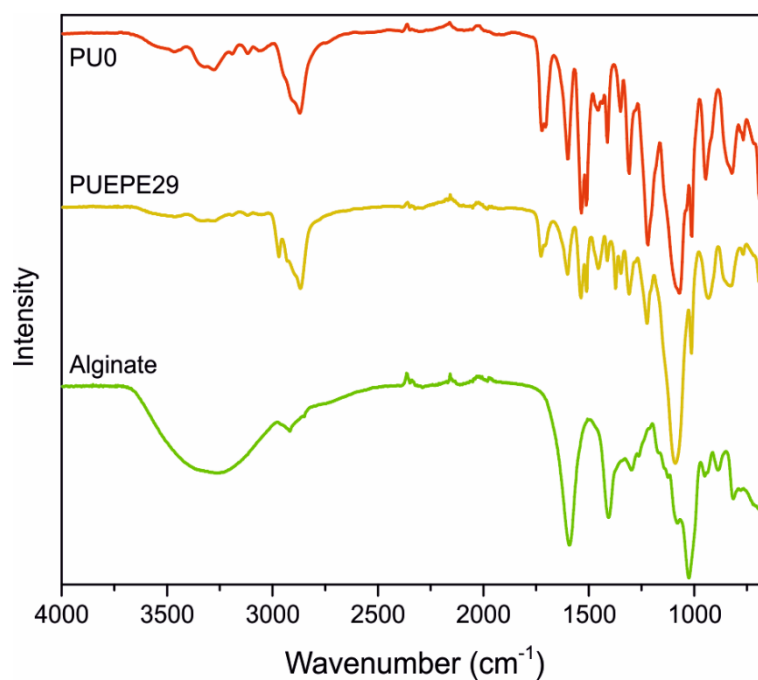


Figure A.8. FTIR spectra of SA, PU0 and PUEPE29 employed for the preparation of the designed hydrogels.

TGA of TiO_2 -PUEPE19 and TiO_2 -PUPEP27 nanocomposites

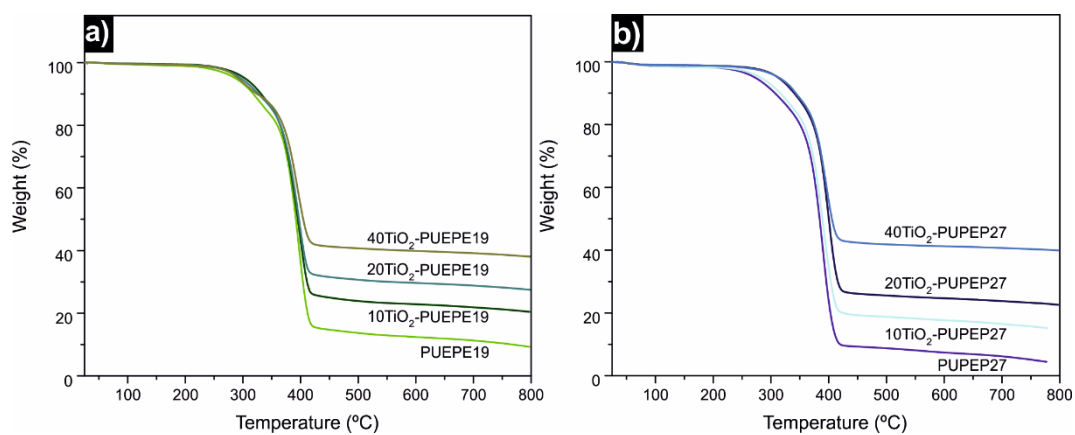


Figure A.9. TGA curves of designed TiO_2 -PUEPE19 and TiO_2 -PUPEP27 nanocomposite films.

TGA and dTGA of SA, PU0 and PUEPE29

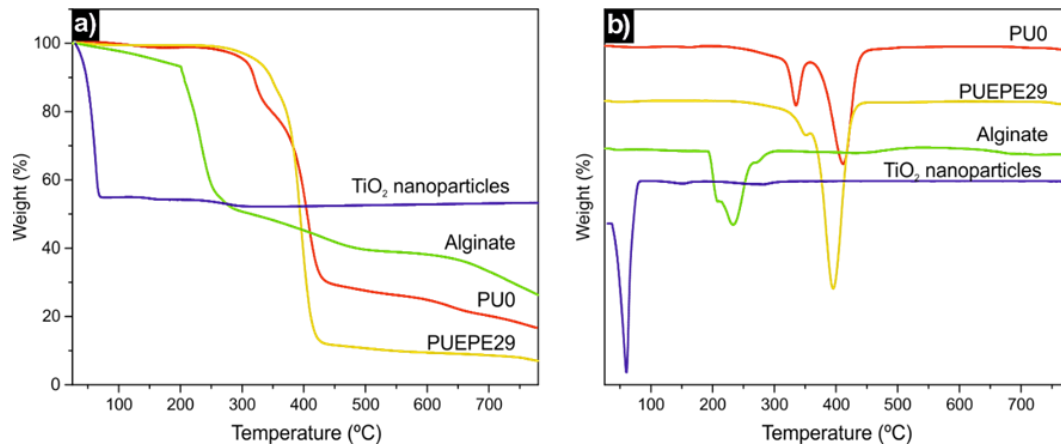


Figure A.10. (a) TGA and (b) dTGA curves of SA, PU0, PUEPE29 and TiO₂ nanoparticles employed for the preparation of designed hydrogels.

Strain-stress curves

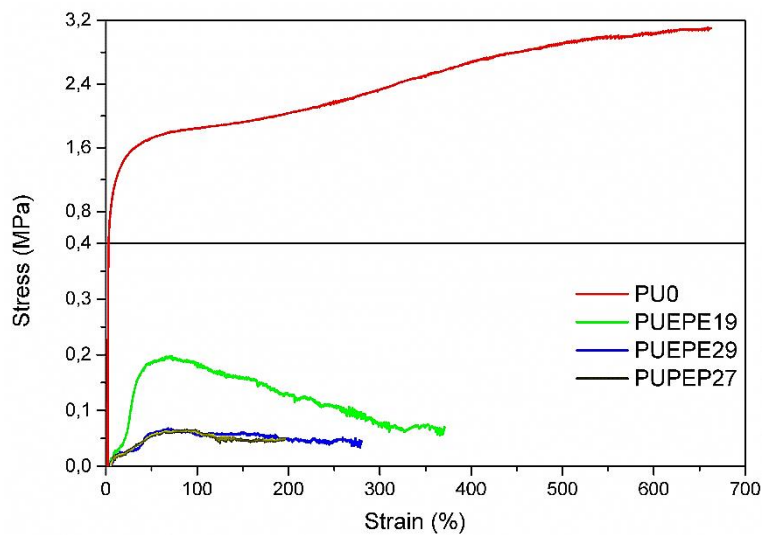


Figure A.11. Stress-strain curves of PU0, as reference, and triblock copolymers based waterborne poly(urethane-urea)s.

Strain-stress curves of self-healed films

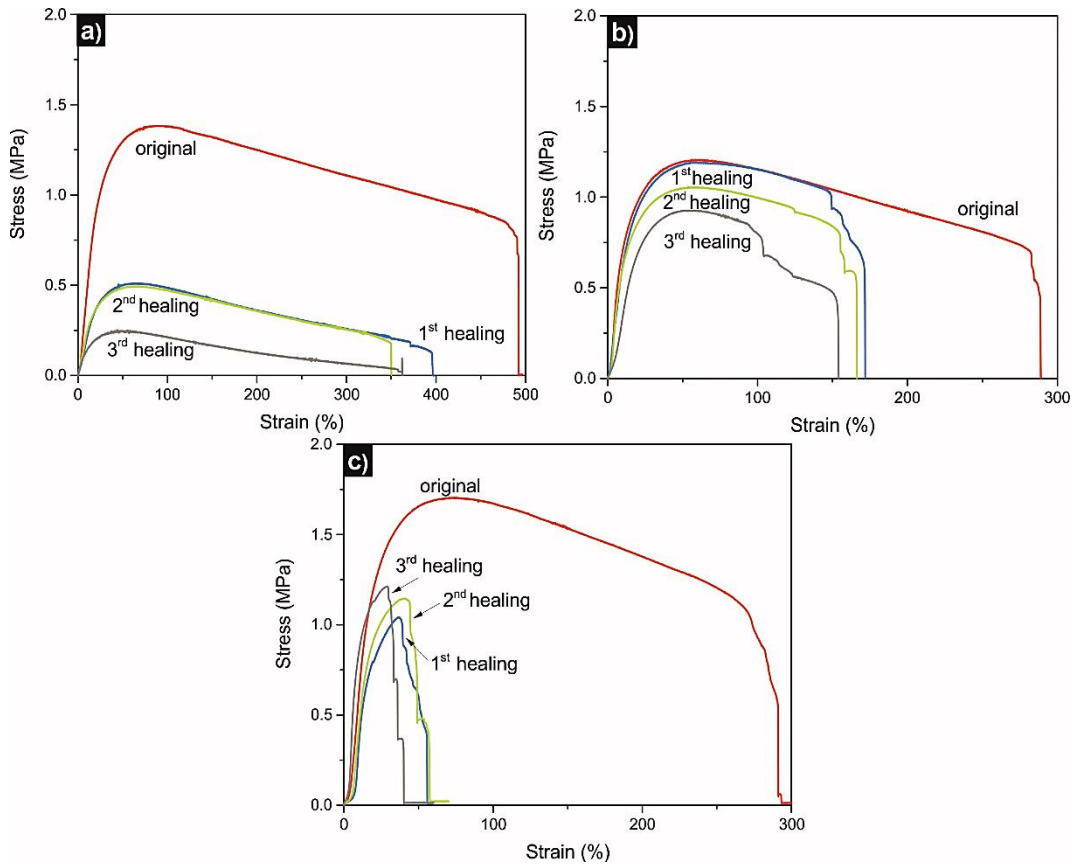


Figure A.12. Stress-strain curves of original and self-healed films of (a) PU0, (b) 10TiO₂-PU0 and (c) 20TiO₂-PU0.

A.2. List of tables

Chapter 2: Materials and characterization techniques

Table 2.1. Raw materials employed for the synthesis of waterborne poly(urethane-urea). Their chemical structure, molecular weight and PEO content	42
--	----

Chapter 3: Waterborne poly(urethane-urea)s based on a bio-based macrodiol

Table 3.1. Designation of samples, molar composition, MDI-SBBS segment content, acid group content and renewable macrodiol content of synthesized waterborne poly(urethane-urea)s	60
--	----

Table 3.2. Average particle size, experimental solid content and solid content yield of synthesized PEO and P3MG based waterborne poly(urethane-urea) dispersions	61
--	----

Table 3.3. Average weight molecular weight \bar{M}_w and polydispersity index (IP) of synthesized PEO and P3MG based waterborne poly(urethane-urea) films	66
--	----

Table 3.4. Glass transition temperature of the soft segment (T_g) and endotherm temperature (T_E) of synthesized waterborne poly(urethane-urea) films	67
--	----

Table 3.5. Yield stress (σ_y), stress at break (σ_b), Young's modulus (E) and deformation at break (ϵ_b) of synthesized PEO and P3MG based waterborne poly(urethane-urea) films determined from strain-stress curves	69
--	----

Chapter 4: Triblock copolymers as macrodiols for the synthesis of waterborne poly(urethane-urea)s

Table 4.1. Designation of samples, molar composition, MDI-SBBS segment content and acid group content of synthesized triblock copolymers based waterborne poly(urethane-urea)s and PEO based waterborne poly(urethane-urea)	84
--	----

Table 4.2. Average particle size, experimental solid content and theoretical solid content of synthesized triblock copolymers based waterborne poly(urethane-urea) dispersions. PU0 dispersion was analyzed as reference	85
---	----

Table 4.3. Average weight molecular weight (\bar{M}_w) and polydispersity index (IP) of synthesized triblock copolymers	
--	--

based waterborne poly(urethane-urea) films. PU0 film was added as reference.	90
Table 4.4. Glass transition temperature of the soft segment (T_g), melting temperature (T_m) and melting enthalpy (ΔH_m) of synthesized triblock copolymers based waterborne poly(urethane-urea) films. PU0 film was added for comparison	92
Table 4.5. Young's modulus (E), stress at break (σ_b) and deformation at break (ϵ_b) of synthesized triblock copolymers based waterborne poly(urethane-urea) films. PU0 film was added for comparison	95
Chapter 5: Nanocomposites prepared by incorporation of TiO₂ nanoparticles	
Table 5.1. Glass transition temperature (T_g) of neat PU0 and TiO ₂ -PU0 nanocomposite films	111
Table 5.2. Decomposition temperatures of hard (T_1) and soft (T_2) segments as well as TiO ₂ nanoparticles content of neat PU0 and TiO ₂ -PU0 nanocomposite films	113
Table 5.3. Contact angle of investigated neat PU0 and TiO ₂ -PU0 nanocomposite films	116
Table 5.4. Young's modulus (E), tensile strength (σ_{max}), stress at break (σ_b), and deformation at break (ϵ_b) of investigated neat PU0 and TiO ₂ -PU0 nanocomposite films	116
Table 5.5. Glass transition temperature (T_g), melting temperature (T_m) and melting enthalpy (ΔH_m) of investigated TiO ₂ -PUEPE19 and TiO ₂ -PUPEP27 nanocomposite films. Neat PUEPE19 and PUPEP7 were added for comparison.	120
Table 5.6. Decomposition temperatures of (T_1) as well as TiO ₂ nanoparticles content of neat PUEPE19 and PUPEP27 and TiO ₂ -PUEPE19 and TiO ₂ -PUPEP27 nanocomposite films	122
Table 5.7. Contact angle of investigated TiO ₂ -PUEPE19 and TiO ₂ -PUPEP27 nanocomposite films. Neat PUEPE19 and PUPEP27 were added for comparison	126

Chapter 6: Self-healing ability of waterborne poly(urethane-urea) and nanocomposite films

Table 6.1. Contact angle of original investigated neat PU0 and TiO₂-PU0 nanocomposite films and of the healed films **141**

Chapter 7: Development of hydrogels by incorporation of sodium alginate

Table 7.1. Content of PU0, PUEPE29, SA and TiO₂ nanoparticles in prepared hydrogels **156**

Table 7.2. Glass transition temperatures of neat waterborne poly(urethane-urea)s and of the prepared hydrogels **161**

Table 7.3. Decomposition temperatures of neat SA and waterborne poly(urethane-urea)s as well as of the designed hydrogels. Decomposition temperatures were related to SA (T_{SA}), the hard segment (T_1) and the soft segment (T_2) of waterborne poly(urethane-urea)s **163**

Table 7.4. Compressive modulus and compressive stress, at different strains, of designed hydrogels **166**

Chapter 8: Adhesive performance of waterborne poly(urethane-urea)s

Table 8.1. Sample denotation of designed bilayers systems based on PU0 and PUEPE29 **181**

Table 8.2. Surface energy (γ_{PU}), calculated interfacial energy (γ_{PUP}) and thermodynamic work of adhesion (W_{adh}) of synthesized waterborne poly(urethane-urea)s **185**

Annexes

Table A.1. Hydroxyl index of employed macrodiol as determined by ASTM D4274-99 **215**

A.3. List of figures

Chapter 1: Introduction

Figure 1.1. Most common reactions of isocyanate group	7
Figure 1.2. Most common diisocyanates	8
Figure 1.3. Structure of segmented poly(urethane-urea)s	9
Figure 1.4. Structure of the triblock copolymers based on PEO and PPO blocks	12
Figure 1.5. Scheme of the poly(urethane-urea) matrix and the polymer matrix nanocomposite after dispersion of the nanofiller	13
Figure 1.6. Estimated disposal method of global plastic wastes. In black, discarded, in red, incinerated, and in green, recycled plastic wastes	14
Figure 1.7. Crack healing mechanism	15
Figure 1.8. General methods for preparation of hydrogels	17
Figure 1.9. Adhesion failure mechanisms depending on the adhesion-cohesion balance	20
Figure 1.10. Percentage of the market value (in millions of \$) of adhesive applications of polyurethanes	22
Figure 1.11. Schematic description of the work presented in this thesis	24

Chapter 2: Materials and characterization techniques

Figure 2.1. Structures of sodium alginate, sodium β -D-mannuronate (M) and sodium α -L-guluronate (G)	43
---	----

Chapter 3: Waterborne poly(urethane-urea)s based on a bio-based macrodiol

Figure 3.1. Reactions and reactivity of aliphatic amines (-Al-NH ₂) and aromatic amines (-Ar-NH ₂) compared to hydroxyl groups and water with diisocyanate group	57
Figure 3.2. Schematic illustration of synthesized PEO and P3MG based waterborne poly(urethane-urea)s	59

Figure 3.3. Visual appearance of synthesized PEO and P3MG based waterborne poly(urethane-urea) dispersions	60
Figure 3.4. Visual aspect of synthesized PEO and P3MG based waterborne poly(urethane-urea) films	61
Figure 3.5. Proposed scheme for the particle arrangement in synthesized waterborne poly(urethane-urea)s regarding their chain extension yield	62
Figure 3.6. Proposed arrangement for core-shell particles of synthesized PEO and P3MG based waterborne poly(urethane-urea) dispersions	63
Figure 3.7. FTIR spectra of synthesized (a) PEO and P3MG based waterborne poly(urethane-urea) films and (b) amplification of their carbonyl stretching region	65
Figure 3.8. DSC heating scan curves of PEO and P3MG macrodiols as well as of synthesized PEO and P3MG based waterborne poly(urethane-urea) films	67
Figure 3.9. AFM phase images (750 nm x 750 nm) of synthesized (a) PU0, (b) PU60, (c) PU70, (d) PU80, (e) PU85 waterborne poly(urethane-urea) films	68
Figure 3.10. UV-vis spectra of synthesized PEO and P3MG based waterborne poly(urethane-urea) films	70
Chapter 4: Triblock copolymers as macrodiols for the synthesis of waterborne poly(urethane-urea)s	
Figure 4.1. Schematic illustration of the synthesis of triblock copolymers based waterborne poly(urethane-urea)s	83
Figure 4.2. Visual appearance of synthesized triblock copolymers based waterborne poly(urethane-urea) dispersions. PU0 dispersion was added as reference	84
Figure 4.3. Visual appearance of triblock copolymers based waterborne poly(urethane-urea) films. PU0 film was added for comparison purpose	85
Figure 4.4. Proposed arrangements of core-shell particles of synthesized triblock copolymers based waterborne poly(urethane-urea) dispersions	87
Figure 4.5. Dynamic viscosities of synthesized triblock copolymers based waterborne poly(urethane-urea) dispersions	88
Figure 4.6. FTIR spectra of synthesized (a) triblock copolymers based waterborne poly(urethane-urea) films and (b) amplification	

of their carbonyl stretching region. FTIR spectra of PU0 was added for comparison	89
Figure 4.7. DSC heating scan curves of synthesized triblock copolymers based waterborne poly(urethane-urea) films. DSC curve of PU0 was added for comparison	91
Figure 4.8. AFM phase images (3 μm x 3 μm) of (a) PUEPE19, (b) PUEPE29, (c) PUPEP20 and (d) PUPEP27 synthesized triblock copolymers based waterborne poly(urethane-urea) films. AFM phase images of (e) PU0 film was added for comparison	93
Figure 4.9. UV-visible spectra of synthesized triblock copolymers based waterborne poly(urethane-urea) films. PU0 was added for comparison	95
Chapter 5: Nanocomposites prepared by incorporation of TiO₂ nanoparticles	
Figure 5.1. Schematic description of the procedure for the preparation of the nanocomposites	109
Figure 5.2. FTIR spectra of neat PU0 and TiO ₂ -PU0 nanocomposite films	109
Figure 5.3. DSC curves of neat PU0 and TiO ₂ -PU0 nanocomposite films	110
Figure 5.4. (a) Thermogravimetric analysis and (b) dTGA curves of neat PU0 and TiO ₂ -PU0 nanocomposite films.	112
Figure 5.5. AFM phase images (3 μm x 3 μm) of investigated (a) PU0, (b) 10TiO ₂ -PU0, (c) 20TiO ₂ -PU0 and (d) 40TiO ₂ -PU0 films. The inset in each AFM image corresponds to OM micrograph.	113
Figure 5.6. EFM phase images (3 μm x 3 μm) of investigated (a) 10TiO ₂ -PU0, (c) 20TiO ₂ -PU0, (e) 40TiO ₂ -PU0 films and their simultaneously obtained AFM phase images (3 μm x 3 μm)	115
Figure 5.7. FTIR spectra of investigated (a) TiO ₂ -PUEPE19 and (b) TiO ₂ -PUPEP27 nanocomposite films. Neat PUEPE19 and PUPEP7 were added for comparison	117
Figure 5.8. DSC curves of investigated (a) TiO ₂ -PUEPE19 and (b) TiO ₂ -PUPEP27 nanocomposite films. Neat PUEPE19 and PUPEP7 were added for comparison	119
Figure 5.9. dTGA curves of investigated (a) neat PUEPE19 and TiO ₂ -PUEPE19 as well as (b) neat PUPEP27 and TiO ₂ -PUPEP27 nanocomposite films.	121

Figure 5.10. AFM phase images (3 μm x 3 μm) of investigated (a) neat PUEPE19, (b) 10TiO₂-PUEPE19, (c) 20TiO₂-PUEPE19 and (d) 40TiO₂-PUEPE19 nanocomposite films **123**

Figure 5.11. AFM phase images (3 μm x 3 μm) of investigated (a) neat PUPEP27, (b) 10TiO₂-PUPEP27, (c) 20TiO₂-PUPEP27 and (d) 40TiO₂-PUPEP27 nanocomposite films **124**

Figure 5.12. EFM phase images (3 μm x 3 μm) of investigated (a) 20TiO₂-PUEPE19 (b) 40TiO₂ PUEPE19, (c) 20TiO₂-PUPEP27 and (d) 40TiO₂-PUPEP27 nanocomposite films **125**

Chapter 6: Self-healing ability of waterborne poly(urethane-urea) and nanocomposite films

Figure 6.1. Schematic description of how specimens were cut in half for each cut/recovery cycle **137**

Figure 6.2. Schematic representation of the hydrogen bonds formed in the poly(urethane-urea) network **138**

Figure 6.3. Digital images of the original, cut and self-healed samples of (a) neat PU0, (b) 10TiO₂-PU0 and (c) 20TiO₂-PU0 films **139**

Figure 6.4. The healing efficiency of investigated neat PU0, 10TiO₂-PU0 and 20TiO₂-PU0 films determined from stress-strain curves for (a) Young's modulus, (b) tensile strength, (c) stress at break and (d) deformation at break **140**

Figure 6.5. OM micrographs during self-healing process for investigated (a) neat PUEPE19, (b) 10TiO₂-PUEPE19, (c) 20TiO₂-PUEPE19 and (d) 40TiO₂-PUEPE19 films **142**

Figure 6.6. OM micrographs during self-healing process for investigated (a) neat PUPEP27, (b) 10TiO₂-PUPEP27, (c) 20TiO₂-PUPEP27 and (d) 40TiO₂-PUPEP27 films **143**

Chapter 7: Development of hydrogels by incorporation of sodium alginate

Figure 7.1. Schematic illustration of the egg-box model in which Ca²⁺ cations are accommodated between α -L-guluronate blocks of the alginate chains **154**

Figure 7.2. Schematic description of the protocol followed for the preparation of hydrogels, as well as the proposed hydrogen bonding between SA and waterborne poly(urethane-urea)s **155**

Figure 7.3. Visual aspect of prepared hydrogels based on synthesized waterborne poly(urethane-urea)s. (a) 20SA-PU0, (b)

30SA-PU0, (c) TiO ₂ -SA-PU0, (d) 20SA-PUEPE29, (e) 30SA-PUEPE29 and (f) TiO ₂ -SA-PUEPE29	156
Figure 7.4. Frequency dependence of G' (solid symbols) and G'' (open symbols) of prepared hydrogels based on (a) PU0 and (b) PUEPE29 waterborne poly(urethane-urea)s	157
Figure 7.5. FTIR spectra of designed hydrogels based on (a) PU0 and (b) PUEPE29 waterborne poly(urethane-urea)s	159
Figure 7.6. DSC curves of hydrogels based on (a) PU0 and (b) PUEPE29 waterborne poly(urethane-urea)s	160
Figure 7.7. dTGA curves of designed hydrogels based on (a) PU0 and (b) PUEPE29 waterborne poly(urethane-urea)s	162
Figure 7.8. Proposed hydrogen bonding interactions between SA, TiO ₂ nanoparticles and both PU0 and PUEPE29 waterborne poly(urethane-urea)s regarding their different soft segment compositions	164
Figure 7.9. SEM images of cross-section of (a) 20SA-PU0, (b) 30SA-PU0, (c) TiO ₂ -SA-PU0, (d) 20SA-PUEPE29, (e) 30SA-PUEPE29 and (f) TiO ₂ -SA-PUEPE29	165
Figure 7.10. Swelling degree of prepared hydrogels based on (a) PU0 and (b) PUEPE29 waterborne poly(urethane-urea)s in acidic pH (solid symbols)	168
Figure 7.11. In vitro cell proliferation (MTT method) of prepared hydrogels after Human Fibroblast cell culture (48 h) in the presence or not of different treated materials. (Control x 20SA-PU0 $p < 0.0006$, Control x 30SA-PU0 $p < 0.0003$, Control x 20SA-PUEPE29 $p < 0.0008$, Control x 30SA-PUEPE29 $p < 0.0002$)	169
Chapter 8: Adhesive performance of waterborne poly(urethane-urea)s	
Figure 8.1. Schematic illustration of the arrangement of designed bilayer systems for probe-tack adhesion measurement. Thickness refers to the thickness of the applicator	181
Figure 8.2. Representative probe-tack curves of synthesized waterborne poly(urethane-urea)s for measurements carried out with both (a) steel and (b) PP probes	186
Figure 8.3. Representative probe-tack curves of designed different thickness top layer bilayer systems measured with (a) (c) steel and (b) (d) PP probes. The sample names are defined in Table 2	188

Figure 8.4. Representative probe-tack curves of the prepared PUEPE29/PU0 blends using both steel and PP probes	190
Figure 8.5. Maximum tack stress of synthesized waterborne poly(urethane-urea)s, prepared blends, and designed Bilayer029 systems for both (a) steel and (b) PP probes	191
Figure 8.6. Debonding energy calculated from the area under the probe-tack curves of synthesized waterborne poly(urethane-urea)s, prepared blends, and designed Bilayer029 systems for both (a) steel and (b) PP probes	192
Figure 8.7. Peel force determined for the designed Bilayer029-P system by 180° peel-off test on glass (solid bars) and aluminum (striped bars) surfaces with either PP (blue) or PET (green) backing layer. Results of a commercial tape (purple) are also presented for comparison purpose	194

Annexes

Figure A.1. ¹ H-NMR spectra of PEO	181
Figure A.2. ¹ H-NMR spectra of P3MG	186
Figure A.3. Evolution of the amount of free NCO groups in the reaction between MDI and PEO, as well as of MDI and BCPEPE19	188
Figure A.4. SEC curves obtained from the PEO/P3MG based waterborne poly(urethane-urea) films	220
Figure A.5. SEC curves obtained from the triblock copolymers based waterborne poly(urethane-urea) films	191
Figure A.6. DSC curves of triblock copolymers	192
Figure A.7. DSC curves of SA, PU0 and PUEPE29 employed for the preparation of the hydrogels	194
Figure A.8. FTIR spectra of SA, PU0 and PUEPE29 employed for the preparation of the designed hydrogels	188
Figure A.9. TGA curves of designed TiO ₂ -PUEPE19 and TiO ₂ -PUPEP27 nanocomposite films.	220
Figure A.10. (a) TGA and (b) dTGA curves of SA, PU0, PUEPE29 and TiO ₂ nanoparticles employed for the preparation of designed hydrogels	191

Figure A.11. Stress-strain curves of PU0, as reference, and triblock copolymers based waterborne poly(urethane-urea)s **192**

Figure A.12. Stress-strain curves of original and self-healed films of (a) PU0, (b) 10TiO₂-PU0 and (c) 20TiO₂-PU0 **194**

A.4. List of abbreviations

PA	Polyamide
TDI	Toluene diisocyanate
MDI	4,4'-diphenylmethane diisocyanate
HDI	Hexamethylene diisocyanate
HMDI	Hydrogenated MDI
VOC	Volatile Organic Compound
PEO	Poly(ethylene oxide)
PPO	Poly(propylene oxide)
PSA	Pressure sensitive adhesive
P3MG	Poly(trimethylene ether glycol)
SA	Sodium alginate
M	Sodium β -D-mannuronate
G	Sodium α -L-guluronate
DBSA	2,4-diamino-benzenesulfonic acid
SDBS	Sodium 2,4-diamino-benzene sulfonate
BCPEPE	Poly(ethylene oxide-b-propylene oxide-b-ethylene oxide)
BCPPEP	Poly(propylene oxide-b-ethylene oxide-b-propylene oxide)
DLS	Dynamic light scattering

FTIR	Fourier transformed infrared
SEC	Size exclusion chromatography
IP	Polydispersity index
DMF	Dimethylformamide
PS	Polystyrene
UV-Vis	Ultraviolet-visible
DSC	Differential scanning calorimetry
TGA	Thermogravimetric analysis
DMA	Dynamic mechanical analysis
AFM	Atomic force microscopy
OM	Optical microscopy
SEM	Scanning electron microscopy
EFM	Electrostatic force microscopy
WCA	Water contact angle
MTT	3-(4,5-dimethylthiazol-2-yl)-2,5diphenyltetrazolium bromide
DMSO	Dimethyl sulfoxide
PP	Polypropylene
PET	Polyethylene terephthalate
DBBTM	Dibutylamine back titration method

Annexes

PCL	Poly(ϵ -caprolactone)
PDMS	Poly(dimethylsiloxane)
PTHF	Poly(tetrahydrofurane)
$^1\text{H-NMR}$	Proton nuclear magnetic resonance

A.5. List of symbols

λ	Wavelength
\bar{M}_w	Weight average molecular weight
\bar{M}_n	Number average molecular weight
G'	Storage modulus
G''	Loss modulus
γ	Imposed deformation
η^*	Complex viscosity
$\tan \delta$	Tangent of phase angle
T_g	Glass transition temperature
T_m	Melting temperature
ΔH_m	Melting enthalpy
E	Young's modulus
σ_{max}	Tensile strength
σ_b	Stress at break
ϵ_b	Deformation at break
R_a	Roughness average
R_q	Root mean square roughness
W_0	Weight of freeze-dried hydrogels
W_w	Wet weight of hydrogels

%SD	Swelling degree
σ	Stress
F	Force
A	Contact area
ϵ	Strain
d	Travel distance
h_{film}	Thickness of the film
W_{deb}	Debonding energy
T_{E}	Temperature endotherm
T_{room}	Room temperature
T_1	Decomposition temperature 1
T_2	Decomposition temperature 2
T_{SA}	Decomposition temperature related to sodium alginate
ϵ_{max}	Failure at strain
W_{adh}	Thermodynamic work of adhesion
γ_{PU}	Interfacial free energy between the poly(urethane-urea) and air
γ_{P}	Interfacial free energy between the probe and the air
γ_{PUP}	Interfacial free energy between the poly(urethane-urea) and the probe
Φ	Dissipation of the polymer

*“La gente olvidará lo que dijiste, la gente olvidará lo que hiciste,
pero la gente nunca olvidará lo que les hiciste sentir.”*

(Maya Angelou)

